UCL INSTITUTE OF OPHTHALMOLOGY
LONDON

Genetic and phenotypic heterogeneity in autosomal recessive retinal disease

Panagiotis Sergouniotis

Institute of Ophthalmology, University College London

Submitted to the University College of London for the Degree of Doctor of Philosophy

April 2012

Supervisors: Dr Andrew R Webster
Professor Anthony T Moore

DECLARATION

I, Panagiotis Sergouniotis, confirm that the work presented in this thesis is my own. Where information has been derived from other sources, I confirm that this has been indicated in the thesis.

Panagiotis I Sergouniotis

ABSTRACT

Molecular genetics has transformed our understanding of disease and is gradually changing the way medicine is practiced. Genetic mapping provides a powerful approach to discover genes and biological processes underlying human disorders. Recent advances in DNA microarray and sequencing technology have significantly increased the power of genetic mapping studies and have ushered in a new era for biomedicine. In this thesis, linkage analysis (including homozygosity mapping), exome sequencing and candidate gene sequencing have been utilised to genetically dissect autosomal recessive retinal disease. Subsequently, clinical findings from patients found to be similar in terms of molecular pathology have been pooled. DNA and basic phenotypic data from over 500 unrelated individuals were available for the project. Disease-causing variants in three genes that have not been previously associated with human recessive disorders are reported: (a) biallelic mutations in *TRPM1* abrogate ON bipolar cell function and cause complete congenital stationary night blindness; (b) biallelic mutations in *KCNJ13*, a gene encoding an inwardly rectifying potassium channel subunit cause Leber congenital amaurosis; (c) biallelic mutations in *PLA2G5*, a gene encoding group V phospholipase A_2, cause benign fleck retina. The consequences of mutations in these and other disease-related genes (*RDH5*, *GRM6*, *KCNV2*, *OAT* and *SAG*) on retinal structure (spectral domain optical coherence tomography, fundus autofluorescence imaging) and visual function (electrophysiology, perimetry testing) have been studied; features that may have mechanistic relevance have been identified. Additionally, DNA sequence variation of a highly polymorphic gene (*C2ORF71*), recently associated with photoreceptor degeneration, has been studied and quantified in patient and control samples. Basic bioinformatics tools to analyse genomic data have been developed (bash, perl, python and R programming languages). Overall, results presented in this thesis contribute to an understanding of Mendelian retinal disease that is not only observational but also mechanistic.

ACKNOWLEDGEMENTS

I would like to thank my supervisors Dr Andrew Webster and Professor Tony Moore for giving me the opportunity to undertake this project and for the unconditional trust they bestowed upon me over the last three years. They have been an inspiration to pursue a career in ophthalmic genetics. Special thanks to Dr Zheng Li, Dr Alice Davidson, Dr Donna Mackay and all the members of the Webster/Moore research group, past and present, for their encouragement, help and scientific guidance. I am grateful to Professor Graham Holder and Dr Tony Robson for their collaborative inputs and for introducing me to retinal electrophysiology. I am greatly indebted to Dr Vincent Plagnol for the very fruitful and fun collaboration; his kindness, high quality of expertise, collaborative spirit and general enthusiasm for science made working with him a joy.

I would like to thank the Markideion Foundation, the Alexander S. Onassis Foundation, the British Retinitis Pigmentosa Society (RP Fighting Blindness), the Special Trustees of Moorfields Eye Hospital and the National Institute for Health Research UK (Moorfields Eye Hospital and UCL Institute of Ophthalmology Biomedical Research Centre) for the financial support.

I wish to thank my friend Thomas Daskalakis for his help with python programming and for introducing me to computational thinking. I also wish to express my gratitude to the families that contributed to the study. It has been a great pleasure to meet them in clinic and they have been a genuine source of inspiration to me.

Finally, I wish to dedicate this thesis to my family (Efi, Ilias, Angeliki, yiayia Foteini) and especially to my brother Fotis for paving the way.

TABLE OF CONTENTS

LIST OF FIGURES

LIST OF TABLES

ABBREVIATIONS

A	ampere
APEX	arrayed primer extension
ARMS	amplification refractory mutation system
BMI	body mass index
BRLMM	Bayesian Robust Linear Model with Mahalanobis distance classifier
BSA	bovine serum albumin
CCD	charge-coupled device
cd	candela
cDNA	coding deoxyribonucleic acid
cM	centiMorgan
CPT	central point thickness
CSF	central subfield thickness
CSNB	congenital stationary night blindness
dB	decibel
ddNTP	dideoxy nucleoside triphosphate
dH_20	distilled H_20
dNTP	deoxyribonucleoside triphosphate
DMSO	dimethylsulfoxide
DNA	deoxyribonucleic acid
ECACC	European collection of cell cultures
EDTA	ethylenediaminetetraacetic acid
EOG	electro-oculogram
ERG	electroretinogram
ETDRS	early treatment of diabetic retinopathy study
EVS	Exome Variant Server, NHLBI Exome Sequencing Project, Seattle, USA, http://snp.gs.washington.edu/EVS
FEVR	familial exudative vitreoretinopathy
g	gram
GDP	guanosine diphosphate
GRM6	glutamate receptor, metabotropic 6

GSP	gene specific primer
GTP	guanosine triphosphate
GWA	genome-wide association
HGMD	Human Gene Mutation Database, Cardiff, UK, http://www.hgmd.cf.ac.uk
HRA	Heidelberg retinal angiograph
HRM	high resolution melting
HRR	Hardy-Rand-Rittler
Hz	herz
IPTG	isopropyl-*β*-D-thiogalactoside
IS/OS	inner and outer segment
ISCEV	International Society for Clinical Electrophysiology of Vision
Kv	voltage-gated potassium channel
LCA	Leber congenital amaurosis
LDL	low-density lipoprotein
LOD	logarithm of odds
logMAR	logarithm of the minimum angle of resolution units
M	molar
m	meter
MLPA	multiplex ligation-dependant probe amplification
MEH	Moorfields Eye Hospital, London, UK
mRNA	messenger RNA
NCBI	National Centre for Biotechnology Information
OCT	optical coherence tomography
OD	right eye
OLM	outer limiting membrane
OS	left eye
pERG	pattern electroretinogram
PCR	polymerase chain reaction
PLA_2	phospholipase A_2
PLP	pyridoxal phosphate
PolyPhen	polymorphism phenotyping
POD	probably damaging

POS	possibly damaging
PRD	proline rich domain
psi	pound per square inch
PSIC	position-specific independent counts
RACE	rapid amplification of 5' and 3' cDNA ends
RFLP	restriction fragment length polymorphism
RNA	ribonucleic acid
RP	retinitis pigmentosa
RPE	retinal pigment epithelium
rpm	revolutions per minute
rRNA	ribosomal ribonucleic acid
RT PCR	reverse transcription polymerase chain reaction
SD OCT	spectral domain optical coherence tomography (also known as Fourier domain optical coherence tomography)
SIFT	sorting intolerant from tolerant
SNP	single nucleotide polymorphism
SOC	super optimal broth with catabolite repression
SQL	structured query language
TBE	tris-borate-EDTA
U	unit of enzyme
UV	ultraviolet
V	volt
v/v	volume in volume
VEP	visual evoked potentials
w/v	weight in volume

MAGNITUDES

n	nano
µ	micro
m	milli
k	kilo

1 INTRODUCTION

1.1 Genetics

1.1.1 A Brief History of Genes and Linkage

1.1.1.1 Chromosomes carry genes

The term “gene” along with the terms “genotype” and “phenotype”, were introduced by the Danish plant physiologist and geneticist Wilhelm Johannsen in 1909 [1-2]. Johannsen was born in Copenhagen in 1857, two years before the publication of *the Origin of Species* and a decade before *The Variation of Animals and Plants under Domestication*, Darwin’s first attempt to explain heredity. In the concluding remarks of this book, Darwin proposed that organisms throw off tiny particles which he called gemmules introducing his theory of pangenesis [3]. Meanwhile, in St Thomas's Abbey in Brno, Gregor Mendel has started cultivating and testing pea plants (*Pisum sativum*) [4]. Mendel published the results of his over 10-year long experiment in 1866, implicating the existence of genes and laying the foundation of genetics [5], a discipline to be baptised 40 years later in a personal letter dated April 18, 1905 by the British geneticist William Bateson [6-7].

Despite the fact that Darwin had put heredity at the heart of his theory of evolution, Mendel’s work had little impact and was referenced only four times before 1900 [2]. The birth of classical modern genetics is usually dated at 1900 when Hugo de Vries in Holland [8-9], Erich von Tschermak in Austria [10] and Carl Correns in Germany [11] rediscovered the laws of heredity. De Vries also coined the term “mutation” as the driving force of evolution [12-13] and the term “pangens” as "the smallest particles, of which each represents one hereditary characteristic” [14]. This term was abbreviated to “genes” two decades later in Wilhelm Johannsen’s book *Elemente der exakten*

Erblichkeitslehre [1]. In the same book a conceptual distinction between genotype and phenotype, the foundation stones of genetics, is drawn and the basic principles of the statistical analysis, which is essential to render genetics an exact and quantitative science, are laid out [15-16].

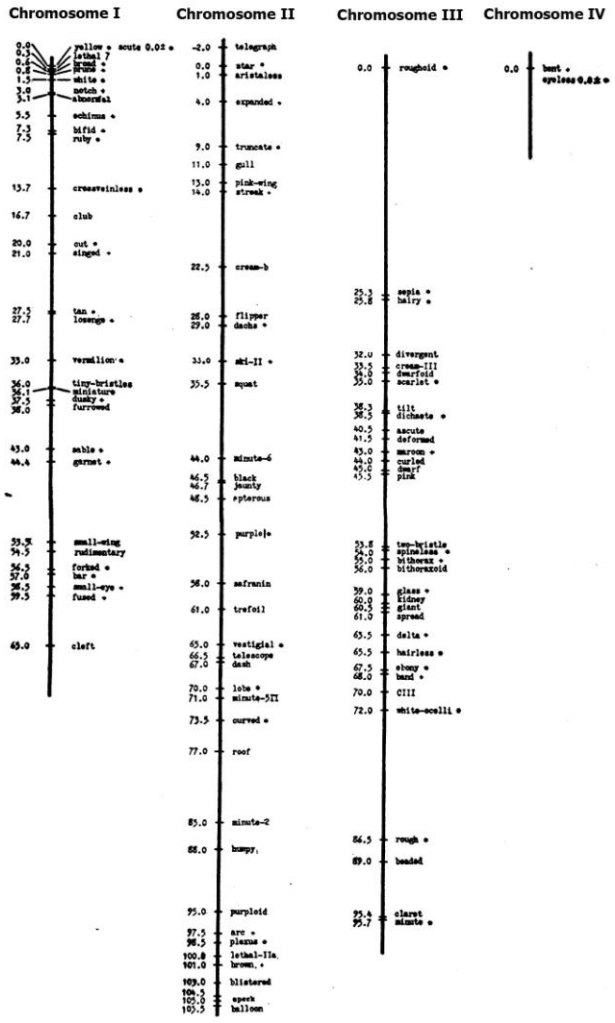

Figure 1-1. Genetic map published in 1921 from Morgan's laboratory showing the distribution of mutant loci in the four chromosomes of *Drosophila melanogaster* [17].

At around the same time, Thomas Morgan, an American embryologist, turned from Mendel's plants to the study of animals, particularly the fruit fly (*Drosophila melanogaster*), soon to become a major model organism in genetics. The initial purpose of his study was to find an occasional fly that had undergone a "mutation" (defined as a sudden change in body form) [18]. This phenomenon had been previously described in plants by de Vries [12]. In 1910, after two years of breeding, a spontaneous mutation occurred with Morgan noticing a white-eyed mutant male among the red-eyed wild-types and naming the mutated gene "white". Further experiments and observations proved that each character resides on a particular chromosome with "white" being carried with the sex chromosome [19-20]. This findings confirmed and elaborated the, independently developed in 1902 by Boveri [21-22] and Sutton [23], chromosomal theory of heredity with Morgan proposing that "each chromosome contains a collection of small units called genes" [24]. In the same paper and in more detail in his seminal book *The Mechanism of Mendelian Heredity* [25], after the study of over a hundred

mutant Drosophila characters and their interactions, Morgan and his colleagues inferred the process of chromosome recombination and hypothesised the phenomenon of crossing over, soon to be elaborated in a thesis by Muller [26]. They proposed that the frequency of a recombination event between two genes is associated with their distance on the chromosome. This led Alfred Sturtevant, Morgan's student, to develop the first genetic maps [27-28]. Haldane, in 1919 introduced the centiMorgan as a unit for measuring the distance between genes on a chromosome [29].

Fifty years after Mendel's discovery, the abstract idea of hypothetical factors was shaped into the physical reality of specific genes residing at specific locations along a chromosome. During the following years, by correlating cytological observations of chromosomes under the binocular microscope [30-31] with breeding results, the role of genes and chromosomes in inheritance would be firmly established [32].

It was a matter of time until Beadle and Tatum would discover in 1941 that enzymes are encoded by genes, linking genetics and biochemistry [33-35] and Avery, MacLeod and McCarty would demonstrate in 1944 genes to be the chemical substance DNA, revealing it as the genetic material [36-37].

1.1.1.2 Genes can be linked

Another important contribution of Morgan’s group was the expansion of the understanding of gene linkage, the tendency of certain characters to be inherited together breaking Mendel’s law of independent assortment. The term “linkage” in the sense that it is used today is attributed to Morgan and Lynch and their phrase: “the linkage of two factors in Drosophila that are not sex-linked” [38-39].

The first report of linkage was by Correns in 1900. It was a case of complete linkage, without recombination, between the characters of flower colour and leaf type in stocks [11]. Incomplete linkage (with demonstrated recombination)

was first reported in 1905 by Punnett and Bateson in sweet pea for the characters of flower colour and grain shape with the authors concluding that: "'there is, therefore, some coupling of pollen-shape and colours" [2, 40]. In man, linkage was first implied in 1911 for colour-blindness gene and the X chromosome [41] although this "peculiar mode of inheritance had of course long been noted (and from 1820 sometimes called Nasse's Law after C.F. Nasse who studied the inheritance pattern of haemophilia)" [39]. The first successful attempt to explain linkage, was by Lock in 1906, a few years before Morgan and Sturtevant set up their "fly room" [2, 42]. After the observation and explanation of linked traits, the next challenge was the quantification and statistical estimation of linkage (recombination fraction). According to Edwards, "in 1914 the first statistical estimate proper was made by Yule & Engledow" but "unfortunately this path-breaking paper (...) has never entered the linkage-estimation literature, which is commonly taken to start with Haldane (1919), who did not refer to it" [43]. Indeed Engledow and Yule's paper introduces the method of minimum x^2 and has only been referenced once before Edwards' paper [44-45]. Linkage estimation literature was enriched with the contribution of Muller [26], Haldane [29, 46] and Fisher; notably, the latter introduced the method of maximum likelihood, opening a new era in linkage analysis [47].

By 1930, the statistical problems of recombination fraction estimation in experimental organisms have been solved and linkage estimation in humans, where mating cannot be arranged as we wish and loci are scattered across 23 chromosomes, was the question.

A major problem was that disease-disease mapping was hard or even not possible in humans. The development of human genetic markers provided the solution and made disease-marker mapping feasible. Marker genetic maps, prerequisite for the latter, had been constructed and evolved from the approximately 20 blood group markers (1910-1960) to the over 40 million SNPs of the NCBI dbSNP Build 135.

Table 1-1. Development of human linkage analysis between loci over the 20th century

y-score	First analysis of linkage in human	Bernstein (1931)
Sib-Pair Method	First autosomal human linkage between Lewis and Lutheran blood groups [48]	Penrose (1935)
Maximum Likelihood Method	First ad hoc method; accurate estimate of recombination fraction (θ) between protan and haemophilia loci [49-51]	Fisher (1922), Bell and Haldane (1937), Smith and Haldane (1947)
μ-score	Link between y-score and z-score	Fisher (1935)
LOD score (Z-score)	Most efficient statistic way of evaluating pedigrees for linkage. Formulae for $Z(\theta)$ described [52]	Morton (1955)
Peeling methods	Fast and exact calculation of LOD score in large pedigrees for few markers [53]	Elston and Stewart (1971)
	Calculation of LOD score for simultaneous study of any number of loci provided not too large a pedigree [54]	Lander and Green (1987)

With the increasing availability of genetic markers and the main methodological and statistical problems worked out (mainly by Morton [55]; table 1-1) attention started to shift towards the computational challenges. In 1958, Simpson described a computer program written for the Elliott 401 at Rothamsted (Harpenden, UK) [56], making the first attempt to compute recombination fraction (θ) using a computer (flow diagram of calculation is presented in figure 1-2) [49]. The Elston-Stewart algorithm, developed in 1971 [53], is the basis for programs performing linkage analysis such as LIPED [57], LINKAGE [58] and VITESSE [59], while the 1987 Lander-Green algorithm is implemented in GENEHUNTER [60-61], ALLEGRO [62] and MERLIN [63].

Linkage analysis has had a pivotal role in the evolution of genetics. Since first conceived in Drosophila by Sturtevant in 1913 [28], it has been extensively used to elucidate biological processes underlying heritable traits. Its tremendous impact on human genetics is discussed in the next pages.

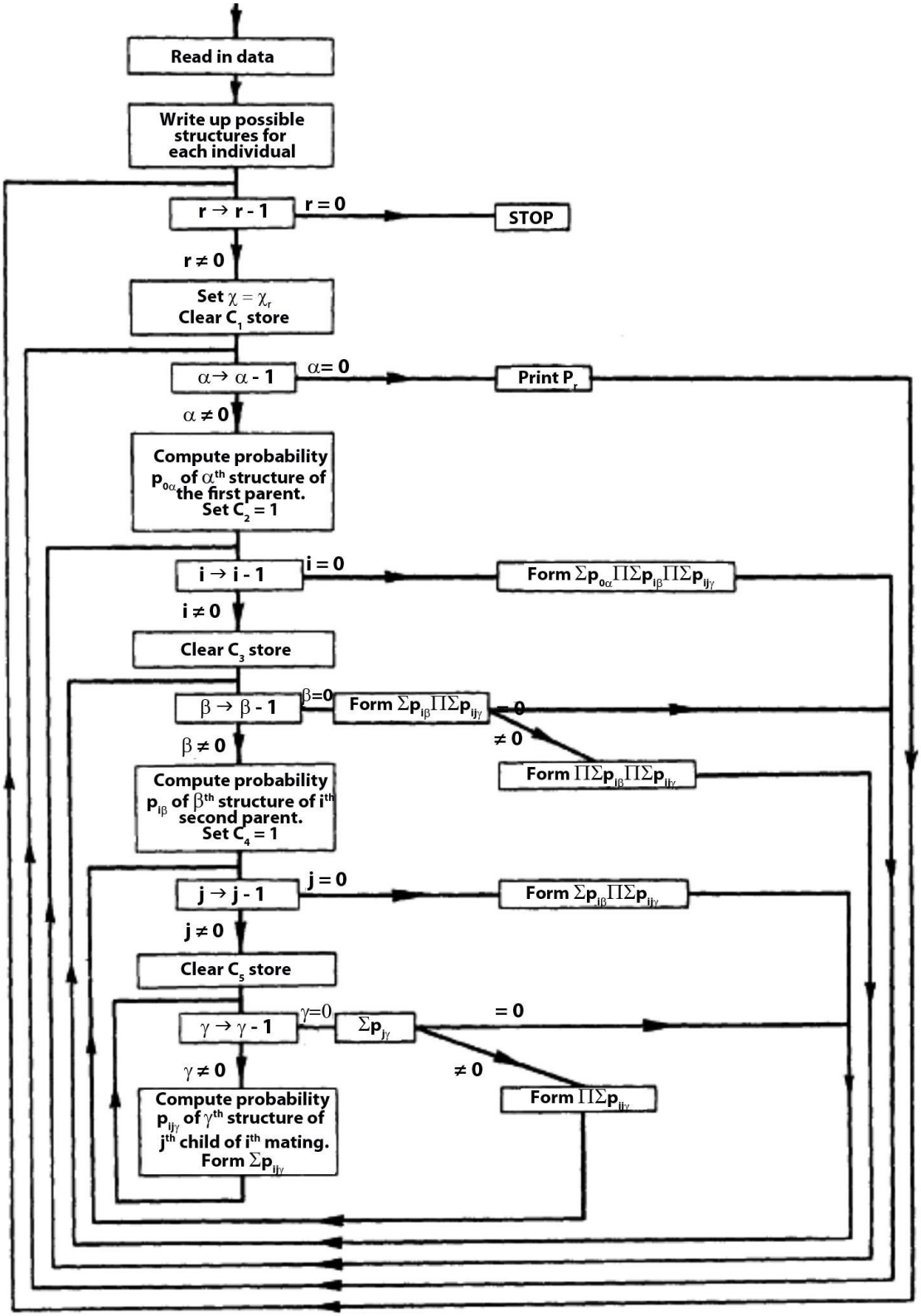

Figure 1-2. Flow diagram of calculations performed in Simpson's first computer program for linkage analysis (modified from [56]).

1.1.1.3 Linkage analysis

Genetic mapping allows localisation of genes associated with phenotypes by demonstrating co-segregation of the trait locus with genetic markers, without the need for prior hypotheses about biological function [64]. Linkage analysis, the simplest form of genetic mapping, uses observations of related individuals to map loci [65-66]. Despite having merits for the identification of genes underlying complex traits, it has been predominantly used to genetically dissect Mendelian disorders; these are characters in which a particular genotype is both necessary and sufficient for the disease phenotype to be expressed.

1.1.1.3.1 Human genetic mapping of Mendelian characters

Although many conditions have been considered by the medical profession since ancient times to be influenced by heredity, it was after the rediscovery of Mendel's laws when physicians started to propose the mode of inheritance for human disease; this was the necessary first step in the search for the chromosomal location of trait loci.

Recessive inheritance was initially suggested for alkaptonuria (1902) [67], arguably the first example of human genetic disease [68], and albinism (1903) [69]. In 1906, at a talk before the Neurological Society of London, Bateson would propose dominant inheritance in a family, originally described by Farabee, with bone deformity in fingers and toes as well as in two families with congenital cataract brought to his attention by Nettleship. In the same talk, Bateson would also discuss X-linked red-green colour blindness, in cases again by Nettleship, and haemophilia; these were the first human traits to be mapped to a chromosome [70].

In 1968, Donahue *et al.* reported the "first assignment of a specific gene locus to a specific autosome in man" providing evidence that "the Duffy blood group locus, already believed to be linked to a congenital cataract locus, is close to

this uncoiler element Un, and that all three are probably on chromosome no. 1" [71].

For most of the 20th century, position-independent methods (functional cloning, candidate gene cloning) were employed to identify disease-associated genes and candidates were suggested by knowledge of the underlying biochemical or cell biology defect (phenylketonuria, haemophilia A, sickle cell disease). Nevertheless, to date, the majority of human disease-related genes have been detected through position-dependent methods using genetic mapping.

The breakthrough in genetic mapping came in the 1980s following the advances in recombinant DNA technology that provided a source of polymorphic markers (restriction fragment length polymorphisms or RFLPs). The groundwork was set in a 1980 paper by Botstein *et al*. [72] and by 1983, the first disease-associated genes mapped using RFLP linkage analysis were reported [73-75]. In 1986, three years after the development of PCR, based on genetic linkage data, chromosome walking within a defined region and hybridization with an enriched cDNA probe, Royer-Prokora *et al.* have identified a 379-amino-acid protein as the cause of chronic granulomatous disease [76]. This is considered the first success for the positional cloning scheme of gene identification (reviewed in [77] and [78]). Over the next decades, this approach would play an important role in gene identification both in isolation (as in the case of retinoblastoma [79] and cystic fibrosis [80-82]) or, more often, combined with the candidate gene approach to avoid amplifying the full length of the interval refined by genetic mapping (as in the case of rhodopsin RP [83]).

A quarter of a century after, studies of Mendelian disease utilising linkage analysis have both enhanced our understanding of the molecular pathology of heritable disorders and altered our perception of disease transmission [64]. Some important lessons have emerged including:

(a) The candidate gene approach method of gene identification [84-85] is inadequate; most disease-associated genes were unsuspected on the basis of previous knowledge.

(b) Compartmentalising genetic disorders into “monogenic/Mendelian, simple and rare” and “multifactorial, complex and common” is an oversimplification. The concept of a monogenic disorder in its strict sense was inaccurate and our view of diseases as monogenic has often been a conceptual artefact [86-87]. A greater complexity was revealed (locus heterogeneity, variable expressivity, incomplete penetrance) and important clues to understanding common disease were provided [88-89].
(c) Linkage analysis has led to many notable successes in mapping variants that confer susceptibility to common diseases [65] (*BRCA1* and *BRCA2* genes with breast cancer [90-91], *INS* with diabetes [92], *APOE* with Alzheimer’s disease [93-94]); this was possible mainly through studying rare Mendelian subtypes of such disorders. Nevertheless, linkage studies have low power and resolution for variants of modest effect [95] and can only explain a small proportion of the familial clustering observed in common diseases.
(d) A large number of Mendelian disorders remain for which no disease-related gene has been identified. Furthermore, striking genetic heterogeneity has been observed in several Mendelian conditions and, for many disorders, mutations in previously identified disease-associated genes explain only a fraction of cases. Elucidation of further pathogenic loci calls for the development of alternative strategies and tools [89, 96].

1.1.1.3.2 Present and future of linkage analysis

Over the past few years, linkage analysis has lost its predominance in favour of association or linkage equilibrium association mapping (comparison of frequencies of genetic variants among affected and unaffected individuals) [65]. Although genetic association analysis is based on an old idea (the principle was applied in 1954 to reveal correlation between blood group and peptic ulceration [84]), the tools for reproducible studies on a genome-wide basis only became available over the past decade [97]. GWA studies have detected a large number of genetic variants robustly associated with common human diseases, providing valuable insights into their genetic architecture. However, for any particular complex trait, the identified sequence alterations

explain only a fraction of total genetic variance calculated from family studies; this gap has been termed “missing heritability” [98-99]. The search for this missing heritability has recently led to a renewed interest in family-based methods and linkage analysis (reviewed in [65]).

Despite the profound success of linkage in mapping Mendelian disease, allelic variants underlying fewer than half of all known or suspected Mendelian disorders have been discovered [100-101]; limiting factors include availability of families, reduced penetrance, locus heterogeneity and reduced reproductive fitness [102]. An alternative, more efficient, approach has emerged over the last few years as sequencing complete human genomes is becoming increasingly feasible and affordable [103]. The first demonstration of a method coupling targeted capture with high-throughput sequencing to genetically dissect Mendelian disease in 2009 [102], can be probably regarded as the beginning of a new era in human genetics. This powerful novel approach (exome sequencing, sequencing the protein coding subset of the genome; section 2.4.17) can both identify disease-related variants in circumstances in which conventional approaches would fail and provide a means for accelerating discovery [101]. However, a key challenge has emerged: how to identify disease-causing alleles among the background of nonpathogenic genomic variation and sequencing errors [101, 104]. The use of family-based filtering strategies (linkage approaches) can substantially narrow the genomic search space for candidate causal alleles. In this study, homozygosity mapping [105], a subtype of parametric linkage analysis, combined with either biological candidate gene or exome sequencing has been utilised to identify novel Mendelian retinal disease-associated genes.

1.1.1.4 Genes in pedigrees and populations (quantitative genetics)

Reginald Punnett was a British geneticist who created the Punnett square, a tool used to predict the probability of an offspring having a particular genotype. Moreover, he had a minor role in the formulation of an important principle of population genetics. In 1908, Punnett was asked at a lecture to explain why in

a random-mating population the dominants did not in the course of time drive out the recessives. Punnett could not answer the question and in turn asked the mathematician G.H. Hardy. Out of this conversation came the Hardy-Weinberg law stating that gene frequencies and genotype ratios in a randomly breeding population remain constant from generation to generation [106-108]. Wilhelm Weinberg a German geneticist and physician, reached and published the same conclusion simultaneously [109].

During the first two decades of the 20th century a huge debate raged around the relevance of Mendelism to evolution. In the *Stanford Encyclopedia of Philosophy* we read that: “many of the early Mendelians did not accept Darwin's ‘gradualist’ account of evolution, believing instead that novel adaptations must arise in a single mutational step” (saltationism); conversely, “many of the early Darwinians did not believe in Mendelian inheritance, often because of the erroneous belief that it was incompatible with the process of evolutionary modification as described by Darwin” (biometric school) [110].

The development of population genetics in the 1920s provided the synthesis between those two schools of thought. In the next few decades, Ronald A Fisher, J.B.S. Haldane and Sewall Wright would weld Mendelism and Darwinism together to create what is known as the “evolutionary synthesis” proving that natural selection was compatible with Mendel’s laws and shifting the level at which evolution works from organisms and individuals (Darwinism) to genes, phenotypes and populations.

It was R.A. Fisher, a British statistician and geneticist who in 1918 first interpreted biostatistic results in accordance with Mendelian inheritance [111]. Part of the Mendelian-Darwinian controversy was due to the belief that discrete inherited factors (genes) did not conform to the Darwinian concept of continuously varying evolution [112]. How could small variations and gradual selective pressure account for the vast differences observed among species? In Fisher’s 1918 paper the question is answered by demonstrating that if a continuous trait is associated with a large number of overall minimally contributing Mendelian factors (genes), then the trait would show an

approximately normal distribution in the population. In the same paper, the term “variance” as the square of the standard deviation, is coined for the first time [111]. In 1922 Fisher introduced a theoretical approach based on the method of maximum likelihood, an important tool for statistical estimation [47]. Finally, Fisher’s 1930 textbook *The Genetical Theory of Natural Selection* brought genetics together with evolution and set the foundations of population genetics [113].

Fisher’s analysis was confirmed and applied to real world paradigms by J.B.S. Haldane, a British biologist and keen experimenter, in his series of papers *A Mathematical Theory of Natural and Artificial Selection* (1924-1934).

Sewall Wright, an American geneticist, conducted pioneering work in quantitative genetics, animal breeding and path analysis. In the 1921 series on *Systems of Mating* Wright defined inbreeding coefficient and explored the methods to compute it in pedigrees and populations [114-119]. This work had a major and lasting effect on the theory and application of genetics.

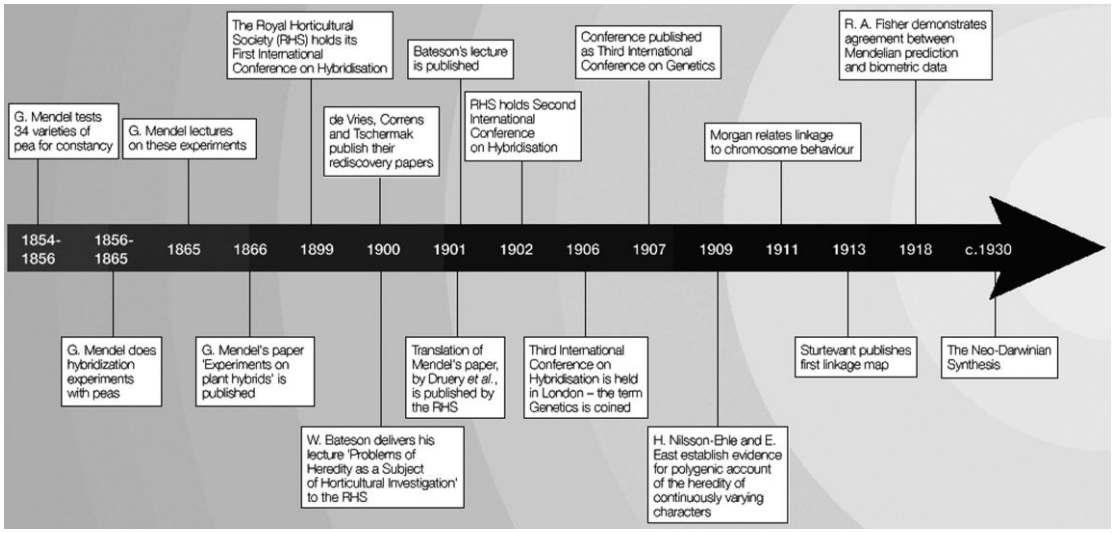

Figure 1-3. History of early Mendelian genetics (modified from [120]).

1.1.2 Molecular Medicine: from Phenotype to Genomic Variation

Understanding the relationship between genotype and phenotype is a central task for biology and medicine. This can be split into two main goals: elucidating the genetic basis of human phenotypes (disease to genes) and computing the Bayesian predictive power of a genotype (genes to disease). This thesis focused on genetic mapping, whose primary value is “not risk prediction but providing novel insights about mechanisms of disease” [64]. A prerequisite to this is the precise delineation of variants and alleles associated with hereditary disorders.

1.1.2.1 Hereditary disease

Hereditary diseases are characterised by familial aggregation, *i.e.* tendency of relatives to be more phenotypically similar than unrelated individuals. Importantly, familial aggregation does not *a priori* suggest genetic involvement as environmental factors may be partially or wholly explanatory [121]. Understanding phenotypic clustering within families is the first step in determining whether and to what extent a genetic aetiology exists for a specific trait. Trying to address this issue, Sewall Wright and R.A. Fisher introduced the concept of heritability, a term used to describe the proportion of phenotypic variance in a population that is due to genetic variation [122-123]. Although essentially a population parameter, heritability significantly determines statistical power in genetic mapping studies and holds a key role within the gene discovery hierarchy (figure 1-4). Once a strong correlation between phenotype and genotype is established (large heritability), subsequent segregation and DNA analysis can be undertaken to elucidate the underlying genetic component [121].

Hereditary disorders are often viewed as either Mendelian or multifactorial. This traditional distinction is most of the time blurred although purely Mendelian traits have been identified. Despite the main genetic contribution to morbidity and mortality being through the genetic component of common

multifactorial disease, Mendelian disorders are the focus of this thesis. Five basic Mendelian pedigree patterns are observed: autosomal dominant, autosomal recessive, X-linked recessive, X-linked dominant and Y-linked. These patterns are subject to basic complications including nonpenetrance (*e.g.* RP [124]), pseudodominant inheritance (*e.g.* Stargardt disease [125]), variable expressivity (*e.g.* FEVR [126]), anticipation and uniparental isodisomy (*e.g.* LCA/RP [127]). Some atypical modes of inheritance that can be viewed as an expansion of Mendelian concepts include mitochondrial (*e.g.* Leber hereditary optic neuropathy [128]) and digenic (*e.g.* RP [129]) [130].

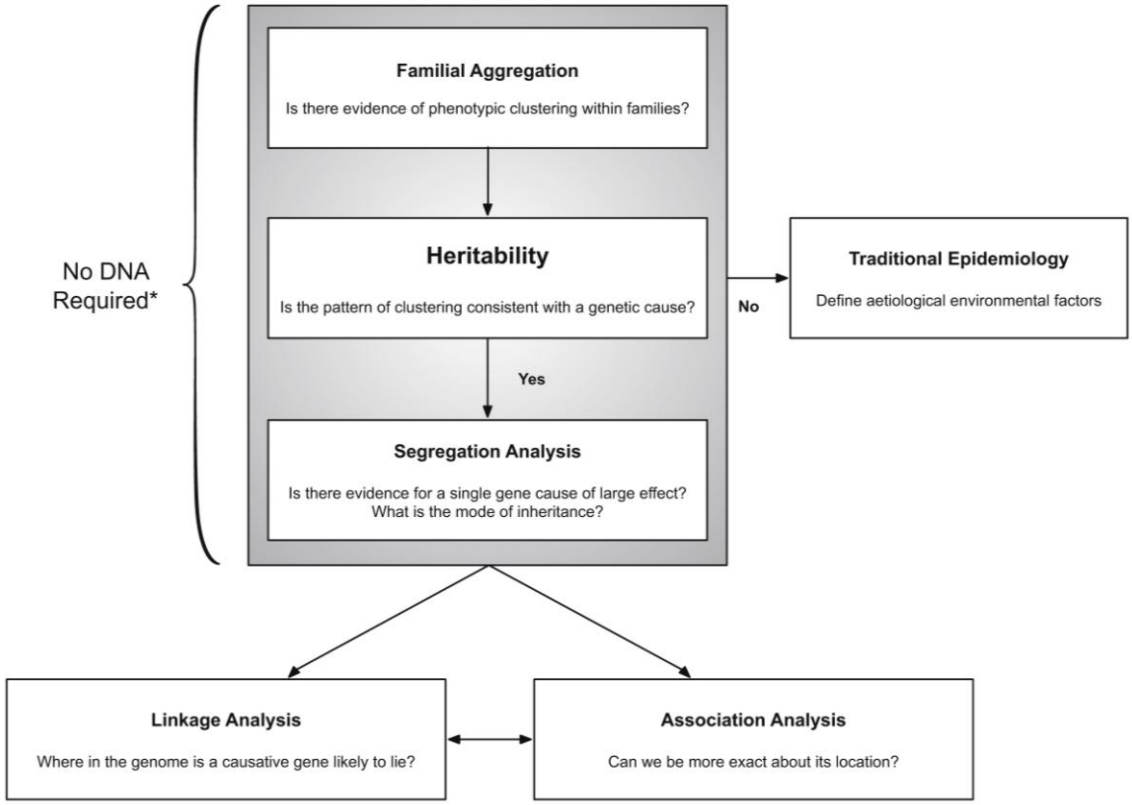

Figure 1-4. Flowchart illustrating the role of heritability within the gene discovery framework [121].

This study is detailing retinal disease exhibiting known or suspected autosomal recessive inheritance. It is noteworthy that one to one genotype-phenotype correspondence is the exception rather than the rule in these disorders. This is mainly due to three types of heterogeneity: locus heterogeneity (*e.g.* complete CSNB, sections 3.1.6 and 3.2.3), allelic heterogeneity (*e.g.* gyrate atrophy, section 3.1.7) and clinical heterogeneity (*e.g. SAG* retinopathy, section 3.1.3).

1.1.2.2 Human genomic variation

Inherited information regarding disease risk, anthropometric characteristics and response to environment can be associated with several, often interacting, mechanisms; these include genetic, epigenetic, ecological and cultural inheritance as well as parental effects [131]. Despite increasing awareness that nongenetic information can be inherited, genetic variation is still considered to be responsible for nearly all the heritable aspects of human individuality. Human genetic variation is common (on average two copies of the human genome are expected to differ by 0.5% of the DNA sequence [132]) and occurs on many different scales, ranging from gross karyotype alterations to single nucleotide changes [133]. While most sequence alterations exert no direct effect on phenotype or gene/protein function, a subset of them has functional consequences (ranging from beneficial to highly deleterious). Consequently, an individual may carry alleles that produce no product (null), reduced amount or activity of product (hypomorphic), increased amount or activity of product (hypermorphic), a novel activity or product (neomorphic) or an antagonistic to the normal protein activity or product (antimorphic) [134]. Variants that form such alleles often cause or predispose to disease and pinpointing them among the background of nonpathogenic variation is the ultimate goal of genetic mapping.

With the advent of high-throughput sequencing, whittling down a list of candidate variants to those that are causal became increasingly challenging, so that currently, the main obstacle is interpretation rather than data collection [104]. This interpretation challenge is in fact a multiple hypothesis testing problem with the prior probability of any given genetic variation being causal, tending to zero. A number of approaches, computational or experimental (summarised in [104]), can be utilised to more accurately estimate this prior probability. Genetic mapping can significantly contribute to this Bayesian predictive model (*a priori* or *a posteriori*) despite both linkage analysis and GWA studies often being insufficiently powered to solely delineate phenotypically important genetic variation.

In Mendelian autosomal recessive disorders, the allelic spectrum of loci tends to be moderately diverse [135] and disease-causing variants tend to be rare and highly penetrant; thus amenable to linkage analysis. However, presumed recessive disease in a number of phenotypes characterised by simplex cases could result from inheriting a *de novo* autosomal dominant or X-linked germline mutation [136] or be caused by a "total mutational load" (epistasis [137]) rather than straightforward autosomal recessive alleles.

1.1.3 Hereditary Disease and the Eye

Looking back at the century passed after the assignment of colour blindness to the X chromosome [41, 70, 138], the pivotal role of ophthalmology and retinal disease in the evolution of human genetics is omnipresent (see [139] and figure 1-5 for a timeline of historic discoveries). The main reason is that both structural defects and functional abnormalities related to the eye, the most important of the sense organs, have been well documented over the centuries from the Pre-Hippocrates and Galen to Dalton, Cuniers and Stargardt. Therefore, the hereditary nature of many eye conditions was brought to the attention of geneticists from the early days (as the above mentioned collaboration between Nettleship and Bateson in 1906).

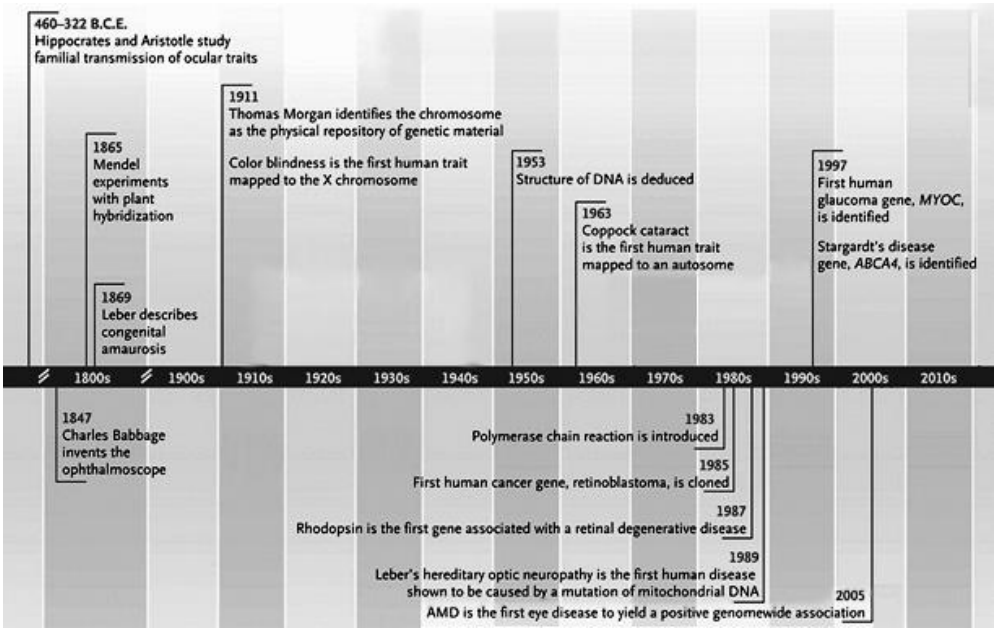

Figure 1-5. Timeline of landmarks in ophthalmic genetics (modified from [140]).

1.2 The Retina

"If you are going to study how the brain works, it is a good idea to start with the simplest part."

Jeremy Nathans

The retina is the most accessible part of the central nervous system and can be characterised as an outpost of the brain. It is the first level of vision and a major source of sensory input.

The term retina comes indirectly from Greek through Latin and Arabic, to Medieval Latin réte, meaning net [141]. It was introduced by Galen to describe the mesh of blood vessels at the back of the eye. The modern retina is defined as the innermost layer of the eye that captures the light and converts it into a neural response. It is derived from the neuroectoderm (optic cup) and is composed of two laminar structures: an outer RPE and an inner neurosensory retina. The central region of highest visual acuity is known as the fovea.

1.2.1 The Retinal Pigment Epithelium

The RPE consists of a single layer of hexagonal melanin-containing epithelial cells. Like the whole retina, the RPE exhibits regional differences with its diameter varying from 10 to 60 μm (taller and thinner in the fovea) and its cell density decreasing from the fovea to the periphery [142]. Like other epithelial cells, the RPE is polarised. The basal end is folded and attached to a basal lamina that forms the inner layer of Bruch's membrane of the choroid. The apical region has multiple villous processes, 5 to 7 μm long, that are embedded in a glycosaminoglycan matrix (interphotoreceptor matrix) and surround the photoreceptor outer segments. These microvilli increase the photoreceptor-RPE surface of contact, optimizing metabolic efficiency. Adjacent RPE cell membranes are firmly attached to each other in the basal region by the zonula adherens and in the apical region by the zonula occludens. These intercellular junctional complexes provide structural stability

and maintain a selective blood-retinal barrier.

The RPE nuclei occupy the basal aspect of the cytoplasm, whereas the apical part and microvilli contain numerous melanin granules (figure 1-6). These granules, called melanosomes, are synthesised *in utero* and remain virtually unchanged thereafter [143]. This is not the case with the other main class of pigment found in the RPE, lipofuscin, which accumulates during life [144]. To prevent the toxic effects of accumulated photooxidative products, photoreceptor cells undergo a daily renewal process wherein ~10% of their volume is shed and subsequently phagocytosed by RPE cells. Lipofuscin granules are the products of incomplete lysosomal activity on the phagosomes containing phagocytosed photoreceptor outer segment debris [145]. Lipofuscin is a heterogeneous material containing a mixture of different compounds, predominantly byproducts of light-related vitamin A cycling [146]. These compounds contain an extended system of conjugated double bonds that allow the absorption of light with subsequent emission of fluorescence; therefore, *in vivo* visualization with fluorescence microscopy is enabled. The excitation wavelength ranges from 300 to 600 nm and the emission spectrum from 480 to 800 nm (maximum around 620 nm) [147].

The RPE has numerous functions. These include absorption of light energy focused by the lens onto the retina (reduction of scatter), bidirectional transport of metabolites between photoreceptors and the choriocapillaris, phagocytosis of shed photoreceptor membranes and uptake, storage and metabolism of vitamin A [148].

Many RPE expressed genes are involved in retinoid metabolism, ion transport or extracellular matrix maintenance and, when mutated, lead to retinal dystrophies. For example, mutations in the RPE genes encoding 11-*cis* retinol dehydrogenase (*RDH5*) and retinaldehyde-binding protein (*RLPB1*), both essential components in rhodopsin regeneration, cause autosomal recessive retinal disease [149-150]. Importantly, retinal disease due to mutation in the RPE expressed gene *RPE65* has been shown to respond to gene-replacement therapy in patients [151-153].

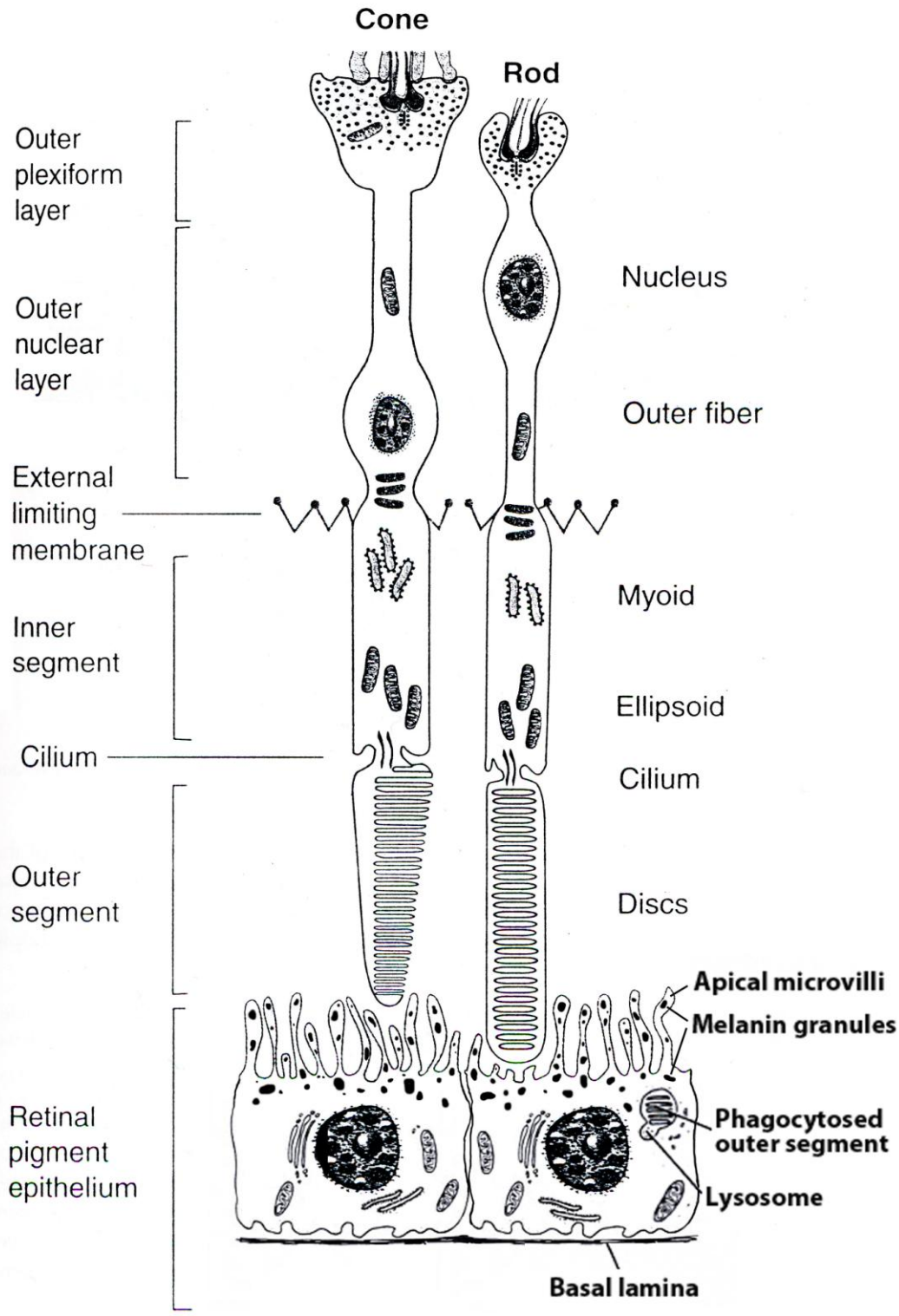

Figure 1-6. Sensory retina and RPE.

1.2.2 The Neurosensory Retina

The neurosensory retina is a laminated structure composed of mainly neuronal but also glial and vascular elements, ranging in thickness from 100 µm (ora serata) to 400 µm (near the optic disc). Six major neuronal cell classes that can be further divided into many subtypes for a total of over 60 different neurons are found in this highly specialised tissue.

Three zones of clustered nuclei separated by two layers called the plexiform or synaptic layers can be seen in an unstained vertical section.

Table 1-2. Major neuronal cell types in the human retina [141, 154]

Cell classes	Characteristic Cell Types	Number
Photoreceptors	Rod; L-cone; M-cone; S-cone	4
Bipolar cells	Diffuse (ON-OFF); midget (ON-OFF) ; S-cone; giant	13
Horizontal cells	HI; HII	2
Ganglion cells	Parasol (on-off); midget (on-off); small bistratified; biplexiform; photosensitive; projecting to the LGN	>20
Amacrine cells	A2, AII, A8, A13, A17, A18, A19, A20, A22, starburst	~30
Interplexiform cells		

The neurosensory retina can be divided into an outer photoreceptive, glutamatergic sensory retina where phototransduction takes place and an inner neural retina where the first steps of visual processing are carried out.

1.2.2.1 The Sensory Retina

The sensory retina contains rod and cone photoreceptors, long, narrow cells whose names describe the shape of their free ends (figure 1-6). Each photoreceptor cell consists of an outer and an inner segment connected through a nonmotile “9+0” primary cilium (connecting cilium), a cell body (nucleus) and a synaptic terminal. The outer segment contains multiple laminated lipid bilayer discs and envelops the visual pigments responsible for

photon absorption. Rod outer segments are made up of a stack of discrete discs unattached to the ciliary plasma membrane, whereas cone outer segments differ by having a series of invaginations continuously connected to the membrane. The connecting cilium originates from the inner segment basal body. In addition to its structural role, it plays a critical role in molecular transport; it transfers disc membrane lipids and phototransduction proteins to the outer segment that is incapable of protein synthesis. The inner segment, in which the protein synthesis occurs, consists of the ellipsoid (outer part) and the myoid (inner part). The ellipsoid contains the basal body and mitochondria and the myoid the endoplasmatic reticulum, ribosomes and a Golgi apparatus. The myoid is continuous with the main cell body. The innermost part of the photoreceptor contains the synaptic terminal. The rod synaptic terminal is termed a spherule and is formed by a single invagination that accommodates two horizontal cell processes and one ON bipolar cell dendrite. The cone synaptic terminals, the pedicles, are located inner to the rod spherules, are larger and contain a number of invaginations. Each invagination contains the processes of two horizontal cells and the processes of two or more ON bipolar cells. Additionally, mainly OFF, bipolar cell processes lie near the invaginations. Just posteriorly to each spherule or pedicle invagination lays a synaptic ribbon, a structure allowing photoreceptors to sustain continuous release of synaptic vesicles.

The human retina possesses a single rod type and three cone types (L-, M- and S-cones). Rods account for 95% of all photoreceptors and are exquisitely sensitive to light but have a low photon saturation threshold. They function optimally in low light settings and are sensitive to contrast, brightness and motion. Cones account for 5% of photoreceptors, have a high saturation threshold, a fast photoresponse but relatively low sensitivity. The different types of cones provide high acuity and discern colour differences. Colour vision is based on differences in the photon catch rate of the three different cone types. Maximum sensitivity and absorbance for S-cones is 420 nm, for L-cones 534 nm and for M-cones 564 nm; for rods it is 498 nm [141, 155].

Cone and rod photoreceptor density varies throughout the retina. The

periphery is rod-dominated whereas the macula contains a cone-dominated fovea surrounded by a parafoveal ring at 5 mm containing maximum rod spatial density [156].

Photoreceptors convert the energy of absorbed photons to an electrical neural signal, the receptor potential. This is achieved by opsins, cell membrane proteins that bind a light absorbing chromophore. The chromophore, 11-*cis* retinal, is a derivative of *β*-carotene, a vitamin A analogue entirely derived from the diet. Light transforms 11-*cis* retinal to its isomer all-*trans* retinal, changing the opsin to its catalytically active form; consequently, the exchange of GTP to GDP on a membrane bound G-protein (transducin) is catalysed. Subsequently, one of the activated transducin subunits binds to and activates a phosphodiesterase. Through a number of intermediate steps, the photoreceptor membrane hyperpolarises. This, following the general rule for all neurons in all species, leads to a decrease in the rate of neurotransmitter (glutamate) release at the photoreceptor terminal synapse. Numerous proteins are involved in photoactivation and photorecovery in cone and rod photoreceptors with mutations in the genes encoding them often leading to retinal disease (table 1-3).

1.2.2.2 The Neural Retina

The neural retina includes an inner nuclear layer containing the cell bodies of horizontal, bipolar and amacrine cells and a ganglion cell layer containing ganglion cells and displaced amacrine cells. In the neural retina, signals from the rods and cones undergo complex processing. The output takes the form of action potentials in ganglion cells whose axons converge at the optic nerve.

The most direct pathway from the photoreceptors to ganglion cells is through bipolar cells (vertical pathway). All types of bipolar cells respond to changes in photoreceptor glutamate release rate by forming graded potentials. However, different bipolar types express different glutamate receptors at subsynaptic sites and can react to a certain stimulus either by hyperpolarizing or

depolarizing their plasma membranes. These different, glutamate-gated, bipolar cell responses are associated with expression of either ionotropic (sign-conserving; OFF bipolar cells) or metabotropic (sign-inverting; ON bipolar cells) glutamate receptors on bipolar cell dendrites. Importantly, mutations in the ON bipolar metabotropic glutamate receptor (mGluR6) cause CSNB [157]. The full mGluR6 cascade has not been resolved.

Ganglion cells form the innermost nuclear layer and are the final output neurons of the human retina. There are over 20 distinct types of ganglion cells, all firing action potentials (sign-conserving to glutamate). Each type carries different channel of visual information and specialises for coding some particular aspect of the visual world (contrast, colour, movement and others). Ganglion cell axons are partially myelinated with the myelinated parts being outside the eye.

1.2.3 Non-neuronal Elements

In addition to the three major classes of neurons, the retina is also populated by three types of glia: Müller cells, microglia, and astrocytes. Müller cells are the predominant retinal glial cells. Their cell bodies are located in the inner nuclear layer, extending vertically and their processes form the outer and the inner limiting membrane. Other processes of the Müller cells make extensive contacts with the basal lamina of the retinal blood vessels. These vessels contain nonfenestrated endothelial cells whose tight junctions maintain the inner blood-retinal barrier. A basal lamina covers the outer surface of the endothelium and is covered by an interrupted layer of pericytes surrounded by their basement membrane. Astrocytes provide many of the same functions as Müller glia, but are restricted almost entirely to the nerve fiber layer of the retina. Unlike astrocytes and Müller cells, the third glial subtype, microglia, may arise from myeloid tissue. Microglia play a central role in the elimination of neuronal debris and in the initiation of immunological signaling through the release of chemokines, cytokines or neurotoxic factors [158].

1.3 Inherited Retinal Disease

The term inherited retinal disease denotes a group of genetically determined conditions that differ from one another in mode of inheritance, pattern of visual loss and fundus appearance. Most of these conditions share an important feature: the loss or dysfunction of photoreceptor cells as a primary or secondary event [159]. Both clinical and genetic heterogeneity is observed; over 170 genes have been implicated and at least another 40 chromosomal loci have been determined (RetNet; figure 1-7). Notably, mutations in genes previously associated with retinal degenerations explain the disease in only a fraction of patients [160]. Due to the complicated and intricate structure and function of the retina, an even higher degree of genetic heterogeneity is expected with more genes remaining to be identified.

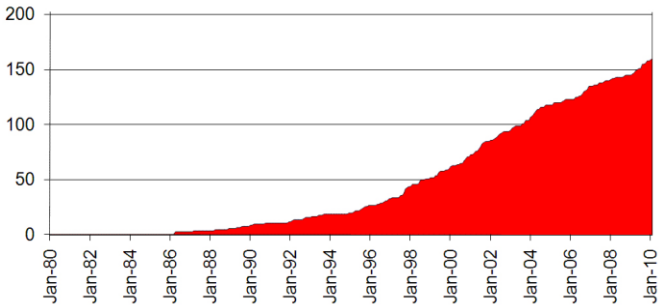

Figure 1-7. Number of genes associated with retinal disease over time (modified from www.sph.uth.tmc.edu/retnet/).

In the past, retinal dystrophies have been diagnosed and subdivided into several groups on the basis of clinical features (*e.g.* RP, Stargardt disease). It is clear, however, that entities like RP are sole clinical manifestations of many genetically determined disorders. In the presence of molecular genetic information a more accurate diagnosis and classification is possible (*e.g. ABCA4* retinopathy, rhodopsin RP, ciliopathies). Nevertheless, genetic testing has traditionally been limited by availability, cost and time requirements. With molecular diagnosis unavailable in most cases, age of onset, mode of inheritance and correlation of electrophysiology with retinal morphology are key to the diagnosis and classification of retinal disease.

A brief overview of genes associated with relatively common forms of inherited retinal disease is found in table 1-3.

Table 1-3. Summary of main monogenic inherited retinal disorders

Nonsyndromic inherited retinal disease				
Rod or rod cone dysfunction; RP	Progressive disease	Childhood- or adult-onset	Autosomal recessive	*ABCA4, BEST1, C2ORF71, CDHR1, CERKL, CNGA1, CNGB1, CRB1, DHDDS, EYS, FAM161A, IDH3B, IMPG2, LRAT, MERTK, MFRP, NPHP5, NR2E3, NRL, OAT, PDE6A, PDE6B, PDE6G, PRCD, PROM1, RBP3, RBP4, RDH12, RGR, RHO, RLBP1, RP1, RPE65, SAG, SPATA7, TTC8, TULP1, USH2A*
			Autosomal dominant	*CA4, CRB1, CRX, FSCN2, GUCA1B, IMPDH1, KLHL7, NR2E3, NRL, PRPF3, PRPF6, PRPF8, PRPF31, RDH12, RDS, RHO, ROM1, RP1, RP9, RPE65, RGR, SEMA4A, SNRNP200, TEAD1, TOPORS*
			X-linked	*REP1, RP2, RPGR, RS1*
		Infantile-onset; LCA	Autosomal recessive	*AIPL1, CABP4, CEP290, CRB1, CRX, GUCY2D, IQCB1, KCNJ13, LCA5, LRAT, RD3, RDH12, RPE65, RPGRIP1, SPATA7, TULP1*
			Autosomal dominant	*CRX, IMPDH1, OTX2*
	Stationary disease; CSNB	Autosomal recessive	With fundus abnormalities	*RDH5, RHOK, SAG*
			Complete	*GPR179, GRM6, TRPM1*
			Incomplete	*CABP4, CACNA2D4*
			Other (Riggs-like type)	*SLC24A1*
		Autosomal dominant (Riggs or Nougaret type)		*GNAT1, PDE6B, RHO*
		X-linked	Complete	*NYX*
			Incomplete	*CACNA1F*
Maculopathy	Autosomal recessive			*ABCA4, CFH, BEST1*
	Autosomal dominant			*BEST1, C1QTNF5, EFEMP1, ELOVL4, FSCN2, GUCA1A, GUCA1B, GUCY2D, HMCN1, PROM1, RDS, RIMS1, RP1L1, TIMP3*
	X-linked			*RS1, RPGR*
Cone or cone rod dysfunction	Autosomal recessive	Rod monochromacy		*CNGA3, CNGB3, GNAT2, PDE6C, PDE6H*
		Other		*ABCA4, ADAM9, CACNA2D4, C2ORF71, C8ORF37, CDHR1, CERKL, KCNV2, R9AP, RAX2, RGS9, RPGRIP1*
	Autosomal dominant			*AIPL1, CRX, GUCA1A, GUCY2D, OPN1SW, PITPNM3, PROM1, RDS, RIMS1, SEMA4A, UNC119*
	X-linked			*CACNA1F, RPGR, OPN1LW/OPN1MW*
Optic nerve disease	Autosomal recessive			*TMEM126A*
	Autosomal dominant			*OPA1*
	Mitochondrial			*LHON*
FEVR, Norrie disease	Autosomal recessive			*LRP5, TSPAN12*
	Autosomal dominant			*FZD4, LRP5, TSPAN12*
	X-linked			*NDP*
Retinoblastoma	Autosomal dominant germline or somatic			*RB1*
Syndromic inherited retinal disease				
Usher Syndrome	Autosomal recessive			*CDH23, CLRN1, DFNB31, GPR98, MYO7A, PCDH15, USH1C, USH1G, USH2A*
Albinism	Autosomal recessive			*OCA2, SLC45A2, TYR, TYRP1*
	X-linked			*GPR143*
Bardet-Biedl syndrome	Autosomal recessive			*ARL6, BBS1, BBS2, BBS4, BBS5, BBS7, BBS9, BBS10, BBS12, INPP5E, MKKS, MKS1, TRIM32, TTC8*
Other syndromic retinal disease	Autosomal recessive			*ABCC6, AHI1, ALMS1, CC2D2A, CDH3, CEP290, CLN3, CNNM4, COL9A1, INPP5E, INVS, IQCB1, MTTP, NPHP1, NPHP3, NPHP4, OPA3, PANK2, PEX1, PEX7, PHYH, PXMP3, RPGRIP1L, SDCCAG8, TTPA, WFS1*
	Autosomal dominant			*ATXN7, COL11A1, COL2A1, JAG1, KCNJ13, PAX2, TREX1, VCAN*
	X-linked			*OFD1, PGK1, TIMM8A*

1.3.1 Clinical Diagnosis

The invention of the ophthalmoscope by Babbage in 1847 [161] helped ophthalmologists to describe and classify familial forms of retinal disease. Some of the most frequently used terms to characterise genetic conditions of the retina were introduced by ophthalmologists in the 19th century.

Detailed history, visual field and colour vision assessment as well as dilated fundoscopy, with examination including not only the affected individual but also potential carriers and other family members, usually allow a specific nosological entity (*e.g.* RP or Usher syndrome) to be diagnosed. On rare occasions (*e.g.* choroideremia, Best and Sorsby disease, familial dominant drusen), those investigations will point to a specific gene or even a specific mutation.

Thorough structural and functional assessment of the retina can be performed with the use of electrophysiology (section 1.3.2), psychophysics (static and kinetic perimetry), fundus autofluorescence imaging (section 1.3.3.2), OCT (section 1.3.3.3) and fluorescein angiography.

1.3.2 Electrophysiology

Electrophysiology is the gold standard for investigating neuronal signalling. In the early 19th century, Luigi Galvani was the first to discover that the function of the nervous system is intrinsically linked to electrical activity [162]. Changes in the light flux on animal eyes were first reported to produce electrical signals by the Swedish physiologist Frithiof Holmgren in 1865 [163-164]. The first human subject was tested with success by Dewar in 1877 [165]. However, it was the work of Finnish Ragnar Granit and American Haldan K Hartline, two of the three winners of the 1967 Nobel in Medicine, that provided the basis for understanding retinal electrophysiology [166-167].

Electrophysiology is critical to the accurate diagnosis and appropriate

management of individuals with inherited retinal disease. The main tests are the EOG, which assesses the function of the RPE; the full field ERG, which reflects the function of the photoreceptors and inner nuclear layers of the retina; the pERG, which examines the function of the macular photoreceptors and ganglion cells; the VEP which examines the intracranial visual pathways. Other tests include multifocal ERG that spatially evaluates macular function and dark adaptometry that quantitatively determines the kinetics of rod and cone recovery following a bright flash [168]. The ISCEV, has published recommendations and minimum standards relating to the performance of these tests [169-174].

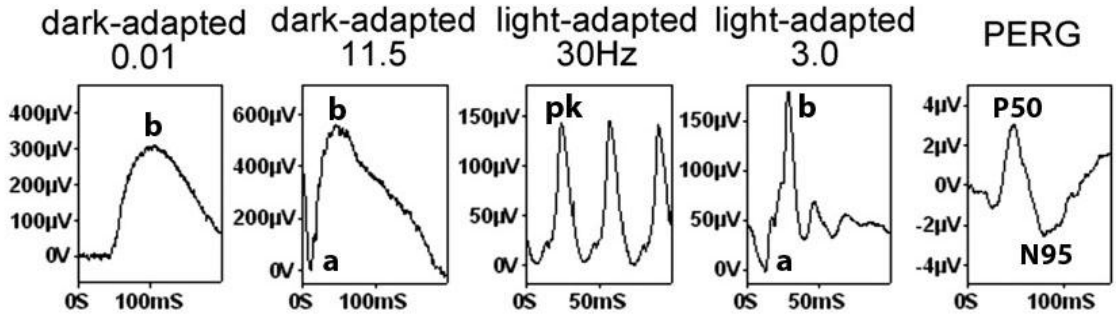

Figure 1-8. Normal examples of ISCEV full field and pERGs. The bright flash was 0.6 log units brighter than the ISCEV standard flash to better demonstrate the a-wave (courtesy of Dr Anthony G Robson).

Some electrophysiological phenotypes are highly suggestive of specific inherited retinal diseases. For example: reduced EOG light rise and normal full field ERGs are usually associated with Best disease; severely reduced light-adapted and preserved dark-adapted ERGs in a young child are commonly associated with rod monochromacy (or other stationary cone dysfunction); undetectable ERGs in a young child imply LCA; electronegative ERG with normal a-wave is associated with X-linked retinoschisis, X-linked or recessive CSNB and some acquired diseases; VEP interhemispheric amplitude/latency difference is a feature of albinism. On two occasions of inherited retinal disease, ERGs can be “pathognomonic”. Those are: cone dystrophy with supernormal rod ERG (*KCNV2* retinopathy) [175-176] and enhanced S-cone syndrome (*NR2E3* retinopathy) [177-178]. The unique ability of electrophysiology to localise dysfunction in the visual system is summarised in table 1-4 [179-180].

Table 1-4. Correlation between electrophysiological findings and visual pathway level of dysfunction

Electrophysiological findings	Site of dysfunction
Abnormal EOG light rise, normal full field ERGs	RPE dysfunction
Abnormal dark-adapted 0.01 ERG b-wave and 11.0 ERG a-wave	Rod photoreceptor dysfunction
Abnormal dark-adapted 0.01 ERG b-wave, normal a-wave and markedly subnormal b-wave in dark-adapted 11.0 ERG (electronegative)	Postreceptoral disease
Normal dark-adapted 11.0 ERG, abnormal light-adapted responses	Cone dysfunction
Normal full field ERG, abnormal pERG P50 or multifocal ERG	Macular dysfunction
Normal full field ERG, preserved pERG P50, abnormal pERG N95	Ganglion cell dysfunction
Normal pERG, abnormal VEP	Optic nerve dysfunction
Asymmetrical VEP, crossed asymmetry	Chiasmal dysfunction or misrouting
Asymmetrical VEP, uncrossed asymmetry	Retrochiasmal dysfunction

1.3.3 Retinal Imaging

It appears that the interior of the human eye was first observed by Purkinje who wrote in his 1823 thesis that when light was thrown back “the whole pupil lit up in a beautiful orange colour” [181-182]. Over the next decades, researchers realised that the observer had to stand in the path of the emerging rays in order to view the fundus. An English mathematician, Charles Babbage solved the problem in 1847 by using a mirror but his prototype ophthalmoscope was rejected by an ophthalmologist and laid aside [183]. Helmholtz is claimed to note that the instrument would have worked if a concave lens of four or five dioptres had been inserted to correct the convergent rays [184]. Hermann von Helmholtz is generally credited with the invention of the ophthalmoscope. His instrument was published in 1851 [185] and he was lucky to see it quickly accepted by prominent ophthalmologists like Donders and von Graefe [186]. Soon there was a flood of publications describing both observations and technical variations of the instrument. In 1852 Christian Theodor Georg Ruete established indirect fundoscopy [187-

188] and in 1911 Allvar Gullstrand, one of the few Ophthalmologists to receive a Nobel prize [189], developed the slit lamp [190]. Fundoscopic appearance of inherited retinal disease was reported early with Ernst Coccius describing RP in 1853 [191]. Since these early days ophthalmic imaging has played an important role in the documentation and diagnosis of inherited retinal disease.

1.3.3.1 Fundus photography

Photography as a practical procedure draws its origin in the 1830s. The challenges of imaging the fundus have been addressed early; the first technique for photographing the retina of a living human subject was proposed in 1886 [192] and the first commercial camera was produced in 1926 by Carl Zeiss Company. Nowadays, the high resolution digital fundus CCD cameras work on the principle of indirect ophthalmoscopy, except that the image is stored as electronic data. They are placed 2 to 3 cm from the subject and image an angle of 30° creating an imaging plane 2.5 times life size [193]. An imaging mode frequently supplementing colour photography is infrared imaging. It enables enhanced detail through poor media and more comfort for the patient (no flash). In inherited retinal disease, retinal photography is widely used to document fundus abnormalities, create illustrations for publication and education and track disease progression through serial photography.

1.3.3.2 Fundus autofluorescence imaging

The first use of a confocal scanning laser ophthalmoscope to produce autofluorescence signal from the retinoid fluorophores in a clinical setting was done in 1995 in the UCL Institute of Ophthalmology, London, UK [194]. Autofluorescent phenomena of the human fundus have been described in the early days of fluorescein angiography, mainly before the injection of the fluorescent dye, and were initially treated as a problem in fluorescein angiogram interpretation [195]. The use of a regular fundus camera posed two important limitations: the low intensity of the emitted autofluorescence and the

significant fluorescence deriving from tissues anterior to the retina, particularly the lens. The first problem was resolved with the use of a scanning laser ophthalmoscope. This device was developed in 1980 [196] and uses a different approach to imaging from the fundus camera: a spatially coherent, low-divergence, narrow beam from a laser rather than irregular cathode ray tube illumination is swept over the retina, delivering its energy to a very small spot for a very short time. Light returned from that spot is detected and decoded to form an image [197-198]. The problem associated with high noise from anterior structures was resolved with the introduction of confocal optics. Confocal imaging mode uses a small aperture size (2 mm) in order to suppress light scattered from layers other than the point of illumination and ensures that reflectance is collected from the same optical plane [199-200]. Several images are recorded, aligned and used to compute a mean image.

One of the few commercially available confocal scanning laser ophthalmoscope devices for fundus autofluorescence imaging is the HRA (Heidelberg Engineering, Heidelberg, Germany). It uses an excitation wavelength of 488 nm and a 500 nm short wavelength cutoff filter. Two different lenses allow 35° or 55° field of view. One limitation is posed by the fact that the mean image's pixel values are normalised; therefore the absolute amount of fundus autofluorescence cannot be assessed.

The concept of using naturally occurring fluorescence to provide an indicator of RPE health makes fundus autofluorescence imaging an invaluable tool for the assessment of retinal dystrophies. It not only discloses information above and beyond those obtained by fundoscopy, but also specific fundus autofluorescence patterns seem to correlate with distinct patterns of dysfunction [201-202]. In short, it facilitates diagnosis and phenotype-genotype correlations and allows more sensitive assessment of disease progression.

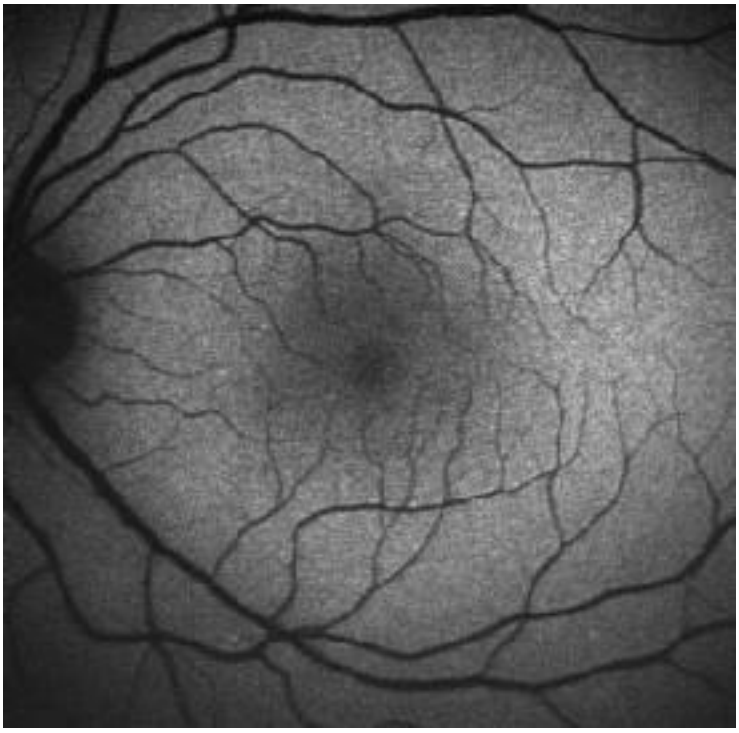

Figure 1-9. Normal fundus autofluorescence image: the optic nerve head typically appears black due to abscence of RPE. At the fovea, autofluorescence is reduced due to absorption mainly from the foveal “blue light filter” (peaking at 460 nm), the macular pigment and secondarily due to increased melanin deposition. The macular pigment (lutein and zeaxanthin) concentration is highest in the prereceptoral axon layer of the fovea and its density can be assessed by subtracting the 514 nm fundus autofluorescence image from the regular 488 nm one. This is a result of the minimal absorpion of over 500 nm wavelengths by macular pigment [203-204].

1.3.3.3 Optical coherence tomography

OCT generates cross sectional or three-dimensional images by measuring time delay and magnitude of backscattered or reflected light [205]. It is analogous to a radar or an ultrasound except that it measures reflectivity to an infrared signal (around 820 nm) rather than radio waves (1 mm to 100 m for radars; FM radio around 3 m, TV around 5 m, AM radio around 400 m) or “higher frequency than normal hearing” sound waves (in air: 0.1 mm to 1.5 mm for diagnostic ultrasound; audible sound wavelengths: 17 mm to 17 m). The optical signal that OCT uses is much shorter in wavelength to ultrasound; therefore, resolution is much higher (one to two orders of magnitude higher than conventional ultrasound) and probe-tissue contact is not necessary.

Two dimensional OCT was developed in 1991 [206] and became fast enough for *in vivo* studies two years later [207]. The first OCT instrument became commercially available in 1995 and over the next 15 years almost all technological OCT parameters have significantly improved. Every imaging modality is characterised by five main technological parameters: axial resolution, transverse (lateral) resolution, measurement (data acquisition) time, detection sensitivity, image penetration depth in tissue and image contrast [205]. Axial resolution, perhaps the most significant parameter of OCT, has reduced from 20 μm [207] to 2 μm [208-209] enabling comprehensive visualisation of the intraretinal morphology. Application of the Fourier transform, a mathematical formula, to signal processing in order to extract the frequency spectrum of a signal, has considerably improved image acquisition speed and resolution [210]. The first generation of instruments (time domain) was comparing echo delays of light from different retinal layers while the novel frequency domain technology, using Fourier transformation, measures all echoes of light simultaneously rather than sequentially. The common feature of both technologies is a Michelson interferometer measuring the effect of combining two light waves from the sample and a reference arm [211]. The first demonstration of Fourier domain OCT was in 2002 [212]. The consequent dramatic increase in imaging speed has led to an increased “line rate” (up to 312,000 A-scan per second) making three-dimensional reconstructions feasible [213-217].

Several studies have focused on the interpretation of OCT images and their correlation with retinal morphology. We are close to establishing a precise interpretation of OCT layers although one to one correspondence with histology cannot be expected [205, 209, 218-220]. Notably, the OCT contrast may often not be sufficient to visualise structures like ganglion cell layer or Bruch’s membrane. Advances in technology as well as observational studies have increased our understanding of the, crucial for the assessment of retinal dystrophies, outer retinal OCT appearance in health and disease [221-223]. Throughout this study outer retina morphology interpretation would be as suggested by Srinivasan *et al.*[221].

In inherited retinal disease the introduction of OCT has clearly changed clinical practice enabling early diagnosis and accurate assessment of disease progression or response to treatment. The role of OCT imaging in research is also key and the overall impact of this technology on our understanding of the pathology of retinal dystrophies has ushered in a new exciting era, turning the page that Babbage and Helmholtz have opened 150 years ago.

1.4 Aims of this Thesis

(a) To identify novel genes and loci associated with human retinal phenotypes.

(b) To characterize the clinical consequences of mutations in genes associated with human retinal disease.

(i) To determine the structural and functional effects of mutation in the retina.

(ii) To determine the variability within and between families.

More specifically, this thesis focuses on

- screening genes previously associated with retinal disorders,
- combining linkage analysis (including homozygosity mapping), exome sequencing and candidate gene sequencing to identify novel genetic determinants of autosomal recessive retinal disease and
- characterising the consequences of mutations identified on retinal structure and visual function.

2 MATERIALS AND METHODS

2.1 Study Subjects

2.1.1 Ethical Approval and Consent

Approval for this study was obtained from the MEH Research Ethics Committee (project number MOOA1005) and from the Moorfields & Whittington Hospitals Research Ethics Committee (WEBA1006; 05/Q0504/38). All individuals involved in this study provided fully informed written consent.

2.1.2 Control Panels

Two control panels were used:
(a) a control population of 192 anonymised, randomly selected, unrelated, UK Caucasian blood donors (HRC-1 and HRC-2, Health Protection Agency Culture Collections, Salisbury, UK),
(b) a panel of 50 DNA samples from unrelated patients of South Asian origin and no history of eye disease (as part of a collaboration with Professor Eamonn R Maher and Birmingham University Women's Hospital, Birmingham, UK).

2.1.3 Linkage Study

Experiments conducted prior to this study had generated genotyping data for 162 individuals from 48 families; genome-wide genotyping microarray technologies (Human Mapping 10K, 50K and 250K Arrays, Affymetrix, Santa Clara, CA, USA) had been utilised. The molecular diagnosis had been determined in 22 families. In the remaining 26 (table 2-1), pedigree and phenotyping information were collected and genotyping data were

reprocessed and reanalyzed. Regions identified in families with similar clinical phenotypes were examined for overlap.

Table 2-1. Families genotyped prior to this study in which the molecular diagnosis was unclear

Autosomal Recessive Condition	Number of previously genotyped families with unclear molecular diagnosis
LCA / RP/ EARLY-ONSET RETINAL DYSTROPHY	11
CSNB	2
MACULAR DYSTROPHY	4
SYNDROMIC EYE DISEASE	4
ROD MONOCHROMACY	3
FLECK RETINA SYDROMES	2
TOTAL	**26**

Additional 21 individuals from 14 families were genotyped using a SNP array containing over 50,000 markers of genetic variation (GeneChip Human Mapping 50K Array Xba, Affymetrix, Santa Clara, CA, USA; section 2.4.18.2.1). Genomic DNA ethanol precipitation, restriction enzyme digestion, ligation, PCR, PCR purification, fragmentation and labelling steps were performed in the laboratory as part of this study (sections 2.4.5, 2.4.6, 2.4.7, 2.4.9 and 2.4.14). Hybridisation, staining and scanning steps were performed at the Wolfson Institute, UCL, London, UK as part of the UCL Genomics Microarray Facility genotyping support services.

After the first year of this study, more powerful genotyping solutions became available. Genotyping using denser arrays (Genome-Wide Human SNP Array 6.0, Affymetrix; section 2.4.18.2.2) was performed in 63 individuals from 49 families. Genomic DNA preparation (sections 2.4.4, 2.4.5 and 2.4.8) was performed in the laboratory with all other steps conducted by Drs Jill Urquhart and Sarah Daly in the St. Mary's Hospital Academic Medicine Department, Manchester Academic Health Sciences Centre, University of Manchester, Manchester, UK as a service.

2.1.4 Exome Sequencing Study

High-throughput sequencing platforms have become increasingly available and the cost of sequencing during the course of this study has dropped 40x (http://www.genome.gov/sequencingcosts/). A grant application was prepared (principal applicants Dr Donna S Mackay, PS and Dr Alice E Davidson; collaboration with Dr Vincent Plagnol, UCL Genetics Institute, London, UK) and funding was secured to perform exome sequencing in individuals affected with retinal disease (October 2010).

Twelve unrelated patients, members of families previously studied using SNP genotyping arrays, were selected. Individuals were affected with: RP (3), LCA (1), rod monochromacy (3), cone-rod dystrophy (1), syndromic RP and cataract (1), FEVR (1), macular dystrophy (1) and benign fleck retina (1).

Quantification using a microvolume spectrophotometer (NanoDrop 2000, Thermo Fisher Scientific, Wilmington, DE, USA; section 2.4.4) and inspection of genomic DNA on a 1% w/v agarose gel (section 2.4.8) were performed in the laboratory. Subsequently, 5 to 10 µg of high molecular weight DNA were sent to Beijing Genomics Institute, Shenzhen, China through UCL Genomics Whole Genome Sequencing support services.

2.1.5 Mutation Detection Study

A panel of 288 unrelated patients diagnosed with recessive adult-onset rod cone or cone rod dystrophy was collected using an SQL query in the MEH and UCL Institute of Ophthalmology Inherited Eye Disease Database. The genomic DNA extracted from peripheral blood leukocytes of the donated blood samples was quantified (sections 2.4.3 and 2.4.4) and samples with sample purity (260:280 ratio) over 1.80 and two consistent concentration measurements over 50 ng/µL were diluted to 50 ng/µL and added to 96-well plates.

A second panel with 192 unrelated probands diagnosed with autosomal recessive LCA or childhood-onset retinal dystrophy was also available for the study (courtesy of Drs Donna S Mackay and Louise Ocaka). The majority of patients were recruited in Professor Anthony T Moore's clinics by Drs Robert H Henderson, Philip Moradi and Arundhati Dev Borman. The panel is enriched for novel mutations as patient DNA had been screened and excluded for previously identified LCA-related variants through an APEX genotyping microarray (LCA Chip, Asper Biotech, Tartu, Estonia; section 2.4.18.1).

On the basis of suggestive phenotypic features, smaller panels were collected for the following recessive retinal disease-associated genes: *CRB1, NR2E3, KCNV2, MERTK, GRM6, RDH5, RLBP1, CLRN1, ADAM9, OAT, PDE6C*. In a similar fashion, panels were collected for disorders such as benign fleck retina, occult maculopathy, rod monochromacy, oligocone trichromacy, foveal hypoplasia and FEVR.

2.2 Phenotyping

As part of this study, over 250 individuals with retinal dystrophy have been examined in the Genetic Clinic, MEH Medical Retina Department under Dr Andrew R Webster. Phenotyping information of further patients was collected retrospectively from the MEH electronic databases and patient clinical and genetic notes.

A detailed clinical history covering age of onset and symptoms at presentation (*e.g.* central vision loss, night blindness, photophobia, colour blindness, peripheral vision problems), age at diagnosis, progression of symptoms and current symptoms (in light, in dark, visual acuity, colour vision, peripheral vision) was taken.

A careful past medical history was enquired after. Patients were directly questioned for suggestion of exposure to retinotoxic medication (chloroquine, hydroxychloroquine, thioridazine, quinine, deferoxamine) or syndromic associations. Questions were asked regarding hearing (for Usher syndrome), anosmia and neuropathy (for Refsum disease), digit abnormalities and polydactyly (for Bardet-Biedl syndrome and Refsum disease), urinary tract abnormalities and amenorrhea (for Bardet-Biedl syndrome) as well as renal failure (for Senior-Loken syndrome).

Family history was taken including detailed pedigree, ethnicity background information and history of consanguinity (or origin from a small gene pool resulting in high coefficient of inbreeding) in parents and the patient's marriage.

Best corrected Snellen visual acuity was obtained by an ophthalmic nurse prior to the instillation of dilating drops. As part of the clinical examination, confrontation visual fields to pick up gross defects were examined and colour vision testing with HRR plates (American Optical Company, New York, NY,

USA) and/or 24-plate Ishihara colour vision test (Kanehara and Co. Ltd, Tokyo, Japan) was conducted.

General ophthalmic examination including slit lamp biomicroscopy was performed on all subjects. Most patients underwent retinal imaging including fundus photography (section 1.3.3.1), fundus autofluorescence imaging (section 1.3.3.2) and SD OCT (HRA2 and Spectralis HRA+OCT, Heidelberg Engineering; section 1.3.3.3). In the majority of cases, imaging was performed by medical photographers (MEH Medical Illustration Department). Fundus autofluorescence and SD OCT images were obtained in over 80 subjects as part of this study.

Electrophysiological testing (section 1.3.2) was performed in the MEH Electrophysiology Department and the results were interpreted and reported by Professor Graham E Holder or Dr Anthony G Robson.

2.3 Bacteriological Procedures

2.3.1 Bacterial Strain

High efficiency (at >10^8 cfu/µg) *E.coli* competent cells (JM109 strain; Promega, Madison, WI, USA) were used. The JM109 strain [224] is sensitive to all common antibiotics and deficient in *β*-galactosidase activity; its genotype is: *end*A1, *rec*A1, *gyr*A96, *thi*, *hsdR17*(r_K-, m_K+), *rel*A1, *sup*E44, Δ(*lac-proAB*), [F', *tra*D36, *pro*AB, *lac*I^qZΔM15].

2.3.2 Transformation of Chemically Competent Cells

After thawing and gently flicking the tubes of frozen *E.coli* competent cells (JM109 strain; Promega), 50 µl were transferred into chilled tubes containing DNA solution; the latter was either 2 µl (approximately 200 ng) of each cloning/ligation reaction (sections 2.4.7 and 2.4.13) or 0.1 ng of uncut plasmid (to determine transformation efficiency). Subsequently the tubes were placed on ice for 30 minutes followed by heat shock at 42 °C for 50 seconds and incubation on ice for a further minute. Finally, transformation reactions were diluted to 1 ml by addition of 900 to 950 µl of SOC medium prior to an incubation period of 2 hours at 37 ºC and with shaking at 225 rpm.

2.3.3 Preparation of Growth Medium for Blue/White Screen

LB Agar was prepared (7.5 g of LB Broth and 4.5 g of LB Agar powders were suspended in 0.5 litres of dH_2O) and sterilised by autoclaving for 15 minutes at 15 psi (around 103,400 Pascal). After air-cooling to 50 °C, agar was prepared for blue-white screening and antibiotic resistance selection. Ampicillin (final concentration 50 µg/ml), X-gal in dimethylformamide (20 mg/ml; final concentration 50 µg/ml) and IPTG (final concentration 0.1 mM) were added.

Using aseptic techniques, the solution was poured into sterile Petri dishes and allowed to harden at room temperature.

2.3.4 Screening Bacterial Colonies and Bacterial Culture Growth

Plates containing the aforementioned growth medium (section 2.3.3) were inoculated with 100 to 200 µl of each transformation culture (section 2.3.2) and once the inoculum had been absorbed, incubated at 37 °C in an inverted position for 12 to 16 hours. After removing the plates from the incubator and allowing the blue colour to develop (at 4 °C), colonies carrying recombinant plasmids (white) were identified. Single colonies were isolated, transferred to a sterile tube containing LB Broth and ampicillin (final concentration of 100 µg/ml) and incubated for 12 to 16 hours at 37 °C in a shaker incubator (250 rpm). Finally, the bacterial cells were harvested by centrifugation at 3,500 rpm for five minutes at room temperature and removal of the supernatant.

All reagents used for growth media preparation and selection of recombinants were purchased from Sigma-Aldrich, Poole, UK.

2.4 Nucleic Acid Procedures

Understanding information macromolecules, DNA and RNA, is a primary concern of molecular genetics. As RNA is unstable and can easily be converted into DNA with reverse transcription, nucleic acid research has focused on how to study DNA sequence. Amplifying and detecting the target sequence are the necessary steps. The general approaches used in this study are summarised in figure 2-1.

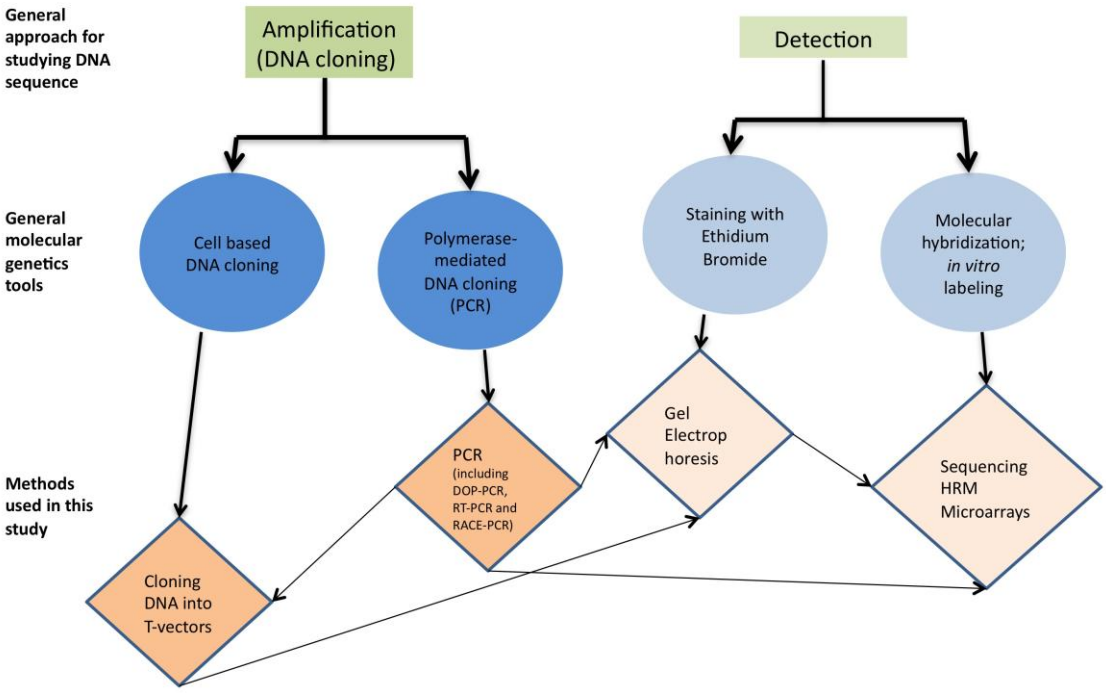

Figure 2-1. Overview of basic nucleic acid procedures performed in the course of this study.

2.4.1 RNA Electrophoresis

Total RNA integrity and purity prior to RT PCR was assessed using microfluidic separation technology (Experion Automated Electrophoresis System and Experion RNA StdSens Analysis Kit, Bio-Rad, Hercules, CA, USA) according to the manufacturer's instructions. After the automated steps (including electrophoresis, separation, staining, imaging, band detection and basic data analysis), electropherogram and simulated gel views of separation were inspected.

To assess mRNA integrity the assumption that rRNA quality reflects that of the underlying mRNA population was made. This is because mRNA represents only 1 to 3% of total RNA samples and is not readily detectable while rRNA makes up over 80% of total RNA samples. The majority of rRNA is comprised by the 28S and 18S rRNA species with eukaryotic 28S and 18S rRNA size in kb ratio being relatively constant. In case of contamination or degradation, the

28S:18S ratio is decreased [225-226]. In 2006, the RNA integrity number (RIN) was introduced as an alternative predictor of RNA integrity [227].

2.4.2 Reverse Transcription

Reverse transcription reactions were carried out using 20 U/µl of SuperScript III reverse transcriptase (Invitrogen, Carlsbad, CA, USA) with 1 µg of total RNA and 2 µM of gene-specific primer according to the manufacturer's instructions. All resultant cDNA was stored at 4 °C and used within five days of synthesis.

The reaction was performed to produce cDNA of various *TRPM1* transcripts in skin and retina (section 3.2.3). After the integrity of total RNA samples from retina (Clontech, Mountain View, CA, USA) and skin (Stratagene, La Jolla, CA, USA) was assessed (section 2.4.1), a 3' end *TRPM1*-specific primer (in exon 27; 5' CCTGTCCATGTATCACATCTGTTTTAT 3') was used for first-strand cDNA synthesis. The cDNA was utilised as template for the ensuing PCRs.

As part of the RACE protocol (GeneRacer Kit, Invitrogen; section 2.4.12), reverse transcription was performed using two different modules: SuperScript III RT Module for both 5' and 3' RACE; Cloned AMV RT Module for 3' RACE. The aforementioned gene-specific primer for 5' RACE and an oligo-dT primer (different dT tail for each module) for 3' RACE were used to prime the first-strand cDNA synthesis according to the manufacturer's instructions.

2.4.3 DNA Extraction

Peripheral venous blood samples were collected in 10 ml tubes containing sodium EDTA as an anticoagulant and stored at 4 °C for less than five days to avoid DNA degradation. Extraction was carried out using either the BACC-2 Kit (Tepnel Life Sciences, Manchester, UK) or the Gentra Puregene Blood Kit (Qiagen, Hilden, Germany). After extraction, DNA was stored at 4 °C if for

immediate use or at -20 °C if for longer term storage. The majority of blood samples were collected by Ms Genevieve Wright and Mrs Sophie Devery while most of DNA extraction was performed by Ms Bev Scott and Dr Naushin Waseem.

2.4.4 Quantification of DNA

DNA samples were quantified using a UV-Vis spectrophotometer (NanoDrop 2000, Thermo Fisher Scientific). Analysis of 0.5 to 2.0 µl of stock sample was performed by measuring ultraviolet light absorbance at wavelengths of 260 nm and 280 nm. Using the Beer-Lambert law the amount of light absorbed was related to the concentration of the absorbing molecule. Double-stranded DNA absorbs maximally at 260 nm while proteins absorb maximally at 280 nm [225]. The concentration (ng/µl) of each DNA sample was calculated using the absorbance value obtained at 260 nm ($A_{\text{bsorbance}}^{260\text{nm}}$ = 1 is equivalent to 50 µg/ml of DNA); the $A_{\text{bsorbance}}^{260\text{nm}}$:$A_{\text{bsorbance}}^{280\text{nm}}$ ratio was used as a marker of sample purity. Pure DNA has a ratio of approximately 1.80 and a ratio of less than 1.50 indicates that the sample has significant protein contamination.

2.4.5 Ethanol Precipitation of DNA

Ethanol precipitation was performed in order to concentrate and purify DNA samples. This procedure allows charged phosphate groups present on DNA backbones to form stable ionic bonds and precipitate out of aqueous solutions.

In general, 95% v/v ethanol (2.5x sample volume) and 3 M sodium acetate (pH 5.3; 0.1x sample volume) were added to each sample and the mix was stored overnight at -20 °C. Subsequently, precipitated DNA was collected by centrifugation in a microcentrifuge tube at 12,000 rpm for 20 minutes in a 4 °C environment. After centrifugation the supernatant solution was removed and 1 ml of 70% v/v cold ethanol was added to the pellet (salt removal step). The suspension was centrifuged again at 12,000 rpm for 10 minutes to once again

pellet DNA. After the supernatant solution had been removed, the pellet was air-dried for 10 minutes. Finally, DNA was resuspended in 10 mM Tris-Cl, pH 8.5 (Buffer EB, QIAgen Spin Kits, Qiagen).

2.4.6 Digestion of DNA

Restriction enzyme digestion [228-229] of genomic DNA was performed in this study as part of and according to the Affymetrix GeneChip Mapping 50K Xba Assay Kit protocol (section 2.4.18.2.1). The assay utilises a strategy that reduces the complexity of genomic DNA up to 10-fold by first digesting it. The Xba I restriction enzyme (New England Biolabs, Ipswich, MA, USA) was used and BSA (New England Biolabs) was added to enhance enzymatic activity.

Restriction enzyme digestion of PCR products was utilised to assay the prevalence of c.352C>A, p.Arg118Ser variant in *GRM6* within control populations (section 3.1.6.1.3). The enzyme SacII (New England Biolabs) was chosen on the basis of its ability to differentiate wild-type and mutant alleles (assessed by http://tools.neb.com/NEBcutter2/). Initially, 5.0 µl of PCR product for each individual were incubated with 1x NEBuffer 4 (New England Biolabs), 3.5 µl dH_2O and 0.1 U/µl of enzyme for one hour at 37 °C. Subsequently, 5.0 µl of digested product were run on a 2% w/v agarose gel with a 25 to 500 separation range DNA ladder (HyperLadder V, Bioline, London, UK).

EcoR I (New England Biolabs), whose recognition sites flank the insert position of the PCR product in the plasmid sequence of both pCR4-TOPO (Invitrogen) and pGEM-T easy (Promega) vectors, was used to digest eluted plasmid DNA. After fractionating the restricted DNA by agarose gel electrophoresis, band sizes were measured confirming the identity of the cloned fragment.

2.4.7 Ligation of DNA

In the Affymetrix GeneChip Mapping 50K Xba Assay Kit protocol, the digestion of genomic DNA step is followed by a universal adapter ligation step (section 2.4.18.2.1). In general, 0.25 µM of adapter (GeneChip Human Mapping 50K Xba Adaptor, Affymetrix), 10 U/µl of T4 DNA Ligase and 1x T4 DNA Ligase Buffer Ligase (New England Biolabs) were added to the digested DNA and incubated according to the assay protocol.

A ligation reaction was also performed as part of the MLPA DNA detection/quantification protocol (section 2.4.11). This reaction involved two probe oligonucleotides and was followed by PCR.

T4 DNA Ligase was the first DNA ligase to be characterised [230] and originates from the T4 bacteriophage. In addition to the aforementioned protocols, this enzyme was also used to allow PCR inserts to ligate efficiently with pGEM-T Easy Vectors (Promega; reaction was performed according to the manufacturer's instructions). One example was the use of DNA inserts from the genomic region around *PLA2G5* exon 3 (insert size 343 base pairs) in a benign fleck retina patient carrying two *PLA2G5* variants (c.145G>A, p.Gly49Ser and c.157C>T, p.Arg53X; section 3.2.5). Insert to vector molar ratios ranging between 3:1 and 1:3 were used for ligation reactions. A vector-only ligation was employed as a negative control every time ligation reactions were performed.

2.4.8 Agarose Gel Electrophoresis

Electrophoresis through agarose gel, a technique having its roots in the mid-1960s [231], was used to separate, identify and purify DNA fragments. PCR products and restriction enzyme digests were analysed using this technique. Gels were prepared by adding the appropriate amount of agarose (typically 2% w/v for 100 to 2,000 base pair product size; Bio-Rad Laboratories, Berkeley, CA, USA) in 1x TBE buffer (Eppendorf, Hamburg, Germany). After

dissolving the agarose, ethidium bromide [232] to 0.5 µg/ml final concentration was added and the gel was allowed to set. DNA was mixed with 1x DNA loading dye (Bioline), loaded into wells next to a standard size marker (Bioline) and run until desired separation was achieved, typically 150 mV for 30 minutes in 1x TBE buffer. The DNA was visualised on a transilluminator (UV light of wavelength 210 nm) and photographed using a camera with orange filter (BioDoc-It 210, UVP, Upland, CA, USA).

2.4.9 PCR

PCR [233-234] was usually performed using either MolTaq (Molzym, Bremen, Germany) or BioTaq (Bioline) DNA polymerase. Two of the protocols used are described in table 2-2.

Table 2-2. Standard protocols for PCR

Components		**MolTaq protocol**		**BioTaq protocol**	
		Volume	**Final Concentration**	**Volume**	**Final Concentration**
Buffer		3 µl of Buffer; 0.3 µl of Enhancer (Molzym)	1x	2.5 µl of NH_4 Buffer (Bioline)	1x
$MgCl_2$			1.5 mM	0.75 µl of 50mM $MgCl_2$ (Bioline)	1.5 mM
dNTP mixture		0.24 µl (Promega)	0.2 mM each	0.2 µl (Promega)	0.2 mM each
10 µM Primer	Forward	1 µl	0.33 µM	0.5 µl	0.2 µM
	Reverse	1 µl	0.33 µM	0.5 µl	0.2 µM
Taq Polymerase		0.2 to 0.3 µl of MolTaq (5 U/µl; Molzym)	0.03 to 0.05 U/µl	0.1 µl of BioTaq (5 U/µl; Bioline)	0.02 U/µl
DNA Template		1 µl	10 to 50 ng/µl	2 µl	100 to 200 ng/µl
dH_2O		23.16 to 23.26 µl	-	18.15 µl	-
Total Volume		30 µl	-	25 µl	-

Occasionally, extra $MgCl_2$ or DMSO up to 10% v/v were added to PCR reactions to enhance efficiency. For difficult/problematic PCR applications different polymerases were used including: Bio-X-Act long DNA Polymerase (Bioline), GC-RICH PCR System (Roche, Mannheim, Germany), Platinum Taq DNA Polymerase High Fidelity (Invitrogen) and Platinum Pfx DNA Polymerase (Invitrogen), all according to the manufacturers' instructions.

The standard PCR cycling parameters used are stated below in table 2-3.

Table 2-3. PCR cycling parameters

Cycling stage	Temperature (°C)	Time	Cycles
Initial denaturation	94 to 95 °C	3 to 5 minutes	x 1
Denaturation	94 to 95 °C	30 to 45 seconds	
Annealing	50 to 70 °C	30 seconds	x 35
Extension	72 °C	1 minute·kb^{-1}	
Final Extension	72 °C	5 to 7 minutes	x 1
Hold	4 °C	hold	x 1

2.4.10 Amplification Refractory Mutation System

ARMS is an amplification strategy in which a PCR primer is designed in such a way that it is able to discriminate among templates that differ by a single nucleotide residue [235]. In ARMS, the primer pair is designed so that the terminal 3' nucleotide of one primer coincides with a DNA variant in the target sequence. When the primer mismatches, the amplification is not allowed to proceed to the same degree as under optimal hybridisation. A DNA polymerase possessing no 3'-5' exonuclease (proofreading; like Taq [236-237], unlike Pfu [238] polymerase) activity was used.

An ARMS test was used to assess the presence of a heterozygous mutation, c.2991+1655A>G, p.Cys998Stop, in *CEP290* in two siblings affected with retinal dystrophy, their mother and a control DNA (section 3.1.1). DNA templates were amplified using

5' ACCGCACCTGGCCCCAGTTGTAATTGTGGG 3' as forward primer and

5' AGTAAGGAGGATGTAAGACTGGAGATAGAG 3' as reverse primer.

This primer pair was designed to mismatch with the wild-type and match with the mutant DNA template sequence. Annealing temperature was 67 °C and product size was 137 base pairs. 0.25 U of Taq DNA polymerase (Bioline) per 20 µl reaction was used. The protocol was optimised by Dr Donna S Mackay.

2.4.11 Multiplex Ligation-dependent Probe Amplification

MLPA is a PCR based method permitting multiple targets to be amplified with a single primer pair. It is mainly used to test genomic DNA sequences for abnormal copy numbers. Notably, in MLPA, it is not target sequences that are amplified, but MLPA probes that hybridise to the target sequence. An MLPA probe consists of two probe oligonucleotides each containing one of the PCR primer sequences. In case both the oligonucleotides' immediately adjacent target sequences are present in the sample, the probes hybridize next to each other allowing connection by ligation. Only ligated probe pairs will be exponentially amplified during the subsequent PCR reaction and the amount of PCR product is a measure for the number of target sequences [239].

The SALSA MLPA P221 LCA probemix-1 (MRC-Holland, Amsterdam, Netherlands) containing probes for *AIPL1, CRB1, CRX* and *RPE65* genes was used according to the manufacturer's instructions in order to identify duplications or deletions in five unrelated patients with a single heterozygous *CRB1* mutation (section 3.1.1).

2.4.12 Rapid Amplification of 5' and 3' cDNA Ends

RACE is a PCR-based technique which was developed to facilitate the cloning of full length cDNA 5' and 3' ends [240]. RACE, also called one-sided [241] or anchored PCR [242], differs from conventional PCR in that it requires knowledge of only a small region of sequence within the target cDNA. Therefore, only one sequence-specific primer is used with the second primer being complementary to a general feature of the target. In general, 3' RACE takes advantage of the natural poly-A tail in mRNA as a generic priming site for PCR amplification. In the case of 5' RACE, protocols tend to slightly vary. The first experimental step of the GeneRacer Kit (Invitrogen) protocol that was used in this study involves RNA dephosphorylation and mRNA 5' cap structure removal. Subsequently, an RNA oligonucleotide that supplies a known 5' end priming site is ligated to the decapped mRNA. After reverse transcription

(section 2.4.2), cDNA is amplified and cloned into a vector. The flowchart in figure 2-2 outlines the RACE experiment.

To investigate the full-length *TRPM1* transcripts in retina and skin, 5′ and 3′ RACE were performed (section 3.2.3). After assessment of RNA integrity, ligation of RNA oligonucleotide and cDNA synthesis (sections 2.4.1 and 2.4.2), amplification was performed. For 5' RACE, a *TRPM1*-specific reverse primer was used together with the GeneRacer 5' primer. PCR reactions were setup according to the manufacturer's instructions with an annealing temperature of 68 °C. Subsequent nested PCR was also performed at 65 °C. In a similar fashion, two rounds of PCR for 3' RACE were setup (a *TRPM1*-specific forward primer and a nested *TRPM1*-specific forward primer with corresponding primers in the kit) using the same conditions as in the 5' RACE. The experiments were optimised and conducted with the assistance and supervision of Dr Zheng Li.

Table 2-4. Rapid Amplification of 5' and 3' cDNA Ends primer sequences

GeneRacer 5' primer	CGACTGGAGCACGAGGACACTGA
TRPM1 5' GSP-reverse	GGAGCAGTGAGTCTGGCTTGGTGTCATA
GeneRacer 5' nested primer	GGACACTGACATGGACTGAAGGAGTA
TRRM1 5' GSP-nested	GGCAGAGGGGGGATATGCTGGTTGGTGAA
GeneRacer 3' primer	GCTGTCAACGATACGCTACGTAACG
TRPM1 3' GSP-forward	CCCAGATGGCAGTCACCTTGCAGTAGAT
GeneRacer 3' nested primer	CGCTACGTAACGGCATGACAGTG
TRPM1 3' GSP-nested	CCTCGAATCCCTCGCTTGTCCCTAA

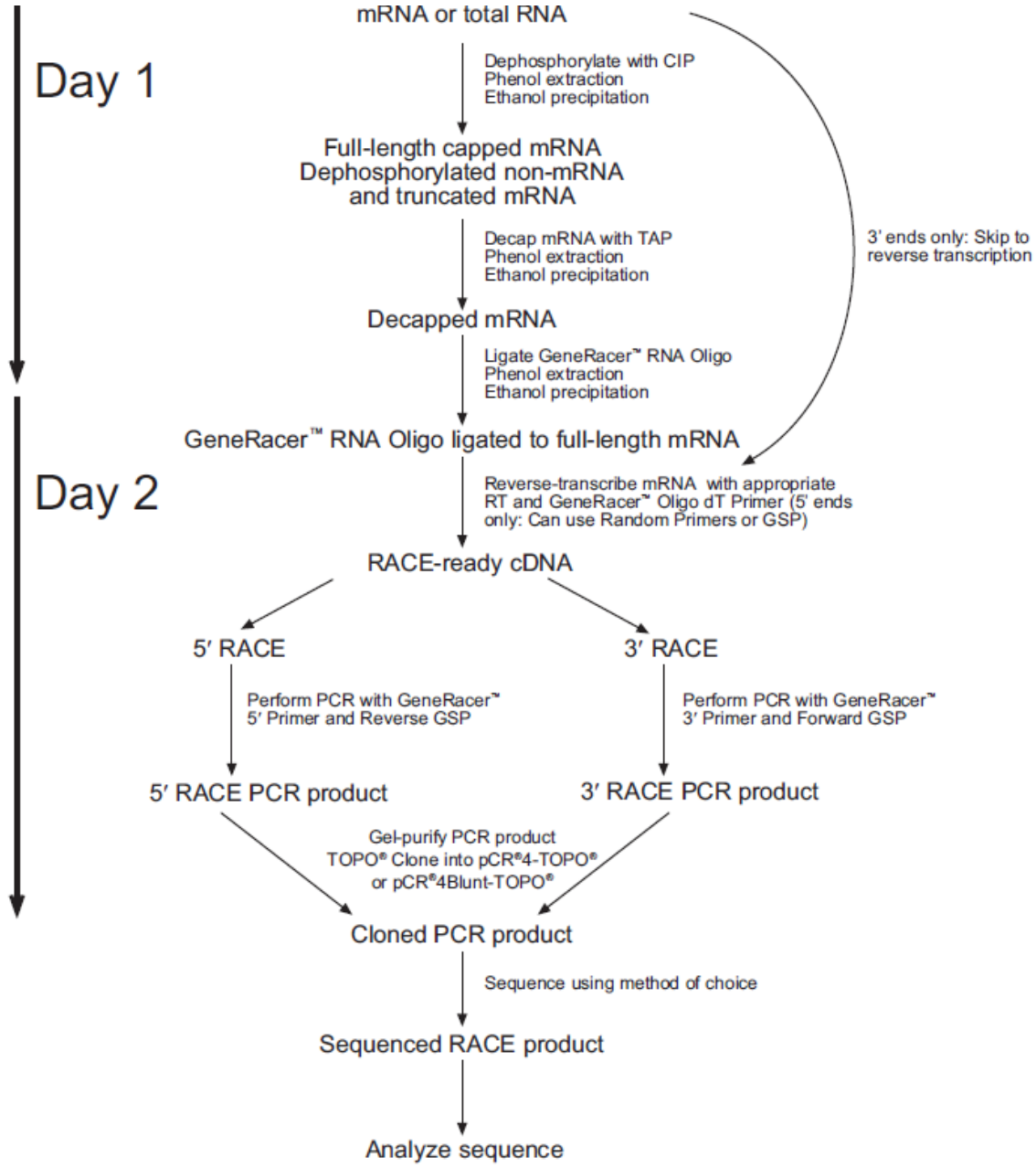

Figure 2-2. Flow chart showing the RACE experiment outline as presented in the Invitrogen GeneRacer Kit instruction manual.

2.4.13 Cloning PCR Products into T Vectors

Taq polymerase generated PCR products were cloned into a vector (T vector) containing a complementary unpaired 3' thymidyl residue [243]. After PCR products were purified from an agarose gel, they were inserted to either a linearised pCR4-TOPO (Invitrogen) or a pGEM-T easy (Promega) vector. The main difference between these two cloning kits is that the first does not require

DNA ligase and uses topoisomerase I [244-245] while the second one is a typical, ligase based, T vector system (section 2.4.7).

2.4.14 Purification of PCR Products and Plasmid DNA

Typically, PCR fragments were purified using vacuum-based, size exclusion separation with a small volume, 96-well filter device (Montage PCR_{96} cleanup kit, Millipore, Watford, UK) according to the manufacturer's instructions.

On some occasions, the QIAquick gel extraction kit (Qiagen) was used to isolate the amplified DNA contained in excised bands from agarose gels. The manufacturer's instructions were followed in order to bind the amplified DNA to the anionic silica membrane of appropriate columns after centrifugation.

As part of the Affymetrix GeneChip Mapping 50K Xba Assay Kit protocol (section 2.4.18.2.1), pooled PCR products were purified with a MinElute 96 UF PCR Purification kit (Qiagen).

For purification of high copy plasmid DNA from *E.coli* cultures, a QIAprep spin (Qiagen) or a Genelute plasmid (Sigma-Aldrich) miniprep kit were used according to the manufacturer's instructions; a microcentrifuge was utilised.

2.4.15 High Resolution Melting Analysis

HRM is a rapid and cost effective method for targeted genotyping and mutation screening [246]. It is based on the analysis of the melting profile of amplified DNA and uses saturating fluorescent dye to monitor the transition from unmelted to melted polynucleotide. The approach was first introduced in 1997 [247-248] and recent advances in instrumentation and DNA binding dyes have increased its sensitivity, accuracy and clinical utility.

HRM analysis was performed using the LightScanner System (Idaho Technology, Salt Lake City, UT, USA), which allows DNA sequence variation scanning in two steps: amplification (with a fluorescent dye) and amplimer melting.

Amplification was performed either using the 2.5x LightScanner High Sensitivity Master Mix (Idaho Technology) or the following mix (final reaction volume 10 µl):

1x reaction buffer, 0.2x of enhancer (Molzym),
0.125 mM of each dNTP,
1 µM of forward and reverse primer,
10 to 50 ng of genomic DNA,
10 U of Taq polymerase (MolTaq, Molzym) and
1x of LCGreen Plus DNA dye (Idaho Technology).

Each reagent concentration in this mix was titrated and optimised by comparing the agarose gel band appearance of control DNA amplified with this method to the one amplified with 2.5x LightScanner High Sensitivity Master Mix (Idaho Technology). 15 µl of mineral oil (Sigma-Aldrich) were added in each well before starting the reaction to avoid evaporation.

PCR cycling parameters were used as described in the manufacturer's instructions with annealing temperature ranging from 67.5 to 70 °C.

Following PCR, amplimer melting was performed in 96-well plates. The LightScanner System (Idaho Technology) collected data from 77 to 95 °C at a ramp rate of 0.10 °C per second. Images of DNA melting were captured by CCD camera and sample-to-sample comparisons of these images were used to interrogate the sequences of the amplified DNA.

Interpretation of data was performed using the Lightscanner Instrument and Analysis software with Call-IT function version 2.0 (Idaho Technology). After defining the negative control, raw melting data of different samples were normalised; lower temperature ranged between 83 and 93 °C and upper

temperature ranged between 90 and 95 °C. The default value of 5% was chosen for the melting temperature curve shift function. Samples were clustered into groups using various curve shape matching algorithms. Different sensitivity levels were tried (all over 0.25) and both normalised melting curve and difference plots were inspected. Samples with significant differences in fluorescence were selected, purified and sequenced bidirectionally.

2.4.16 DNA Sequencing Using Sanger Method

Nucleotide sequence of PCR fragments and plasmid DNA was determined using Sanger's dideoxy mediated chain termination method [249-250]; the BigDye terminator v3.1 (>500 base pairs) cycle sequencing kit (ABI, Foster City, California, USA) was utilised. The sequencing reaction consisted of the following components: 10 to 50 ng of purified amplified DNA, 1 µM sequencing primer, 1x BigDye sequencing buffer, 0.5 µl of BigDye terminator and dH_20 (up to 10 µl).

The standard cycle sequencing conditions used were: 96 °C for 1 minute followed by 25 cycles of 96 °C for 10 seconds, 50 °C for 5 seconds and 60 °C for 4 minutes. Extension products were purified using a vacuum-based protocol with size-exclusion filter plates (Montage SEQ_{96} Sequencing Reaction cleanup kit, Millipore). Automated capillary electrophoresis was performed on a multi-colour fluorescence-based DNA analysis system with 48 capillaries operating in parallel (ABI PRISM 3730 Genetic Analyser). As a result, electropherogram files (AB1 files using the ABIF binary file format) were generated.

2.4.17 Targeted Capture and High-throughput DNA Sequencing

Sanger's method has provided the backbone technology for genome analysis for the past 30 years. There has recently been a shift away from this approach [251]; in 2005, the beginning of a new era characterised by a "dizzying free-fall

in sequencing costs" [252] was heralded by two publications [253-254] introducing massively parallel, high-throughput DNA sequencing (figures 2-3 and 2-4). Nevertheless, six years after and despite the cost of DNA sequencing dropping by approximately four orders of magnitude (http://www.genome.gov/sequencingcosts/), sequencing a human genome in its entity is still an expensive endeavour. Additionally, the costs associated with downstream data handling often match or surpass the data acquisition costs [251]. As an interim solution, target-enrichment methods in which specific genomic regions are selectively captured from a DNA sample prior sequencing, have been developed [255-257]. Such strategies often target the protein coding subset of the genome, *i.e.* the exome. Over the past couple of years "whole exome sequencing by high-throughput sequencing of target-enriched genomic DNA" (exome sequencing) has been widely used to cost-effectively interrogate this interpretable subset of the genome.

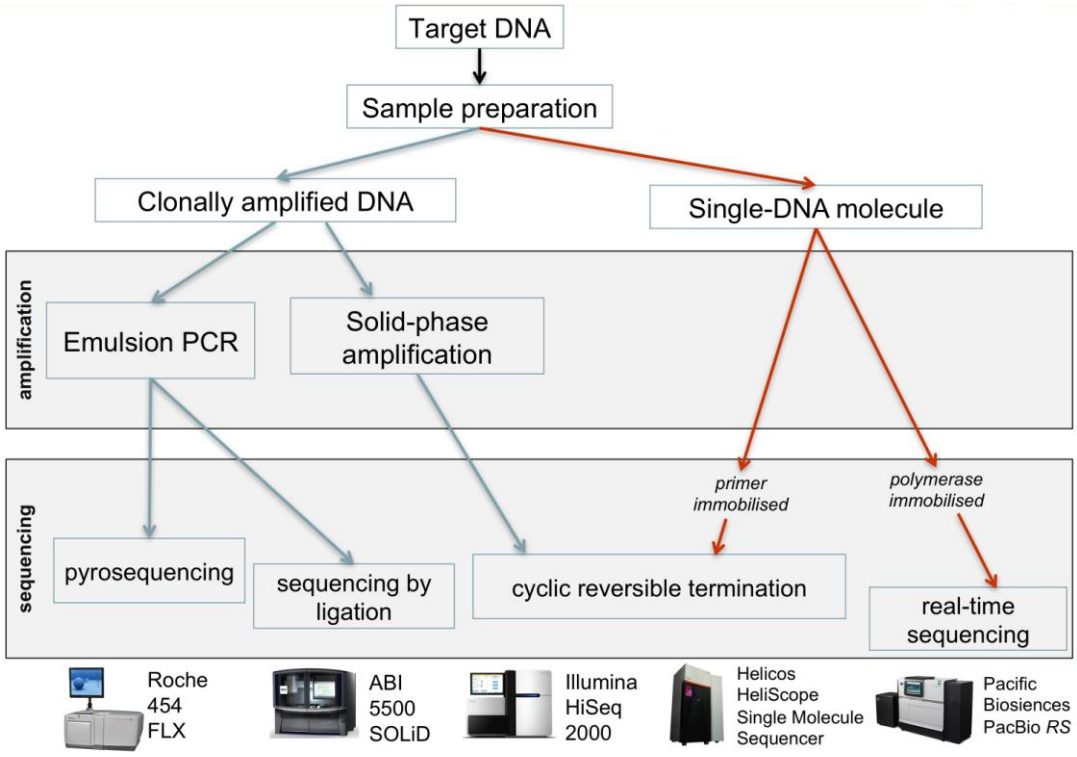

Figure 2-3. Overview of commercially available high-throughput sequencing technologies and the combination of different protocols used. The methods included are diverse and can be broadly grouped as template preparation and sequencing.

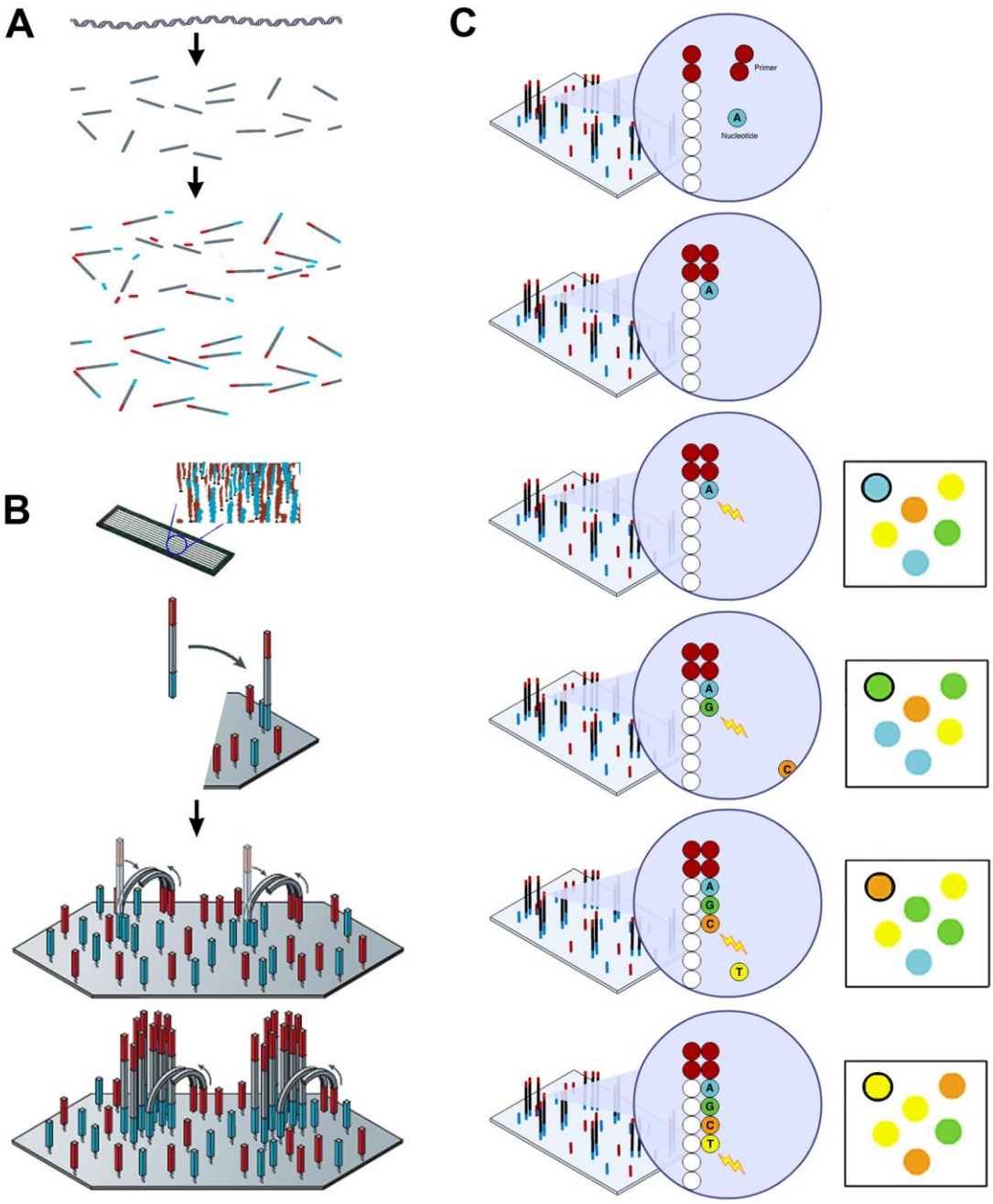

Figure 2-4. Illumina reversible terminator-based sequencing method (modified from [251] and http://genome.wellcome.ac.uk/doc_WTX056439.html).
[A] Random fragmentation of genomic DNA into small sizes (~100 to 300 base pairs; ultrasound technology is typically used) is followed by end-repair (converts the overhangs resulting from fragmentation into blunt ends), adenylation of 3' ends (to prevent fragments from ligating to one another during the adapter ligation reaction and allow efficient ligation to the complementary overhang-containing adapter) and adapter ligation.
[B] The next step (amplification) is performed on an optically transparent surface similar to a microscope slide called the flow cell. The flow cell is partitioned into eight lanes/channels and high-density forward and reverse primers are bound to the its surface; these anchored oligonucleotides are complimentary to the adaptors used in the previous step. Adapted single-stranded DNAs are randomly bound to the flow cell and amplified by solid-phase PCR (bridge-amplification). In each PCR cycle, priming occurs by arching of the template molecule such that the adapter at its free end hybridizes to and is primed by a free oligonucleotide in the near vicinity on the flow cell surface. This process results in randomly distributed ("raindrop pattern"), clonally amplified clusters from fragment templates on a glass surface [251, 258-259].

[C] A cyclic reversible termination method utilising fluorescently modified nucleotides is used for sequencing. Initially, labelled terminators (3'-blocked nucleotides; each of A, T, C and G is bound to a different fluorophore), primer and DNA polymerase are applied to the flow cell. Subsequently, a three-step cycle which includes nucleotide incorporation, imaging and cleavage is repeated a number of times. In the first step, a dye-labelled modified nucleotide, complementary to the template base, is incorporated; this leads to termination of DNA synthesis. In the second step, remaining unincorporated nucleotides are washed away and the fluorescent signal at each cluster is recorded. Following imaging, a cleavage step removes the fluorophore from each incorporated base, unblocking the 3'-OH group. Washing is performed before starting the next incorporation step [251, 258-259].

As part of this study, solution-phase hybrid capture with biotinylated RNA baits was used to target 38 Mb (SureSelect Human All Exon Kit, Agilent, Santa Clara, CA, USA [256]) of genome sequencing from each of 12 patient DNA samples (sections 2.1.4 and 3.2.2). The enriched library was amplified and then sequenced on a HiSeq2000 (100 base pair paired-end mode; Illumina, San Diego, CA, USA). All experimental procedures were carried out according to the manufacturers' protocols in BGI Shenzhen, China. Data were returned as two FASTQ files [260] per patient sample.

2.4.18 DNA Microarrays

Microarrays utilise a reverse hybridization assay to test for sequence variation in known target sequences, or to monitor for RNA expression levels. The idea that labelled nucleic acid molecules could be used to interrogate DNA attached to a solid support dates back to 1975 when Southern blot, the first DNA array, was introduced [261]. Key innovations in miniaturization, fluorescence-based detection [262-263], genome amplification [264-265] and oligonucleotide high density chemical synthesis [266-268] during the 1990s have provided a scale-up in hybridization assay technology, introducing oligonucleotide microarrays. Currently, microarrays are a standard tool of biomedical research and clinical diagnostics [269-270].

In this study different types of arrays have been used to identify and genotype mutations and polymorphisms.

2.4.18.1 Arrayed Primer Extension Microarray

APEX technology was first introduced as a novel method for DNA analysis in 1996 [271-272]. The APEX reaction involves several simultaneous mini-sequencing reactions on a solid support (figure 2-5). Numerous 5′ modified, sequence specific oligonucleotides (probes) are arrayed on a glass surface with their 3′ end designed immediately adjacent to a variable site. PCR amplified and fragmented DNA from target samples is hybridised to the array. DNA polymerase-driven extension of the immobilised probes' 3′ ends with ddNTPs is performed. The pattern of binding at different spots gives a visual record of the genotype.

A number of patient samples were sent to Asper Ophthalmics, Tartu, Estonia for analysis with the LCA [273], recessive RP or ABCA4 chip [274] (Asper Biotech, Tartu, Estonia).

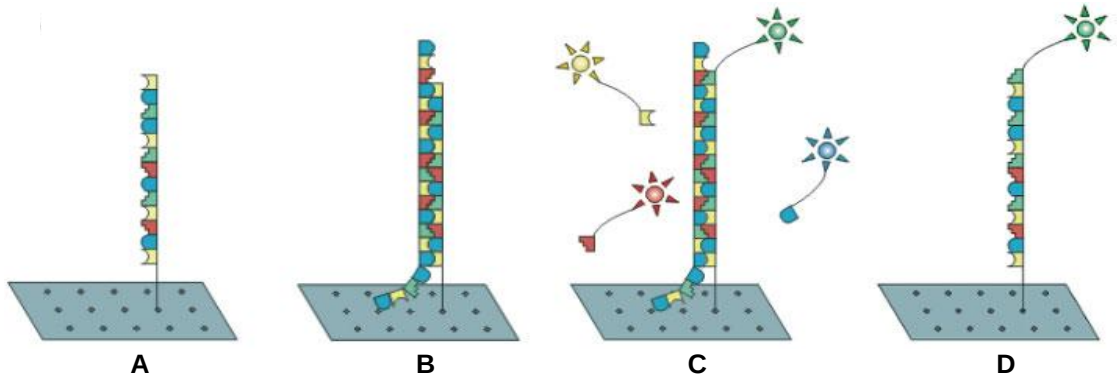

Figure 2-5. Overview of APEX technology.
[A] Oligonucleotide probes are arrayed on a glass slide.
[B] Complementary fragments of PCR amplified target sample DNA are annealed to the probes.
[C] DNA polymerase-mediated, sequence-specific single nucleotide extension of the 3′ ends of the probe with fluorescent ddNTPs.
[D] DNA fragments and unused ddNTPs are washed off followed by signal detection (modified from [274]).

2.4.18.2 Genome-Wide Genotyping SNP Arrays

Affymetrix GeneChip arrays were used in order to perform large scale, genome-wide linkage analysis. GeneChip probe arrays are high density, solid-phase arrays (quartz chips), containing up to a million of different

oligonucleotide sequences on their glass surface. The different DNA probes are constructed by *in situ*, light-directed synthesis in sequential steps as opposed to being prepared in advance and then spotted onto the surface (*e.g.* APEX chips).

2.4.18.2.1 Affymetrix GeneChip Human Mapping 50K Array Xba

DNA samples from 21 individuals (section 2.1.3) have been processed with the Affymetrix GeneChip Mapping 50K Xba Assay Kit, enabling genotyping of over 50,000 SNPs per sample. Genomic DNA was digested with Xba I and ligated to adaptors that recognised the cohesive overhangs (sections 2.4.6 and 2.4.7). A universal primer annealing to the adapter sequence was then used to amplify the adaptor-ligated fragments in a PCR reaction. The amplified DNA was then fragmented to a size range of 250 to 2,000 base pairs. Fragmented PCR products were then labelled and transferred to the Wolfson Institute, UCL, London, UK for hybridisation to the Affymetrix GeneChip Human Mapping 50K Array Xba. All steps were performed according to the manufacturer's instructions.

2.4.18.2.2 Affymetrix Genome-Wide Human SNP Array 6.0

During the course of this study, as the array information capacity increased and the array price dropped, a decision to switch from the Affymetrix GeneChip Human Mapping 50K Array Xba to the Affymetrix Genome-Wide Human SNP Array 6.0 was made. The former features 1,800,000 genetic markers, including more than 906,600 SNPs and more than 946,000 probes for the detection of copy number variants (figure 2-6).

For each subject (section 2.1.3), 500 ng of genomic DNA were sent to St. Mary's Hospital Academic Medicine Department, University of Manchester. Subsequently, ARR (array attribute), CEL (probe results) and GQC (genotype quality control) files were received and analysed.

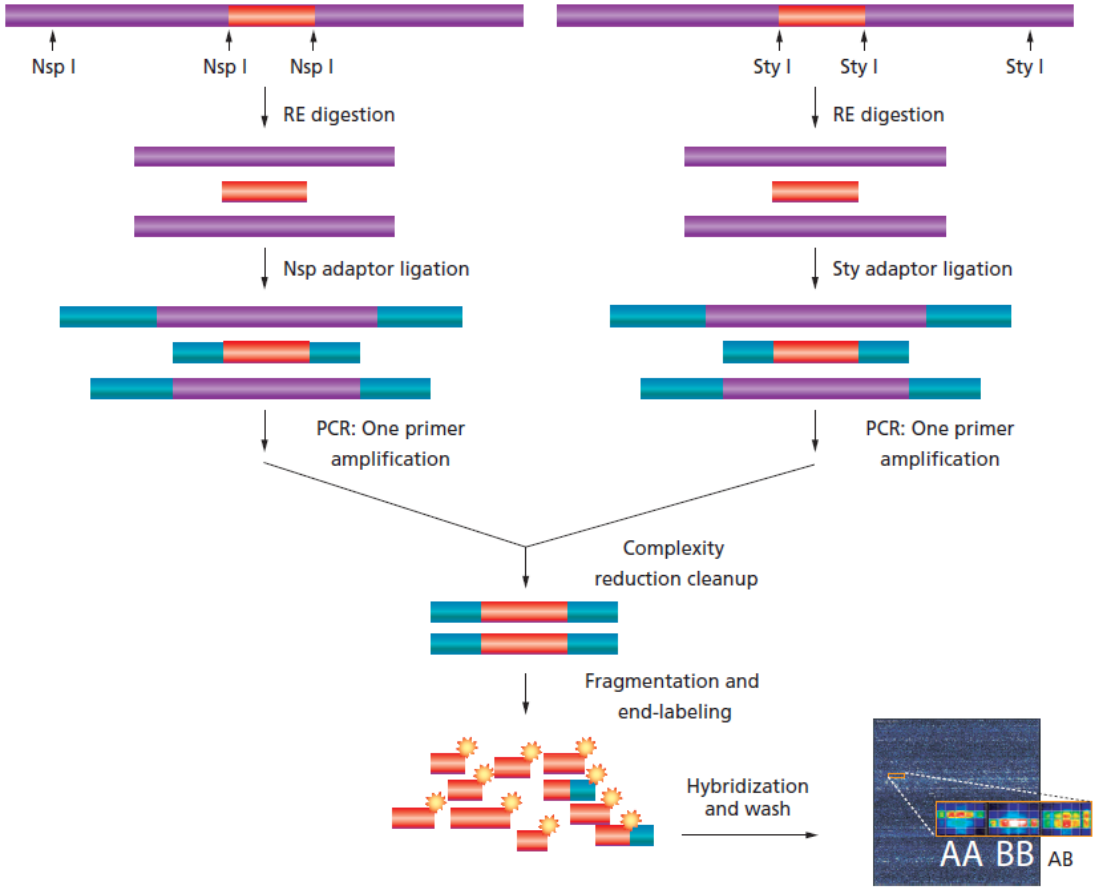

Figure 2-6. Overview of the Affymetrix Genome-Wide Human SNP Nsp/Sty Assay 6.0 (from the Affymetrix datasheet). A similar principal applies to the Affymetrix GeneChip Mapping 50K Xba Assay although digestion with one (Xba I) rather than two restriction enzymes is performed.

2.4.19 Microsatellite Markers

Microsatellites are short runs (usually less than 100 base pairs) of tandem repeats of a very simple DNA sequence, usually 1 to 4 base pairs [134]. Genotyping with microsatellite markers was introduced in 1989 [275] and due to their abundance and high degree of polymorphism they became the primary tool for genetic mapping during the 1990s.

Markers on 19p were chosen from the Généthon map [276] and fluorescently labelled microsatellite primers were ordered (ABI PRISM Linkage Mapping Set version 2.5). Microsatellite PCR reactions were performed according to the manufacturer's instructions with an annealing temperature of 55 °C. The PCR products were diluted and (either multiplexed or alone) loaded onto an ABI

PRISM 3730 Genetic Analyser. Raw sample files (FSA files using the ABIF binary file format) were generated and fragment genotyping analysis was performed with the ABI GeneMapper Software (version 4.1).

To further refine the candidate region, additional microsatellite primers were designed and labelled using a different approach, first described by Schuelke [277]. A sequence-specific forward primer with an M13(-21) tail at its 5′ end was designed. This oligonucleotide was subsequently added to the PCR mix together with a sequence-specific reverse primer and a FAM-labelled universal M13(-21) primer; amplification was carried out as previously described [277].

2.5 Bioinformatics

Despite the fact that computers were important tools in molecular biology a decade before DNA sequencing became feasible [278], the term bioinformatics was not used until 1978 when Dutch biologist Paulien Hogeweg coined the term as “the study of information processes in biotic systems” [279-281]. Today, bioinformatics is used to describe the application of computational tools and techniques to capture, manage and analyse biological data (figure 2-7). Bioinformatics main aims are [282-285]:

(a) To organise data in a way that allows researchers to access existing information and submit new entries.

(b) To develop tools and resources that aid in the analysis of data and interpretation of the results in a biologically meaningful manner.

Publically available bioinformatics databases and tools used in this study are summarised in table 2-5.

Table 2-5. Publically available bioinformatics databases and tools used in this study

Bioinformatics method:	**Link**
primer designing software	http://www.basic.northwestern.edu/biotools/oligocalc.html http://frodo.wi.mit.edu/primer3/
genomic databases and genome browsers	http://www.ensembl.org/ http://genome.ucsc.edu/ http://www.ncbi.nlm.nih.gov/sites/entrez?db=genome
DNA variation databases (accessed 20/11/2011 unless otherwise stated)	http://browser.1000genomes.org/index.html http://snp.gs.washington.edu/EVS/ http://www.ncbi.nlm.nih.gov/projects/SNP/ http://www.hgmd.cf.ac.uk/ac/ http://hapmap.ncbi.nlm.nih.gov/
tools for sequence alignment	http://www.ebi.ac.uk/Tools/clustalw2/ http://www.tcoffee.org/ http://genome.ucsc.edu/cgi-bin/hgBlat/
tools predicting impact of DNA variants on the structure and function of a protein	http://genetics.bwh.harvard.edu/pph2/ http://genetics.bwh.harvard.edu/pph/ http://sift.bii.a-star.edu.sg/ http://bg.upf.edu/group/projects/condel.php http://mmb2.pcb.ub.es:8080/PMut/ http://www.ncbi.nlm.nih.gov/Class/FieldGuide/BLOSUM62.txt http://www.fruitfly.org/seq_tools/splice.html http://www.cbs.dtu.dk/services/NetGene2/ http://rulai.cshl.edu/cgi-bin/tools/ESE3/esefinder.cgi http://cubweb.biology.columbia.edu/pesx/ http://genes.mit.edu/burgelab/rescue-ese/
expression databases and software modelling	http://www.genenetwork.org/ http://www.ncbi.nlm.nih.gov/dbEST/

gene regulatory dynamics and networks	http://www.ncbi.nlm.nih.gov/unigene http://neibank.nei.nih.gov/EyeSAGE/ http://omicspace.riken.jp/PosMed/ http://bioinfo.wilmer.jhu.edu/morenet/
tools for prediction of gene and protein structure and function	http://swissmodel.expasy.org/ http://www.pymol.org/ http://www.umass.edu/microbio/rasmol/ http://opm.phar.umich.edu/ http://www.ebi.ac.uk/Tools/InterProScan/ http://www.ebi.ac.uk/pdbsum/ http://www.pdb.org/pdb/home/home.do http://www.psipred.net/ http://pfam.sanger.ac.uk/ http://smart.embl-heidelberg.de/
tools for analysis of genome-wide genotyping data	http://bioinf.wehi.edu.au/software/linkdatagen/ http://www.sph.umich.edu/csg/abecasis/merlin/ http://pngu.mgh.harvard.edu/~purcell/plink/ http://dna.leeds.ac.uk/autosnpa/ http://www.affymetrix.com/estore/browse/level_seven_software_products_only.jsp?productId=131535&categoryId=35625#1_1 http://www.affymetrix.com/estore/browse/level_seven_software_products_only.jsp?productId=131408&categoryId=cat40006#1_1
tools for analyzing exome sequencing data	http://www.novocraft.com/main/page.php?s=novoalign http://bio-bwa.sourceforge.net/ http://samtools.sourceforge.net/ http://picard.sourceforge.net/index.shtml http://code.google.com/p/bedtools/ http://samtools.sourceforge.net/tabix.shtml http://vcftools.sourceforge.net/ http://www.openbioinformatics.org/annovar/ http://snp.gs.washington.edu/SeattleSeqAnnotation131/ http://www.broadinstitute.org/software/igv/ http://genomesavant.com/ http://compbio.charite.de/index.php/ibd2.html http://main.g2.bx.psu.edu/ ftp://ftp.ensembl.org/pub/current_fasta/homo_sapiens/dna/ http://www.ncbi.nlm.nih.gov/nuccore/251831106/ http://bzip.org/ http://www.r-project.org/ http://www.gnu.org/software/bash/
other	http://www.omim.org/ http://www.uniprot.org/ http://www.ensembl.org/biomart/ http://www.sph.uth.tmc.edu/retnet/ http://www.hgvs.org/mutnomen/ http://phenome.jax.org/ http://www.sanger.ac.uk/mouseportal/ http://www.komp.org/ http://www.proteinatlas.org/ https://putt.eng.uiowa.edu/ http://bioweb.pasteur.fr/phylogeny/intro-en.html http://www.open-bio.org/ http://www.bioconductor.org/ http://tools.neb.com/NEBcutter2/

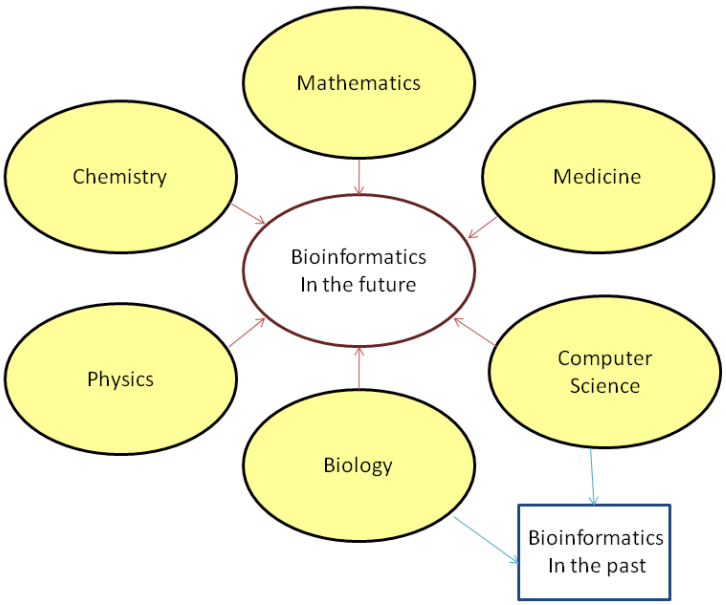

Figure 2-7. Disciplines related to bioinformatics. In the past bioinformatics focused on practical applications of informatics to genomics. As data-driven is replaced by principle-driven biology, bioinformatics will become a more fundamental discipline encompassing other fields of basic science (concept from [286]).

2.5.1 Primer Design

Primers were designed to avoid the known polymorphisms; their properties were evaluated with OligoCalc [287]. Typically, PCR primers (a) between 18 and 28 nucleotides long, (b) with GC content ideally between 50 and 60% and (c) with minimal hairpin loop formation and self-complementarity were chosen. All primer sequences were submitted to the NCBI BLAST site and the ones with more than 90% similarity with a nucleotide sequence of the human genome other than the target sequence were rejected. The two primers of a primer pair had closely matched melting temperatures (difference <5 °C). Amplimer length for standard PCR was up to 1,000 base pairs.

2.5.2 DNA Sequence Analysis

2.5.2.1 Sanger Sequencing Data

The Seqman Pro application (Lasergene version 8.02 sequencing analysis software suite, DNASTAR Inc., Madison, WI, USA) was used to assemble and analyse sequencing data (AB1 files). On occasion, the ABI Sequence Scanner

Software v1.0 or the Sequencher 4.10.1 (Gene Codes Corporation, Ann Arbor, USA) tools were utilised to inspect the raw signal data.

2.5.2.2 Exome Sequencing Data

Mining data sets generated from high-throughput sequencing platforms poses several hurdles for analysis and storage; thus high-performance computational infrastructure is essential [288]. A computer cluster optimised for many classes of computationally intense applications was used (UCL Genetics Institute cluster running OpenBSD 4.5, a unix-like operating system).

Raw sequencing data were shipped in a storage drive from BGI, Shenzhen, China. For each patient sample, two compressed (gzip) Solexa/Illumina FASTQ files [260] were received. Initially, a high-quality data compressor (bzip2 1.0.6) was used. Subsequently, the relatively short (~100 base pair), paired-end reads generated by the Illumina HiSeq2000 sequencer were aligned against a reference sequence [289]. The novoalign short-read mapper (v2.05 and v2.07, Novocraft, Selangor, Malaysia; arguably the most accurate aligner to date: http://lh3lh3.users.sourceforge.net/NGSalign.shtml) and the novoindex utility (Novocraft) were used. The g1k (NC_012920.1) version of the mitochondrial genome and the GRCh37.p5 human coverage assembly were combined into a reference sequence. A tab-delimited text file containing alignment information (SAM file format [290]) was generated for each pair of FASTQ files. SAM files were then imported into the SAMtools software package [290], converted into a highly compressed binary form (BAM files created), sorted and had duplicate reads removed (using Picard's MarkDuplicates tool with REMOVE_DUPLICATES option). The resulting file was indexed (BAI file created) and the output was one _sorted_unique.bam file with its respective _sorted_unique.bam.bai file for each sequenced sample.

BAM is a key file format separating the alignment step from downstream analysis enabling a "generic or modular approach to the analysis of genomic

sequencing data" [290]. Importantly, most assembly programs and alignment tools directly produce SAM/BAM files and the space-efficient BAM format is routinely used for storing and sharing raw high-throughput sequencing data [291].

Each BAM file was imported in a number of alignment viewers (including Savant [292] and IGV [293]); these tools allow to visually understand the alignment and validate variant calls and structural variation. Other downstream analysis of BAM files included obtaining index statistics (*e.g*. count of aligned and unaligned reads; Picard's BamIndexStats tool was used) or mapping statistics (*e.g.* coverage in the targeted/exome regions; Picard's CalculateHsMetrics tool was used) and producing pileup datasets (using SAMtools pileup option). In the pileup format, each line represents a genomic position, consisting of chromosome name, coordinate, reference base, read bases, read qualities and alignment mapping qualities. Notably, information on match, mismatch, insertions-deletions and mapping quality are encoded at the read base column (http://samtools.sourceforge.net/samtools.shtml). Processing the resulting pileup files with SAMtools enabled calling single nucleotide variants and short insertions-deletions as well as storing them in tab-delimited text files (VCF file format [294]); functional annotation of detected genetic variation was performed by processing these VCF files with the ANNOVAR tool [295]. Finally, sequential filtering of variants was carried out using R scripts or spreadsheet applications.

Most software used (bzip2, novoalign, SAMtools, Picard and ANNOVAR) have been designed to work on a stream. Consequently, several commands were combined in unix pipes. The reference pipeline code (in bash) was written by Dr Vincent Plagnol under whose supervision all the exome sequencing data analysis was performed.

2.5.3 Expression Analysis Databases

Expression of genes can be tested by RT PCR followed by Sanger sequencing, whole transcriptome shotgun sequencing (RNA-Seq), Northern blotting, *in situ* hybridization against mRNA in tissue section, SAGE and expression microarrays. Furthermore, immunohistochemistry using labelled antibodies is a widely used method to assess protein expression in different parts of a biological tissue.

From a list of genes within a chromosomal region identified by linkage, one would look for a gene that shows appropriate expression and/or appropriate function. Genes paralogous or orthologous to a relevant gene should also be tested [134].

To assist selection and prioritisation of genes for mutation screening, an SQL database has been created. In general, genes preferentially or specifically expressed in the retina or knowingly associated with retinal disease have been included. The database contains the Retinal Information Network dataset (http://www.sph.uth.tmc.edu/retnet/) and results from experiments using either DNA microarrays or SAGE to analyse expression patterns [296-314]. Data from experiments using chromatin immunoprecipitation followed by high-throughput sequencing (ChIP-seq) to identify binding sites for the transcription factor *CRX* across the mouse genome (genome-wide protein-DNA interaction or *cis*-regulatory mapping) [315] have also been included in the devised database.

Further to the database, four different datasets were queried:
(a) dbEST (http://www.ncbi.nlm.nih.gov/dbEST) [316]: a database of over eight million deposited expressed sequence tags (generated by RT PCR and cDNA sequencing) from human tissue.
(b) The EyeSAGE database (http://neibank.nei.nih.gov/EyeSAGE/) [297]: a database summarising the results from SAGE experiments [317] on donor

eyes; frequency data for genes expressed in retina, RPE, macular and peripheral retinal tissue are included.

(c) Genenetwork (http://www.genenetwork.org): a database of mouse phenotypes including the levels of expression of several genes in the retina (generated by expression microarrays) [318]. Often genes of similar function or genes involved in the same biochemical pathway have expression levels that are tightly correlated in different mouse strains.

(d) Positional Medline (http://omicspace.riken.jp/PosMed) [319] a database that interrogates pubmed (http://www.ncbi.nlm.nih.gov/pubmed/) for occurrences of both search terms and all genes within a specified genomic region.

2.5.4 Genome-wide Genotyping Data Analysis

Primary data (CEL files) analysis was performed with the Genotyping Console Software (Affymetrix). Either the BRLMM (for the Affymetrix GeneChip Human Mapping 50K Array Xba; http://array.mc.vanderbilt.edu/microarray/dna/brlmm.pdf) or the birdseed v2 (for the Affymetrix Genome-Wide Human SNP Array 6.0; http://www.broadinstitute.org/mpg/birdsuite/birdseed.html) algorithm was used to genotype SNP data; the canary algorithm was used for copy number data [320].

For SNPs, a call confidence score threshold was set (typically ≤0.01) and genotyping results were exported to a comma-separated values (CSV) file for further analysis. For copy number probes, analysis was performed on the Chromosome Analysis Suite (ChAS) software (Affymetrix).

2.5.4.1 Excel visual basic

A macro was written by Dr Andrew R Webster in Visual Basic programming language within the Microsoft Excel spreadsheet application (Microsoft, Redmond, WA). Detection of genomic regions of shared haplotype

(homozygosity) and regions of linkage in family data as well as sex checks based on X chromosome SNPs and testing for non-Mendelian transmission were enabled.

2.5.4.2 Perl

The aforementioned macro code (section 2.5.4.1) was translated to Perl programming language (v5.12; http://www.perl.org/) and further enriched. In the Perl version, after a threshold of consecutive SNPs fitting a certain criterion (homozygosity or linkage) is set, regions of interest and a results summary table are automatically exported into a spreadsheet format (XLS file).

Perl is a flexible, high-level, general-purpose, interpreted, dynamic programming language that borrows features from C and is extensively used in bioinformatics. It has become popular with biologists because it is well-suited to several bioinformatics tasks [321]: (a) it has a well supported biological suite, (b) it has an extensive library of modules to support bioinformatics/ genomics work (BioPerl, http://bioperl.org/; http://www.cpan.org/) [322] and (c) it can be integrated with other languages such as R and C (both of which are common in bioinformatics).

2.5.4.3 Python

In order to be able to analyse the large amount of SNP data generated by the Affymetrix Genome-Wide Human SNP 6.0 Arrays, an approach skipping the initial processing in a spreadsheet application and indexing the data was necessary. Due to the first step being the merging of selected columns from the appropriate annotation files (available in http://www.affymetrix.com/) with the genotyping data (AA, AB, BB, NoCall), processing in a database environment was required. MySQL (www.mysql.com), a relational database management system that runs as a server providing multi-user access to a

number of databases [323], was used to store and annotate the data. A python (www.python.org/) script interacting with a MySQL database and allowing identification of regions of homozygosity or linkage was composed (section 6.2). The program is running on a Ubuntu 10.04 Linux machine with python 2.6.5, MySQL 5.1 and a python-mysqldb 1.2.2-7ubuntu1 module.

Python (www.python.org/) is a general-purpose, high-level programming language whose design philosophy emphasizes code readability [324]. Python's collection of modules intended for bioinformatics (BioPython, http://biopython.org/) was founded in 1999, four years after BioPerl.

3 RESULTS

3.1 Screening Genes Knowingly Associated with Retinal Disease

3.1.1 Mutation Detection

Once the first links between a list of genes and a list of well recognised clinical entities have been drawn, attention must turn to identifying genotypically homogeneous groups of patients and carefully obtaining information on their phenotype. Over the last two decades a wide variety of mutations in a number of different genes have been shown to cause dysfunction and premature death of the photoreceptor cells. However, as we are still in the early days of practical genetic tests, the “boundaries that are inherent in focused prospective studies funded by research organizations” [325] have not been broken and our knowledge of the phenotype and clinical course of inherited retinal disorders is still limited.

One part of this study aims to review and take advantage of the knowledge accumulated so far in order to examine small portions of the retinal disease-associated gene set (RetNet) in carefully selected groups of patients (*e.g. NYX, GRM6, TRPM1* in individuals with CSNB). Once a sequence variant had been identified and statistically significantly associated with disease, the consequences on retinal function and structure were investigated in the light of this new information. Clinical observations of genetically similar patients were pooled and data on variability (phenotypic range) and natural history of disease were generated.

Understanding and, ultimately, predicting the downstream events that occur in response to a specific genotype is invaluable for two main reasons. Firstly, counselling and prognosis: specific outcomes can be predicted years before they occur. Secondly, treatment: better design of clinical therapeutic trials,

better judgement of the risk/benefit ratio of treatment and more informed interpretation of the therapeutic benefits are enabled.

Over twenty genes previously reported to be associated with recessive retinal disease have been sequenced in selected panels of patients; many likely disease-causing variants have been detected and the retinal phenotype of subjects with biallelic changes has been characterised. These results are discussed in this chapter (sections 3.1.2, 3.1.3, 3.1.4, 3.1.5, 3.1.6 and 3.1.7) and have contributed to published (*MFRP, MERTK, CRB1, C2ORF71, RDH5, KCNV2, GRM6, OAT*) [326-331] or under preparation (*CYP4V2, NR2E3*) manuscripts.

Likely disease-associated variants identified as part of this study can be found in table 3-1. Mainly biallelic changes with convincing pathogenic effect (previously reported or segregating with disease and not identified in control DNAs) are included.

Table 3-1. Summary of knowingly associated with retinal disease genes screened and pairs of likely disease-associated variants identified.

Gene	Allele 1	Reference	Proven or Presumed Allele 2	Reference
CRB1 OMIM 604210	c.2401A>T, p.Lys801X	den Hollander *et al. [332]*	c.3320T>C, p.Leu1107Pro	Hanein *et al.* [333]
	c.2843G>A, p.Cys948Tyr	den Hollander et al. [334]	c.2688T>A, p.Cys896X	Hanein *et al.* [333]
	c.2843G>A, p.Cys948Tyr	den Hollander et al. [334]	c.2955insAG, p.Asn986AlafsX2	novel
	c.2843G>A, p.Cys948Tyr	den Hollander et al. [334]	c.727_743delCTGGGG GCCTATTTCT, p.Leu243AlsfsX50	novel
	c.2843G>A, p.Cys948Tyr	den Hollander et al. [334]	c.936T>G, p.Asn312Lys	novel
	c.2506C>A, p.Pro836Thr	den Hollander *et al. [332]*	c.470G>C, p.Cys157Ser	novel
	c.584G>T, p.Cys195Phe	den Hollander *et al. [332]*	c.3442C>T, p.Cys1148Arg	novel
	c.584G>T, p.Cys195Phe	den Hollander *et al. [332]*	*not identified*	
	c.2842+5G>A	den Hollander et al. [334]	*not identified*	
KCNV2 OMIM 607604	c.1381G>A, p.Gly461Arg	Thiagalingam *et al.* [335]	c.377T>A, p.Leu126Gln	Wu *et al.* [175]
	c.1381G>A, p.Gly461Arg	Thiagalingam *et al.* [335]	c.966G>C, p.Ala322Pro	novel
	c.451T>C, p.Phe151Leu	novel	*not identified*	
	c.1199delT, p.Phe400fsX53	novel	c.8_11delAACA, p.Lys3fsX93	novel
	c.568delG, p.Gly189fsX21	novel	c.568delG, p.Gly189fsX21	novel
	c.1318C>T, p.Asn439Ile	novel	c.1318C>T, p.Asn439Ile	novel

NR2E3 OMIM 604485	c.119-2A>C	Haider *et al.* [336]	c.119-2A>C	Haider *et al.* [336]
	c.119-2A>C	Haider *et al.* [336]	c.767C>A, p.Ala256Glu	Sharon *et al.* [337]
	c.119-2A>C	Haider *et al.* [336]	c.1018G>A, p.Glu340Lys	novel
	c.932G>A; p.Arg311Gln	Haider *et al.* [336]	c.1112C>G, p.Leu371Trp	novel
	c.572-2A>C	novel	c.572-2A>C	novel
	c. 646G>A, p.Gly216Ser	novel	c. 646G>A, p.Gly216Ser	novel
	c.166G>A, p.Gly56Arg	Coppieters *et al*. [338]	Dominant inheritance	
GRM6 OMIM 604096	c.2122C>T, p.Gln708X	Dryja *et al.* [157]	c.1054C>T, p.Arg352Cys	novel
	c.2029C>T, p.Arg677Cys	novel	c.2029C>T, p.Arg677Cys	novel
	c.2030G>A, p.Arg677His	novel	c.2030G>A, p.Arg677His	novel
	c.712C>T, p.Arg238X	O'Connor *et al.* [339]	c.2029C>T, p.Arg677Cys	novel
	c.2267G>A, p.Gly756Asp	novel	c.2267G>A, p.Gly756Asp	novel
	c.575delG, p.Val193fsX15	novel	c.575delG, p.Val193fsX15	novel
	c.823G>A, p.Gly275Asp	Zeitz *et al.* [340]	c.2062delC, p.Pro689fsX24	novel
TRPM1 OMIM 603576	c.220C>T, p.Arg74Cys	novel	c.3004A>T, p.Ile1002Phe	novel
RDH5 OMIM 601617	c.712G>T, p.Gly238Trp	Yamamoto *et al.* [149]	c.712G>T, p.Gly238Trp	Yamamoto *et al.* [149]
	c.712G>T, p.Gly238Trp	Yamamoto *et al.* [149]	c.310+1 G>A	novel
	c.346_348insGCA, p.Gly116_Ile117insSer	novel	c.346_348insGCA, p.Gly116_Ile117insSer	novel
	c.346G>C, p.Gly116Arg	novel	c.710A>C, p.Tyr237Ser	novel
RLBP1 OMIM 180090	c.12+2delT	novel	c.141+2T>C	novel
	c.346+3delG	novel	*not identified*	
CYP4V2 OMIM 608614	c.998C>A, p.Thr333Lys	novel	c.998C>A, p.Thr333Lys	novel
	c.283G>A, p.Gly95Arg	Shan *et al.* [341]	c.637_641delAGTAA, p.Ser213X	novel
	c.792-8_del17insGC	Lai *et al.* [342]	c.792-8_del17insGC	Lai *et al.* [342]
	c.792-8_del17insGC	Lai *et al.* [342]	*not identified*	
CNGA3 OMIM 600053	c.1279C>T, p.Arg427Cys	Wissinger *et al*. [343]	c.1279C>T, p.Arg427Cys	Wissinger *et al*. [343]
	change found in homozygous state in an unaffected member of the family			
	c.1688G>A, p.Arg563His	Wissinger *et al*. [343]	c.106_109delCACT, p.His36fs	novel
CNGB3 OMIM 605080	c.1208G>A, p.Arg403Gln	Michaelides *et al.* [344]	c.1208G>A, p.Arg403Gln	Michaelides *et al.* [344]
	c.1208G>A, p.Arg403Gln	Michaelides *et al.* [344]	c. 1908G>T, p.Arg636Ser	novel
LCA5 OMIM 611408	c.835C>T, p.Gln279X	den Hollander *et al.* [345]	c.1756A>T, p.Lys586X	novel
CEP290 OMIM 610142	c.2991+1655A>G, p.Cys998X	den Hollander *et al*. [346]	c.5254C>T, p.Arg1752Trp	novel
MFRP OMIM 606227	c.492delC, p.Asn167ThrfsX25	Sundin *et al.* [347]	c.492delC, p.Asn167ThrfsX25	Sundin *et al.* [347]
	c.492delC, p.Asn167ThrfsX25	Sundin *et al.* [347]	c.1622_1625 delTCTG, p.Val541AlafsX188	novel
CLRN1 OMIM 606397	c.144T>G, p.Asn48Lys	Adato *et al.* [348]	c.144T>G, p.Asn48Lys	Adato *et al.* [348]
RP1L1 OMIM 608581	c.133C>T, p.Arg45Trp	Akahori *et al.* [349]	Dominant inheritance	
GPR143 OMIM 300808	c.793 C>T, p.Arg245X	Schnur *et al.* [350]	X-linked inheritance	

3.1.2 A Study of DNA Sequence Variation in the *C2ORF71* Gene

In 2009 Baye *et al.* [351], followed by Nishimura *et al.* [352] and Collin *et al.* [353], used linkage analysis to identify missense and truncating mutations in the *C2ORF71* gene in five families affected with autosomal recessive retinal dystrophy. Three additional families were subsequently reported [354-355]. Most affected individuals in these reports had adult-onset rod cone dystrophy [352-354]. Nevertheless, early-onset disease [354], a cone rod pattern of dysfunction [353, 355] and considerable intra-familial variability with both childhood-onset and adult-onset disease [352] have also been described.

Human *C2ORF71* is a two exon gene spanning a 12.5 kb region on 2p23. The gene is conserved in vertebrates and, in human, it encodes a 1288-amino-acid, photoreceptor-specific protein. Subcellular localisation is hypothesised to be within the outer segment and/or the connecting cilium of the photoreceptor cells [352]. C2ORF71 function remains unknown. The gene does not contain any known functional domains but does include motifs suggesting that the encoding protein may undergo post-translational lipid modification [352]. From the expression patterns in the developing mouse eye, *C2ORF71* is presumed to play a role in retinal development [353].

In this section, HRM (section 2.4.15) was combined with PCR and Sanger sequencing (sections 2.4.9 and 2.4.16) to perform *C2ORF71* variation analysis in a cohort of probands with various forms of autosomal recessive retinal degeneration and controls.

3.1.2.1 Methods

3.1.2.1.1 Subjects

(also see sections 2.1.5 and 2.1.2)

Overall, 286 unrelated affected individuals were evaluated for DNA variants; 95 of these were affected with LCA or autosomal recessive childhood-onset retinal dystrophy. The remaining 191 individuals had a diagnosis of autosomal recessive adult-onset rod cone or cone rod dystrophy. DNA from 151 European and 40 South Asian control individuals with normal vision was also screened. Parental DNA was tested to determine the phase of interesting variants.

3.1.2.1.2 Genetic analysis

Amplimers were designed to cover the two previously reported exons (NM_001029883.1). Two methods of mutation screening were utilised. On the basis of the reported polymorphisms in *C2ORF71* at the time of the experiment design (18 polymorphic sites, NCBI dbSNP130 database, accessed November 2009) amplimers were divided in two groups:
(a) Four out of ten amplimers (group 1), covering two or more polymorphic sites each, were amplified by PCR and mutation analysis was performed by direct sequencing of all PCR products (sections 2.4.9 and 2.4.16).
(b) Six out of ten amplimers (group 2), covering one or no polymorphic sites each, were analysed using PCR (with highly saturating fluorescent dye), HRM analysis and Sanger sequencing (sections 2.4.15 and 2.4.16).

To avoid false positive results, DNA variants within group 2 fragments identified in less than three control or patient DNA samples were confirmed by independent regular PCR followed by direct sequencing.

3.1.2.1.3 Genetic variation quantification

As a large amount of DNA sequence alterations were being identified, it was deemed appropriate to quantify coding sequence variation and allelic complexity of *C2ORF71* and compare it with other genes. The total expected amount of heterozygosity and its number density per nucleotide were used as

measures of genetic variation. Expected heterozygosity (h_E) is defined as the probability of an individual being heterozygous at a site. The probability of heterozygosity at a site equals one minus the probability of homozygosity for each allele. The individual probabilities from *m* randomly associated sites can be algebraically summed to give a total value of heterozygosity in a sample. Its value assuming Hardy-Weinberg equilibrium is:

$$\sum_{j=1}^{m}(1-\sum_{i=1}^{n}p_{ij}^{2})$$

where p_{ij} denotes the prevalence of the i^{th} of *n* alleles (maximum of two alleles per site in this case) at the j^{th} of *m* sites. The total heterozygosity density per nucleotide is equal to the average heterozygosity $\hat{H}$ as defined by Nei and Roychoudhury [356]:

$$\hat{H}=\sum_{j=1}^{m}h_j/m=\sum_{j=1}^{m}(1-\sum_{i=1}^{n}p_{ij}^{2})/m$$

where h_j denotes the expected heterozygosity at the j^{th} of *m* sites.

On the assumption of the standard neutral model and taking into account the many sites tested, the low average MAF of the detected polymorphisms and the large number of control subjects, $\hat{H}$ of a sample of controls estimates the expected average heterozygosity in a population and is a good measure of genetic variability, comparable to nucleotide diversity (π) [357-358] and Watterson's estimate (θ_w) [359].

3.1.2.2 Results

A total of 40 DNA sequence variants were identified (table 3-2). A number of changes that are not reported in dbSNP130 were detected: (a) 17 (eight missense, seven synonymous, one three base pair deletion and one two base pair insertion-deletion) of them were found in controls; (b) the remaining 11 (six missense, five synonymous) were found in 20 alleles of 19 affected individuals (3.5% of all patient alleles) and not in controls. No truncating variants were identified. Two missense changes, p.Pro177Leu and

p.Glu227Lys, were identified in a recessive RP patient *in trans*. Segregation analysis revealed her unaffected father to be homozygous for p.Glu227Lys (figure 3-1B). Multiple primer pairs were used to exclude allele-specific amplification caused by a variant underlying the primer. All *C2ORF71* DNA variation identified in the cohort of 286 patients and 191 controls screened is summarised in table 3-3.

Table 3-2. Overview of variants in *C2ORF71* identified in patient and control DNAs

Type of change	**Controls** (n=191)	**Patients** (n=286)	**Total**
Synonymous	12	5	***17***
Missense	14	6	***20***
Other	3 (1x delCAinsAG 1x delCCC 1x dupAGC)	0	***3***
Total	***29***	***11***	***40***

The proportion of polymorphic sites in *C2ORF71* was found to be 5% (64/1288). The mean expected heterozygosity of the coding region in unaffected control subjects was 2.728 (value for affected individuals: 2.48). Therefore, on average, 2.728 nucleotides will differ in the *C2ORF71* sequence of two randomly chosen chromosomes of the population. The probability of each nucleotide being nonidentical between two randomly chosen control subject sequences is approximately the average hetrozygosity $\hat{H}$ and in *C2ORF71* equals 21.18×10^{-4} (19.26×10^{-4} in affected individuals). Consequently, if two chromosomes have been chosen at random, a sequence variation would have been identified every 472 base pairs. These values are higher than those of *BEST1* (0.14 sites, 0.8×10^{-4} sites per nucleotide), *EFEMP1* (0.003 sites, 0.03×10^{-4} sites per nucleotide) and *ABCA4* genes (1.28 sites, 1.8×10^{-4} sites per nucleotide) in unaffected subjects [360] suggesting that the *C2ORF71* coding sequence is more variable in the control population.

.

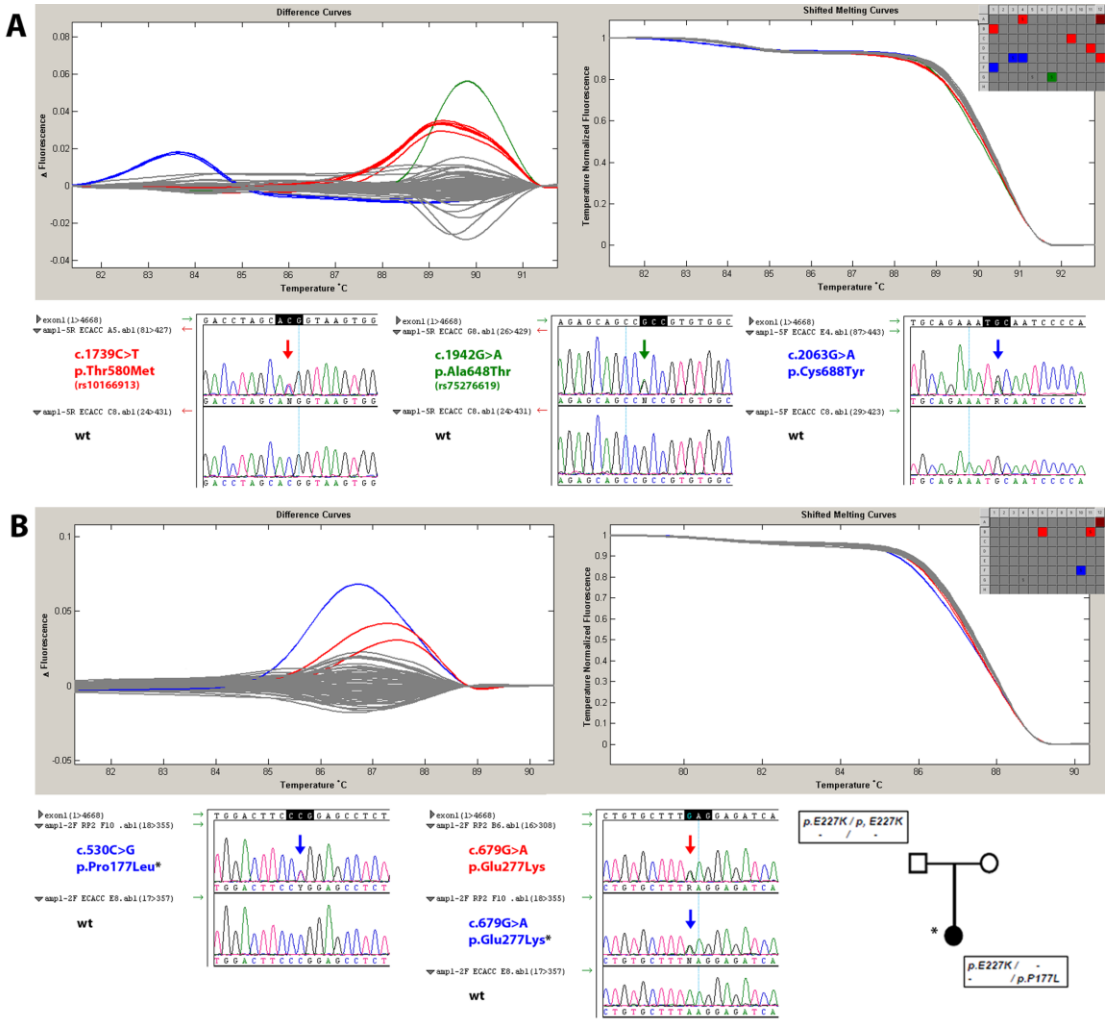

Figure 3-1. Normalised melting curve and difference plots and electropherograms generated by downstream sequencing of the amplified product.
[A] Amplimer 1_5 for European control plate 1: two clusters of samples (blue and red groups) and one isolated sample (green group) demonstrate melting difference plots significantly deviating from the majority of control DNAs screened in the plate (grey group). When sequenced, samples from the same group contained the same missense change in heterozygous state (c.1739C>T, p.Thr580Met for the red group; c.2063G>A, p.Cys688Tyr for the blue group and c.1942G>A, p.Alal648Thr. for the green group).
[B] Amplimer 1_2 for RP panel plate 2: three samples demonstrate differences in fluorescence compared to the majority of the examined samples. Sequencing revealed two samples being heterozygous for c.679G>A, p.Glu277Lys (red group) and one sample being compound heterozygote for c.530C>G, p.Pro177Leu and c.679G>A, p.Glu277Lys (blue group). None of those two changes was identified in the control DNA panels studied. Family members of the patient in the blue group were screened with unaffected father being homozygous for c.679G>A, p.Glu277Lys

Table 3-3. Summary of *C2ORF71* sequence variants; predicted impact on C2ORF71 protein and frequency in patients and controls**.**

DNA Variants			SIFT		PolyPhen and PolyPhen-2				Frequency in (chromosomes)	
Nucleotide	Protein	dbSNP130	Prediction	Tolerance Index (0-1)	Prediction§		PSIC Score Difference (0-4)	Hum Div Score (0-1)	Controls	Patients
					Ver1	Ver2				
c.37A>T	p.Ser13Cys	rs10084168	intolerant	0.01	POS		1.548	0.774	0/364	1/572
c.60G>A	p.(=)	rs35929540			*not applicable*				82/364	101/572
c.99G>A	p.(=)				*not applicable*				1/364	2/572
c.158 C>T	**p.Ala53Val**		tolerated	0.26	Benign		1.129	0.022	0/364	1/572
c.258G>A	p.(=)	rs62132765			*not applicable*				77/364	111/572
c.530C>T	**p.Pro177Leu**		intolerant	0.00	POD		2.550	0.999	0/382	1/572
c.531G>A	**p.(=)**				*not applicable*				0/382	1/572
c.679G>A	**p.Glu227Lys**		intolerant	0.01	Benign	POD	1.409	0.949	0/382	3/572
c.1262A>G	p.Lys421Arg	rs17007544	tolerated	0.47	Benign	POS	1.047	0.665	3/190	0/572
c.1387G>T	p.Val463Phe		tolerated	0.05	Benign	POS	1.284	0.375	1/190	1/572
c.1452C>T	p.(=)	rs13385188			*not applicable*				81/190	153/572
c.1739C>T	p.Thr580Met	rs10166913	intolerant	0.01	POS		1.665	0.798	5/190	0/572
c.1844T>A	**p.Val615Asp**		tolerated	0.40	POS	POD	1.970	0.925	0/190	1/572
c.1942G>A	p.Ala648Thr	rs75276619	tolerated	0.59	Benign		0.211	0.022	1/190	11/572
c.2063G>A	p.Cys688Tyr		tolerated	0.52	POD		2.938	0.996	3/190	0/572
c.2112T>C	p.(=)	rs10200693			*not applicable*				123/380	168/572
c.2234G>A	p.Arg745Lys		tolerated	0.92	Benign	POS	1.132	0.788	1/380	0/572
c.2374C>G	p.Leu792Val	rs17744093	tolerated	0.30	Benign	POS	1.017	0.426	66/380	103/572
c.2406A>G	p.(=)				*not applicable*				1/380	1/572
c.2498C>T	**p.Pro833Leu**		intolerant	0.01	POD		2.550	0.994	0/380	1/572
c.2499G>A	p.(=)	rs34253433			*not applicable*				70/380	106/572
c.2502T>C	**p.(=)**				*not applicable*				0/382	1/572
c.2600C>T	p.Pro867Leu		tolerated	0.72	Benign		0.213	0.20	1/380	2/572
c.2864G>A	p.Arg955Gln		tolerated	0.81	Benign		0.192	0.192	1/190	0/572
c.2875G>A	p.Ala959Thr		tolerated	0.23	Benign		0.995	0.109	2/190	1/572
c.2889C>T	p.(=)				not applicable				2/190	3/572
c.3037C>G	p.Pro1013Ala		tolerated	0.23	POD		2.100	0.908	1/372	0/572
c.3058_3059 delCAinsAG	p.Gln1020Arg		tolerated	0.52	Benign		0.900		2/372	3/572
c.3264_3266 delCCC	p.Pro1089del				*not applicable*				1/372	6/572
c.3291G>A	p.(=)				*not applicable*				1/372	3/572
c.3395A>C	p.Glu1132Ala	rs78874550	tolerated	0.32	Benign		1.350		1/174	1/572
c.3447G>A	p.(=)				*not applicable*				1/174	5/572
c.3522C>T	p.(=)				*not applicable*				1/174	2/572
c.3609G>A	**p.(=)**				*not applicable*				0/174	1/572
c.3626A>G	**p.Asp1209Gly**		tolerated	0.43	POS		1.575		0/174	1/572
c.3673_3675dup3		rs72183347, rs72122505			*not applicable*				43/300	84/572
c.3739G>A	p.Gly1247Ser		tolerated	1.00	Benign		0.225		3/300	4/572
c.3780C>T	**p.(=)**				*not applicable*				0/300	1/572
c.3789G>A	p.(=)				*not applicable*				1/300	4/572
c.3840G>A	**p.Ala1280Ala**				*not applicable*				0/300	2/572

3.1.2.3 Comment

To improve molecular testing of retinal genes in panels of affected individuals and controls the advances of HRM technology were exploited. To date, over 60 genes have been analysed by this method including *ABCA4* [361-362]. In this study, HRM analysis using the LightScanner System was utilised to study the parts of the *C2ORF71* sequence containing one or no reported polymorphisms (dbSNP130). Standard PCR and Sanger sequencing were performed in the remaining amplimers as the presence of three or more polymorphic sites could potentially hinder the analysis and interpretation of melting curves.

HRM had previously been markedly efficient in detecting heterozygous variants and is widely used as a method to detect carriers in *BRCA1* and *BRCA2* genes [363-364]. For heterozygous sequence alterations, sensitivity and specificity approach 100% for all categories of substitution as well as insertions and deletions small enough to be amplified by PCR (reviewed by Taylor [365]). Such variants are detectable at any location in the PCR amplimer, including those within a few base pairs of the primers [366]. Homozygous changes are harder to distinguish from wild-type sequence and 16% of SNPs demonstrate minimal or no differences between the melting temperatures of the two homozygous states [361]. Compared with the wild-type sequence, most homozygous changes produce a melting temperature shift with symmetric melting transitions [367-368] whereas heterozygous samples are identified by differences in melting curve shape (distortion) with a more gradual, complex transition [246, 369-370]. Only one sequence alteration (c.1452C>T) was detected in homozygous phase in the *C2ORF71* amplimers analysed with HRM. The low carrier frequency of the remaining 16 heterozygous changes could explain the absence of homozygotes (x^2 test). Despite the fact that the average coefficient of inbreeding in the studied cohorts is likely to be low, it may still be possible that a homozygous change could not be detected with the method used.

Common variants may be recognised by characteristic melting patterns [371] although this is debated [365]. In this study, common polymorphisms were identified by melting curve identity and rare sequence variants by sequencing. On average, 12% (11 samples) of each 96-well plate was sequenced; numbers widely varied between amplimers and runs. Unnecessary downstream sequencing was generated by HRM false positive results. Importantly, on one occasion, a false positive result could not be resolved by sequencing directly after HRM analysis (figure 3-2). Independent regular PCR followed by Sanger sequencing revealed that both patients, initially tagged as heterozygotes for a p.Pro1083Leu mutation, were wild-type. It can be speculated that this substitution occurred due to a "hot spot" for polymerization errors in the sequence of the target DNA [372]. This observation resulted in modification of study design: all variants identified in three or less patient or control samples were independently amplified and sequenced.

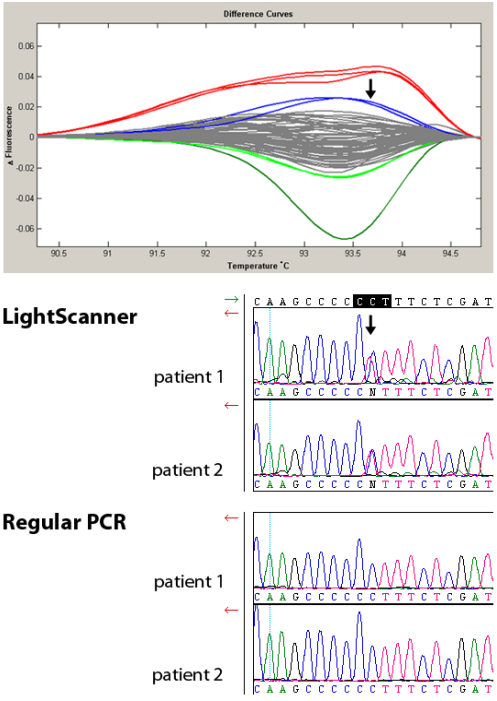

Figure 3-2. Melting curve difference plots for amplimer 1_8 in LCA panel are presented. Among the different groups, two samples with similar melting behaviour can be observed (blue group). Electropherograms of amplimer 1_8 in those two individuals affected with LCA were generated. Rows 1 and 2 are the result of sequencing the product of amplification using HRM protocol while rows 3 and 4 show the same samples amplified through normal PCR. A c.3248C>T, p.Pro1083Leu variant was suspected initially but could not be confirmed in either patient.

During the study it became evident that the total number of *C2ORF71* sequence variants discovered in controls or reported in dbSNP130 (48 in total) was disproportionately greater compared to other retinal genes even without accounting for gene size. However, analysing the proportion of polymorphic nucleotides does not assess how variable the coding sequence of the gene is in a population. This is more obvious in *C2ORF71* as most sequence alterations were found to have small minor allele frequencies. Average heterozygosity ($\hat{H}$) was used to

summarise variation as a function of both the number of polymorphic sites and their frequencies in the population. $\hat{H}$ calculates the probability of nonidentity of two randomly chosen chromosomal sites [356]. *C2ORF71* demonstrated greater genetic variability compared to *BEST1, EFEMP1* and ABCA4 [360].

Comparison of the C2ORF71 peptide sequence with its orthologs revealed minimal conservation. Notably, multiple “islands” of conserved sequence are observed between amino acids 173 and 359. Four out of seven previously reported mutations (p.Gln186X [353], p.Ile201Phe [351-352], p.Asn316MetfsX5 [353] , p.Trp253X [352]) fall within this 173-359 interval. No polymorphisms in this region were detected in the control DNA panels studied and only an unaffected parent was found homozygous for a p.Glu227Lys change. Other regions, completely conserved between species, included the first 3 amino acids of the protein and amino acids 830 to 834. The significance of complete conservation of glycine at position two and cysteine at position three (G2/C3), a motif subject to lipid modification, also found in *RP2*, has been investigated by Nishimura *et al.* [352]. In the region between amino acids 830 and 834, three variants were identified: a known polymorphism, c.2499G>A, p.(=) (rs34253433); a missense change, c.2498C>T, p.Pro833Leu, in one LCA patient; and a silent change, c.2502T>C, p.(=), in another LCA patient. All three were only identified in the heterozygous state; no second change was identified in either of the two affected individuals.

C2ORF71 does not harbour any known functional domains and results from protein analysis tools (section 2.5) were negative. The region between amino acids 176 and 331 is predicted as a potential globular domain by GlobProt [373] but this might be falsely positive because of the conservation observed in this region. A region of compositional bias is described in UniProt (http://www.uniprot.org/uniprot/A6NGG8) with proline being over-represented within the subsection between amino acids 1013 and 1095. There is little functional knowledge on COOH-terminal PRDs. Importantly, PRDs are implicated in a number of aberrant protein interactions and certain protein-interaction domains prefer ligand sequences that are proline-rich [374].

Recently, a PRD in a microtubule-associated protein, mainly existing in neurons, has been shown to mediate interactions with actin [375]. The photoreceptor connecting cilium contains clusters of actin [376] and previous work suggests interaction of C2ORF71 with the connecting cilium [352]. A number of genes like *TULP1* [377] and *MYO7A* [378] interacting with actin are also associated with nonsyndromic or syndromic RP.

HRM and Sanger Sequencing were utilised to detect mutations in *C2ORF71* and the technical challenges of screening a polymorphic gene with numerous rare variants were encountered. The high degree of genetic variability was quantified and the implications of the polymorphic site distribution were interrogated. There was no convincing evidence that biallelic mutations in *C2ORF71* were responsible for the retinal degeneration in any of the 286 families tested. *C2ORF71* variants must therefore be a rare cause of RP.

3.1.3 Nonsense Mutation in *SAG* Causes Oguchi Disease

The *SAG* gene encodes S-antigen, a visual/*β* arrestin abundant in rod photoreceptor cells. S-antigen binds to light-activated rhodopsin preventing further interaction with transducin during the recovery phase of phototransduction [379-381]. Mutations in *SAG* are primarily associated with Oguchi disease, a rare autosomal recessive form of CSNB characterised by yellow-gold discolouration of the fundus that disappears in the dark-adapted state and reappears shortly after the onset of light (Mizuo phenomenon) [382-383]. Typically patients with mutations in *SAG* have no obvious signs of photoreceptor degeneration [384]. However, significant inter- and intra-familial phenotypic variability have been described and a number of cases with biallelic *SAG* mutations developing RP have been reported [385-388].

The clinical and electrophysiological findings in a case of Oguchi disease harbouring a homozygous nonsense mutation in *SAG* (c.874C>T, p.Arg292X) are presented. *SAG* screening (NM_000541.4) was performed by Dr Alice E Davidson using standard PCR and Sanger sequencing (sections 2.4.9 and 2.4.16). The proband was a 7-year-old girl of South Asian origin referred for evaluation of congenital nyctalopia. Visual acuity was 0.12 logMAR in each eye. Fundus examination revealed widespread golden discolouration and peripheral RPE mottling (figure 3-3A). Fundus autofluorescence imaging was normal (figure 3-3B). SD OCT is presented in figure 3-3C. In the foveola, three hyperreflective bands representing the IS/OS junction of the photoreceptors, the cone outer segment tips and the RPE/Bruch's membrane complex are visible. Outside the fovea, the hyporeflective band corresponding to the outer segments is not apparent. These findings were consistent on three different tests over a one year interval. SD OCT of an age-matched control is also presented in figure 3-3D.

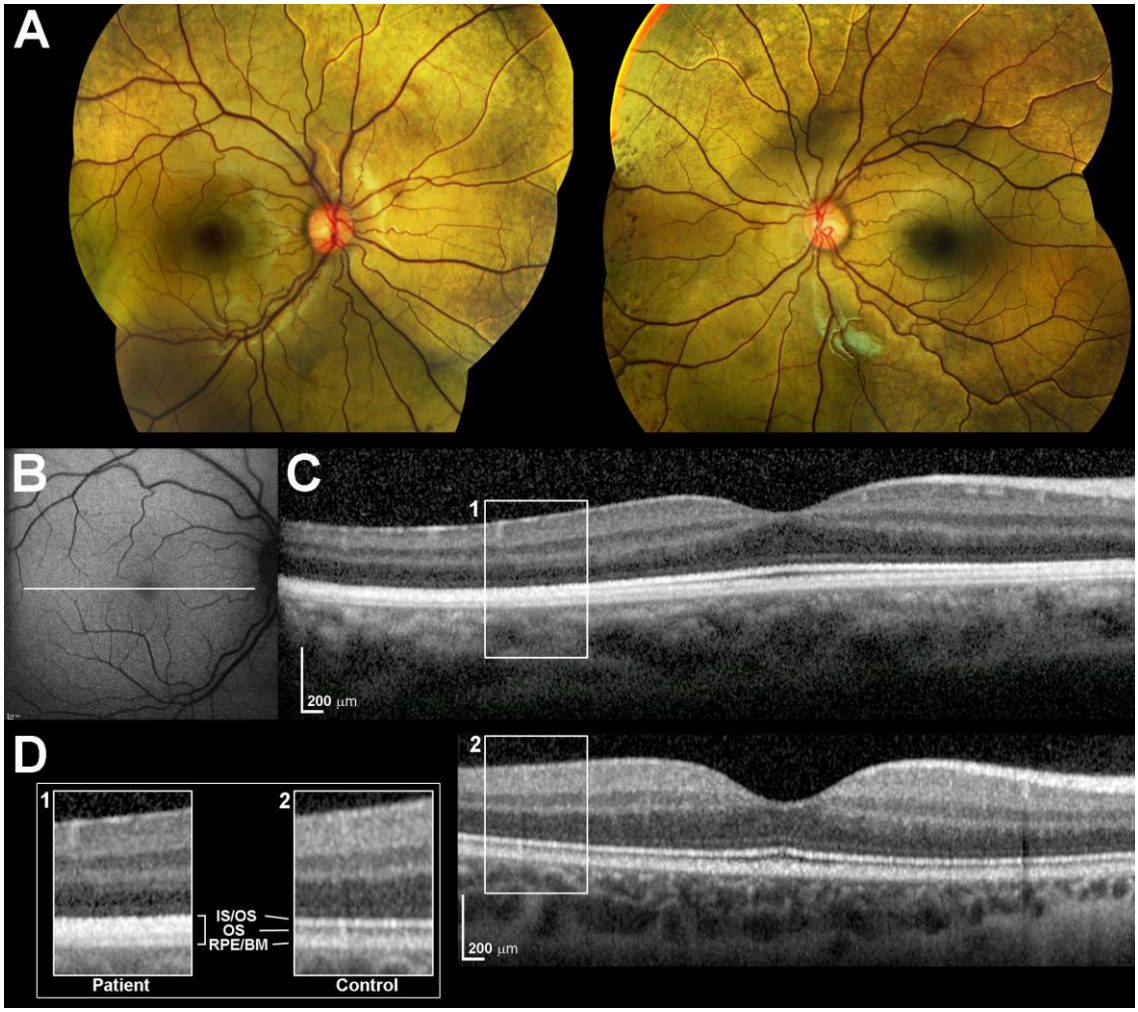

Figure 3-3
[A] Colour fundus photography of both eyes showing typical golden fundus reflex and pigment mottling in the far periphery. Discolouration is less profound in the macular area.
[B] Fundus autofluorescence imaging of the right eye demonstrating no abnormality.
[C] Axial cross sectional image of the proband's right macula obtained using SD OCT. In the parafovea, SD OCT failed to detect the hyporeflective band (outer segments; OS) that is observed between the hyperreflective layers associated with the IS/OS junction (IS/OS) and the RPE/Bruch's membrane complex (RPE/BM).
[D] SD OCT of the right eye of a 9-year-old control individual.
Scans in C and D are to scale and acquired using the same SD OCT protocol. A panel with enlarged images of boxed regions (1, patient; 2, control) shows outer retina in detail.

ISCEV standard full field ERGs were consistent with severe generalised rod photoreceptor dysfunction. Prolonged dark adaptation resulted in partial ERG recovery, in keeping with abnormally slow rod dark adaptation. There was marked desensitization following a single bright flash (figure 3-4). Generalised cone function was normal. PERG revealed no evidence of macular dysfunction.

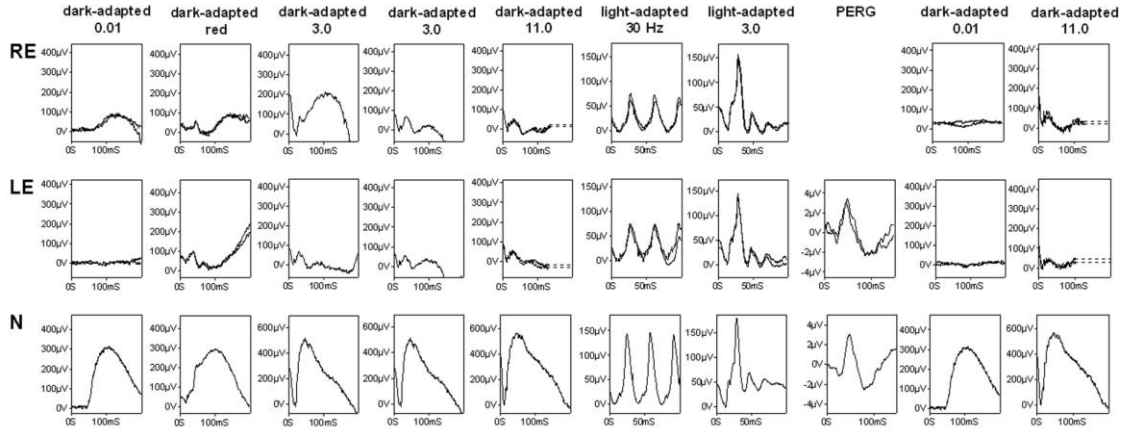

Figure 3-4. Full field ERGs from the right (RE) and left (LE) eyes of the patient and normal examples (N) for comparison. After 25 minutes dark adaptation, left eye rod ERGs were undetectable and bright flash ERGs had a waveform that resembled the early component of the red flash ERG, consistent with a dark-adapted cone system origin. After overnight dark adaptation of the right eye, ERGs showed partial recovery but a second bright flash (3.0 $cd \cdot s \cdot m^{-2}$; inter-stimulus interval 60 seconds) resulted in marked ERG attenuation. Light-adapted ERGs revealed no evidence of generalised cone system dysfunction. The pERG (left eye only) revealed no evidence of macular dysfunction. After photopic testing, ERGs were repeated following an additional 20 minutes dark-adaptation of both eyes (last two columns).

To test for the Mizuo-Nakamura phenomenon, the patient's right eye was dark-adapted overnight and images were obtained with a nonmydriatic camera in a totally darkened room. This type of camera was selected as it uses an infrared illumination source instead of the common white light to view the fundus prior to flash photography. Fundus appearance was initially normal in the dark-adapted eye but after 10 to 15 flashes, the golden sheen appeared (figure 3-5).

Oguchi disease has been previously shown to be caused by mutations in either *SAG* or *GRK1*, a gene encoding rhodopsin kinase [389-390]. Mutated *GRK1* alleles are considered the commonest cause of Oguchi in South Asians and, to date, only one Indian family has been reported to harbour *SAG* mutation [391].

SD OCT findings similar to the proband have been previously described in two nongenetically confirmed Oguchi cases [392-393]; this outer retinal appearence has been attributed to microstructural changes [392-393] and could indicate increased reflectivity in the light-adapted state. Additional outer

retinal attenuation demonstrated in two cases (aged 31 and 43 [388, 392]), was not evident in the presented case.

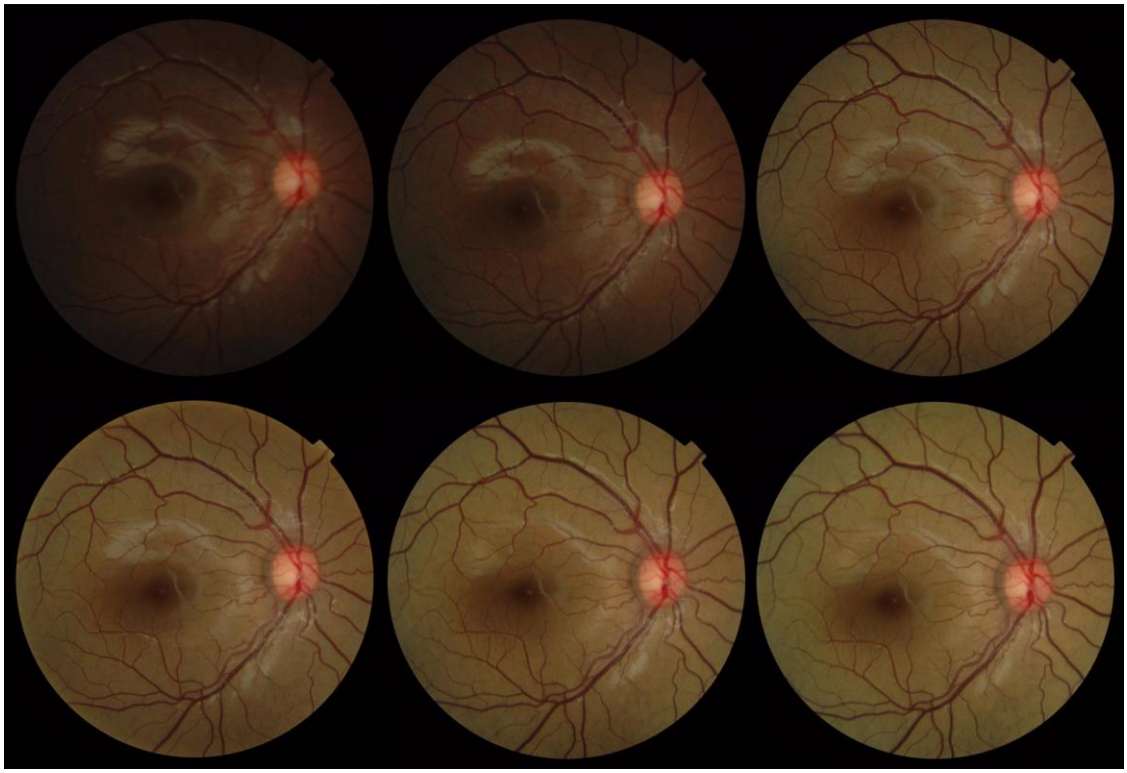

Figure 3-5. Colour fundus photography of the posterior pole of the right eye using a nonmydriatic camera (TRC-NW65, Topcon, Tokyo, Japan; images obtained by Mr Kulwant Sehmi). After overnight (12 hour) dark adaptation, a series of images were obtained over a 20 minute interval. Disappearance of the golden reflex can be seen in the first image taken (top left). The golden colour gradually reappears after 10 to15 flashes. Bottom right image is after 20 minutes and 32 flashes.

A retinal sheen similar to Oguchi disease can be associated with *RS1* mutations. Furthermore, partial or complete ERG recovery following prolonged dark adaption can occur in *RDH5*- or *RLBP1*-related disease (section 3.1.4) [329, 394-396] and rapid ERG attenuation to successive flashes can result from *RGS9/R9AP* mutation [397-398] but the combination of normal cone function, delayed rod ERG dark adaptation and marked rod desensitisation to a bright flash is distinctive for Oguchi disease.

3.1.4 Phenotypic Variability in *RDH5* Retinopathy

The 11-*cis* retinol dehydrogenases are stereo-specific enzymes capable of oxidising 11-*cis* retinol to 11-*cis* retinaldehyde, the universal vertebrate chromophore of visual pigments [399-402]. Retinol dehydrogenase 5 (RDH5) is a protein found in abundance in the smooth endoplasmic reticulum of the RPE [403]. Its enzymatic activity accounts for most of the 11-*cis* retinol dehydrogenase activity in the retina [149, 404-407]. Human RDH5 is a highly conserved among species, 318-amino-acid, protein [408].

Mutations in the *RDH5* gene are usually associated with fundus albipunctatus [149], an autosomal recessive disorder characterised by night blindness, delayed dark adaptation and distinct fundus abnormalities [384, 409]. Individuals with fundus albipunctatus have numerous white-yellow subretinal spots scattered in the mid-periphery and parafovea; spot shape and number tend to vary with age [410-412]. Importantly, both dark adaptometry and rod-specific ERGs have been reported to normalise following sufficiently prolonged dark adaptation [384, 413-414]**.**

Since the first identification of clinically significant changes of the *RDH5* sequence in 1999, there have been reports of missense, in-frame and frameshift mutations [411-412, 415-433]. Most affected individuals had nonprogressive night blindness, normal visual acuities and severely abnormal rod ERGs. Additional cone ERG abnormalities and/or macular dysfunction have been reported, as has disease progression [412, 417-419, 423, 425-426, 429-430]. Notably, biallelic null *RDH5* alleles have been associated with stationary night blindness and white spots [432].

This section addresses phenotypic variability in patients with *RDH5* mutations. Comprehensive ERG recordings in the dark-adapted state were performed in order to gain insight into the retinal function of these patients. Four of the cases have been described in a preliminary report [434]; *RDH5* mutation screening in these four patients was performed by Dr Zheng Li. Analysis of

electrophysiological data was supervised or performed by Dr Anthony G Robson and Professor Graham E Holder. Extended testing in the dark-adapted state in one subject was performed by Dr Vikki A McBain.

3.1.4.1 Methods

3.1.4.1.1 Subjects

Nine affected individuals from eight families with electrophysiological or fundoscopic suggestion of *RDH5* retinopathy were ascertained. All had congenital night blindness. Blood samples were collected for DNA extraction and subsequent mutation screening of *RDH5* (sections 2.4.3, 2.4.9 and 2.4.16). The proband of one family declined to donate DNA for analysis and screening was performed on maternal DNA.

3.1.4.1.2 Retinal imaging and electrophysiology

Fundus autofluorescence imaging was performed in six and SD OCT in three affected inidividuals. Electrophysiological assessment routinely included the recording of dark-adapted ERGs to a red flash enabling the assessment of dark-adapted cone function. Photopic ON-OFF ERGs were performed in eight cases using an orange stimulus (560 $cd \cdot m^{-2}$, duration 200 ms) superimposed on a constant green background (150 $cd \cdot m^{-2}$). Short wavelength flash ERGs were also performed; a blue stimulus (445 nm, duration 5 ms, 80 $cd \cdot m^{-2}$) superimposed on a constant orange background (620 nm, 560 $cd \cdot m^{-2}$) was utilised. Full field ERG recordings were either repeated following two hours of dark adaptation (subjects RD2 and RD8b) or performed after overnight patching of one eye (seven cases). In order to address the nature of the electronegative waveform and the recovery of the b-wave during prolonged dark adaptation, extended testing was performed in one patient (subject RD5). His right eye was patched overnight to achieve extended dark adaptation and

his left eye was exposed to a 100 cd·m^{-2} bleach for ten minutes prior to ERG recording. Sequential scotopic responses (11 cd·s·m^{-2}) were acquired every 2 to 5 minutes for 90 minutes until the response from the left eye resembled that from the dark-adapted right eye. A series of progressively increasing intensity backgrounds (0.1, 0.3, 1.6 and 6.3 cd·m^{-2}) were then applied (10 minutes for the first intensity, 6 minutes for subsequent intensities) while sequential bright flash responses were recorded as during the period of dark adaptation.

Dark adaptometry at two test locations (3° and 9°) was performed in two patients (subjects RD4 and RD5). The Humphrey field analyser (Carl Zeiss Meditec, Inc., Jena, Germany) used was controlled by a computerised program (PS/2 model 50; International Business Machines, Armonk, NY, USA).

3.1.4.1.3 Genetic analysis

Primers were designed to cover the coding region and intron-exon boundaries of exons 2 to 5 of *RDH5* (NM_002905.3). For *RLBP1* (NM_000326.4), primers were used as previously described [150].

3.1.4.2 Results

3.1.4.2.1 Clinical Findings

Clinical findings are summarised in table 3-4. Visual acuity was 0.2 logMAR or better in all but one eye of one patient. All affected individuals described night blindness from birth and delay in dark adaptation after exposure to bright light. The individual with poor acuity in one eye complained of progressive visual loss and patchy central vision (subject RD7).

Table 3-4. Summary of clinical findings in individuals with *RDH5*-related disease

Subject	Sex	Age at exam	Visual Acuity		Ishihara colour vision test	Visual Fields	Fundus appearance	Fundus autofluorescence imaging	SD OCT	Comments
			OD	OS						
RD1	Male	18	6/6	6/5	Test plate only	Full to confrontation	Multiple deep whitish dots; subtle RPE changes in the foveal region	High density spots within the arcades that spatially associate with some of the white dots seen on fundoscopy	not performed	
RD2	Female	19	6/5	6/5	17/17	Full to confrontation	Multiple deep whitish dots	not performed	not performed	
RD3	Female	26	6/6	6/6	3/17	Full to confrontation; Normal binocular static perimetry	Multiple deep whitish flecks and dots; subtle RPE changes in the foveal region	High density spots within the arcades that minimally spatially associate with the white dots seen on fundoscopy	not performed	
RD4	Male	36	6/6	6/6	17/17	Monocular static perimetry: mild superior and temporal loss of sensitivity in each eye	Multiple deep whitish dots; subtle RPE changes in the foveal region	Demarcated area of increased autofluorescence inferiorly	Hyperreflective lesions in the outer retina	Dark adaptometry performed: final thresholds severely elevated after 45 minutes dark adaptation. Normal after overnight dark adaptation of the other eye.
RD5	Male	37	6/6	6/6	17/17	Normal binocular static perimetry. Monocular static perimetry: loss of sensitivity in the upper field in each eye	Multiple deep whitish dots; subtle RPE changes in the foveal region	not performed	not performed	Dark adaptometry performed: No evidence of rod cone interaction after one hour of dark adaptation. Rod and cone final thresholds severely elevated
RD6	Female	41	6/6	6/9	3/17	Full to confrontation	Multiple deep whitish dots; subtle RPE changes in the foveal region	Ring of high density around the fovea	not performed	
RD7	Male	55	6/6	3/60	Test plate only	Monocular static perimetry: central loss of sensitivity in each eye	Within normal limits	Irregular autofluorescence around the fovea	Irregular IS/OS junction; debris; wrinkling of the outer retina	Refraction: -1.50/-3.00x15 OD -5.50/-1.00x175 OS
RD8a	Female	7	6/9	6/9	not tested	not performed	Multiple deep whitish flecks	not performed	Hyperreflective lesions in the outer retina	First cousins once removed
RD8b	M	48	6/6	6/5	not tested	Full to confrontation	Multiple deep whitish dots	Irregular autofluorescence around the fovea	not performed	

Fundus photographs and fundus autofluorescence images are shown in figure 3-6. Diffuse subretinal white or pale yellow spots, usually extending into the midperipheral regions, were present in the fundi of all but subject RD7 (figure 3-6F). Pigment irregularity is present in the foveal regions of five individuals (5/9). The oldest study subject (subject RD7, 55 years old) had a normal fundus appearance.

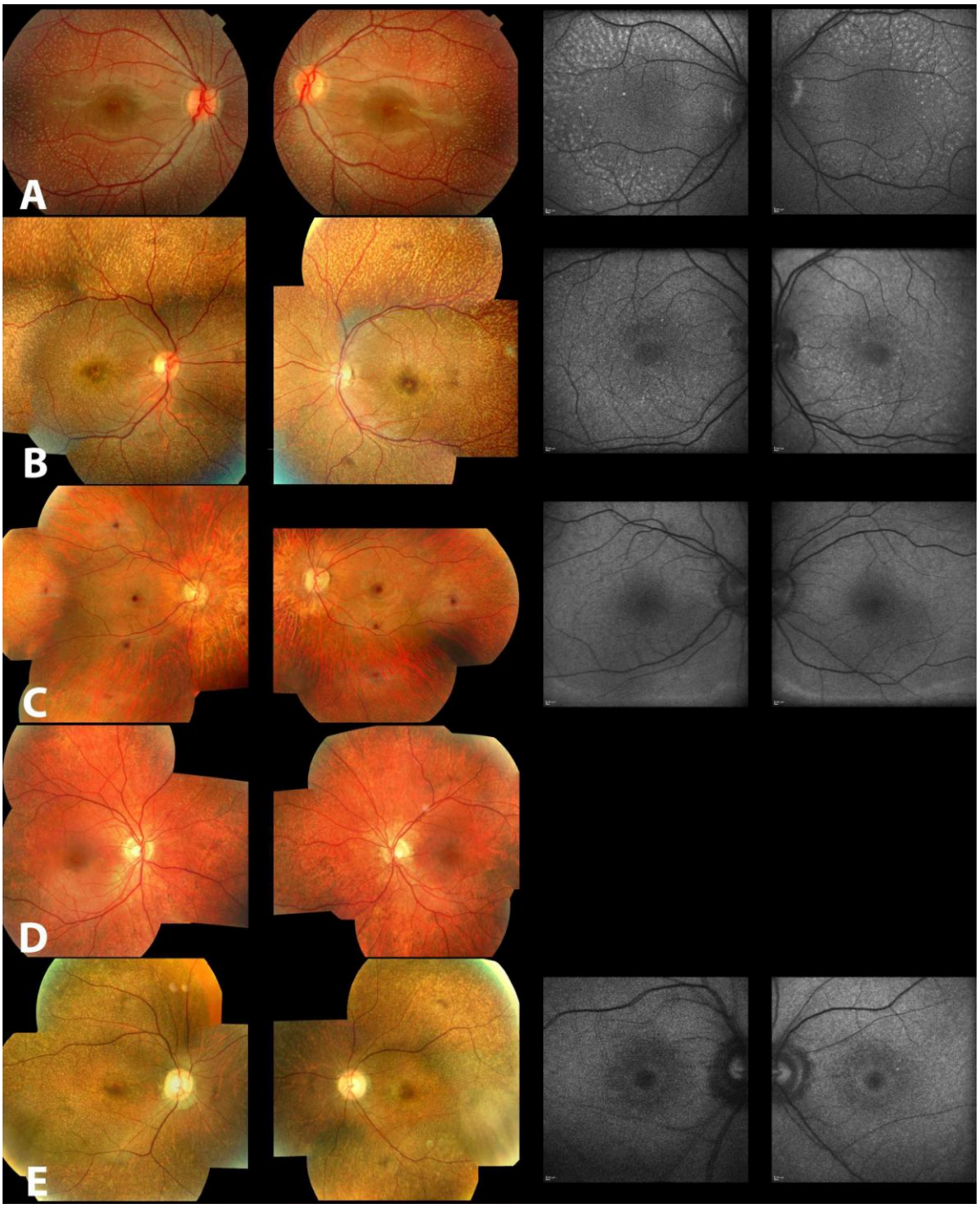

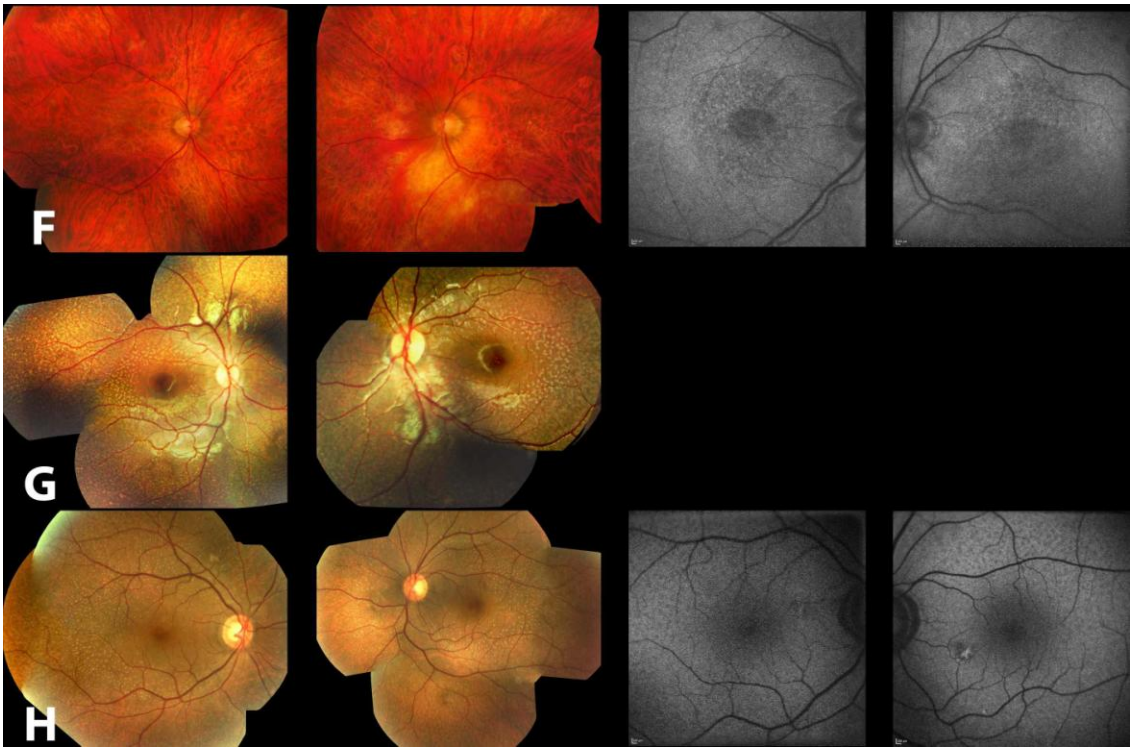

Figure 3-6. Fundus photographs and fundus autofluorescence images of subjects RD1, RD3, RD4, RD5, RD6, RD7, RD8a and RD8b (A to H respectively).

Fundus autofluorescence imaging (n=6) showed a variety of distinct features. High-density foci were noted to associate spatially with some of the white dots in the fundus in one individual (subject RD1, aged 18, figure 3-6A). Similar hyper-autofluorescent lesions associating with white dots in the fundus were also observed in a 26-year-old subject (subject RD3), although most fundoscopic lesions did not autofluoresce (figure 3-6B). A crescent of increased autofluorescence, similar to that reported in RP [435], was seen inferiorly to the temporal vessels of a 36-year-old affected individual (subject RD4, figure 3-6C). Concentric parafoveal rings of high density were present in a 41-year-old subject (subject RD6, figure 3-6E). Fundus autofluorescence image quality in the studied cohort of individuals with *RDH5* retinopathy was compromised and many frames had to be aligned and averaged. Furthermore, signal detection sensitivity had to be near the maximum sensitivity of the system. Digital enhancement artefacts like autofluorescence from the optic disc and large vessels can be observed (figure 3-6). Similar challenges are faced when imaging patients with *RPE65* mutations suggesting abnormal lipofuscin accumulation and low fundus autofluorescence to 488 nm [436].

SD OCT in three affected individuals (subjects RD4, RD7 and RD8a aged 36, 55 and 7 respectively) also revealed a variety of features. Discrete highly reflective lesions extending below the OLM and corresponding in location with the white dots in the fundus were observed in subjects RD4 and RD8a (figure 3-7). In the older patient (subject RD7) disruption and focal loss of the IS/OS junction, debris-like material external to the OLM and remarkable preservation of the OLM were observed (figure 3-7B).

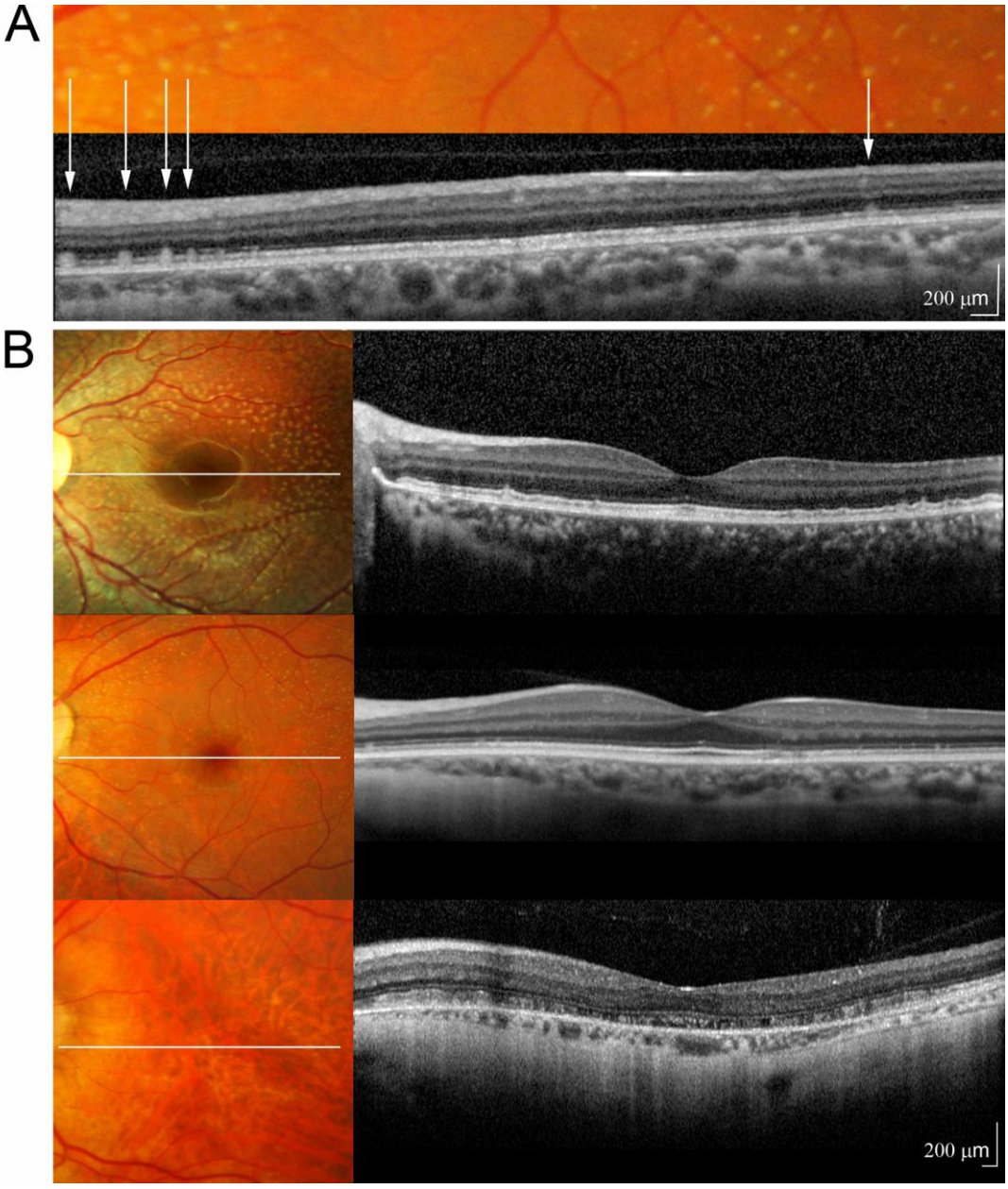

Figure 3-7. SD OCT findings. Spatial association between dots on fundus photography and deep hyperreflective lesions on SD OCT (A). SD OCT of the left eye of subjects RD8a (B), RD4 (C) and right and left eye of subject RD7 (D).

3.1.4.2.2 Electrophysiological findings

Representative examples of full field ERGs are shown in figure 3-8 and electrophysiological data are summarised in figure 3-9.

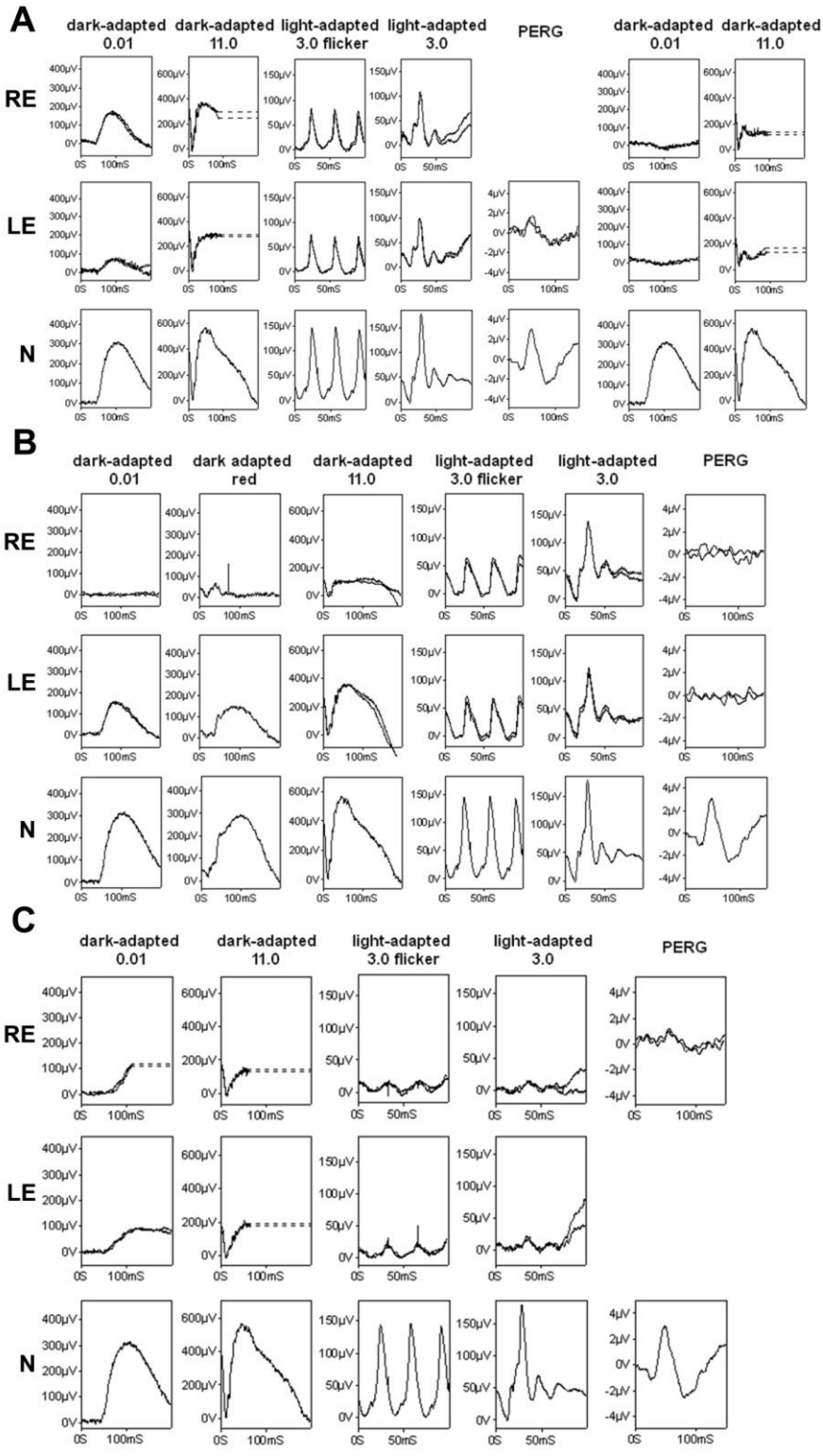

Figure 3-8. Full field ERGs from the right (RE) and left (LE) eyes of subjects RD1 (A), RD7 (B), RD4 (C) and normal traces (N). Dark-adapted ERGs are shown for white flash strengths of 0.01 and 11.0 cd·s·m^{-2}, recorded after standard dark adaptation (left eyes of subjects RD1 and RD7, right eye of subject RD4) or after overnight dark adaptation (right eyes of subjects RD1 and RD7, left eye of subject RD4). Both eyes of subject RD1 underwent subsequent standard dark adaptation and additional recordings were obtained (A, columns 6 and 7). Standard light-adapted full field ERGs are shown for a flash intensity of 3.0 cd·s·m^{-2} (30 Hz and 2 Hz).

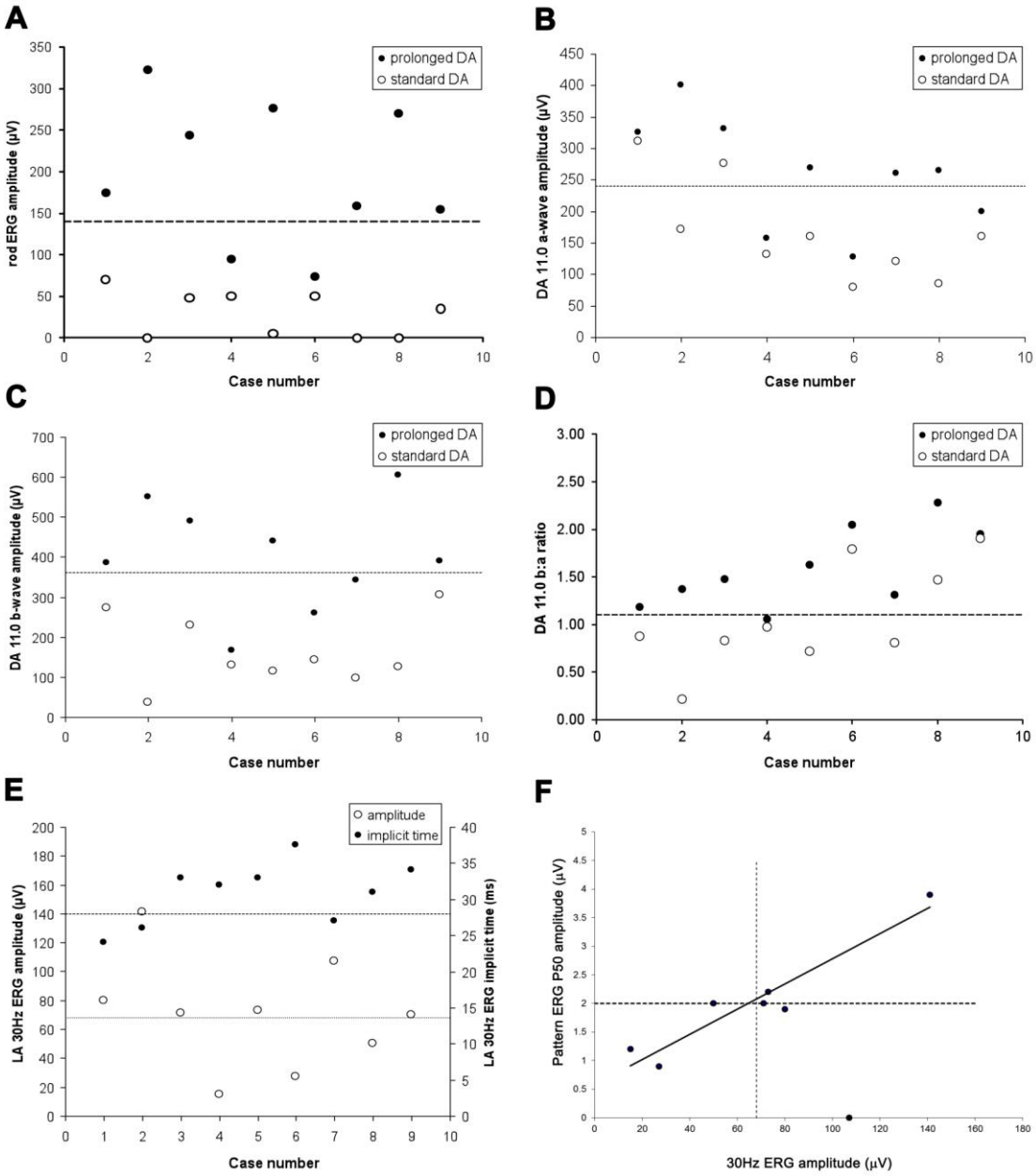

Figure 3-9. Scotopic ERG parameters after standard (20 minutes) and after prolonged dark adaptation shown for the dark-adapted 0.01 cd·s·m^{-2} rod ERG (A) and dark-adapted 11.0 cd·s·m^{-2} (DA 11.0) bright flash ERG a and b-waves (B and C) and the b:a ratio (D). Prolonged dark adaptation was for 2 hours (subjects RD2 and RD9; same eye) or overnight (same eye in case 5; other eye in all others). Standard photopic (light-adapted; LA) 30 Hz flicker ERG and pERG parameters are summarised (E and F). Broken lines show lower limit of normal amplitude or upper limit of normal timing.

(a) Standard (20 minutes) dark adaptation

The dim flash rod-specific ERG (DA 0.01) was undetectable in three subjects and showed moderate-severe reduction in others; maximum amplitude was 47% of normal (subject RD1, figure 3-8A). Red flash ERGs under dark adaptation showed a clear cone component in six of seven cases; the rod component was markedly subnormal or undetectable. The bright flash ERG a-

wave (DA 11.0) showed mild-moderate reduction in seven cases; the b-wave was subnormal in all nine with an electronegative waveform (b:a ratio <1) in six affected individuals (figures 3-8A, 3-8B and 3-9).

(b) Extended dark adaptation

All scotopic responses normalised in two patients after two hours of dark adaptation (subjects RD2 and RD8b; figure 3-9A). Seven affected individuals underwent overnight dark adaptation. Overall, dim flash rod ERGs normalised in seven out of nine cases while in two cases amplitudes increased by 48% (subject RD6) and 90% (subject RD4; figure 3-8C) but failed to attain normal amplitude. The bright flash ERG a- and b-waves normalised in six patients with normalisation of the b:a ratio (figure 3-9B, C). Subject RD4 showed minimal improvement and was the only patient to retain an electronegative ERG after prolonged dark adaptation (figure 3-8D).

(c) Light-adapted ERGs

Photopic 30 Hz flicker ERGs were delayed by 3 to 10 ms in six affected individuals; three showed additional amplitude abnormality (figure 3-9E). Long duration ON-OFF ERGs, performed in all eight adults, contained delayed ON b-waves in the four cases with the greatest flicker ERG delay; the ON b-waves were subnormal in two of those individuals. OFF d-waves were of normal timing in seven cases but were subnormal in the patient with the most severe flicker ERG delay (subject RD6). Short wavelength flash ERGs were of borderline timing in two of eight individuals (subject RD4 and RD5) and were subnormal in subjects RD4 and RD6.

PERG P50 was normal in two patients; markedly or severely subnormal in three patients; and borderline in three patients of the eight in which pERG was performed. PERG reduction was proportional to the flicker ERG amplitude (figure 3-9) in all but subject RD7, who presented with central scotoma, undetectable pERGs and normal photopic full field ERGs.

(d) Extended testing in dark-adapted state

Subject RD5 underwent extended ERG testing. Responses to a bright flash from the right eye, which was dark-adapted overnight, were normal and remained so throughout the 90 minutes of testing under scotopic conditions (figure 3-10). Responses from the left eye were subnormal, with a reduced b:a ratio until approximately 70 minutes of dark adaptation. The a- and b-wave amplitudes gradually increased between 45 and 70 minutes of testing. After 70 minutes the waveform resembled that from the right eye. The a-wave peak time did not significantly differ throughout the 90-minute period of dark adaptation. The peak time of the b-wave was significantly earlier than that from the right eye during the initial 45 minutes of testing, consistent with a predominantly cone system origin; the b-wave peak time then increased in keeping with a greater rod system contribution and normalised after approximately 70 minutes.

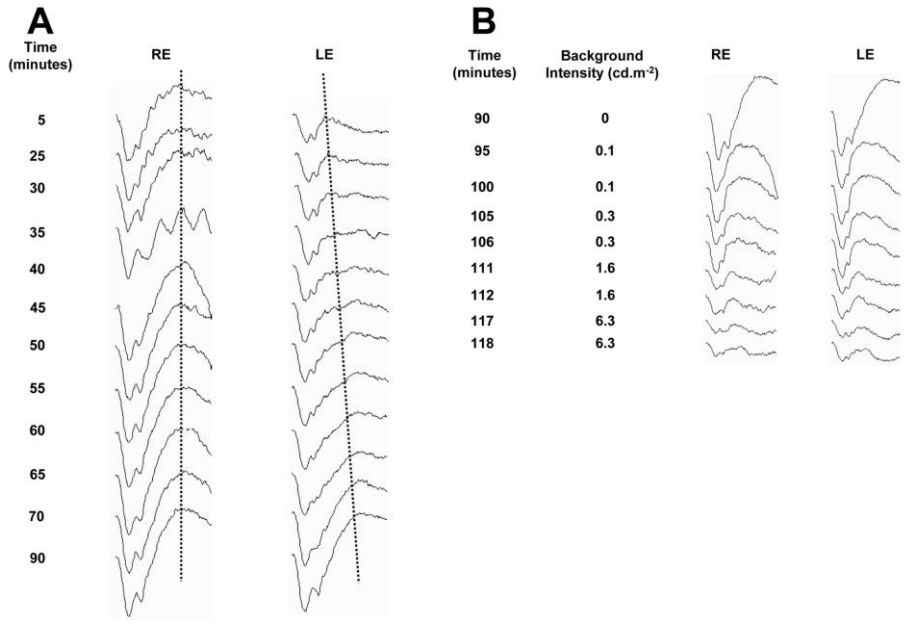

Figure 3-10.
[A] Sequential dark-adapted response traces (11.0 cd·s·m^{-2}) recorded from an overnight dark-adapted eye (RE) and a fully light-adapted eye (LE) during 90 minutes of dark adaptation. Note the changing waveform of the traces from the left, previously light-adapted eye with increasing dark adaptation as the waveform changes from that arising in dark-adapted cones to that arising from the rod system.
[B] Sequential responses (11.0 cd·s·m^{-2}) acquired during a 30 minute period with an increasing intensity adapting background (0.1 to 6.3 cd·m^{-2}). Both eyes were dark-adapted prior to testing (right eye overnight; left eye 1.5 hours). The waveform of the bright flash response changed in both eyes with increasing light adaptation, returning to that seen following standard dark adaptation as the rod contribution becomes effectively bleached out due to impaired regeneration of rhodopsin.

The application of a dim background light (0.1 cd·m^{-2}) significantly reduced the b-wave amplitude in both eyes (figure 3-9B). There was approximately 70%

reduction in amplitude of the b-wave compared with minimal reduction in the a-wave (~15%). Further increase in background light intensity (0.3 $cd \cdot m^{-2}$) produced greater b-wave and a significant a-wave amplitude reduction. With a background intensity of 1.6 $cd \cdot m^{-2}$, both amplitudes decreased further, with the b-wave becoming smaller than a-wave. The final increment in background light intensity (6.3 $cd \cdot m^{-2}$) continued to induce a reduction in the a- and b-wave amplitudes while retaining a reduced b:a ratio (figure 3-9B).

3.1.4.2.3 Genetic analysis results

Either homozygous or compound heterozygous likely disease-associated *RDH5* variants were detected in eight affected individuals from seven families. One patient declined to donate blood but analysis of her mother's DNA disclosed heterozygosity for a previously unreported variant. *RLBP1* sequence was also examined in all study subjects and only previously reported polymorphisms were detected. It is therefore assumed that mutant *RDH5* alleles are disease-causing in all nine patients. Overall, eleven disease-associated variants were identified with two (p.Arg157Gln and p.Gly238Trp) having been previously reported and predicted to severely affect RDH5 *in vivo* enzymatic activity and expression [437]. Nine novel *RDH5* mutations were found; these included five missense (p.Ile33Thr, p.Arg19Gly, p.Gly116Arg, p.Gly139Val, p.Tyr237Ser), one in-frame three base pair insertion (p.Gly116_Ile117insSer) and one mutation affecting pre-mRNA splicing (c.310+1G>A), all altering the catalytic ectodomain in the lumenal compartment of the endoplasmatic reticulum (amino acids 19-288) [403]. One frameshift mutation (p.Arg275fsX60), changing the sequence of the COOH-terminal transmembrane domain (amino acids 289-310), and one nonstop mutation in the translation termination site (p.X319ArgextX32) extending the short cytosolic tail (amino acids 311-319) were also identified [359]. None of these changes were present in DNA from 55 European and 40 South Asian control subjects tested. Nevertheless, testing larger numbers and including samples from control individuals of Middle Eastern origin will provide further insight. These results are summarised in table 3-5.

Table 3-5. *RDH5* mutation analysis results and predicted impact of identified likely disease-associated variants on protein function

Subject	Origin	Mutation Status	Reference	SIFT		PolyPhen-2	
				Prediction	Tolerance index (0-1)	Prediction	HumVar Score (0-1)
RD1	Middle Eastern	c.417G>T, p.Gly139Val^	this study	intolerant	0.00	POD	0.999
		c.956T>C, p.X319ArgextX32^	this study	*not applicable*			
mother of subject RD2	European	c.55A>G, p.Arg19Gly^	this study	intolerant	0.03	POS	0.468
		wild-type					
RD3	Middle Eastern	c.824-825delGA, p.Arg275fsX60*	this study	*not applicable*			
RD4	South Asian	c.470G>A, p.Arg157Gln*	Hajali *et al.*[431]	intolerant	0.00	POD	0.997
RD5	European	c.98T>C, p.Ile33Thr^	this study	intolerant	0.00	POD	0.989
		c.712G>T, p.Gly238Trp^	Yamamoto *et al.*[149]	intolerant	0.00	POD	0.993
RD6	South Asian	c.346_348insGCA, p.Gly116_Ile117insSer*	this study	*not applicable*			
RD7	European	c.346G>C ,p.Gly116Arg^	this study	tolerated	0.52	POS	0.656
		c.710A>C, p.Tyr237Ser^	this study	intolerant	0.00	POD	0.999
RD8a	South Asian	c.712G>T; p.Gly238Trp*	Yamamoto *et al.*[149]	intolerant	0.00	POD	0.993
RD8b	South Asian	c.310+1G>A^	this study	*not applicable*			
		c.712G>T; p.Gly238Trp^	Yamamoto *et al.*[149]	intolerant	0.00	POD	0.993

*homozygous state; ^heterozygous state

3.1.4.3 Comment

Classically, mutations in *RDH5* are associated with fundus albipunctatus, where there is night blindness from birth and white dots in the fundus. All affected individuals in the present series were night blind, but fundus appearance was variable. Patient RD7 had a normal fundus and was initially diagnosed on the basis of the electrophysiological findings (see below). Abnormalities in other patients ranged from minimal white dots (subject RD5) to numerous larger coalescent spots (subject RD8a). Although no clear pattern of longitudinal change emerged, speculative conclusions can be drawn when these data are placed in the context of those in the literature [411-412, 416, 428, 431]. The white spots in the posterior pole have a discrete appearance, are small in size and appear to decrease in number with age. Spots are larger at a young age, in both the mid and far periphery and tend to be confluent and form reticular networks. With increasing age, the spots may become smaller, discrete and less apparent, especially in the far periphery. Disappearance of white dots has been previously described in individuals with *RDH5* retinopathy in association with increasing age or following uveitis [412, 438]. Importantly, a 55-year-old patient in the present series (subject RD7) with life-long night blindness and normal fundus (figure 3-6F) had previously been noted to have a normal fundus at 43 years of age; routine ERG testing after standard dark adaptation revealed severe and selective rod dysfunction (figure 3-8B) that prompted prolonged dark adaptation and additional ERG testing. A normal fundus therefore does not exclude *RDH5*-related retinal dysfunction and appropriate screening is enabled by the electrophysiological findings.

Loss of retinal sensitivity was demonstrated psychophysically in three patients. One proband (subject RD7) presented with patchy central vision and reading problems and perimetry revealed paracentral scotomata. Similar findings have previously been reported [412, 423, 425, 433].

Fundus autofluorescence imaging was performed in six patients; only the two younger adults demonstrated hyperautofluorescent spots. As mutations in the

murine ortholog *Rdh5* do not result in increased N-retinylidene-N-retinyl ethanolamine (A2E) formation compared to double knockout mice of *Rdh8* and *Rdh12* [439], an increase in autofluorescence would not be predicted. Accumulation of 11-*cis* and 13-*cis* retinyl esters seen in the *RDH5*-related disease animal model does not result in autofluorescent substances [406-407]. The only mildly abnormal autofluorescence in the older patients suggests that there is no progressive abnormal accumulation of fluorophores. A low autofluorescent signal was noticed in all six patients, an observation compatible with a recent report of lack of autofluorescence in four individuals with *RDH5* retinopathy [440]. Further studies measuring absolute levels of fundus autofluorescence should assist in the determination of the significance of these observations.

SD OCT imaging of a 47-year-old woman with *RDH5*-related disease has previously been reported to demonstrate dome-shaped lesions and focal loss of IS/OS junction [415]. Discrete hyperreflective elements in the outer retina, spatially associated with the white dots, were recently shown in the SD OCTs of four mutation-positive subjects aged 8, 19, 32 and 35 [440]. Similar lesions and preserved IS/OS junction line were observed in the SD OCTs of two patients in this study (subjects RD4 and RD8a). In an older patient (subject RD7), apparent focal loss of outer segments and hyperreflective material external to the OLM were observed (figure 3-7). Future studies with long-term follow-up will elucidate any possible longitudinal changes in retinal structure.

To date, 68 individuals from 51 families have been reported with likely disease-causing variants in *RDH5* [329]. Despite the fact that in most studies, patients with a diagnosis of fundus albipunctatus were screened, the electrophysiological phenotype is variable. Generalised cone and macular dysfunction have been described in *RDH5* retinopathy although nongenetic factors may have influenced the electrophysiological phenotype [417, 419, 426]. Photopic ERG responses were abnormal in six individuals from the largely Caucasian present series (67% compared with a previously reported Japanese series of 38%) [429]. Macular function, as assessed by the pERG P50 component, was definitely abnormal in three of eight cases.

All patients showed a moderate to severe loss of the rod-specific ERG b-wave following a standard period of dark adaptation. Most showed normalisation of the rod ERG following extended dark adaptation, but recovery was incomplete in two patients (subjects RD4 and RD6). Partial recovery in the rod system sensitivity has been demonstrated in retinitis punctata albescens (Bothnia dystrophy; mutations in *RLBP1*) but only in some individuals after periods of dark adaptation ranging from 10 to 24 hours [394]. Mutations in *RLBP1,* which encodes a soluble 11-*cis* retinoid carrier found in RPE and Müller cells [441] were excluded in all patients in the present series.

A reduced b:a ratio or electronegative ERG is usually associated with dysfunction that is post-phototransduction or inner retinal [442] and, superficially, is perhaps a surprising observation in the context of a disorder primarily affecting rod photoreceptor function. Use of a red flash under dark adaptation in normal subjects elicits an early response arising in the cone system and a later response arising in the the rod system. The intensity of the red flash stimulus is such that in a normal subject the amplitude of the rod component to the red flash is equivalent to that of the rod-specific response to a dim white flash (DA 0.01). In patients with *RDH5* mutations, there is usually a clear cone component but no detectable rod component (figure 3-8B); thus the ERGs under dark adaptation are probably dominated by dark-adapted cone activity rather than rods. Normal cone-mediated ERGs under photopic conditions exhibit a characteristic intensity-response known as the “photopic hill”, such that increasing stimulus intensity initially results in an increase in both photopic a-wave and photopic b-wave but following further increase in stimulus intensity the b-wave starts to reduce in amplitude relative to a continuing increase in a-wave amplitude, giving an electronegative waveform [443]. This has been shown to result from the reduction of the ON component amplitude and the delay in the positive peak of the OFF component at higher stimulus intensities [444]. It has previously been shown in patients with vitamin A deficiency, who lack rhodopsin and typically have a functionally cone-isolated retina, that this phenomenon is a property of dark-adapted as well as light-adapted cones [445]; this suggests that the term “photopic” hill is perhaps inappropriate. The electronegative ERG to a bright flash associated with *RDH5*

mutations is thus consistent with a dark-adapted cone-mediated origin, exposed in the absence of normal rod photoreceptor function and should not be taken to reflect inner retinal rod system dysfunction. Comprehensive recordings in the dark-adapted state performed in one patient support this hypothesis (figure 3-10) and the use of a red flash under dark adaptation is generally recommended to assist accurate ERG interpretation.

Prior to this study, 25 likely disease-causing variants in *RDH5* have been reported [329]; 11 of these were found only in pedigrees of Japanese ancestry. Among the remaining 14 mutations, 12 occur in non-Japanese pedigrees and two in both Japanese and non-Japanese. The families in the present study were either of European, Middle Eastern or South Asian origin (table 3-5). Eleven disease-associated variants were identified, nine of which were novel; the remaining two have been previously reported in Caucasian families [149, 428]. In general, no significant correlation between genotype and severity of electrophysiological or clinical phenotype could be found; this was in agreement with the conclusions of previous studies [427, 429].

The presence of 11-*cis* retinal, the lack of retinal degeneration and the normal dark adaptation kinetics observed in *Rdh5* knockout mice, suggest that RDH5 is not the only enzyme responsible for oxidation of 11-*cis* retinol [407]. The presence of another enzyme, *Rdh11* that can oxidise 11-*cis* retinol has been described in mice but its role in human is debated [446]. Nevertheless, the presence of other 11-*cis* retinol dehydrogenases could explain the relatively mild clinical disease seen in *RDH5*-retinopathy compared to *RLBP1*-related disease, which features more severe and progressive retinal degeneration. Furthermore, there may be alternative pathways responsible for regenerating 11-*cis* retinal and, for cones, this may occur in outer segments rather than in the RPE [405]. Since *RDH5* is situated in the RPE [447], this alternative cone pathway could account for the relative sparing of cone function in patients with biallelic *RDH5* mutations.

To conclude, the clinical and electrophysiological phenotype of *RDH5*-related retinal dysfunction is variable. This may relate to genetic variability and

consequent availability of chromophore but progression of disease may also be a contributory factor. Electrophysiology is fundamental to making the diagnosis, but the ERGs should be performed and interpreted in consideration of the underlying pathophysiological mechanisms.

3.1.5 Optical Coherence Tomography in *KCNV2* Retinopathy

Voltage-gated potassium channels, Kvs, are transmembrane proteins that control excitability of electrically active cells and play a fundamental role in all organs and tissues. The human genome contains 40 Kvs, involved in diverse physiological processes [448]. Each channel is formed by four α-subunits, each containing six transmembrane regions, clustering around a central pore. *KCNV2* encodes *Kv8.2*, a 545-amino-acid Kv subunit highly expressed in the inner segments of rod and cone photoreceptors of the human retina and known to form heteromeric channels with *Kv2.1* subunits [175, 449].

Recessive mutations in *KCNV2* have been shown to cause a specific retinal dystrophy, “cone dystrophy with supernormal rod ERG”, which is the first disorder of the visual system to be associated with a potassium channel defect in man [175]. This condition was initially described in 1983 as a progressive degeneration of the cone photoreceptors associated with unique rod system abnormalities [450]. Patients typically present in the first two decades of life with reduced visual acuity, disturbance of colour vision and photophobia. Nyctalopia may also be a feature of the disorder. Affected individuals are usually myopic, have a normal peripheral retinal appearance and a range of macular abnormalities on fundoscopy and fundus autofluorescence imaging [451]. Early diagnosis and targeted mutation screening is enabled by pathognomonic electrophysiological findings (section 1.3.2) [176, 451].

This section details structural changes associated with *KCNV2* mutations. SD OCT findings in 12 patients with *KCNV2* retinopathy are described and four novel disease-associated variants are reported.

3.1.5.1 Methods

3.1.5.1.1 Subjects

Twelve subjects (eight simplex cases and two sibling pairs) with clinical and/or electrophysiological examination suggestive of *KCNV2*-related disease were ascertained. Blood samples were collected for DNA extraction and subsequent mutation screening of *KCNV2* (sections 2.4.3, 2.4.9 and 2.4.16). The proband of one family (subject KC2) declined to donate blood and screening was performed on parental DNA.

3.1.5.1.2 Retinal imaging and electrophysiology

Clinical assessment included fundus autofluorescence imaging and SD OCT. The Spectralis HRA+OCT with viewing module version 5.1.2.0 (Heidelberg Engineering; 3.9 μm axial resolution) was used to acquire tomographs. The protocol included a horizontal, centred on the fovea, linear scan and a volume scan (19 B-scans, 20° x 15°) for each eye. When subjects were unable to comply the number of frames per B-scan was adjusted.

SD OCT data were analysed qualitatively; comparisons were made between affected individuals and the degree of interocular symmetry was investigated. Central point and retinal thickness in the ETDRS central subfield were assessed. The HEYEX software interface (version 1.6.2.0; Heidelberg Engineering) was used for all measurements. Identification and evaluation of the true dimensions of the outer nuclear layer would be a better indicator of photoreceptor loss compared to global thickness but the technique used to acquire images was not optimal for accurate segmentation and appropriate normative data are lacking [223].

All subjects underwent electrophysiological assessment that included full field and pERG testing that incorporated the minimum ISCEV standards. The protocol also included the recording of dark-adapted ERGs to an intensity

series of flashes ranging from 0.001 $cd \cdot s \cdot m^{-2}$ to 11.5 $cd \cdot s \cdot m^{-2}$ in eight increments.

3.1.5.1.3 Genetic analysis

The *KCNV2* coding region (NM_133497.2) and intron-exon boundaries were amplified and sequenced according to previously described methods [175]. The novel c.1318C>T, p.Thr439Ile variant was tested in 50 ethnically matched control DNAs tested, while the c.964G>C, Ala322Pro variant was tested in 95 control DNAs (ECACC, HRC-2).

3.1.5.2 Results

3.1.5.2.1 Clinical and electrophysiological findings

Clinical findings are summarised in table 3-6. Affected individuals were between 13 and 48 years old and presented with reduced central vision and/or photophobia that had commenced in the first or second decade of life. Visual acuity ranged from 0.20 to 1.30 logMAR (mean 0.71). None of the individuals participating in this study reported history of epilepsy or seizures. Subjects KC2, KC5 and KC8 as well as the sibling pair of KC6 and KC7 were born to consanguineous parents.

PERGs were undetectable in all 11 individuals tested, indicating severe macular dysfunction. Full field ERGs showed the characteristic combination of findings previously described as pathognomonic for “cone dystrophy with supernormal rod ERG”, in all 12 cases (figure 3-11) [451].

Table 3-6. Summary of clinical findings in individuals with *KCNV2*-related disease

Case	Age at examination	Visual Acuity*		Refraction	Ishihara colour vision test	Macular appearance on fundoscopy	Fundus autofluorescence imaging	Foveal appearance on SD OCT
		OD	OS					
KC1	13	0.90	1.10	+5.00/-3.50x165 OD +4.50/-3.50x10 OS	test plate only	Granular macular appearance	Abnormal foveal autofluorescence; small parafoveal ring of increased autofluorescence	Focal disruption of reflective band at IS/OS junction
KC2	13	0.90	0.75	+1.50/+1.00x90 OD +1.50/+1.25x90 OS	test plate only	Normal	Parafoveal area of mildly increased autofluorescence	Complete loss of photoreceptor layers in the fovea
KC3	16	0.45	0.35	myopic prescription	test plate only	Subtle RPE mottling in the fovea	Parafoveal area of increased autofluorescence	Focal disruption of reflective band at IS/OS junction
KC4	18	0.25	0.25	emmetropic	test plate only	Granular macular appearance	Abnormal foveal autofluorescence; small parafoveal ring of increased autofluorescence	Focal disruption of reflective band at IS/OS junction
KC5	18	0.20	0.30	-8.50/-0.50x130 OD -7.00/-0.75x5 OS	test plate only	Granular macular appearance	Parafoveal area of mildly increased autofluorescence	Focal disruption of reflective band at IS/OS junction
KC6	18	0.80	0.80	emmetropic	test plate only	Macular atrophy and flecks	Abnormal foveal autofluorescence; high density foci around the fovea	Optical gap in the fovea with absent IS/OS junction line
KC7	20	0.80	0.80	emmetropic	3/17	Subtle RPE mottling in the fovea	Parafoveal area of increased autofluorescence	Small optical gap with disruption of reflective band at IS/OS junction
KC8	34	0.80	0.80	-12.00/-1.50x180 OD -12.50/-1.50x180 OS	test plate only	RPE mottling in the fovea	Parafoveal area of increased autofluorescence	Focal disruption of reflective band at IS/OS junction
KC9	43	0.60	0.78	emmetropic	test plate only	Normal	Parafoveal area of increased autofluorescence	Focal disruption of reflective band at IS/OS junction
KC10	44	1.00	1.30	-2.75/-1.75x50 OD -5.50 OS	unable to see test plate	Macular atrophy	Central loss of autofluorescence	Complete photoreceptor layers loss; RPE layer loss
KC11	44	0.50	0.80	-9.00/-2.00x180 OD -6.50/-2.00x5 OS	test plate only	Subtle RPE mottling in the fovea	Central area of increased autofluorescence with surrounding area of reduced signal	Loss of photoreceptor layers in the fovea
KC12	48	1.00	1.00	-3.00/-2.00x160 OD ∞/-3.00x30 OS	2/17	Macular atrophy	Central atrophy surrounded by ring of increased AF	Complete photoreceptor layers loss, RPE layer loss

* LogMAR or logMAR equivalent.

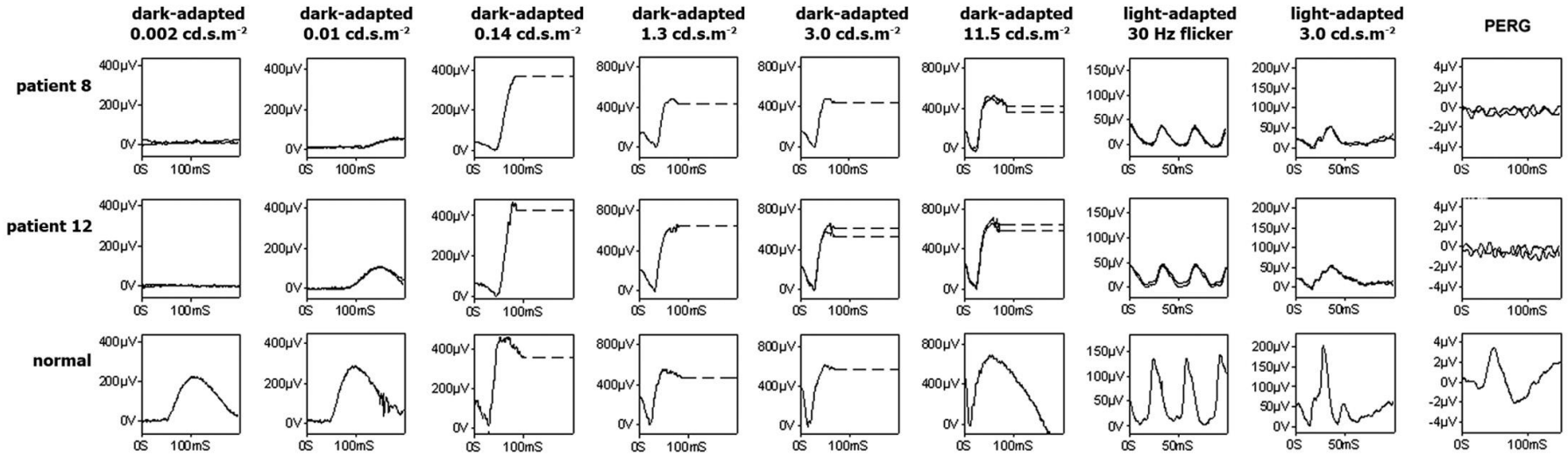

Figure 3-11.
Representative full field and pERG traces. Subject KC8 (upper row) carries biallelic nonsense mutations. Subject KC12 (middle row) is homozygous for a mutation affecting the pore. The lower row shows representative normal traces. Both patients had characteristic findings. The dim flash ERGs are undetectable and the ISCEV standard dark-adapted 0.01 shows a profoundly delayed and subnormal b-wave. With increasing stimulus intensity there is then a rapid increase in b-wave amplitude and shortening of peak time despite relatively small increase in stimulus intensity. The brighter flash (dark-adapted 11.5) ERGs show a normally developing a-wave with a broadened trough and a sharply rising high amplitude b-wave. Cone flicker (light-adapted 30 Hz flicker) and single flash (light-adapted 3.0) ERGs are delayed and reduced. pERGs are undetectable.

Fundus autofluorescence imaging revealed abnormal macular autofluorescence in all affected individuals. The pattern of abnormality was variable and ranged from a small parafoveal ring of increased signal (*e.g.* subject KC1) to a central area of absent autofluorescence corresponding to RPE atrophy (*e.g.* subject KC12) (figure 3-12).

SD OCT demonstrated structural changes in all 23 eyes tested (one eye was not included in the analysis due to unstable fixation). The findings were concordant between eyes in all study subjects. Discontinuous reflectivity of the hyperreflective band corresponding to the photoreceptor IS/OS junction was the predominant feature in eleven eyes (subjects KC1, KC3, KC4, KC5, KC8 and KC9). In four eyes (subjects KC6 and KC7), disruption was more profound and an optical gap was seen (elsewhere described as hyporeflective zone) [452]. The thin reflective line corresponding to the OLM was relatively preserved in both groups. Extensive loss of IS/OS junction reflectivity with significant foveal depth reduction and a preserved RPE/Bruch's membrane complex was seen in four eyes (subjects KC2 and KC11). RPE/Bruch's membrane band thinning was observed in addition to the photoreceptor loss in four eyes (subjects KC10 and KC12). Mean CPT was 141.26 µm (n=23) and mean ETDRS CSF was 204.84 µm (n=19). Both CPT and CSF were significantly reduced compared to normative data (CPT: 227.3 ± 23.2 µm, CSF: 270.2 ± 22.5 µm); although part of this difference may be due to age, sex and axial length variability [453]. Peripheral outer retinal architecture was relatively well preserved on the basis of the 20° x 15° OCT volume scans (n=19 eyes).

In terms of age, two groups can be highlighted in the present cohort. OCTs in the first group (subjects KC3 to KC7, aged 16 to 20) revealed relative preservation of the OLM and focal loss of photoreceptor outer segments. A more severe phenotype was observed in the second group (subjects KC9 to KC12, aged 43 to 48), where there was more marked photoreceptor and/or RPE loss in three out of four affected individuals (figure 3-12).

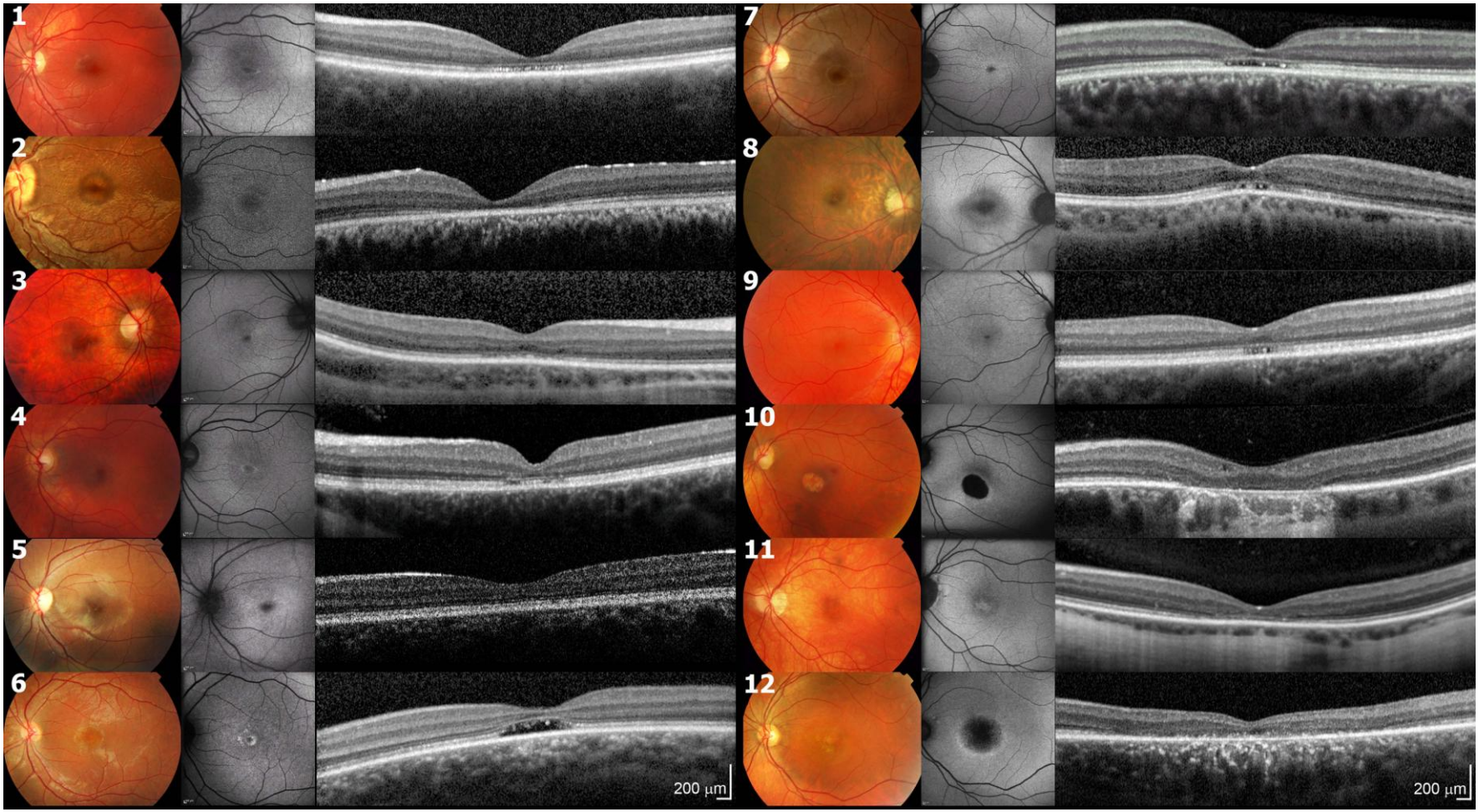

Figure 3-12. Fundus photography, autofluorescence and SD OCT of 12 individuals with "cone dystrophy with supernormal rod ERG" and mutations in *KCNV2*. The number relating to each triplet of images corresponds to case number (KC1 to KC12). Patients are ordered by age. SD OCT image quality in case KC5 was compromised by unstable fixation.

3.1.5.2.2 Genetic analysis results

Either homozygous or compound heterozygous disease-associated variants were detected in all affected individuals within nine families (table 3-7). Only one single heterozygous variant could be detected in one family (subject KC1). Four previously unreported mutations were identified, including two missense variants: one (p.Ala322Pro) altering a residue that is located in the second transmembrane helix and is not particularly conserved and one (p.Thr439Ile) occurring at a site located in close proximity to the pore region (amino acids 446-463) that is fully conserved across vertebrates and highly conserved in other Kvs, [454]. None of these changes was found to be present in the control chromosomes tested.

Table 3-7. KCNV2 mutation analysis results

Subject	**Mutation Status**	**Protein Domain/ Position**	**References** Mutation	Study subject
KC1	c.451T>C, p.Phe151Leu^ not identified	Cytoplasmic (NAB)	Robson *et al*.[176] *not applicable*	case partially detailed in Robson *et al.*[176]
affected mother of KC2	c.427G>T, Glu143X*	Cytoplasmic (NAB)	Wu *et al.*[175]	previously unreported case; family members partially detailed in Wu *et al.*[175] and Robson *et al.*[176]
KC3 & KC4	c.964G>C, p.Ala322Pro^ c.1381G>A, p.Gly461Arg^	Transmembrane(S2) Pore (P loop)	novel Thiagalingam *et al.* [335]	previously unreported cases
KC5	c.1318C>T, p.Thr439Ile^	Extracellular	novel	previously unreported case
KC6 & KC7	c.568delG, p.Gly189fsX21^	Cytoplasmic	novel	cases partially detailed in Robson *et al.*[176]
KC8	c.916G>T, p.Glu306X^	Transmembrane(S2)	Wu *et al.[175]*	case partially detailed in Wu *et al.*[175] *and* Robson *et al*.[176]
KC9	c.1381G>A, p.Gly461Arg^ c.1637T>C.p.X546TyrextX61^	Pore (P loop) Cytoplasmic (COOH-terminus)	Thiagalingam *et al.* [335] Thiagalingam *et al.* [335]	case partially detailed in Robson *et al.*[176]
KC10	c.430C>T, p.Gln145X^ c.776C>T, p.Ala259Val^	Cytoplasmic (NAB) Extracellular (EC1)	Wu *et al.[175]* Wu *et al.*[175]	case partially detailed in Wu *et al.*[175] *and* Robson *et al.*[176]
KC11	c.1199delT,p.Phe400fsX53^ c.8_11delAACA, p.Lys3fsX93^	Cytoplasmic Cytoplasmic (NH_2-termimus)	novel Wissinger *et al.* [455]	case partially detailed in Robson *et al.*[176]
KC12	c.1381G>A, p.Gly461Arg*	Pore (P loop)	Thiagalingam *et al.* [335]	case partially detailed in Robson *et al*.[176]

Subjects KC3 and KC4 and subjects KC6 and KC7 are pairs of siblings. NAB represents the cytoplasmic domain NH_2-terminal A and B box. *homozygous state; ^heterozygous state

Two novel frameshift mutations were also identified; both are one base pair deletions and occur within exon 1 (table 3-7). In the case of c.568delG, p.Gly189fsX21, mRNA would be predicted to succumb to nonsense-mediated decay; if however they were translated, the encoded proteins would be severely truncated and predicted to be nonfunctional since they would lack all transmembrane helices and the pore region. The c.1199delT, p.Phe400fsX53 mutation shifts the protein frame before the fifth transmembrane domain and the pore.

3.1.5.3 Comment

Mutations in Kv channel genes cause many diverse phenotypes both in animal models and man. These include long QT Syndrome and neonatal seizures [456-458]; notably, heterozygosity for missense *KCNV2* variants (p.Arg7Lys and p.Met285Arg) has been recently associated with epilepsy [459].

SD OCT enables high resolution, cross sectional visualization of retinal structure and allows assessment of the structural integrity of the photoreceptor layer, an important parameter for the success of gene therapy or pharmacological modulation strategies (section 1.3.3.3) [205, 460]. Thinning and nonspecific changes in the foveal outer retinal layers were present in all affected individuals. An unusual optical gap similar to that described in individuals with rod monochromacy [452] caused by mutations in *PDE6C* [461] or *CNGA3* [462], occult macular dystrophy [463] and less commonly in Stargardt disease [464], was observed in the SD OCTs of a sibling pair (subjects KC6 and KC7).

In this cross sectional study more severe morphologic changes in SD OCT with increasing age cannot be excluded suggesting that there might be progressive loss of foveal photoreceptors; this is consistent with observations from other reports [176, 465]. However, it is noted that the two youngest individuals in the studied cohort (subjects KC1 and KC2) presented with a

relatively severe OCT phenotype and large longitudinal studies are needed to more accurately determine the natural history of the disorder.

Fundoscopic and gross OCT abnormalities appear to be confined to the central retina. This is despite the fact that *KCNV2* is expressed in both rod and cone photoreceptors and the ERG changes indicate widespread retinal dysfunction. The severity of peripheral retinal dysfunction does not correlate with age and serial recordings, described in a few cases, have shown mild or no deterioration [176, 465]. Colour vision testing has shown relative preservation of S-cone function [451, 466]. These findings together with the OCT changes suggest that foveal cones are particularly susceptible to the deleterious effects of mutant *KCNV2* or that *KCNV2* is more highly expressed in foveal cones. Future studies with cellular-resolution retinal imaging will more accurately map cone abnormalities in the foveal and parafoveal area and provide further insight [467].

Kv8.2 (KCNV2) subunits are not functional in isolation and do not form homomeric potassium channels. Instead, they coassemble with *Kv2.1* to constitute functional heteromers [449, 454]. *Kv2.1* (KCNB1) subunits are expressed in neurons and neuroendocrine cells and can form both homomeric and heteromeric channels [468]. Mutations in *KCNV2* can lead to either completely absent or dysfunctional *Kv8.2/Kv2.1* channels. When *KCNV2* mRNA is not translated, *Kv2.1* homomeric channels are formed [449, 469]. This is predicted to be the case in individuals with biallelic mutations that trigger nonsense mediated mRNA decay. Conversely, mutations affecting the pore forming loop like p.Gly461Arg are expected to result in present but nonfunctional *Kv8.2/Kv2.*1 heteromers [449, 469]. Subjects KC2, KC6, KC7 and KC8 carry alleles in the first category while subject KC12 is homozygous for a mutation in the pore. No significant difference in severity of clinical, electrophysiological, or OCT phenotype emerges when comparing these groups between them or with other study subjects.

KCNV2 retinopathy is a recessive early-onset retinal dystrophy which has a characteristic electrophysiological phenotype. Foveal structural abnormalities

are demonstrated in SD OCT even in the early stages of disease. Undetectable pERG recordings are a consistent feature and suggest that there is widespread macular dysfunction affecting even morphologically intact photoreceptors. Future therapeutic approaches such as gene replacement or pharmacological therapy may restore function to these cells or slow the degenerative process.

3.1.6 Phenotypic Study of CSNB Caused by *GRM6* Mutations

The term CSNB denotes a clinically and genetically heterogeneous group of hereditary retinal disorders associated with lifelong nyctalopia. Types of this condition differ in fundus appearance, mode of inheritance and electrophysiological characteristics [384, 470]. CSNB is usually associated with an electronegative ERG in response to a bright white flash in the dark-adapted eye (section 1.3.2) [471-472]. This selective reduction in the b-wave reflects dysfunction occurring post-phototransduction [442].

CSNB with electronegative ERG has been further subdivided into complete and incomplete forms according to whether there is a rod-specific ERG response to a dim light from the dark adapted eye [473]. Mutations in *NYX* are associated with X-linked complete CSNB [474] whereas mutations in *GRM6* [157] and *TRPM1* [475-477] are associated with autosomal recessive complete CSNB.

GRM6 encodes the 877-amino-acid, retina-specific, metabotropic glutamate receptor 6 (mGluR6) situated on the dendrites of rod and cone ON bipolar cells [478]. Photoreceptors respond to changes in photon catch by changing the release rate of glutamate, a neurotransmitter acting differently on the two fundamental bipolar cell classes: OFF bipolar cells, which have sign-conserving ionotropic receptors and ON bipolar cells, which have sign-inverting metabotropic receptors (mGluR6) [141, 479]. The majority of cones connect with at least two bipolar cells, one of which is ON and the other OFF while rods interact mainly with ON bipolar cells [480-481]. Biallelic *GRM6* mutations result in defective signal transmission from cones and rods to ON bipolar cells and lead to a complete CSNB phenotype [157]. Twelve mutations in eight families with *GRM6*-related retinal dysfunction had been reported prior to this study [157, 339, 482-484].

In this section, novel mutational data and phenotypic detail in nine patients with *GRM6* mutations are reported.

3.1.6.1 Methods

3.1.6.1.1 Subjects

The cohort consisted of nine patients from seven families with a history suggestive of autosomal recessive inheritance and clinical and electrophysiological findings suggestive of complete CSNB. Blood samples were collected for DNA extraction and subsequent mutation screening of *GRM6* (sections 2.4.3, 2.4.9 and 2.4.16).

3.1.6.1.2 Retinal imaging and electrophysiology

Fundus autofluorescence imaging was performed in two affected individuals. All study subjects had electrophysiological assessment. Four younger patients were tested using surface (n=3) or gold-foil (n=1) recording electrodes and a shortened protocol that included light-adapted 30 Hz flicker and dark-adapted ERG testing. Five patients had full field ERGs performed using protocols that exceeded the ISCEV standard [169, 171] and included ON-OFF ERG and short wavelength flash (“S-cone”) ERG testing (detailed in section 3.1.4.1.2). PERGs were performed in five cases without marked nystagmus.

3.1.6.1.3 Genetic analysis

The *GRM6* coding region (NM_000843.3) and intron-exon boundaries were screened. In a sib-pair (subjects GR1 and GR2), prior to *GRM6* sequence analysis, genotyping was performed by Dr Zheng Li (GeneChip Human Mapping 50K Array Xba; sections 2.1.3 and 2.4.18.2.1). Novel missense variants were tested with 50 control DNAs from normally sighted individuals of South Asian origin and 45 DNAs from UK blood donors (ECACC, HRC-2).

3.1.6.1.4 Statistical analysis

Individuals with *GRM6* retinopathy described here and elsewhere (n=19) were split into three groups: those with 0, 1 or 2 alleles harbouring nonsense or frameshift mutation in *GRM6*. A greater effect of nonsense/frameshift than missense mutations on protein expression and function was assumed. Kruskal-Wallis nonparametric analysis of variance for three groups was used to assess correlation between overall mutation impact on patient mGluR6 and the presence or absence of high myopia. Spherical equivalent averaged between the two eyes of -6.00 dioptres or more myopic was considered high myopia.

3.1.6.2 Results

3.1.6.2.1 Clinical findings

The age of affected individuals ranged from 7 to 75 years (mean 24, median 10 years); all but one (subject GR3) presented in the first decade of life. The most common presenting symptoms were reduced visual acuity despite myopic correction and nystagmus. Only two individuals presented with night blindness: subject GR3 in her 20s and subject GR4 at nine years of age. Overall, five of nine complained of nyctalopia. Two had strabismus: one had mild exophoria (subject GR4) and one had manifest esotropia requiring surgery (subject GR8). Five of nine subjects had nystagmus of various amplitudes with one patient (subject GR9) adopting a head posture to utilise a null position. Two sib-pairs with no other family history of retinal disease were included in the studied cohort (subjects GR1, GR2 and GR5, GR6); the remaining five patients were simplex cases. Four of nine had consanguineous parents (subjects GR4, GR5, GR6 and GR8).

The median visual acuity was 0.2 logMAR (ranging from 0.0 to 3.0). Myopic astigmatism was the most common refractive error and a median spherical

equivalent refraction of -5.375 dioptres was observed. Colour vision was normal in all four affected individuals tested. Fundus examination was within normal limits in 15 eyes and revealed signs of severe myopic maculopathy in three eyes (left eye of subject GR1, both eyes of subject GR2). Fundus autofluorescence imaging was normal in both patients tested. The clinical findings in these and other individuals so far reported with *GRM6*-related retinal dysfunction are summarised in table 3-8.

3.1.6.2.2 Electrophysiological findings

In all study subjects that underwent ISCEV standard testing (n=5), the rod-specific ERG was undetectable. The dark-adapted bright flash ERG a-wave was subnormal in the oldest patient and was normal in others; waveforms were markedly electronegative in all and b:a ratios ranged from 0.3 to 0.45 (figure 3-13). Light-adapted 30 Hz flicker ERGs had an abnormal waveform in three of five patients with a broadened trough but no definite delay and normal amplitude. Additional delay was observed in the four eyes of the two oldest subjects, a brother and sister with myopic degeneration. The light-adapted single flash cone ERG was of abnormal waveform in all five individuals with a broadened a-wave and a sharply rising b-wave lacking photopic oscillatory potentials; b:a ratios ranged from 1.5 to 3.5. The ON-OFF ERGs showed severe ON b-wave reduction and sparing of both the a-wave and the OFF response. Short wavelength flash ERGs were subnormal in four of four cases, in keeping with ON pathway dysfunction. The waveforms in the four younger patients that had been tested with a shortened protocol were qualitatively similar to those described above. PERG P50 was variable, being normal in subject GR5, subnormal in subjects GR3 and GR4; and undetectable in subjects GR1 and GR6.

Table 3-8. Clinical characteristics and molecular pathology of subjects with *GRM6* retinopathy reported here and elsewhere

Reference		Sex	Age at exam	Refractive error (dioptres)		VA*		Nystagmus	Molecular diagnosis
				OD	OS	OD	OS		
This study	subject GR1	Male	75	-16.50/-1.00x110	-17.00 (balance)	0.36	3.00	Yes	p.[**Arg352Cys** (+) Gln708X]
	subject GR2	Female	58	-12.00/-2.00x 7	-11.00/-2.00x150	1.78*	0.80*	Yes	p.[**Arg352Cys**(+) Gln708X]
	subject GR3	Female	30	-1.00/-1.25x105	-0.50/-2.50x 50	0.18*	0.18*	No	p.[**Arg677Cys** (+) **Arg677Cys**]
	subject GR4	Female	11	-0.50/-1.00x 80	-0.50/-1.50x105	0.20	0.00	Yes	p.[**Gly756Asp** (+) **Gly756Asp**]
	subject GR5	Female	10	-7.00/-3.50x 10	-7.00/-1.75x175	0.20*	0.18*	No	p.[**Val193fsX15** (+) **Val193fsX15**]
	subject GR6	Female	7	-4.50/-2.75x 20	-6.00/-2.00x180	0.08	0.14	No	p.[**Val193fsX15** (+) **Val193fsX15**]
	subject GR7	Female	9	-3.50/-3.50x180	-3.50/-4.00x180	0.58	0.28	Yes	p.[Arg238X (+) **Arg677Cys**]
	subject GR8	Male	8	-4.25/-1.50x175	-2.50/-1.00x180	0.54	0.2	No	p.[**Arg677His** (+) **Arg677His**]
	subject GR9	Female	7	+0.25/-0.75x 25	+0.25/-1.50x160	0.22	0.2	Yes	p.[Gly275Asp (+) **Pro689fsX24**]
Dryja *et al.* [157]		Male	37	-0.25^ (averaged between two eyes)		0.0	0.0	No	p.[Arg621X] + [Arg621X]
		Male	31	-4.62^ (averaged between two eyes)		0.3	0.3	Yes	p.[Gly150Ser] + [Gln708X]
		Female	14	-5.38^ (averaged between two eyes)		0.1	0.18	No	p.[Glu781Lys (+) Glu781Lys]
Zeitz *et al.* [482]		Male	46	+3.50^	+1.50^	0.3	0.1	Yes	p.[Pro46Leu] + [Val243fs]
		Male	36	-3.00^	-3.00^	0.4	0.4	Yes	p.[Cys522Tyr] + [Cys522Tyr]
		Female	13	-9.00^	-10.00^	1.0	0.2	No	p.[Gly58Arg] + [Leu26fs]
		Female	10	-10.00^	-8.00^	0.1	0.1	Yes	p.[Gly58Arg] + [Leu26fs]
		Female	8	-6.50^	-6.00^	0.5	0.5	No	p.[Gly58Arg] + [Leu26fs]
O'Connor *et al.* [339]		Female	7	-2.50/-3.50x 85	-2.50/-4.00x100	0.3	0.3	Yes	p.[Arg238X (+) Tyr409X]
Leifert *et al.* [484]; Zeitz *et al*.[483]		Female	63	-6.00/-3.00x 80	-9.00/-2.00x 90	0.3*	0.4*	No	p.[Ile405Thr (+) Ile405Thr]

Subjects GR1 and GR2 and subjects GR5 and GR6 are pairs of siblings. Subjects GR1 and GR2 have British origin while subjects GR3 to GR9 originate from South Asia.

* Snellen acuity converted to logMAR equivalent

^ spherical equivalent

Previously unreported changes are in bold font.

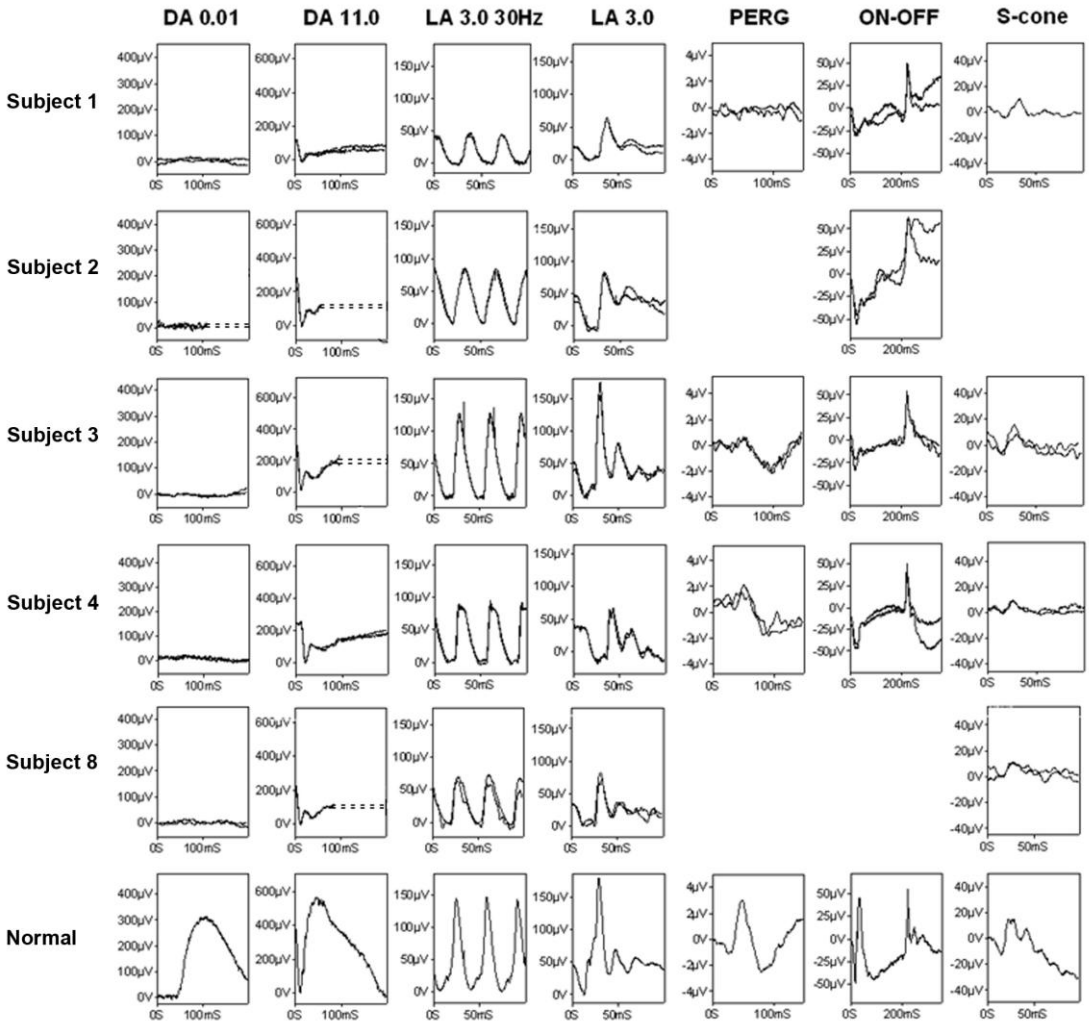

Figure 3-13. Full field ERGs and pERGs from individuals with *GRM6*-related complete CSNB. Normal traces are shown for comparison. Dark-adapted responses are shown for flash strengths of 0.01 and 11.0 cd·s·m^{-2} (DA 0.01; DA 11.0). Photopic ERGs are shown for flash strength 3.0 cd·s·m^{-2} (LA 3.0; 30 Hz and 2 Hz) and for ON-OFF and S-cone system stimulation. All responses show a high degree of inter-ocular symmetry and are for one eye only. A 10 ms prestimulus delay was used in subject GR4. Missing traces in subjects GR2 and GR8 were unrecordable due to nystagmus or eye movement artefact.

3.1.6.2.3 Genetic analysis results

Analysis of array data from subjects GR1 and GR2 (section 2.5.4.2) showed that among the 25% of the genome predicted to be shared between siblings there was a chromosomal segment around *GRM6* but not one around *TRPM1*. Overall, nine mutations in *GRM6* were detected in the seven families studied. Those include five missense variants, two nonsense mutations and two one base pair deletions. Tables 3-8 and 3-9 summarise the results and review the

variants identified in the *GRM6* coding region that are likely to be pathogenic. No statistically significant correlation between severity of mutated alleles per individual and high myopia could be found.

Four novel missense disease-associated variants were identified: the p.Arg352Cys change occurs at a residue located in the extracellular, ligand-binding, part of the receptor without directly affecting the glutamate binding pocket [483]; two novel changes occur at the same site (p.Arg677Cys, p.Arg677His), a highly conserved across species and other group III mGluRs residue that is located in the intracellular part of the protein; the p.Gly756Asp mutation alters an amino acid located in the fifth transmembrane helix. None of these missense changes is predicted to interfere directly with the dimerisation of mGluR6 [483]. Two novel one base pair deletions that cause premature termination codons were also identified (p.Val193fsX15, Pro689fsX24).

Table 3-9. Coding sequence changes in *GRM6* that are likely to be pathogenic and *in silico* analysis of their effect

Nucleotide substitution	Amino acid exchange	Number of alleles in affected	SIFT		PolyPhen-2		Reference
			Prediction	Tolerance index (0-1)	Prediction	HumVar Score (0-1)	
c.57_75dup19	p.Leu26fs	3		*not applicable*			Zeitz *et al*. [482]
67_82delCAGGCGGGCCTGGCGCinsT	p.Gln23_Arg28del5insCys	1		*not applicable*			Xu *et al.* [485]
c.137C>T	p.Pro46Leu	1	intolerant	0.00	POD	1.00	Zeitz *et al.* [482]
c.172G>C	p.Gly58Arg	3	intolerant	0.03	POD	0.91	Zeitz *et al.* [482]
c.448G>A	p.Gly150Ser	1	intolerant	0.00	POD	1.00	Dryja *et al.* [157]
c.575delG	p.Val193fsX15	4		*not applicable*			this study
c.712C>T	p.Arg238X	2		*not applicable*			O'Connor *et al.* [339], this study
c.720_721insG	p.Val243fs	1		*not applicable*			Zeitz *et al.* [482]
c.823G>A	p.Gly275Asp	2	tolerated	0.07	POD	0.94	Zeitz *et al.* [340],this study
c.1054C>T	p.Arg352Cys	2	tolerated	0.07	POS	0.55	this study
c.1214T>C	p.Ile405Thr	2	tolerated	0.29	POS	0.78	Zeitz *et al.* [483]
c.1227C>A	p.Tyr409X	1		*not applicable*			O'Connor *et al.* [339]
c.1537G>A	p.Val513Met	4	tolerated	0.33	Benign	0.01	Xu *et al* .[485]
c.1565G>A	p.Cys522Tyr	2	intolerant	0.00	POD	1.00	Zeitz *et al.* [482]
c.1861C>T	p.Arg621X	2		*not applicable*			Dryja *et al.* [157]
c.2029C>T	p.Arg677Cys	3	tolerated	0.21	POD	1.00	this study
c.2030G>A	p.Arg677His	2	tolerated	0.22	POD	1.00	this study
c.2062delC	p.Pro689fsX24	1		*not applicable*			this study
c.2090A>T	p.Gln697Leu	1	intolerant	0.00	POD	0.96	Zeitz *et al.* [340]
c.2267G>A	p.Gly756Asp	2	tolerated	0.21	POS	0.45	this study
c.2122C>T	p.Gln708X	3		*not applicable*			Dryja *et al.* [157], this study
c.2341G>A	p.Glu781Lys	2	intolerant	0.01	POD	1.00	Dryja *et al.* [157]

3.1.6.3 Comment

Complete CSNB is usually but not always associated with high myopia [473]. Spherical equivalent in six of nine patients in the studied cohort was less myopic than -6.00 dioptres (12 out of 19 in all published cases including this study). Mutations in *NYX* and *GRM6* have been reported to contribute to high myopia without additional features of CSNB [485-486] but further studies are needed to confirm this association.

All affected individuals had a full field ERG phenotype consistent with complete CSNB. There was ON pathway involvement in rod and cone systems and evidence of S-cone system involvement. Two siblings with myopic degeneration showed 30 Hz flicker ERG delay but, as with other causes of complete CSNB, delay was not a prominent feature. A 75-year-old study subject had a subnormal ERG a-wave (DA 11.0), consistent with additional rod photoreceptor involvement. Dark-adapted ERG a-wave reduction was not present in any other patient, although this has been previously documented in two teenage patients without severe myopia [157].

Electrophysiology and family history can assist diagnosing different forms of CSNB and direct molecular genetic testing. Complete forms of CSNB with electronegative ERG can be inherited in an autosomal recessive (*GRM6, TRPM1*) or X-linked (*NYX*) fashion. Mutations in *NYX* are considered the most common cause, even when an X-linked inheritance pattern cannot be convincingly established through family history [340]. Mutations in *GRM6* or *TRPM1* should be suspected when a pedigree is not suggestive of X-linked inheritance. *TRPM1* is considered the most frequently mutated gene in autosomal recessive complete CSNB [476-477]. If the mode of inheritance is unclear, the only difference in electrophysiological phenotype among complete CSNB patients has been described using a dark-adapted 15 Hz flicker ERG [487]; patients with *TRPM1* mutations showed responses similar to those with *NYX* mutations, but different from those with *GRM6* mutations [476, 482].

To conclude, presentation of *GRM6*-related retinal dysfunction can be variable and electrophysiology is fundamental to the diagnosis. Identifying disease-causing variants in *GRM6* confirms autosomal recessive inheritance and facilitates accurate counselling.

3.1.7 Structure, Function and Molecular Pathology in Gyrate Atrophy

Gyrate atrophy of the choroid and retina is an autosomal recessive condition associated with significantly increased plasma ornithine levels [488]. Patients typically report night blindness and/or loss of peripheral vision in the second decade of life; myopia and early cataracts are also features of the disorder. On fundoscopy, sharply demarcated, circular areas of chorioretinal atrophy distributed around the peripheral fundus are observed that, later in the disease process, coalesce and spread posteriorly. The macula and consequently, central vision is often preserved into the fourth or fifth decade of life [489-490]. Over 200 individuals with gyrate atrophy have been reported since it was first described in the late 19th century, with a significant proportion of them being Finnish [491].

The underlying biochemical defect of gyrate atrophy is in OAT, a vitamin B6 dependant mitochondrial matrix enzyme. This enzyme catalyzes the conversion of L-ornithine, a nonproteinaceous amino acid, to proline and glutamic acid. OAT plays a role in cellular detoxification by disposing ornithine derived from dietary arginine thus removing uncoupled ammonia [492-495]. Chronic reduction of plasma ornithine levels with an arginine-restricted diet has been reported to slow disease progression in some instances [496].

The gene that encodes the 439-amino-acid human OAT precursor is expressed in most tissues, including liver, brain, neurosensory retina and RPE [497]. To date, over 50 mutations have been reported in *OAT* (HGMD) with their deleterious consequences largely confined to the eye. As the RPE is considered the primary site of dysfunction in gyrate atrophy, clinical trials of gene replacement therapy targeting the RPE or cellular therapeutic approaches involving induced pluripotent stem cell-derived RPE may be relevant to gyrate atrophy patients [498-501].

Histopathologic study of postmortem tissue and *in vivo* cross sectional imaging with time domain OCT have been previously used to provide insight into

structural changes in gyrate atrophy [502-506]. Retinal histopathology has been reported in human as well as in animal models of gyrate atrophy [498, 502, 507]. In a 98-year-old patient, later identified to be homozygous for a p.Glu318Lys mutation [508], focal areas of photoreceptor atrophy with an underlying hyperplastic RPE were observed in the posterior pole. Near the transition from relatively preserved to atrophic retina, the RPE was either absent or dysmorphic. More peripherally to this transition zone both RPE and photoreceptor cells were absent. At a short distance into the area of atrophic RPE, photoreceptor cell nuclei abutted directly onto Bruch's membrane; the underlying choriocapillaris were preserved. Complete absence of outer retina, RPE, choriocapillaris and most medium and large choroidal vessels was observed in the atrophic region [502]. Regarding *in vivo* investigation, although resolution is relatively low in time domain OCT detection, features such as oedema and macular hole have been described [504-506].

In this section SD OCT (an alternative to time domain OCT with significant sensitivity and speed advantages; section 1.3.3.3) and fundus autofluorescence imaging findings in gyrate atrophy are detailed. Fundus-controlled perimetry (also known as "microperimetry", a method for accurate functional assessment of the central retina with high spatial resolution and continuous fixation monitoring [509]), features and novel mutational data are also reported.

3.1.7.1 Methods

3.1.7.1.1 Subjects

Seven unrelated patients with a diagnosis of gyrate atrophy were ascertained over a 10-year period of time; all had a retinal dystrophy and fundoscopic features compatible with those previously described in gyrate atrophy together with a significantly raised plasma ornithine level. Subjects GA1 to GA7 are numbered according to age (youngest to oldest).

3.1.7.1.2 Retinal imaging and perimetry testing

Fundus autofluorescence imaging, SD OCT and fundus-controlled static perimetry were performed (imaging was performed by Dr Eva Lenassi and PS, perimetry testing was performed by Dr Eva Lenassi). The Spectralis HRA+OCT with viewing module version 5.1.2.0 (Heidelberg Engineering) was used to acquire fundus autofluorescence images (over a 30° × 30° and/or a 55° × 55° field; six patients tested) and tomographs (all seven patients tested). The SD OCT protocol included a horizontal, linear scan (100 B-scans averaged to improve the signal-to-noise ratio) centred on the fovea and a volume scan (minimum of 19 B-scan slices, 20° x 20° or 20° x 15°) for each eye. Retinal thickness in the central and inner macula ETDRS subfields were assessed; the HEYEX software interface (version 1.6.2.0; Heidelberg Engineering) was used for all measurements. Static perimetry (MP1 Microperimeter, Nidek Technologies, Padova, Italy) was performed in six patients. The semi-automatic examination with number of stimuli ranging from 49 to 82, threshold sensitivities from 0 to 20 dB, test spot size Goldmann I, projection time 1000 ms and 4-2 staircase test strategy was used. A smaller than usual stimulus size was chosen as it has been previously suggested that with such stimuli, it is possible to observe little islands with residual function [510].

3.1.7.1.3 Genetic analysis

Blood samples were collected and the *OAT* gene (NM_000274.3) was screened in all affected individuals (screening was performed by Dr Alice E Davidson; sections 2.4.3, 2.4.9 and 2.4.16). When possible, parental DNA samples were screened to establish phase of variants (subjects GA4 and GA6).

3.1.7.2 Results

3.1.7.2.1 Clinical findings

Table 3-10 presents data on the seven affected individuals studied (age range 10 to 52). The mean visual acuity was 0.26 logMAR (range 0.10 to 0.50). Presentation was in the first decades of life: four patients were noted to have abnormal retinal appearance in routine refraction following difficulty reading the blackboard in early school years (subjects GA1, GA2, GA4, GA6); one presented with night vision problems around the age of 12 (subject GA5); one recalls night blindness from a young age and problems with peripheral vision from early teenage years, but medical advice was only sought at age 26 (subject GA7); one presented with poor central vision (1.00 logMAR in each eye) with electrophysiology suggesting that this is caused by functional visual loss. Six of seven affected individuals were night blind and seven of seven had elevated plasma ornithine concentration. Subject GA5 and GA7 had bilateral cataract extractions with intraocular lens implants at age 29 and 41 respectively; subject GA6 had the right eye operated at age 22 and the left at age 26. Subject GA7 had late-onset sensorineural hearing loss and a paternal family history of hearing impairment; hearing problems were also reported for subject GA1. All individuals had a negative family history of retinal disease; subjects GA1 and GA2 were born to consanguineous parents. Fundoscopy revealed typical changes of gyrate atrophy in all seven patients. Importantly, retinal pigment migration was minimal or absent and retinal vessel diameter was relatively preserved. Sharply demarcated areas of increased or preserved signal were observed in autofluorescence images of all six cases tested. Colour fundus photography and fundus autofluorescence imaging are presented in figure 3-14.

Table 3-10. Clinical characteristics and molecular pathology of subjects with gyrate atrophy

Subject	Sex	Age at exam	Refractive error (dioptres)		VA (logMAR)		Colour vision	Presenting complaint (age at diagnosis)	Nyctalopia (age first noticed)	Ornithine levels at diagnosis (µmol/l)	Molecular diagnosis, mutations in *OAT*
			OD	OS	OD	OS					
GA1	Female	10	-6.75/-4.00x180*	-6.50/-4.00x180*	0.34	0.30	HRR full	increasing myopia (9)	yes (8)	1390	p.[**Gly91Glu**];[**Gly91Glu**]
GA2	Female	14	-6.00/-2.50x25	-5.50/-2.50x155	0.10	0.16	HRR full	increasing myopia (11)	no	1152	p.[**Gly51Asp**];[**Gly51Asp**]
GA3	Female	17	-2.00	-1.75/-0.50x170	0.22	0.20	ISH 17/17	poor central vision (17)	yes (17)	775	p.[Glu318Lys];[?]
GA4	Male	30	Myopic astigmatism		0.18	0.20	ISH 17/17	increasing myopia (6#)	yes (14)	908	p.[Pro199Gln];[Pro417Leu]
GA5	Female	34	-13.50/-1.50x75^	-11.00/-1.50x120^	0.50	0.20	ISH test plate only	night blindness (13)	yes (12)	~900	p.[Pro199Gln(;)Pro417Leu]
GA6	Female	38	Myopic astigmatism^		0.10	0.40	ISH 6/17	increasing myopia (9)	yes (27)	~1000	p.[**Gly121Asp**];[Tyr299X]
GA7	Female	52	-9.50/-2.00x177^	-7.75/-3.00x7^	0.50	0.20	ISH 5/17	night blindness (26)	yes (always)	~700	p.[Tyr55His(;)**Arg250X**]

*cycloplegic refraction
^prior cataract surgery
#diagnosed with retinal dystrophy; gyrate atrophy was diagnosed at age 30
Normal plasma ornithine levels: 20 to 114 µmol/l. Novel changes are in bold font

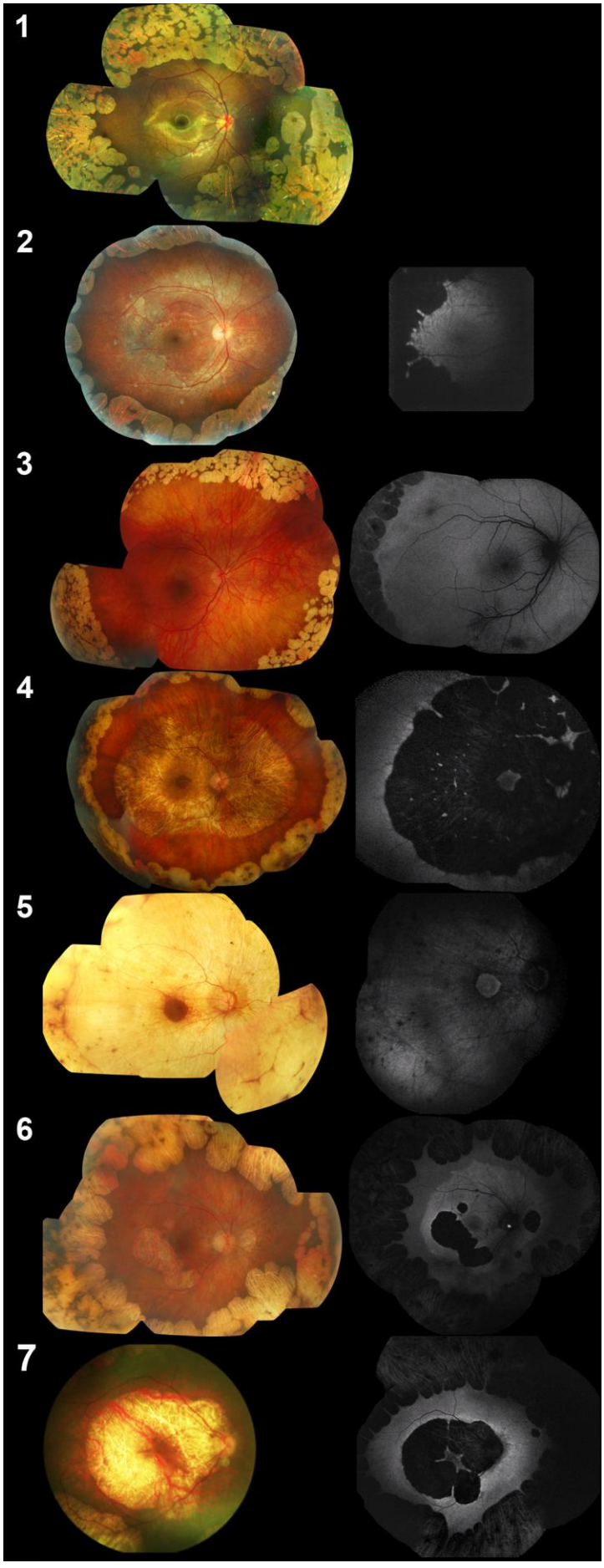

Figure 3-14. Colour fundus photography and fundus autofluorescence imaging of individuals with gyrate atrophy and *OAT* mutations. The number relating to each pair of images corresponds to the case number (subjects GA1 to GA7) and patients are numbered according to age (youngest to oldest; age range 10 to 52). Bone spicule pigmentation is minimal, retinal vessels are relatively preserved and circular areas of chorioretinal atrophy are evident in fundus photography. Sharply demarcated areas of increased or normal signal are observed in fundus autofluorescence images.

SD OCT demonstrated structural changes concordant between eyes in all affected individuals. For subjects GA1 and GA3, SD OCT revealed multiple intraretinal cystic spaces bilaterally and no other significant abnormality (figure 3-15). Hyporeflective cysts varying in size were also detected in the remaining five cases. In these patients (subjects GA2, GA4, GA5, GA6 and GA7), the hyperreflective band corresponding to the photoreceptor IS/OS junction was preserved in the regions where autofluorescence signal was normal or increased. Outside these regions, typically at the edges of foveal scans and at the more peripheral scans of the volume series, extensive loss of IS/OS junction reflectivity and significant thinning were observed. The thinning was not confined to the scattering layers in the outer retina, but also extended to the inner retinal layers, the hyperreflective band corresponding to the RPE/Bruch's complex and the structures often seen posterior to it. Structures corresponding to the external choroidal margins, large choroidal vessels and inner scleral surface were visible on the scans of all affected individuals. A loss of focal hyperreflectivity in the inner choroid was frequently observed and structures resembling large choroidal vessels appeared to be in close proximity to the hyperreflective band interpreted as Bruch's membrane. Vitreomacular traction and/or epiretinal membrane causing irregularity of the retinal surface were observed in the four oldest subjects. An interesting shared feature in the SD OCT of all seven individuals was the presence of hyperreflective deposit in the ganglion cell layer, particularly over the regions of preserved, or at a short distance into the regions of absent, autofluorescence. When the amount of hyperreflective material was increased deposits coalesced and were depicted as vertical hyperreflective lines (for example figure 3-15, subjects GA3 and GA4; figure 3-16B, subject GA4). Another interesting finding was the presence of round or ovoid hyporeflective spaces with hyperreflective borders on SD OCT scans from the four older patients (subjects GA4, GA5, GA6 and GA7). These were typically found in the transition from relatively preserved to atrophic retina (figure 3-17, subject GA4) and previously were termed "outer retinal tubulation" [511]. Finally, when thickness profiles were evaluated, relative thickening was observed in the more central ETDRS subfields of younger subjects (figure 3-16A, subjects GA1, GA2 and GA3).

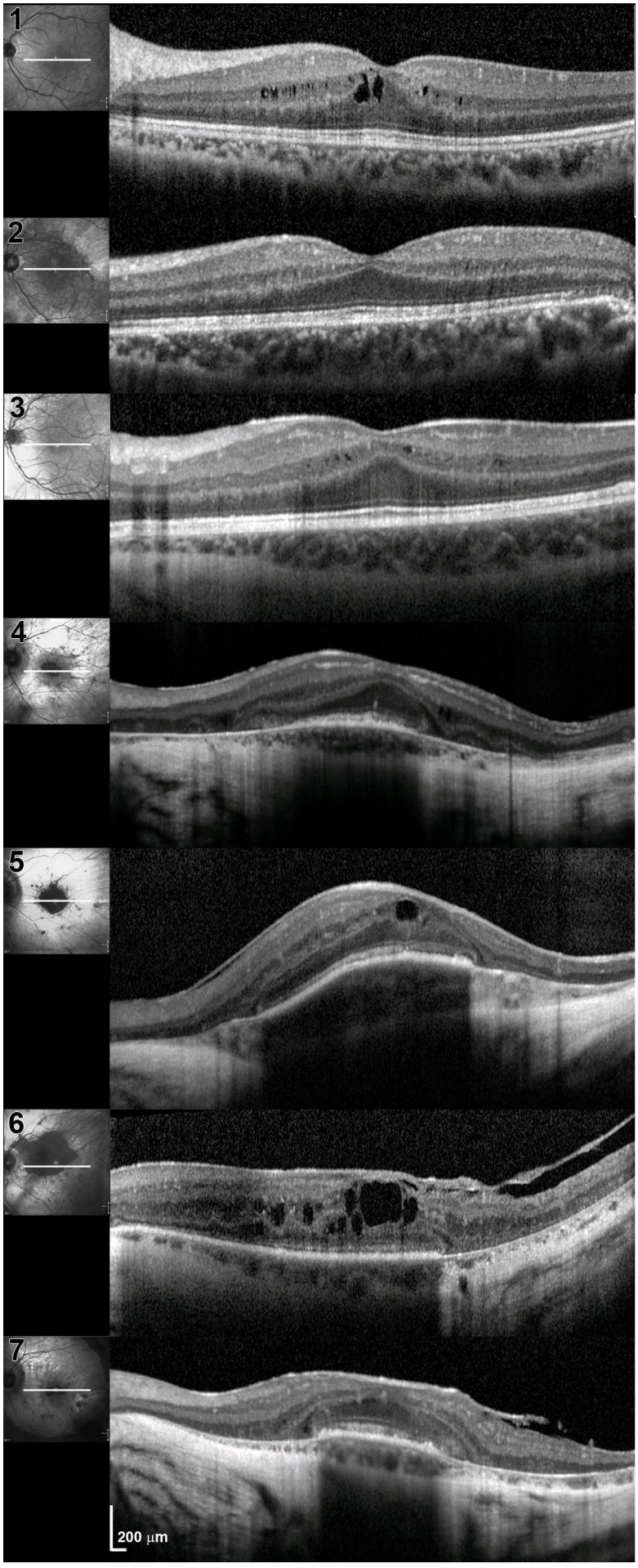

Figure 3-15. Foveal linear SD OCT scans of seven individuals with gyrate atrophy (subjects GA1 to GA7, ordered by age).

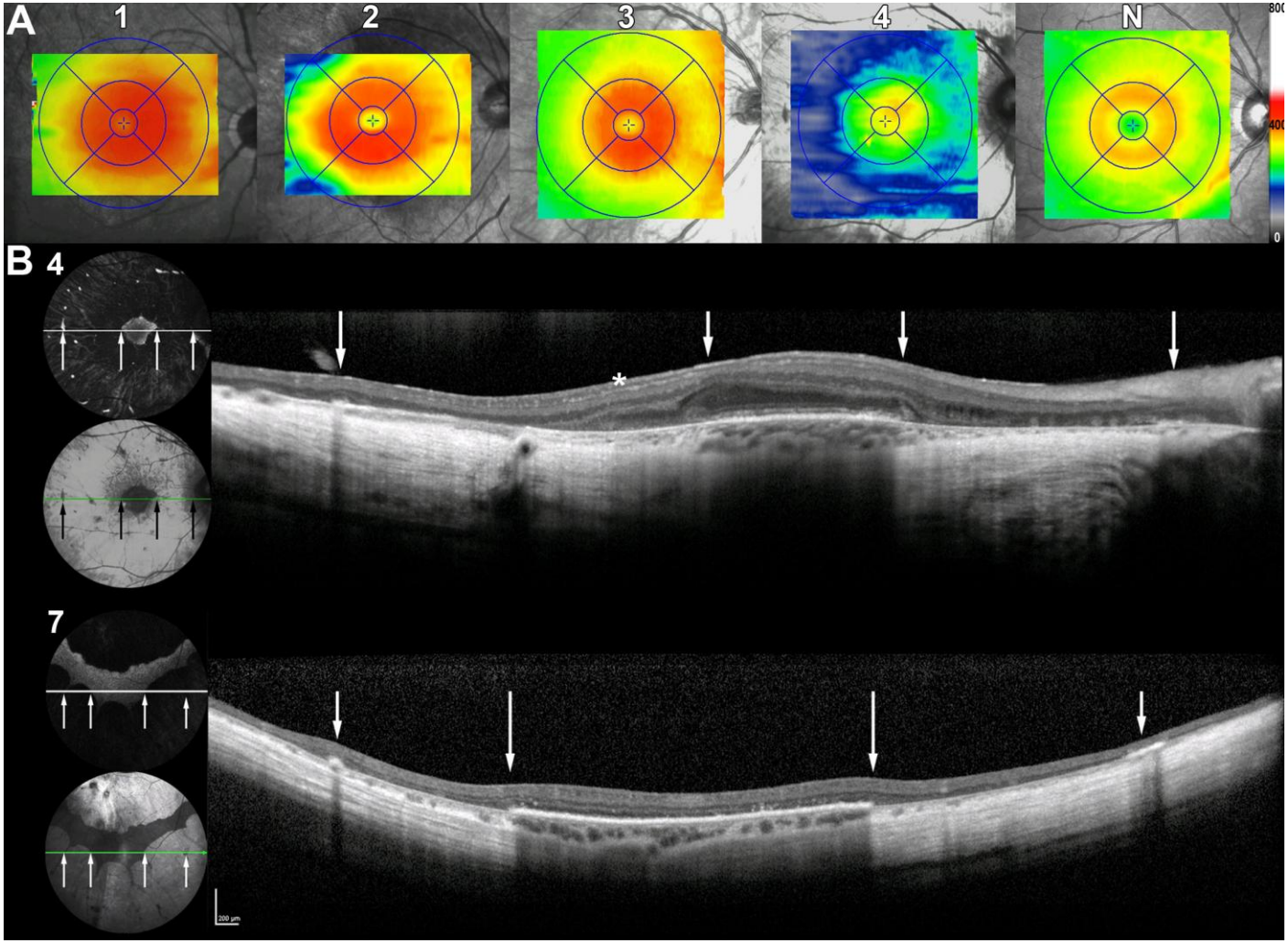

Figure 3-16. SD OCT findings in gyrate atrophy.
[A] Thickness profiles of foveal region of subjects GA1 (aged 10), GA2 (aged 14), GA3 (aged 17) and GA4 (aged 30). A healthy 28-year-old control (N) is also shown. Thickening of the central subfields is evident in the three younger subjects and thinning of midperipheral subfields is demonstrated in the older patient.
[B] 55° field fundus autofluorescence, infrared imaging and SD OCT scans from subjects GA4 (aged 30) and GA7 (aged 52). The borders from preserved to absent autofluorescence correspond to transition zones in SD OCT (arrows). In subject GA4, the structures corresponding to choroidal layers are very thin and the scleral surface is clearly visible. Hyperreflective deposit arranged in a linear pattern is observed in the band corresponding to the ganglion cell layer (asterisk). In subject GA7, a linear scan from a peripheral area of preserved autofluorescence is presented. Preservation of the hyperreflective layer corresponding to the RPE is observed.

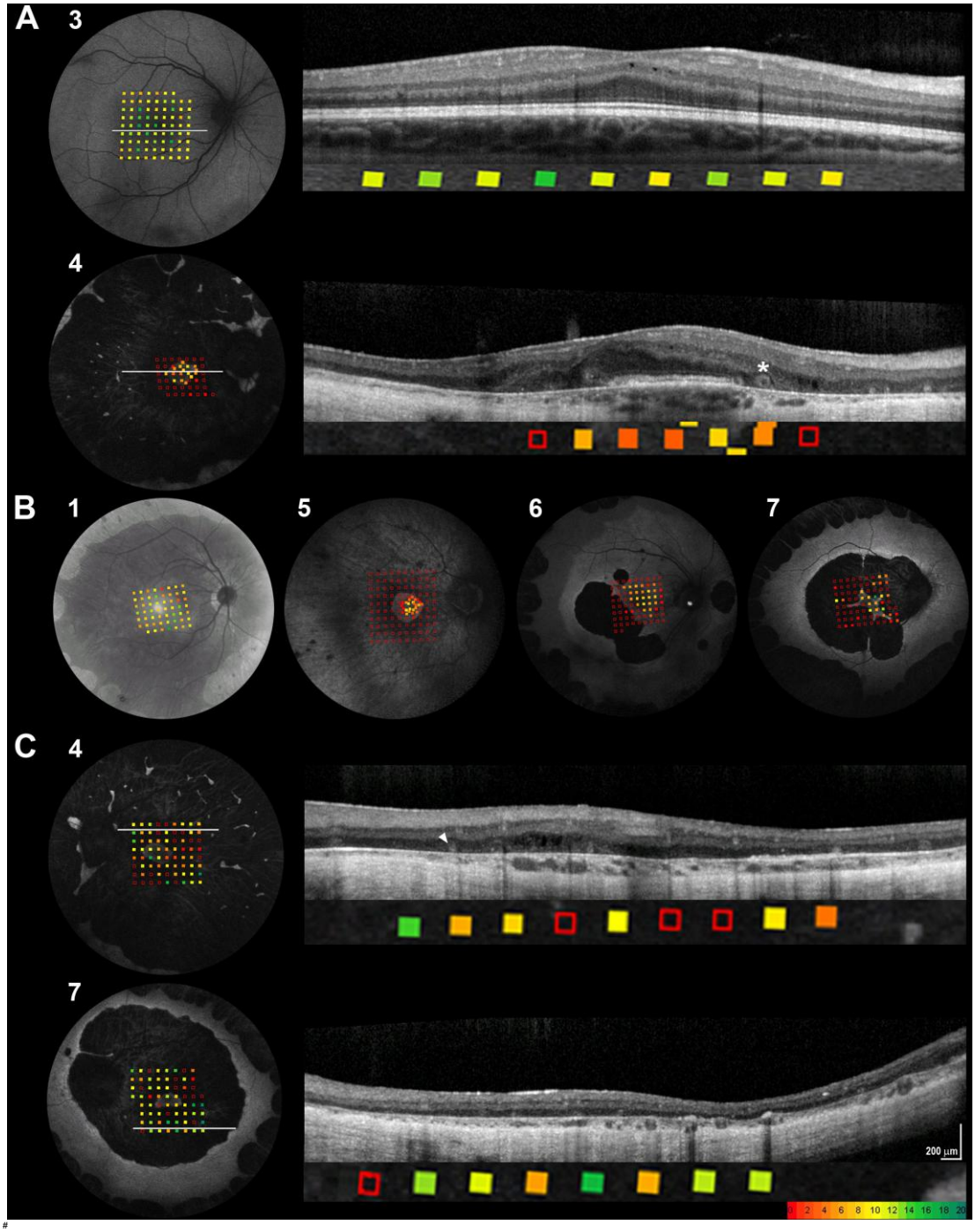

Figure 3-17. Functional assessment of the central retina in six individuals with gyrate atrophy. [A] Static perimetry testing results overlaid with fundus autofluorescence images and SD OCT scans from subjects GA3 (aged 17) and GA4 (aged 30) are presented. Mild reduction of foveal sensitivity is observed in the younger patient were fundus autofluorescence in normal and SD OCT only shows some cystic spaces. In the older patient, sensitivity is reduced over areas of relatively preserved fundus autofluorescence and with an intact IS/OS junction line. However, outside these regions there is no response even to the brightest stimulus. The asterisk marks a round hyporeflective space with hyperreflective borders ("retinal tubulation"). This could reflect photoreceptors forming rosettes in the absence of RPE.
[B] Static perimetry results from subjects GA1 (aged 10), GA5 (aged 34), GA6 (aged 38) and GA7 (aged 52). Datasets have been overlaid with infrared (subject GA1) or fundus autofluorescence (subjects GA5, GA6 and GA7) images. Similarly to subject GA3, subject GA1 presents with mildly reduced retinal sensitivity despite structurally intact retina. Conversely, in the older subjects, retina is functional only over areas of preserved autofluorescence, thus highlighting the clinical value of fundus autofluorescence imaging in

gyrate atrophy.
[C] Static perimetry testing results overlaid with fundus autofluorescence images and SD OCT scans from subjects GA4 (aged 30) and GA7 (aged 52) are presented. Surprisingly, retinal function appears preserved over areas of absent autofluorescence signal (on fundus autofluorescence) and very thin outer and total retina (on SD OCT). The scleral surface is clearly visible and the presence of islands of preserved photoreceptors cannot be excluded (arrowhead).
Threshold values of retinal sensitivity derived from fundus-controlled perimetry are presented according to the pseudocolour scale at the lower right hand corner; numbers indicate the scale in dB (0 to 20 dB). Normal sensitivity is indicated by green colour, and decreased sensitivity is indicated by red colour. Hollow red squares correspond to areas where the brightest perimetry stimulus was not detected by the subject (absolute scotoma).

Static perimetry testing results were overlaid with fundus autofluorescence images and SD OCT and are presented in figure 3-17. Stable fixation was observed in all eyes tested. In patients with structurally preserved posterior pole, although appropriate normative data are lacking, a mild reduction in macular sensitivity is likely (figure 3-17A and B, subjects GA1 and GA3). In the more severely affected individuals (subjects GA4 to GA7), reduced sensitivity was evident over regions of increased or preserved autofluorescence signal (on fundus autofluorescence imaging) and relatively intact IS/OS line (on SD OCT). In six out of eight eyes, outside these areas, patients did not respond even to the brightest stimuli (figure 3-17A and B, subjects GA4, GA5, GA6, GA7). Interestingly, in the remaining two eyes, consistent responses were documented over areas with significant outer retinal (absent IS/OS line on SD OCT) and RPE (no signal on fundus autofluorescence imaging) loss (figure 3-17C, subjects GA4 and GA7).

3.1.7.2.2 Genetic analysis results

Overall, nine likely disease-causing DNA variants in *OAT* were detected in 13 alleles of seven patients; these included seven missense and two nonsense changes (table 3-11). The bioinformatics programs SIFT and PolyPhen-2 both supported the likely pathogenicity of each of the identified missense mutations, including p.Gly51Asp, p.Gly91Glu and p.Gly121Asp which are novel to this study. Furthermore, all novel mutations identified (p.Gly51Asp, p.Gly91Glu, p.Gly121Asp and p.Arg250X) were found to be absent from the 1000 genomes project dataset (628 individuals from the 20100804 sequence and alignment release).

Table 3-11. Missense coding sequence changes in *OAT* that are likely to be pathogenic and *in silico* analysis of their effect

Nucleotide substitution	Amino acid exchange	SIFT		PolyPhen-2		Reference
		Prediction	Tolerance index (0-1)	Prediction	HumVar Score (0-1)	
c.152G>A	p.Gly51Asp	intolerant	0.00	POS	0.867	this study
c.163 T>C	p.Tyr55His	intolerant	0.00	POD	0.980	Kaufman *et al.*[512]
c.272 G>A	p.Gly91Glu	intolerant	0.00	POD	1.000	this study
c.362 G>A	p.Gly121Asp	intolerant	0.01	POD	0.995	this study
c.596 C>A	p.Pro199Gln	intolerant	0.00	POD	0.994	Kaufman *et al.*[512]
c.952 G>A	p.Glu318Lys	intolerant	0.02	POS	0.626	Mashima *et al*.[508]
c.1250 C>T	p.Pro417Leu	intolerant	0.00	POD	0.997	Brody *et al.*[513]

3.1.7.3 Comment

All seven study subjects had myopic refraction, fundus changes typical of gyrate atrophy and greatly elevated plasma ornithine. Six of seven subjects complained of poor night vision and/or increasing myopia as their first symptom. In a previous report, more than 70% of patients presented with myopia [491]. Fundoscopy through dilated pupils in highly myopic children with or without night blindness is key for the early diagnosis of gyrate atrophy. However, it is noted that presentation can be unusual as in subject GA3, a low myope that presented with poor central vision, probably unrelated to the primary retinopathy.

Visual acuity loss in individuals with gyrate atrophy can be the result of disease progression causing central photoreceptor cell death, but also cataract or macular oedema. By the second decade, cataract is considered a uniform finding in gyrate atrophy patients [514]. Cataracts are typically posterior sutural, may have unique histological characteristics and require surgical intervention by the third or fourth decade of life [490, 514]. In the present series, the three older patients (subjects GA5, GA6 and GA7) had already undergone bilateral cataract surgery. Cystoid macular oedema can be another ocular manifestation of gyrate atrophy with at least four cases reported to date; fluorescein angiography and time domain OCT have been used to confirm this macular complication [504-505]. Hyporeflective cystic spaces, predominantly at the inner retina were identified with SD OCT in all affected individuals suggesting that oedema is also a uniform finding. RPE dysfunction/loss leading to disruption of the outer blood-retinal barrier and diffusion of fluid toward intraretinal spaces is likely to be the main mechanism of oedema formation in gyrate atrophy. The fact that it is observed even in younger subjects with structurally intact, although thickened (figure 3-15), retina may suggest RPE dysfunction as an early abnormality leading to photoreceptor cell exposure to toxic agents from choroidal circulation. In older subjects, in addition to the inner retinal hyporeflective cystic spaces, SD OCT detected epiretinal membrane and vitreomacular traction.

Hyperreflective deposits on SD OCT were observed in the ganglion cell layer of all individuals in the present series (figure 3-15, subjects GA3 and GA4; figure 3-16B, subject GA4). This material was more obvious but not confined to the areas near the transition from relatively preserved to atrophic retina. Colourless, elongated glittering crystals, better seen in the fluorescein angiogram and located over or proximal to the preserved areas have been previously described in gyrate atrophy patients [489, 515]. Immunofluorescent localization of glial fibrillary acidic protein in the *Oat*$^{-/-}$ mouse retina, revealed labelling of the astrocytes in the innermost retina [498]. This finding suggests gliotic response to ongoing cell death [516] and one possibility is that the hyperreflective deposits on SD OCT reflect retinal gliosis. Inner retinal globular hyperreflective aggregates, with some similarities to the ones described in this study, have been previously reported in eyes with acute zonal occult outer retinopathy [517].

Another interesting finding in the tomographs of older gyrate atrophy patients was the presence of outer retinal tubulation (figure 3-17, subject GA4). Similar structures were observed in choroideremia and have been previously described in Bietti crystalline dystrophy, pseudoxanthoma elasticum and age-related macular degeneration [511]. It has been proposed that these rosettes are formed by degenerating photoreceptor cells becoming arranged in a circular or ovoid fashion [511]. This could partially explain the relative preservation of visual function over these structures (figure 3-17, subject GA4). As RPE is an early site of dysfunction in all conditions mentioned above, it can be speculated that the first step in the process may be RPE loss. In support to this is evidence from transplantation studies in murine eyes, which suggest that symbiosis of photoreceptors with microglia in rosettes promotes photoreceptor cell survival in the absence of RPE [518].

This study showed that in individuals with gyrate atrophy, perimetry stimuli are recognised over areas of preserved or increased signal in fundus autofluorescence imaging. Surprisingly, in two eyes of two patients (figure 3-17B), preserved retinal function was also observed over areas of absent autofluorescence signal, corresponding to RPE atrophy. When the relevant

perimetry data points were overlaid with SD OCT, a very thin retina with complete loss of IS/OS line was observed (figure 3-17C). It can be speculated that reflection, or scatter, of the stimulus from the sclera, onto preserved and functioning anterior retina, might account for the absence of an absolute scotoma, which would be expected from an area of complete loss of RPE and outer retina. Of the two eyes concerned, the results were reproducible and not evidently the result of poor compliance. When the subjects were asked to report the direction of the stimuli, again this was reproducibly reported, but did not always map to the area stimulated. Each eye had areas of intact anterior retina and the most likely explanation is that scatter towards the functioning areas allowed the subject to "see" these stimuli. Alternative explanations include small areas of preserved retina missed by OCT and fundus autofluorescence imaging and inner-retinal phototransduction. This finding suggests the need for caution in the interpretation of perimetry data when investigating dystrophies such as gyrate atrophy and is particularly relevant to its use in characterising the deficit in choroideremia in preparation for relevant therapeutic trials.

Six of seven individuals in the present series were identified to harbour either proven (subjects GA1, GA2, GA4 and GA6) or presumed (subjects GA5 and GA7) biallelic mutations in *OAT*. Subjects GA4 and GA5, who are not knowingly related, share the same genotype. The observed phenotypic differences between the two patients most likely can be attributed to other currently unidentified genetic factors and/or environmental modifying factors. Subject GA3 was found to harbour only a single previously reported [508] heterozygous *OAT* mutation, p.Glu318Lys. Interestingly, patient GA3 is of British ancestry and all previously reported individuals carrying this mutation are also of British or Irish descent [508].

The Glu318 residue is important for pyridoxal phosphate (PLP; the active form of vitamin B6) cofactor binding to OAT [494] and it has been suggested previously that a p.Glu318Lys substitution disrupts it [502, 508]. This missense change is one of only a handful of *OAT* mutations demonstrated to be responsive to PLP supplementation [508, 519-521]. Importantly, gyrate

atrophy patients reported with PLP responsive genotypes have been noted to have a less severe and progressive clinical presentation [508]; a finding in keeping with the clinical presentation of subject GA3 in this study.

To conclude, structural changes in gyrate atrophy are reported in detail: macular oedema is a common finding, the fovea is relatively thick in early stages of disease, deposits that could suggest retinal gliosis are observed and retinal tubulation is present in advanced disease. Functional testing highlights the importance of fundus autofluorescence imaging as a monitoring tool for gyrate atrophy and suggests that retinal sensitivity can be reduced even over structurally intact retina and in early stages of disease progression.

3.2 Identifying Novel Retinal Disease-associated Genes and Loci

Identifying novel retinal disease-associated genes is important for both scientists and clinicians. For scientists interested in understanding the development, function and structure of the visual system, each discovery elucidates a gene-protein component and biochemical pathway; thus important insights into the complex biochemistry and cellular physiology of the human eye are provided. For clinicians, knowledge of the molecular pathology of an affected individual allows improved counselling and management as well as access to relevant clinical therapeutic trials [522]. A method termed homozygosity mapping [105], both in isolation (section 3.2.3) and combined with exome sequencing (sections 3.2.4 and 3.2.5), was used to identify three novel retinal disease-associated genes.

3.2.1 Homozygosity Mapping

As previously mentioned (section 1.1.1.3), the simplest form of genetic mapping is linkage analysis [28, 64, 523]. Families with recessive retinal disease are small, often containing only one individual; this makes traditional linkage analysis challenging. In addition, the striking genetic heterogeneity of retinal disease (arguably the most genetically heterogeneous class of disorders in man [159]) makes pooling families to increase power unreliable. A genetic mapping strategy proposed by Lander and Botstein in 1987 [105], exploiting the increased power of consanguineous pedigrees, was utilised to tackle these issues.

Table 3-12 summarises some of the families in which homozygosity mapping was performed as part of this study; this work was part of a collaborative project with Drs Alice E Davidson and Zheng Li.

Table 3-12. Summary of families analyzed using SNP arrays on the assumption that affected individuals will be autozygous for a chromosomal region surrounding the mutated gene (homozygosity mapping)

family id	members of family genotyped	level of parental consanguinity	condition	Affymetrix SNP array used (experiment conducted by)	result {presumed disease-associated allelic variants in affected individuals or possible disease-related gene}
hz1786	two affected siblings	first cousins	RP	SNP 6.0 (outsourced)	analysis ongoing; exome sequencing performed
hz3774	three affected and one unaffected siblings; unaffected parents	first cousins	benign fleck retina	50K (Zheng Li)	exome sequencing performed; {***PLA2G5*: p.[Gly45Cys];[Gly45Cys]**}
hz3796	two affected siblings	first cousins	RP	50K (Zheng Li)	analysis ongoing; largest region around RP28 locus {*FAM161A?*}
hz4078	one affected	first cousins	cone rod dystrophy	SNP 6.0 (outsourced)	analysis ongoing; exome sequencing performed
hz4466	two affected siblings	first cousins	Usher syndrome type 1	50K (Zheng Li)	{***USH1C*: c.[446_448delAGG]; [446_448delAGG]**}
hz4665	one affected	multiple consanguineous unions	RP	SNP 6.0 (outsourced)	analysis ongoing; *CERKL* screening negative
hz14463	two affected siblings	third cousins	syndromic retinal disease	50K (PS)	analysis ongoing; small regions on 20p and 16q
hz15567	two affected and two unaffected siblings; unaffected parents	first cousins	syndromic retinal disease	50K (Zheng Li); SNP 6.0 (outsourced)	analysis ongoing
hz15617	one affected	second cousins	RP	SNP 6.0 (outsourced)	analysis ongoing; large region on 6q {*EYS*?}
hz15793	one affected	first cousins	CSNB	50K (PS)	analysis ongoing; *GRM6, TRPM1, NYX* excluded
hz15894	two affected siblings	first cousins	cone rod dystrophy	50K (Zheng Li)	analysis ongoing; largest region around RP58 locus {*ZNF513?*}
hz16071	three affected siblings	first cousins	retinal dystrophy	50K (Zheng Li)	{***MFRP*: p.[His384Profs8X]; [His384Profs8X]**}
hz16128	two affected siblings	first cousins	rod monochromasy	SNP 6.0 (outsourced)	{***CNGA3:* p.[Arg439Trp];[Arg439Trp]**}
hz16138	two affected siblings	first cousins	cone rod dystrophy	50K (PS)	analysis ongoing; large regions on 2p, 11q, 1p; *CNGA3* screening negative
hz16219	one affected	first cousins	cone rod dystrophy	SNP 6.0 (outsourced)	analysis ongoing
hz16329	two affected and one unaffected siblings; unaffected parents	first cousins	RP	50K (Zheng Li)	analysis ongoing; *EYS* screening negative
hz16359	one affected	second cousins	benign fleck retina	SNP 6.0 (outsourced)	{***PLA2G5*: p.[Trp62X];[Trp62X]**}
hz16597	two affected siblings	first cousins	RP	50K (Zheng Li)	analysis ongoing; largest region in chromosome 3 {*IMPG2*?}
hz16857	one affected	first cousins	RP	SNP 6.0 (outsourced)	analysis ongoing

Rows redacted at the request of the author

hz17761	one affected	uncle-niece union	RP	SNP 6.0 (outsourced)	large regions on 16q, 6p, 4q; *CYP4V2* screening negative
hz17775	two affected siblings	first cousins	LCA	SNP 6.0 (outsourced)	exome sequencing performed; {***KCNJ13*: p.[Arg166X];[Arg166X]**}
hz17811	one affected	distantly related	rod monochromasy	SNP 6.0 (outsourced)	{***CNGA3:* p.[Asp260Asn];[Asp260Asn]**}
hz17857	affected proband and two of her mother's sisters (both also affected)	multiple consanguineous unions	rod monochromasy	50K (PS)	analysis ongoing; {proband: *CNGA3:* p.[Arg427Cys];[Arg427Cys] and *CNGB3*: p.[Arg403Gln];[?]; proband's unaffected sister: *CNGA3:* p.[Arg427Cys];[Arg427Cys]; proband's affected maternal aunts: *CNGB3*: p.[Arg403Gln];[Arg403Gln]}
hz17880	one affected	first cousins	RP	SNP 6.0 (outsourced)	analysis ongoing; *NPHP3, RGR, CDHR1* and *CRB1* screening negative
hz17901	one affected	first cousins	RP	SNP 6.0 (outsourced)	analysis ongoing; *NPHP3, RBP3, RD3, CRB1, LRAT* and *GUCY2D* screening negative; {*USH2A* or *C2ORF71?*}
hz17962	one affected	distantly related	FEVR	SNP 6.0 (outsourced)	exome sequencing performed; {***LRP5*: p.[Gly479Arg];[Asp1366Gly]**}
hz17987	one affected	aunt-nephew union	RP	SNP 6.0 (outsourced)	{***CERKL:* p.[Arg364X];[Arg364X]**}
hz18014	one affected and her unaffected husband	first cousins	CSNB	50K (Zheng Li)	{***TRPM1*: c.[2021+2T>C];[2021+2T>C]**}
hz18043	one affected	distantly related	cone rod dystrophy	50K (PS)	analysis ongoing; *FAM19A3* excluded
hz18061	one affected	second cousins	late-onset macular dystrophy	SNP 6.0 (outsourced)	{***ABCC6:* p.[Arg1141X];[Arg1141X]**}
hz18120	one affected	distantly related	RP	SNP 6.0 (outsourced)	analysis ongoing
hz18173	one affected	first cousins	rod monochromasy	SNP 6.0 (outsourced)	{***CNGA3:* c.[1773_1776delCCCC];[1773_1776delCCCC]**}
hz18180	four affected siblings and their affected mother	first cousins	RP	50K (PS) SNP 6.0 (outsourced)	analysis ongoing; only one large region on 6q {*EYS* partially screened and found negative}
hz18193	one affected	first cousins	rod monochromasy	50K (PS)	large region on 8q {***CNGB3***}
hz18196	one affected	distantly related	cone dystrophy	SNP 6.0 (outsourced)	large region on 1p {***GNAT2***}
hz18393	one affected	second cousins	RP	SNP 6.0 (outsourced)	{***TULP1:* c.[190+1G>A];[190+1G>A]**}
hz18419	one affected	first cousins	RP	SNP 6.0 (outsourced)	analysis ongoing
hz18502	one affected	first cousins	late-onset macular dystrophy	50K (PS)	exome sequencing performed; among variants identified was ***CNGB3*: p.[Arg403Gln];[Arg403Gln]**
hz18504	one affected	first cousins	cone dystrophy	50K (PS)	analysis ongoing; largest region on 12q; *ABCA4, ADAM9, GNAT2, CNGB3, CNGA3* and *CLUL1* excluded; {*CEP290?*}
hz18529	one affected	first cousins	cone dystrophy	50K (PS)	{***PDE6C:* p.[Arg102Trp];[Arg102Trp]**}
hz18573	one affected	first cousins	Stargardt disease	SNP 6.0 (outsourced)	largest region on 1p {***ABCA4***}
hz18588	one affected	third cousins	retinal dystrophy	SNP 6.0 (outsourced)	multiple regions; among others 11q {***MFRP***}
hz18598	one affected	first cousins	rod monochromasy	SNP 6.0 (outsourced)	analysis ongoing; exome sequencing performed
hz18603	two affected siblings	first cousins	ocular albinism	50K (PS); SNP 6.0 (outsourced)	multiple regions; *OA1* screening negative but allele shared between the two affected (both male)
hz18610	one affected	first cousins	RP	SNP 6.0 (outsourced)	exome sequencing performed; {***RP1L1*: c.[601delG];[601delG]**}

hz18614	two affected siblings and their affected father	first cousins	RP	SNP 6.0 (outsourced)	analysis ongoing
hz18655	two affected siblings and their affected first cousin	first cousins	RP	SNP 6.0 (outsourced)	analysis ongoing; exome sequencing performed; {proband has *RP1*: p.[Glu487_Glu488delinsGluX]; [Glu487_Glu488delinsGluX]; proband's brother has *RP*1: p.[Glu487_Glu488delinsGluX];[?]; proband's cousin has *RP1*: p.[Glu487_Glu488delinsGluX]; [Glu487_Glu488delinsGluX]
hz18682	one affected	first cousins	fleck retina syndrome	SNP 6.0 (outsourced)	*RLBP1* in large region, *RDH5* excluded and screening negative; {***RLBP1*: p.[Val11Ala];[Val11Ala]**}
hz18730	one affected	first cousins	rod monochromasy	SNP 6.0 (outsourced)	{***PDE6C:* p.[Gly835X];[Gly835X]**}
hz18875	one affected	first cousins	RP	SNP 6.0 (outsourced)	analysis ongoing; *TULP1* screening negative
hz18994	one affected	first cousins	occult maculopathy	SNP 6.0 (outsourced)	analysis ongoing; largest region on 6q
hz19023	one affected	uncle-niece union	cone dystrophy	SNP 6.0 (outsourced)	analysis ongoing; {***GNAT2*?**}
hz19197	one affected	first cousins	RP	SNP 6.0 (outsourced)	analysis ongoing; {*CRB1*?}
hz19277	one affected	first cousins	RP and primary ciliary dyskinesia	SNP 6.0 (outsourced)	analysis ongoing; RPGR exon 6 excluded; {*USH2A*?}
hzbrntn	three affected siblings	first cousins	syndromic retinal disease and cataract	50K (Zheng Li); SNP 6.0 (outsourced)	analysis ongoing; exome sequencing performed; among variants identified was *TRNT1*: p.[Arg99Trp];[Arg99Trp]

3.2.2 Exome Sequencing

Exome sequencing was performed in DNA samples from 12 unrelated affected individuals previously studied using SNP genotyping arrays (section 2.1.4). The Agilent SureSelect 38 Mb exome capture and the Illumina HiSeq2000 sequencer were used (section 2.4.17). Families were selected on the basis of:
(a) Regions of linkage (homozygosity or shared among affected individuals) not containing genes previously associated with a phenotype similar to the proband. In some occasions retinal disease-related genes or obvious candidates were excluded using Sanger sequencing.
(b) A panel of individuals with a similar phenotype being available for screening putative novel genes.
(c) Availability of high molecular weight DNA of sufficient quantity.

This work was part of a collaborative project with Drs Vincent Plagnol and Alice E Davidson and some of the results are summarised in table 3-13.

Table 3-13. Summary of families analysed using a combination of SNP arrays and whole exome sequencing

family id	affected family members with available DNA samples	level of parental consanguinity	condition	number of variants identified in affected proband	result
hz1786	two siblings	first cousins	RP	17,949	analysis ongoing
hz3774	three siblings	first cousins	benign fleck retina	15,611	*PLA2G5*: p.[Gly45Cys]; [Gly45Cys]
hz4078	one	first cousins	cone rod dystrophy	17,835	analysis ongoing
hz17775	two siblings	first cousins	LCA	16,649	*KCNJ13*: p.[Arg166X]; [Arg166X]
hz19762	one	distantly related	FEVR	17,860	*LRP5*: p.[Gly479Arg]; [Asp1366Gly]
hz18502	one	first cousins	late-onset macular dystrophy	17,853	analysis ongoing; one possibility is *CNGB3*: p.[Arg403Gln]; [Arg403Gln]
hz18598	one	first cousins	rod monochromasy	18,075	analysis ongoing
hz18610	one	first cousins	RP	17,397	*RP1L1*: c.[601delG]; [601delG]
hz18655	two siblings, their affected first cousin	first cousins	RP	17,061	analysis ongoing (see also table 3-13)
hzbrntn	three siblings	first cousins	syndromic retinal disease and cataract	18,142	analysis ongoing; one possibility is *TRNT1*: p.[Arg99Trp]; [Arg99Trp]
nhz4040	two siblings	not consanguineous	rod monochromacy	18,374	analysis ongoing
nhz13874	three siblings	not consanguineous	rod monochromacy	15,986	analysis ongoing

3.2.3 Recessive Mutations in *TRPM1* Cause Complete CSNB

As discussed in section 3.1.6, on the basis of electrophysiology, two common subgroups of CSNB have been described [473]: complete CSNB and incomplete CSNB. Prior to this study, recessive mutations in *NYX* (chromosome X [474]) and *GRM6* (chromosome 5 [157]), have been associated with complete CSNB (for incomplete CSNB-associated genes refer to table 1-3, section 1.3). The *TRPM1* gene is located on chromosome 15 and encodes a transient receptor potential cation channel. In 2008, reduced *TRPM1* expression was described in the retinae of horses with a complete CSNB electrophysiological phenotype [524]. This finding together with evidence from other studies [525-526], suggested a possible role for *TRPM1* in the glutamate-mediated ON bipolar cell response.

A consanguineous family of South Asian origin is the basis of this section (family 1 in figure 3-18). The proband (V:1, family 1 in figure 3-18), a 2-year-old girl, was diagnosed with CSNB at eleven months of age. She was noticed to have nystagmus and convergent squint at the age of five months. There are multiple consanguineous marriages within the family and her mother and a maternal uncle also have nonprogressive night blindness. Cycloplegic refraction of the proband at 13 months was -14.00/-1.00x170 in the right and -13.00/-1.00x20 in the left eye. Fundoscopy revealed myopic fundi but was otherwise unremarkable. The proband's father and paternal grandmother had a normal ocular examination. Her mother, aged 28, presented with nonprogressive nyctalopia from an early age as well as convergent squint. She is a high myope (-23 dioptres spherical equivalent in each eye) and best corrected visual acuities were 0.26 logMAR for the right and 0.32 logMAR for the left eye. Fundus examination revealed myopic fundi (figure 3-19A). Electrophysiological findings were typical of complete CSNB, suggesting ON pathway dysfunction. It was not possible to examine the proband's sister (V-2, family 1 in figure 3-18) who developed nystagmus within the first year of life.

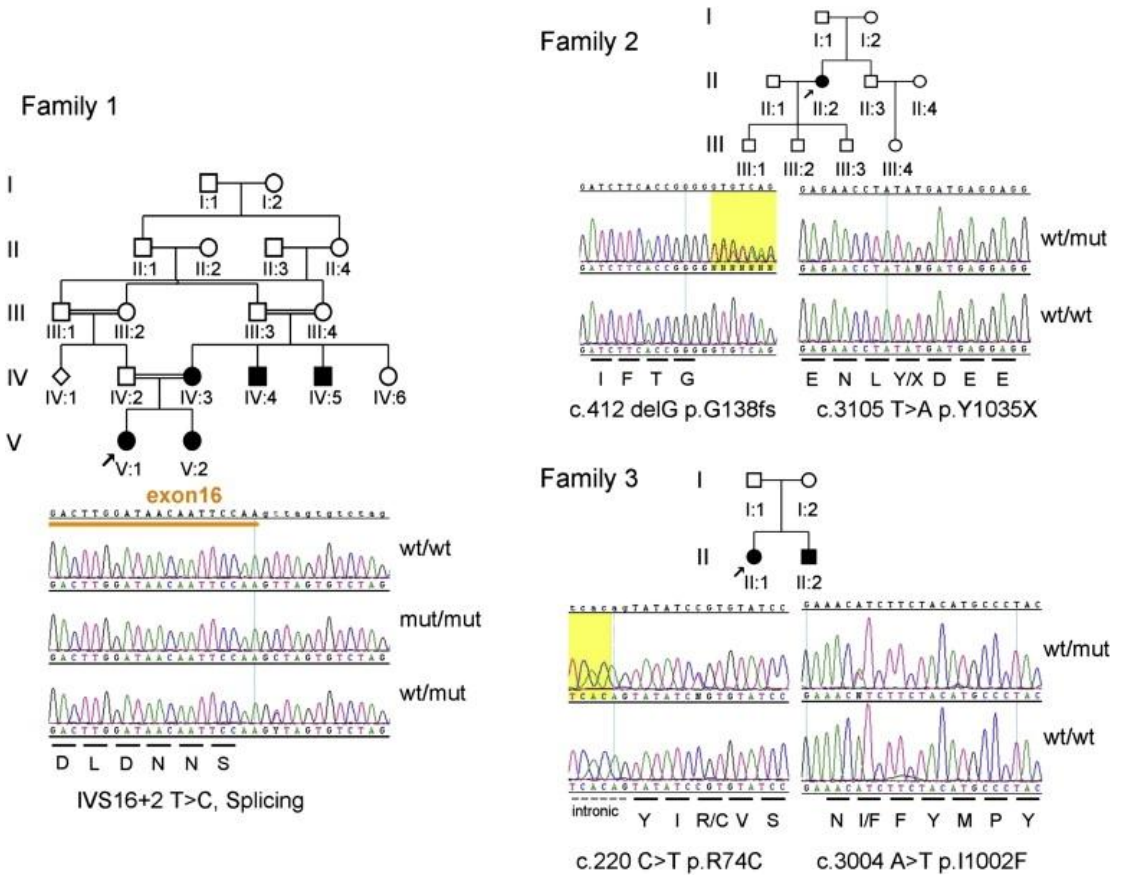

Figure 3-18. Pedigrees from evaluated families.
Electropherograms of DNA sequence surrounding likely disease-causing variants are shown beneath each pedigree.

DNA samples from the proband's unaffected father and affected mother (IV:2 and IV:3, family 1 in figure 3-18) were genotyped using the Affymetrix GeneChip Human Mapping 50K Array Xba (section 2.4.18.2.1; experiment conducted by Dr Zheng Li). The pedigree was consistent with the propagation of a single mutant allele from a recent ancestor such that the unaffected father was heterozygous and the affected mother autozygous for this allele. The largest region obeying this rule consisted of 15.9 Mb and was located on 15q (figure 3-20, section 2.5.4.1). One obvious candidate within this locus was the predominantly expressed in eye and skin gene *TRPM1*. Primers were designed for amplification of the 27 previously reported exons (NM_002420.4; experiment designed and conducted by Dr Zheng Li). A homozygous variant was identified in the affected mother (c.2021+2T>C); the father was heterozygous for this sequence alteration. This change would be predicted to abrogate the canonical donor sequence and affect efficient pre-mRNA splicing of intron 16 of the gene; RNA was not available to test this assertion.

Additional patients with a phenotype consistent with complete CSNB were screened for mutations in *GRM6* (section 3.1.6) and, if male, *NYX*. The cohort was purposefully biased towards female patients in order to be enriched for autosomal genes. Nine families that had negative *GRM6* screening and a pedigree not consistent with X-linked segregation were screened for *TRPM1* (screening by Dr Zheng Li and PS). Likely disease-causing alleles were detected in two families (figure 3-18, table 3-14) of white European descent. Variants identified are summarised in table 3-14.

A 36-year-old female (II:2, family 2 in figure 3-18) with clinical and electrophysiological diagnosis of complete CSNB, was found to harbour two disease-associated variants in *TRPM1*: c.416delG, p.Gly139ValfsX10 and c.3105T>A, p.Tyr1035X. Analysis of a maternal DNA sample revealed that these variants were biallelic. Importantly, both cause a premature termination codon. The patient had onset of nystagmus in the first year of life and was diagnosed with CSNB at age 16. Visual acuities were 1.00 logMAR in the right and 0.84 logMAR in the left eye. She was myopic (-15.50/-1.50x50 and −14.50/−1.00×90 in the right and left eye respectively) and had normal colour vision and full visual fields on kinetic perimetry (figure 3-19B). On examination, right convergent squint and pendular nystagmus were noted; myopic changes were evident on fundoscopy. Fundus autofluorescence imaging was normal (figure 3-19B) and electrophysiology was typical of complete CSNB. In order to determine whether heterozygosity for *TRPM1* mutation had a subclinical effect, the patient's unaffected mother (I:2, family 2 in figure 3-18) underwent electrophysiological testing; no abnormality was detected.

Two rare missense variants (c.220C>T, p.Arg74Cys and c.3004A>T, p.Ile1002Phe) were identified in a 24-year-old female affected with stationary night blindness (II:1, family 3 in figure 3-18). The patient reported nystagmus and a left divergent squint from birth. Difficulties seeing at night and poorer vision in her left eye from an early age were also noted. On examination at age 20, visual acuity was 0.28 logMAR in the right and 1.00 logMAR in the left eye. She was myopic (-4.25 dioptres in each eye), had a left divergent squint

and nystagmus. Fundoscopy revealed bilateral tilted optic discs but was otherwise unremarkable. Electrophysiology was typical of complete CSNB.

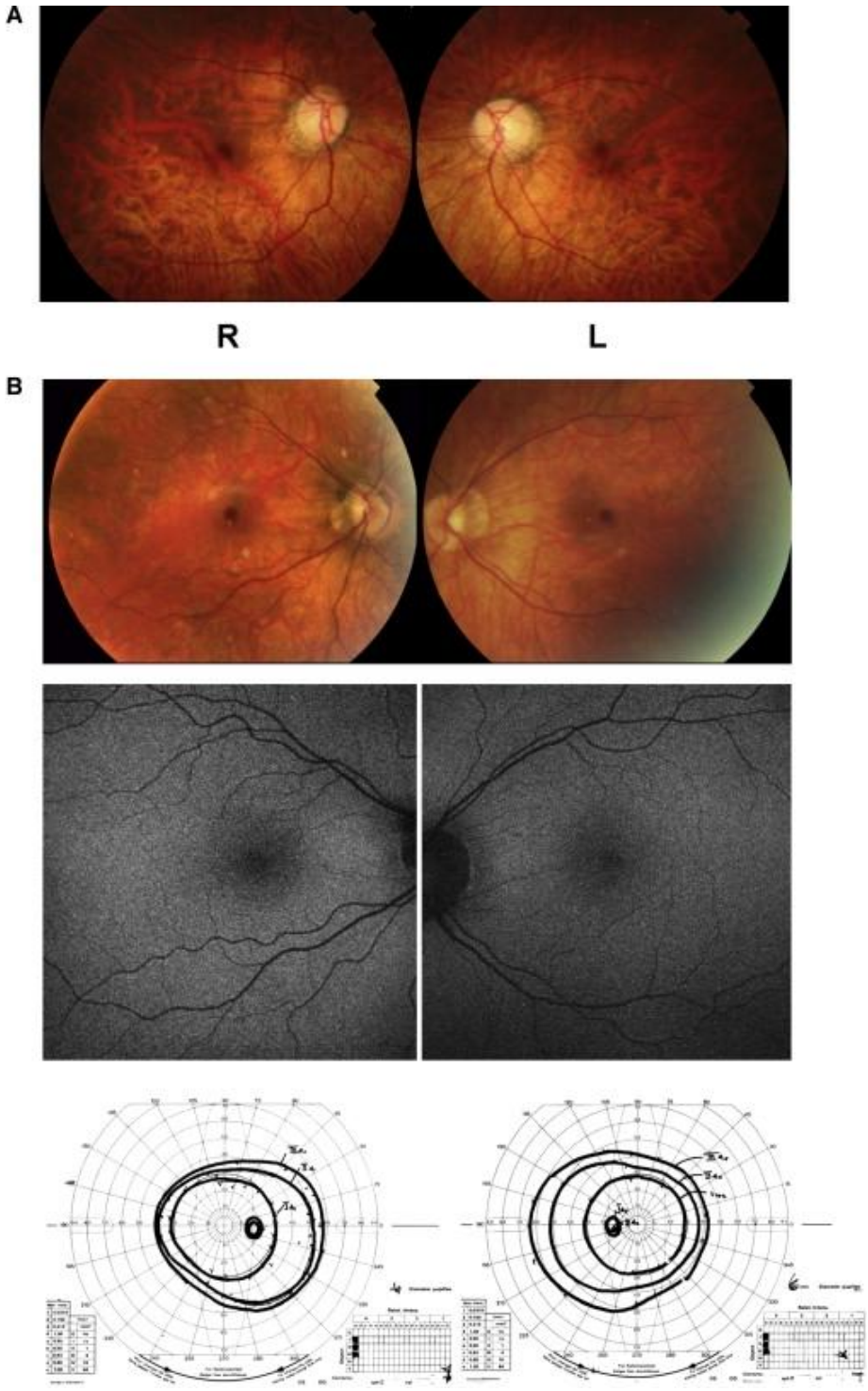

Figure 3-19. Clinical characteristics of *TRPM1* positive individuals.
[A] Colour fundus photographs of patient IV:3 in family 1.
[B] Colour fundus photographs, fundus autofluorescence and Goldmann kinetic perimetry of patient II:2 in family 2. Goldmann perimetry isopters for targets III4a, II4a and I4a are shown. See figure 3-18 for numbering of study subjects

Table 3-14. Summary of *TRPM1* coding and splice site variants in patients and controls

Variant*		**Affected individuals (9 patients)**		**Frequency in controls and EVS**	
Nucleotide	**Protein**	**homozygous or heterozygous**	**family id** (see figure 3-18)	**European control chromosomes**	**EVS [rs id]**
c.2021+2T>C	not known	homozygous	family 1	0/382	not applicable
c.412delG	p.Gly139fs	heterozygous	family 2	0/382	0/3462
c.3105T>A	p.Tyr1035X	heterozygous	family 2	0/382	0/3460
c.220C>T	p.Arg74Cys	heterozygous	family 3	0/382	0/3462
c.3004A>T	p.Ile1002Phe	heterozygous	family 3	0/382	0/3460
c.167A>G	p.Tyr56Cys	heterozygous	each change detected in a simplex complete CSNB case harbouring no second rare variant	0/382	0/3462
c.2162G>A	p.Arg721Gln	heterozygous		0/382	0/3462
c.2648A>G	p.Glu883Gly	heterozygous		0/382	0/3462
c.2872A>C	p.Met978Thr	heterozygous	found in *cis* in a single simplex female patient; no third rare variant detected	0/382	0/3460
c.4312A>G	p.Arg1438Gly	heterozygous		0/382	0/3460
c.2 T>C	p.Met1Thr			76/382	583/3452 [rs4779816]
c.95 G>A	p.Ser32Asn			74/382	757/3462 [rs2241493]
c.1239G>A	p.(=)			148/382	1450/3460 [rs1035705]
c.1813G>A	p.Val605Met			15/382	112/3460 [rs17815774]
c.2307T>C	p.(=)			111/382	934/3454 [rs12913672]
c.2340T>C	p.(=)			68/382	817/3456 [rs2288242]
c.4182G>A	p.Val1395Ile			22/382	140/3454 [rs3784588]

*variant numbering is based on NM_002420.4

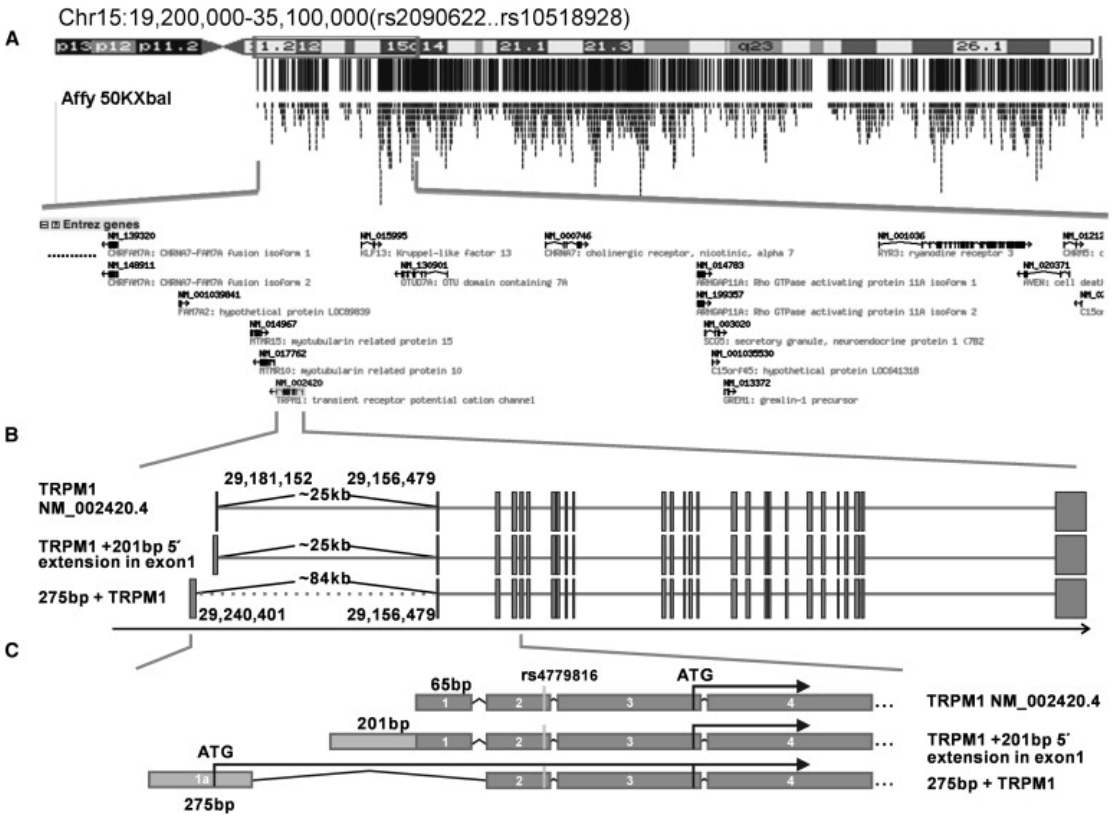

Figure 3-20. Homozygosity mapping and analysis of structure of the *TRPM1* gene.
[A] Largest region of homozygosity for family 1. This region is located on 15q, consists of 15.9 Mb, includes 280 contiguous SNPs and is flanked by rs2090622 and rs10518928. A total of 106 distinct Unigene clusters were found in this chromosomal interval. Only the partial region is shown.
[B] Results of RACE experiments for *TRPM1* transcripts in human retina and skin. One transcript with a 201 base pair 5′ extension of the previously reported exon 1 was found in both skin and retinal tissue. An alternative 5′ exon of 275 base pairs, denoted here as exon 1a, was detected in retina approximately 84,000 base pairs upstream of the previously reported exon 2. Interestingly, splicing was directly to exon 2, omitting exon 1. Approximate physical distances are shown.
[C] The initiation codon of *TRPM1* in the previously reported sequence (NM_002420.4) is shown (rs4779816). Other likely translation intitiation sites in the different transcripts are also presented.

The initially reported sequence (NM_002420.4 [527]) suggested a translation initiation codon within exon 2. Intriguingly, this methionine has been reported to contain a SNP (rs4779816; 2T>C, p.Met1Thr). This variant was tested in 191 control DNAs (ECACC, HRC-1 and 2; section 2.1.2) and a MAF of 0.198 was observed. This suggests that another position in the transcript is used for initiation of protein translation. To investigate the full-length transcripts in human retina and skin RNA, 5' and 3' RACE experiments were performed (designed and optimised by Dr Zheng Li, conducted by Dr Zheng Li and PS under Dr Li's supervision; figure 3-21, section 2.4.12). Firstly, a 5' extension of the initially reported *TRPM1* exon 1 was detected (figure 3-20). This sequence

did not extend the reading frame of the gene and contained three termination codons. Therefore, this 5' extension is unlikely to generate an alternative initiation codon in frame with the downstream sequence. Secondly, an unknown sequence was found at the 5' transcript end in a proportion of retinal clones. Sequence analysis revealed a 275 base pair long fragment that was contiguous with the sequence of exon 2 and contained an extension of the open reading frame (figure 3-20). This exonic sequence was found to be located approximately 84,000 base pairs upstream of exon 2. Exon 1 was absent from these clones. Alignment of *TRPM1* orthologs from diverse vertebrate genomes demonstrated that this novel 5' exon (henceforth referred to as exon 1a) was highly conserved [475].

In order to confirm the presence of this alternatively spliced transcript, RT PCR experiments were undertaken (conducted by Dr Zheng Li and PS, summarised in figure 3-21; section 2.4.2). PCR products containing exon 1a were detected in the retina but not in the skin. It is therefore likely that, at least in the retina, the protein is longer at the amino end than as yet appreciated.

The 3' RACE experiment revealed 3' region sequences identical to the previously reported sequence in both retina and skin (NM_002420.4 [527]). The novel alternative transcripts identified were screened for mutations in all probands; a common coding SNP was found c.16C>T, p.Arg6Trp (ss161641214) but no further variants were detected.

The finding of likely disease-causing mutations in *TRPM1* in individuals with electroretinographic evidence of ON bipolar cell dysfunction (qualitatively identical to that seen in *GRM6* retinopathy [157]) confirms the important role of this cation channel in human ON bipolar cell physiology. Transient receptor potential channels are a group of ion channels located mostly on the plasma membrane of numerous cell types. To date, 28 mammalian transient receptor potential channels have been identified; these demonstrate diverse functions and can be divided into six groups: TRPC, TRPV, TRPM, TRPP, TRPML and TRPA [528-531]. *TRPM1* is the founding member of the TRPM subfamily. It was identified as an RNA sequence in a mouse melanoma cell line and was

subsequently noticed to be expressed in melanomas with lower metastatic potential; thus the protein was termed melastatin [532]. Notably, melanoma-associated retinopathy, a retinal phenocopy for *TRPM1* retinopathy, has been recently associated with autoantibodies against *TRPM1* [533-534].

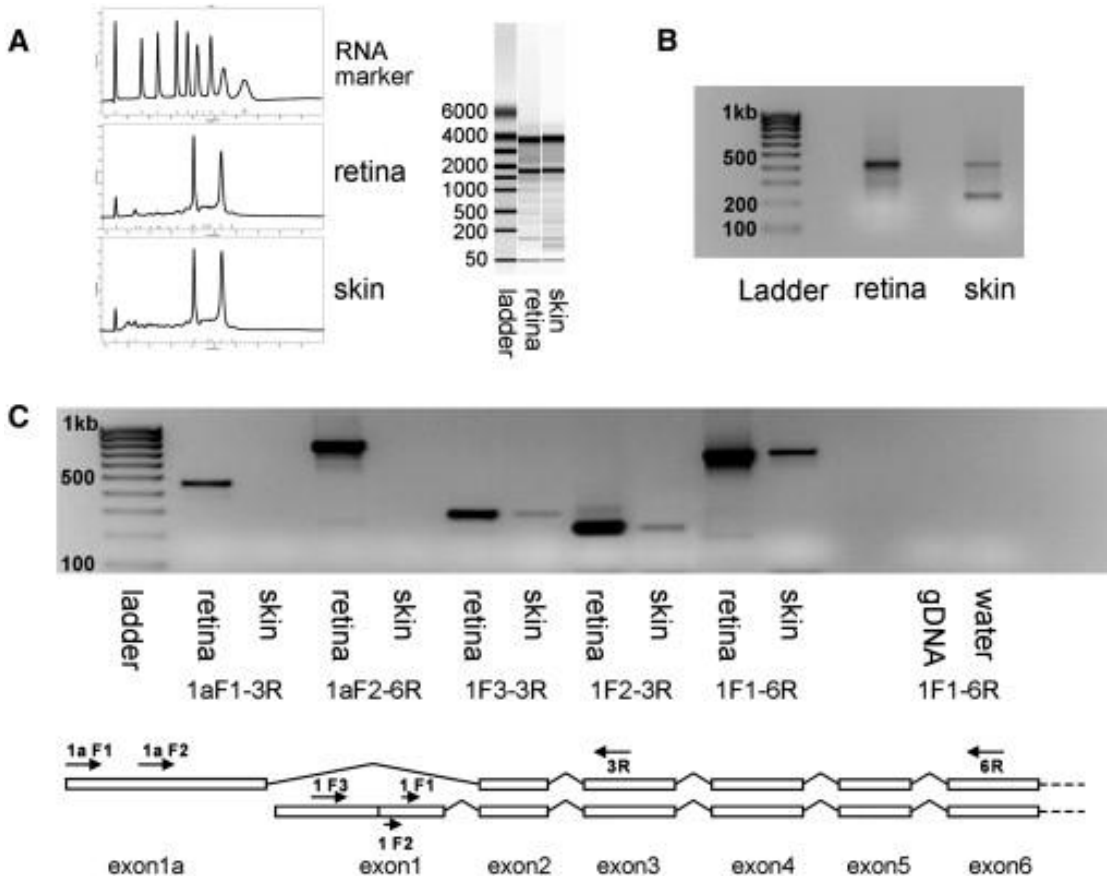

Figure 3-21. Experiments examining *TRPM1* RNA and 5**'** RACE.
[A] The integrity of RNA samples from human retina and skin were assessed (section 2.4.1). The traces show similar peaks and ratios for 28S and 18S RNA molecules (vertical axis, fluorescence intensity; horizontal axis, migration time), suggesting low degradation and comparable quality from both tissues. The right panel shows the data as a computer generated gel image.
[B] Agarose gel image of DNA fragments generated from 5' RACE experiments using the above assessed RNA (section 2.4.12). With the use of a primer complimentary to a 5' adapter oligonucleotide and a *TRPM1*-specific primer complimentary to exon 3, two main bands were produced. The lower band (~200 base pairs) was consistent with the previously reported sequence (NM_002420.4). A higher band (~475 base pairs) corresponding to a mixture of the previously unreported (a) 5' exon 1a and (b) 5' extension of exon 1 was also detected (see text for details). The higher band was predominant in the retina and the lower in skin.
[C] RT PCR experiments were performed on skin and retina RNA (section 2.4.2). A number of primers pairs (schematic) were used to determine the presence of various transcripts in the two tissues. Exon 1a consistently failed to amplify from skin cDNA.

Intriguingly, in the cohort available for this study, there remained a handful of families with a complete CSNB phenotype without mutations in *NYX*, *GRM6* or *TRPM1*, suggesting that there may be additional disease-associated genes. The future identification of such genes will provide further insights into the ON bipolar cell signalling pathway components that link the activation of metabotropic glutamate channels with the permeability state of TRPM1 membrane channels.

3.2.4 Recessive Mutations in *KCNJ13* Cause LCA

RP is a heterogeneous group of genetic disorders that feature progressive loss of photoreceptor cells as a primary or secondary event [159]. Consequent visual impairment usually manifests initially as night blindness and visual field constriction. However, great variability in age of onset, progression, fundus appearance and final visual outcome is observed. LCA represents the most severe end of the phenotypic spectrum, causing severe visual impairment from the first year of life [159, 535]. Genetic heterogeneity of RP and LCA is striking (see table 1-3, section 1.3); inheritance is predominantly monogenic (autosomal and X-linked), but polygenic and mitochondrial inheritance patterns as well as cases with *de novo* mutations have also been reported (RetNet and OMIM). The most prevalent and genetically heterogeneous RP subtype is the autosomal recessive form, with more than 30 genes implicated, accounting for less than 60% of autosomal recessive RP cases [160]. LCA is typically inherited in an autosomal recessive manner and has been linked to over 15 genes, together explaining approximately 70% of families [160]. Half of the LCA genes exhibit clinical heterogeneity with recessive mutations giving rise to both LCA and early-onset RP (see table 1-3, section 1.3). Identifying previously unrecognised causative genes for these conditions is a major challenge, particularly as remaining genes are likely to be less prevalent and less obvious candidates than those already known.

A consanguineous family, of Middle-Eastern origin was recruited. Two affected family members aged 34 (A-2) and 32 (A-3) (V:3 and V:4, family A in figure 3-22) were initially assessed. Both affected siblings were noticed to have nystagmus and were diagnosed with retinal dystrophy shortly after birth. Poor night vision and difficulty reading print from an early age was reported for both patients A-2 and A-3; gradual progression of visual problems affecting central and peripheral vision was also noted. Both had bilateral cataract surgery in their 20s. No other family history of retinal disease was reported. Visual acuities were: 2.0 logMAR in each eye of subject A-2; 1.78 logMAR for the right and 1.48 for the left eye of subject A-3. Fundoscopy revealed significant

pigment at the level of the RPE and in a configuration unlike that of typical RP (figure 3-23A).

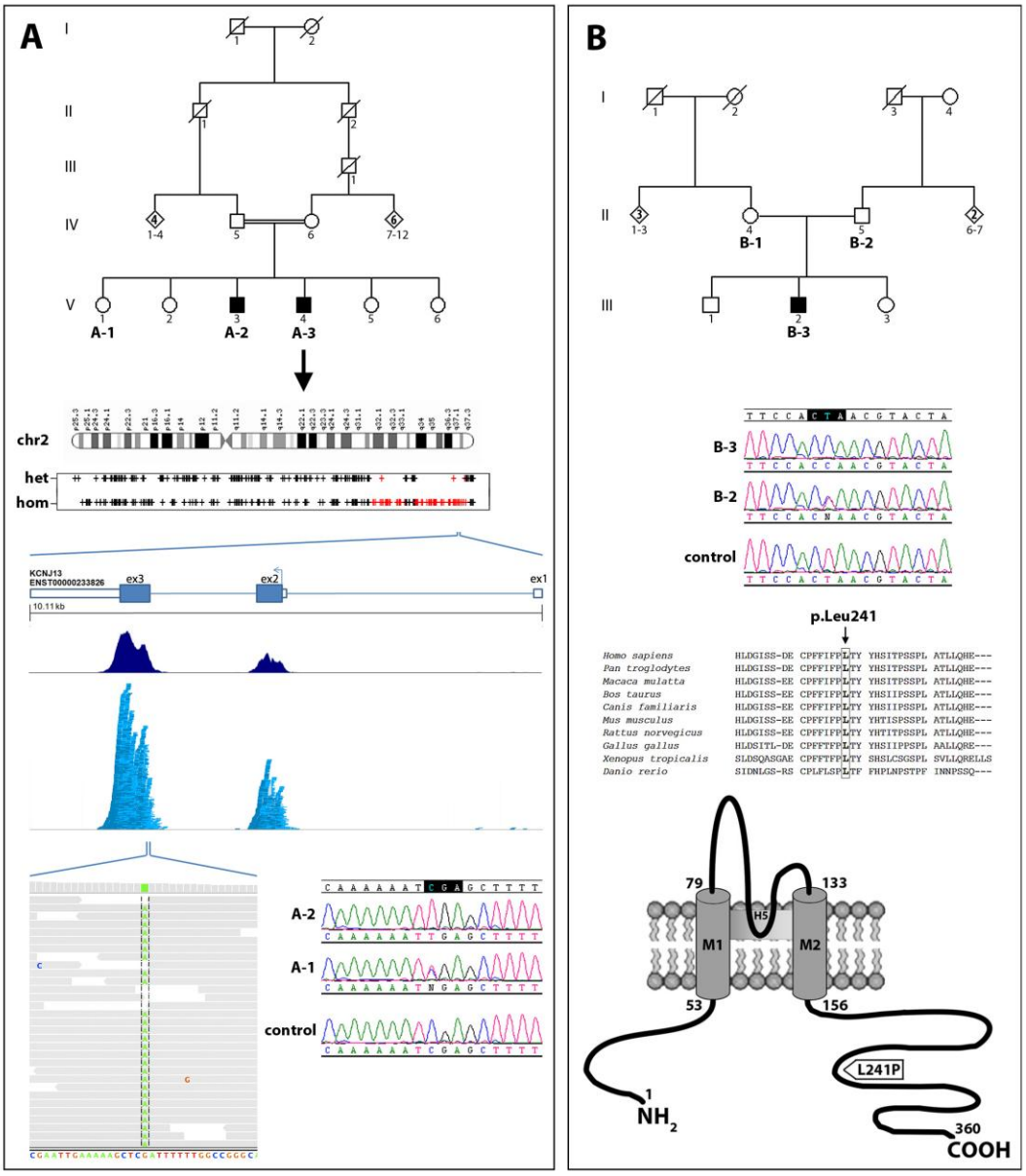

Figure 3-22. Identification of *KCNJ13* mutations in individuals from two families with LCA.
[A] Pedigree of family A**,** exome sequencing data from subject A-3 and Sanger sequencing results in affected brother A-2 and unaffected sister A-1. Pedigree reveals a recent common ancestor. Exome sequencing was performed in DNA from subject A-3. An R script assessing and plotting homozygous or heterozygous state of detected SNPs was composed. In chromosome 2, long regions of homozygosity were detected; SNPs within them are represented as red lines. Within the largest region of homozygosity, a nonsense mutation was identified in *KCNJ13* (c.496C>T, p.Arg166X). Gene structure of *KCNJ13* is presented (reverse strand) comprising of 3 exons. Coverage depth distribution of the mapped reads along the three exons is shown. Sequencing reads showing the homozygous nonsense mutation are presented (80 reads total: 11 forward and 69 reverse,100% adenine). Electropherograms of DNA sequence surrounding the p.Arg166X mutation are shown for affected brother A-2 and unaffected sister A-1.
[B] Pedigree of family B, electropherograms of DNA sequence surrounding the c.722T>C, p.Leu241Pro mutation in subjects B-3 and B-2, multiple alignment of ten *KCNJ13* orthologs around the mutated amino acid, and schematic representation of Kir7.1.[536]. The schematic representation of Kir7.1 highlights the structural domains and the location of mutated residue identified.

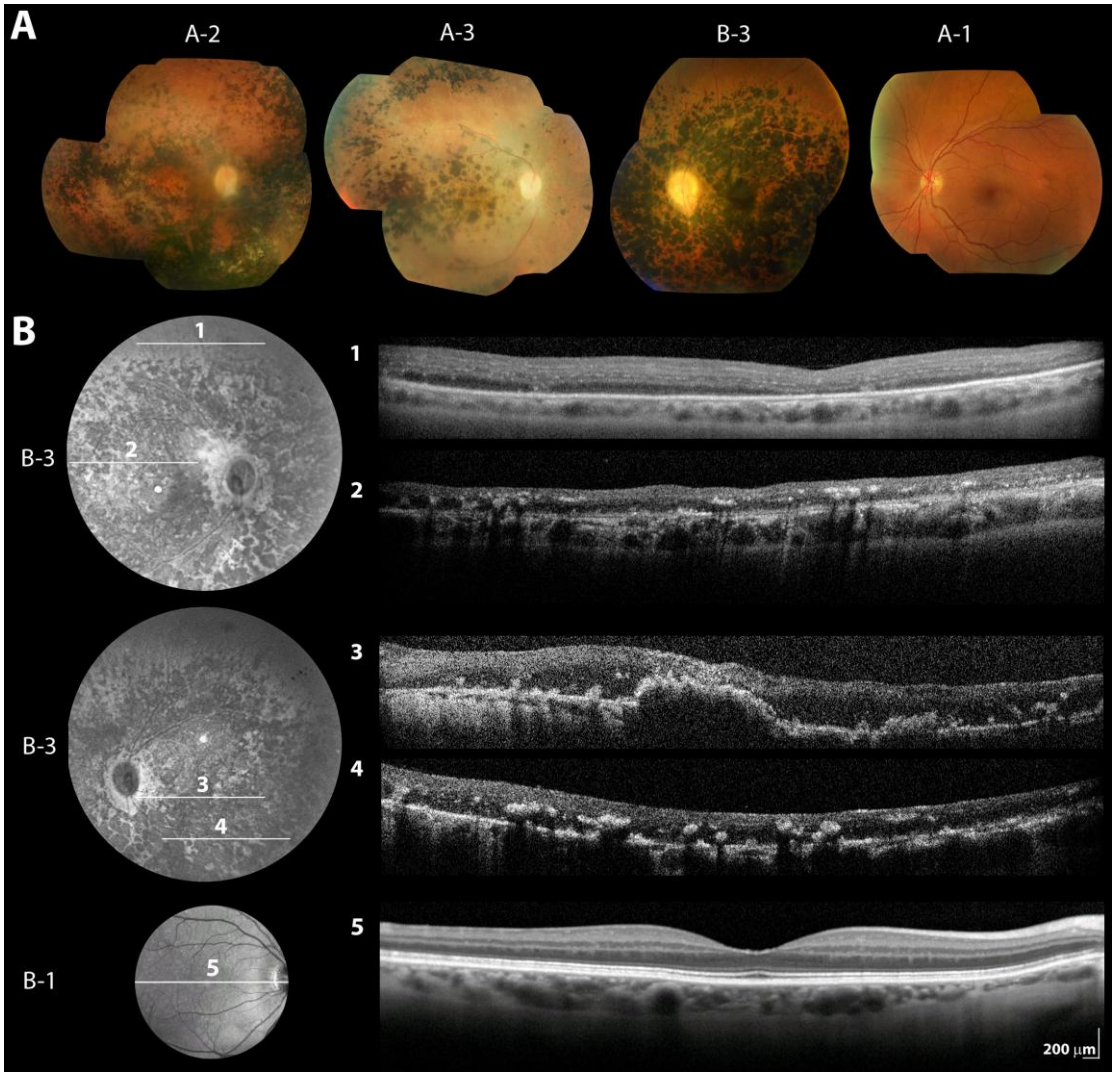

Figure 3-23.
[A] Colour photographs of right fundi of subject A-2 (aged 34) and subject A-3 (aged 32) in family A as well as left fundus of subject B-3 in family B (aged 33); normal left fundus of 39-year-old unaffected c.496C>T, p.Arg166X carrier (A-1, family A) is also shown.
[B] Infrared image and linear SD OCT of right (1, 2) and left (3, 4) retina of subject B-3 in family B. Right retina of his 64-year-old unaffected mother (B-1) is also shown for comparison (5). On some occasions, image quality was compromised by unstable fixation caused by nystagmus or posterior capsule opacification.

Initially, DNA from subject A-2 was analyzed using an APEX microarray chip containing previously reported disease-causing variants in six LCA genes (LCA Chip, Asper Biotech; section 2.4.18.1); no disease-associated alleles were detected. As the phenotype exhibited some features previously associated with mutations in *RDH12* (heavy pigmentation and macular atrophy) and *CRB1* (nummular pigmented lesions), the coding region and intron-exon boundaries of these genes were sequenced and found to be normal. Subsequently, homozygosity mapping was performed. Genotypes of

both subjects A-2 and A-3 were generated using Affymetrix Genome-Wide Human SNP 6.0 Arrays (section 2.4.18.2.2). The birdsuite set of algorithms was used to detect and report SNP genotypes (birdseed v2, threshold 0.0025), common copy number polymorphisms and novel or rare copy number variants in the processed samples (section 2.5.4) [320]. A python script interacting with a MySQL database was used to detect shared regions of homozygosity and rank them by genetic distance (section 2.5.4.3). Four chromosomal segments over 10 cM were identified, the largest being a 45 cM region located on 2q (table 3-15).

As mutations were not detected in candidate genes observed within shared regions of homozygosity (*SAG, PDE6D, WDR17*) and no pathogenic copy number variants were identified, exome sequencing was undertaken. Solution-phase hybrid capture with biotinylated RNA baits was used to target 38 Mb of genomic sequence from subject A-3 (Agilent SureSelect Human All Exon Kit; section 2.4.17). The enriched library was amplified and then sequenced on a single lane of an Illumina HiSeq2000, generating 12.2 Gb of mappable sequence as 100 base pair paired-end reads. Novoalign version 2.05 was used to align these reads to the hg19 reference sequence (section 2.5.2.2). The average sequencing depth on the 38 Mb target region was 61 with 85% of the bases covered with a depth of at least 10x. A total of 16,649 exonic calls with respect to the reference sequence were detected (table 3-16). The exome data were used to identify regions of homozygosity and the results were consistent with the findings from SNP genotyping. Owing to the prior belief that the causal variant is rare, calls that were found in the 1000 genomes pilot dataset were filtered. The remaining variants were filtered further on the basis of the linkage data and the regions of homozygosity shared by both affected individuals (table 3-16). A single loss-of-function homozygous rare variant was identified, p.Arg166X in *KCNJ13*.

Table 3-15. Regions of homozygosity that are shared by both affected siblings A-2 and A-3

Chromosome	From	To	Genetic Distance (Marshfield linkage map)	Genes screened by direct sequencing
chr2	207,725,616 [rs10192834]	236,528,938 [rs10199178]	45 cM	*SAG, PDE6D*
chr2	5,518,359 [rs6727034]	19,331,655 [rs13420305]	27.5 cM	
chr3	194,826,729 [rs6785310]	197,793,905 [rs12639242]	9 cM	
chr4	172,881,246 [rs332971]	178,027,773 [rs2580061]	5.5 cM	*WDR17*
chr9	140,693,181 [rs4876947]	140,991,359 [rs3812541]	4 cM	
chr5	170,215,394 [rs3792811]	172,822,805 [rs6556073]	3.5 cM	

Genotypes of both subjects A-2 and A-3 were generated (section 2.4.18.2.2). A python script interacting with a MySQL database was written to detect shared regions of homozygosity and rank them by genetic distance (section 2.5.4.3). Regions of homozygosity were considered significant if >3 cM.

Table 3-16. Number of variants (departures from hg19) identified in exome sequencing data of subject A-3 and filtering on the basis of genotyping data

	Total	Nonsynonymous heterozygous variants not in 1000 genomes	Nonsynonymous homozygous variants not in 1000 genomes	Nonsense/splice site/frameshifting insertion-deletion heterozygous variants not in 1000 genomes	Nonsense/splice site/frameshifting insertion-deletion homozygous variants not in 1000 genomes
Full exome	16649	329	42	80	37
Within segments where both parental haplotypes are shared with affected sibling	2914	69	12	26	10
Within regions of homozygosity	577	2	6	0	4
Within regions of homozygosity shared with affected sibling	161	2	2*	0	1

A threshold of 5 cM was used for segments where both parental haplotypes are shared in the two affected siblings. Regions of homozygosity were considered significant if larger than 3 cM. The 20100804 sequence and alignment release of the 1000 genomes project was used (628 individuals).
*These two variants [p.Glu180Val in *ARMC9* (rs1626451) and p.Arg302His in *GEN1*] cannot be fully excluded but, on the basis of biology, the loss-of-function *KCNJ13* change is much more likely disease causing.

KCNJ13 is a three exon gene encoding Kir7.1, a 360-amino-acid low-conductance inward rectifying potassium channel (Kir) that functions as a homotetramer [537-539]. Like other Kir subunits, Kir7.1 contains two transmembrane regions (M1 and M2), one pore-forming loop (H5) and cytosolic NH_2- and COOH-termini [540]. The protein is localised at the plasma membrane of a variety of ion-transporting epithelia; high gene expression has been found in intestines, thyroid, choroidal plexus, prostate, kidney and retina (Unigene, [538-539, 541]). Within the retina, Kir7.1 is primarily localised to the apical membranes of RPE [541-543]. The mutant allele, if the transcript is not subjected to nonsense-mediated decay, would produce a peptide lacking almost the entire COOH-terminal intracellular segment of 204 amino acids. Such a protein product is unlikely to form functional homotetramers, as this portion is known to be critical for Kir channel subunit assembly [540]. Additionally, the COOH-terminus is required for correct targeting of Kir7.1 to the apical membrane of epithelial cells [544] and its absence in this mutant would likely lead to mislocalization.

Previously, a missense mutation in *KCNJ13* (p.Arg162Trp) has been associated with a distinct ocular condition, autosomal dominant snowflake vitreoretinal degeneration in a large pedigree comprised of 14 affected family members [543]. The disorder's name is derived from the presence of small inner retinal crystalline-like deposits that are often observed in the fundi of affected individuals [545]. Other ocular features include corneal guttae, early-onset cataract, fibrillar vitreous degeneration, optic nerve head dysmorphism, normal macular appearance and granular changes near the equatorial fundus [546]. Increased predisposition to retinal detachment has also been reported [547]. Visual acuity is normal and retinal function testing reveals only mild abnormalities [547]. Although the term snowflake vitreoretinal degeneration has been used in another eight families, currently, these do not appear to be the same condition by clinical or genetic evaluation [545-546, 548-552].

To assess whether mutations in *KCNJ13* are a common cause of autosomal recessive retinal dystrophy, bidirectional Sanger sequencing of the entire coding region and intron-exon boundaries of the gene in 333 additional

unrelated patients was performed. Among those affected individuals, 132 were affected with recessive LCA or childhood-onset retinal dystrophy; this panel was enriched for mutations in novel genes, as the patients' DNA had been screened and excluded for previously reported LCA-causing variants through a microarray chip (LCA Chip, Asper Biotech; sections 2.1.5 and 2.4.18.1). The remaining 201 individuals were diagnosed with autosomal recessive adult-onset rod cone or cone rod dystrophy and had unknown molecular diagnosis (section 2.1.5). A homozygous missense variant (p.Leu241Pro) was identified in an individual of white European descent with a remarkably similar phenotype to that observed in family A. This sequence change has not been previously reported (EVS, dbSNP135 and 1000 genomes) and was absent from 382 ethnically matched control chromosomes. The mutated amino acid is highly conserved across a broad range of species [536]; among other human Kir family members, it is either conserved or replaced by another nonpolar hydrophobic residue (Ile, Met or Val; figure 3-24).

Figure 3-24. Amino acid sequence alignment of 15 Kir channel subunits around the mutated Kir7.1 residue Leu241. Subunits have been classified into four functional group in accordance with Hibino *et al*. [540]. The alignment was performed with ClustalW2 using appropriate Ensembl transcripts [536].

In order to further evaluate the physiological significance of the p.Leu241Pro change, homology modelling was performed. Leu241 is located in the cytosolic COOH-terminus of Kir7.1 and is the first of six amino acids to form a *β*-sheet (*β*I) [553]. The mutant Pro241 residue does not take part in this *β*-sheet formation, alters the orientation of the *β*-sheet and distorts a proximal similar

structure, thus inducing a considerable conformational change (figure 3-25).

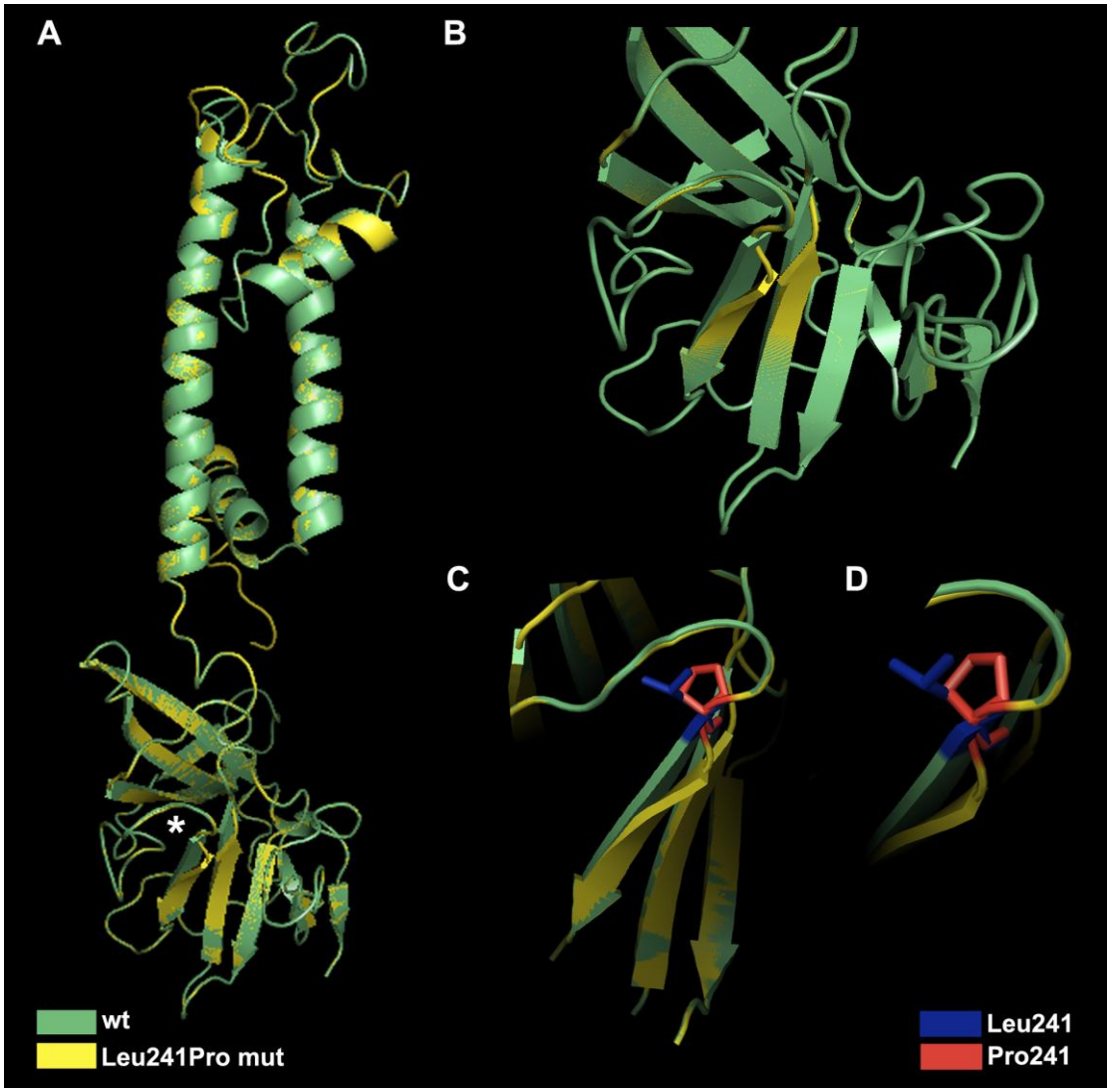

Figure 3-25. Predicted protein structure of the human Kir7.1 subunit
[A] Overlay of wild-type (wt; green) and mutant (yellow) Kir7.1 monomer models. Similar to other Kir family members, the Kir7.1 monomer is comprised of an α helical membrane domain and an intracellular domain primarily composed of *β*-sheets (asterisk highlights the position of the p.Leu241Pro).
[B] Detail of the region around the 241st amino acid. Distortion of the protein secondary structure is evident in the mutant when compared to the wild-type monomer.
[C] The side chains of the Leu241 (wild-type; blue) and Pro241 (mutant; red) residues are highlighted; the cyclic R group structure of proline bends the amino acid chain.
[D] Detail of C.
The structural model was generated by using the SWISS-MODEL protein homology modeling server; the crystal structure of KirBac1.1 (Protein Data Bank code 1q7b) was used as a template. Similar findings were observed when the structure of cKir2.2 (Protein Data Bank code 3jycA) was used as a template. PyMOL was used to view the three-dimensional molecular structures (table 2-5, section 2.5).

The proband, a 33-year-old male (B-3; III:2, family B in figure 3-22), was noticed to have strabismus, nystagmus and poor vision before the age of one. At two years of age, the diagnosis of retinal degeneration was made. Only mild

progression was reported with night vision having most noticeably deteriorated. He is a moderate myope, had strabismus surgery at age 2 and an ERG at the age 10 years showed no consistent rod- or cone-driven responses. Bilateral cataract surgery was undertaken in his early 20s. There was no family history of retinal disease and his parents originate from the same isolated geographic area making the existence of a recent common ancestor highly likely. Visual acuities were 1.45 logMAR in each eye. There was bilateral nystagmus and confrontational visual field testing showed severe field loss but relative preservation of the inferior field. Fundus examination revealed areas of nummular pigment at the level of the RPE, especially over the posterior pole (figure 3-23A). *In vivo* cross sectional imaging using SD OCT revealed loss of outer retinal structures, thinning of the hyperreflective band corresponding to RPE/Bruch's membrane and a coarse lamination pattern (figure 3-23B). The distorted retinal microanatomy in an area of the fundus in which cell-death was not evident may suggest that the early development of the human neurosensory retina is disturbed.

Other sequence alterations identified in the studied patient cohort included three previously unreported (EVS, dbSNP135 and 1000 genomes) missense variants in the heterozygous state. A p.Gln117Arg change was found in an individual of white European ancestry with early-onset retinal dystrophy and heavily pigmented fundi. Gln117 is located in an evolutionarily conserved region of the protein that corresponds to the pore-forming loop; this glutamine is also conserved among the majority of other Kir family members [538]. A p.Arg162Gln was identified in heterozygous state in each of two unrelated male affected individuals of Turkish ancestry (aged 33 and 42). Interestingly, this change occurs in the same amino acid as the dominant mutation causing snowflake vitreoretinal degeneration (p.Arg162Trp) [543]. Both patients carrying heterozygous p.Arg162Gln have been diagnosed with adult-onset RP, are night blind and have field of vision reduced to less than 10°. Notably, one of the two (42-year-old) is the product of a first cousin marriage; he is the only affected family member and fundoscopy on his parents was unremarkable. The identification of a heterozygous *KCNJ13* variant in this proband suggests that the region is not homozygous by descent and therefore less likely to be

the disease locus [105]. Moreover, the phenotype is very different to that seen in families A and B, suggesting a different causative gene. A third missense variant (p.Glu276Ala), altering a highly conserved amino acid in the cytosolic COOH-terminus, was identified in an individual of South Asian origin with adult-onset RP.

In order to study the effect of the p.Arg166X and p.Leu241Pro mutations in the heterozygous state, additional family members from families A and B were ascertained. For family A, the parents were not available for examination but it was possible to examine two siblings. Subject A-1 (V:1, family A in figure 3-22), a 39-year-old female, was found to carry the mutation in heterozygous state. She was asymptomatic and fundus examination, 55° fundus autofluorescence imaging and SD OCT were normal. Importantly, there were no signs of snowflake vitreoretinal degeneration. In family B, Sanger sequencing confirmed heterozygosity for the p.Leu241Pro change in maternal (B-1; II:4, family B in figure 3-22) and paternal (B-2; II:5, family B in figure 3-22) DNA. The 64-year-old father is a high myope, had cataract operations in his 50s and is treated for glaucoma. He was diagnosed with benign prostatic hyperplasia and unilateral acoustic neuroma, but was otherwise well. The 62-year-old mother reports no symptoms and no history of disease. Fundoscopy, 55° fundus autofluorescence imaging and SD OCT were normal in both and there were no signs of snowflake vitreoretinal degeneration. These results suggest that haploinsufficiency in *KCNJ13* does not cause ocular disease. *In vitro* patch clamp studies have demonstrated that the snowflake vitreoretinal degeneration-associated mutation, p.Arg162Trp, produces a nonselective cation current, unlike its wild-type counterpart, when overexpressed in CHO-K1 cells [543]. However, it remains to be determined how this mutant protein behaves in the presence of wild-type Kir7.1. It can be speculated that, p.Arg162Trp, is unlikely to exert a dominant negative effect on Kir7.1 channel function; this would be inconsistent with the LCA phenotype in families A and B, which presumably represents the null Kir7.1 phenotype in humans. The electrophysiological effects of p.Arg162Trp and p.Leu241Pro on Kir7.1 channel with and without the presence of wild-type Kir7.1 merits further investigation. It seems likely that the different snowflake vitreoretinal

degeneration ocular phenotype is explained by a novel function of the mutant p.Arg162Trp allele in the heterozygous state (gain of function).

Retinal disease caused by *KCNJ13* mutations adds to a small group of disorders caused by reduced or abrogated expression of genes encoding inward-rectifying potassium channel subunits. These diseases involve glucose homeostasis (familial hyperinsulinaemia hypoglycaemia type II, *KCNJ11*) [554], renal sodium and potassium reabsorption (Bartter syndrome type II, *KCNJ1*) [555], the glial cell membrane resting potential (SeSAME/EAST syndrome, *KCNJ10*) [556] and the excitability of the cardiac and skeletal muscle (Andersen-Tawil syndrome, *KCNJ2*) [557].

Table 3-17. Summary of DNA variants in the *KCNJ13* coding region reported here and elsewhere

Coding DNA Variants		SIFT		PolyPhen-2		Frequency (chromosomes)		
Nucleotide	**Protein**	**Prediction**	**Tolerance Index (0 to 1)**	**Prediction**	**HumVar score (0 to 1)**	**in individuals with recessive retinal disease (n= 666+4)**	**in European controls (n=382)**	**Reference**
c.17G>C	p.Cys6Ser	tolerated	1.00	Benign	0.001	0/670	0/382	EVS (MAF 0.02%)
c.27T>A	p.(=)		*not applicable*			0/670	0/382	EVS (MAF 0.02%)
c.53G>A	p.Arg18Gln	tolerated	0.77	Benign	0.004	0/670	0/382	EVS (MAF 0.02%)
c.208G>T	p.Val70Phe	tolerated	0.50	Benign	0.043	0/670	0/382	dbSNP132 [rs79005659]
c.214G>T	p.Ala72Ser	intolerant	0.02	POD	0.978	0/670	0/382	dbSNP132 [rs77818131]
c.344A>G	p.Glu115Gly	intolerant	0.00	POD	0.991	0/670	0/382	dbSNP132 [rs112079468]
c.350A>G	p.Gln117Arg	intolerant	0.00	POD	0.945	1/670	0/382	this study [LCA panel]
c.438C>T	p.(=)		*not applicable*			0/670	0/382	EVS (MAF 0.02%)
c.484C>T	p.Arg162Trp	intolerant	0.00	POD	0.972	0/670	0/382	Hejtmancik *et al.*[543]
c.485G>A	p.Arg162Gln	tolerated	0.20	POD	0.937	2/670	0/382	this study [RP panel]
c.496C>T	p.Arg166X		*not applicable*			4/670	0/382	this study [family A]
c.511C>T	p.(=)		*not applicable*			0/670	0/382	EVS (MAF 0.02%)
c.524C>T	p.Thr175Ile	tolerated	0.38	Benign	0.001	212/670	109/382	dbSNP132 [rs1801251], EVS
c.528A>G	p.(=)		*not applicable*			0/670	0/382	EVS (MAF 0.02%)
c.607C>T	p.(=)		*not applicable*			0/670	0/382	EVS (MAF 0.02%)
c.652T>C	p.Tyr218His	tolerated	0.74	Benign	0.001	0/670	0/382	1000 genomes, EVS
c.722T>A	p.Leu241Gln	tolerated	0.07	Benign	0.001	0/670	0/382	EVS (MAF 0.02%)
c.722T>C	p.Leu241Pro	intolerant	0.02	POD	0.997	2/670	0/382	this study [LCA panel; family B]
c.725C>T	p.Thr242Met	intolerant	0.03	POD	0.998	0/670	0/382	EVS (MAF 0.02%)
c.807A>G	p.(=)		*not applicable*			0/670	0/382	EVS (MAF 0.02%)
c.827A>C	p.Glu276Ala	intolerant	0.03	POD	0.987	1/670	0/382	this study [RP panel]
c.869C>A	p.Pro290Gln	intolerant	0.02	POD	0.945	0/670	0/382	dbSNP132 [rs17853727]
c.925G>T	p.Gly309Cys	intolerant	0.00	POD	0.998	0/670	0/382	dbSNP132 [rs17857137]
c.980C>T	p.Thr327Ile	intolerant	0.01	Benign	0.113	0/670	0/382	EVS (MAF 0.02%)

3.2.5 Recessive Mutations in *PLA2G5* Cause Benign Fleck Retina

Benign fleck retina is a term used to refer to an autosomal recessive condition associated with a distinctive retinal appearance and no apparent visual or electrophysiological deficits [558]. Affected individuals are asymptomatic but fundus examination reveals a striking pattern of diffuse, yellow-white, fleck-like lesions extending to the far periphery but sparing the foveal region [559-562]. The benign fleck retina phenotype was first described in 1980 in seven affected siblings born to consanguineous parents [559]. A similar clinical appearance was subsequently reported in three unrelated individuals originating from diverse ethnic backgrounds [560-562].

A consanguineous family of South Asian origin is the basis of this section (family J, figure 3-26). Initially, subject J-4, a healthy, asymptomatic 10-year-old girl (IV-2, family J in figure 3-26), was referred after abnormal retinal appearance was noticed on a routine eye test. No family history of retinal disease was reported. Visual acuity was normal. Fundus examination revealed multiple, discrete, polymorphous, yellow-white flecks at the level of the RPE; the flecks affected both fundi in a symmetrical pattern, spread peripherally, beyond the major vascular arcades and spared the maculae (figure 3-27). Other family members including three siblings and both parents were also examined. Similar findings to the proband were obtained in subjects J-5 (aged 9; IV-3, family J in figure 3-26) and J-6 (aged 7; IV-4, family J in 3-26); normal retinal appearance was observed in subject J-3 (IV-1, family J in figure 3-26) and parents J-1 (III-6, family J in figure 3-26) and J-2 (III-7, family J in figure 3-26). Electrophysiological assessment was performed. Full field ERGs, pERGs and EOGs were normal in all three affected subjects and a diagnosis of benign fleck retina was confirmed. The clinical findings are summarised in table 3-18.

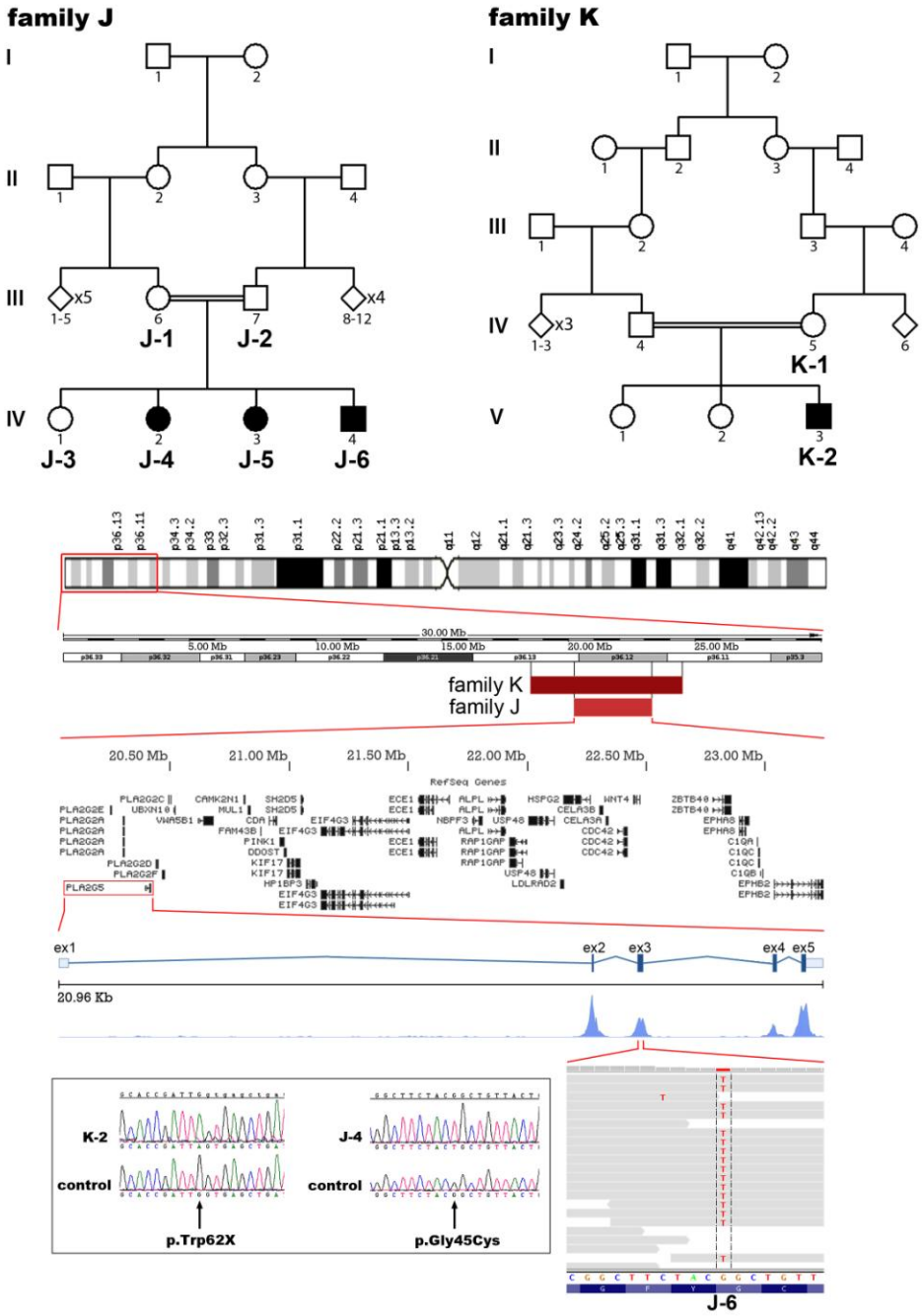

Figure 3-26. Identification of *PLA2G5* mutations in individuals from two families with benign fleck retina

Pedigrees of families J and K are shown. Homozygosity mapping using DNA from subject K-2 revealed a 12 cM region on 1p (flanked by rs10796459 and rs12407356). DNA samples from subjects J-1, J-2, J-3, J-4, J-5 and J-6 were also genotyped and a 5 cM region (flanked by rs3738122 and rs1832047) was found to be homozygous in all affected and consistent with disease segregation. Refseq genes contained in this shared region between families K and J are shown. Exome sequencing using DNA from subject J-6 revealed a rare homozygous missense change, c.133G>T, p.Gly45Cys in *PLA2G5.* Gene structure of *PLA2G5*, coverage depth distribution of the mapped reads along its five exons (Savant Genome Browser) and sequencing reads corresponding to this variant are presented (IGV viewer; 34 reads total: 10 forward and 24 reverse,100% thymine). Subsequently, bidirectional Sanger sequencing confirmed segregation of the p.Gly45Cys change in family J and identified a homozygous nonsense mutation in K-2 (c.185G>A, p.Trp62X). Electropherograms of DNA sequences surrounding these two variants are shown. Both sequences are displayed in the forward orientation.

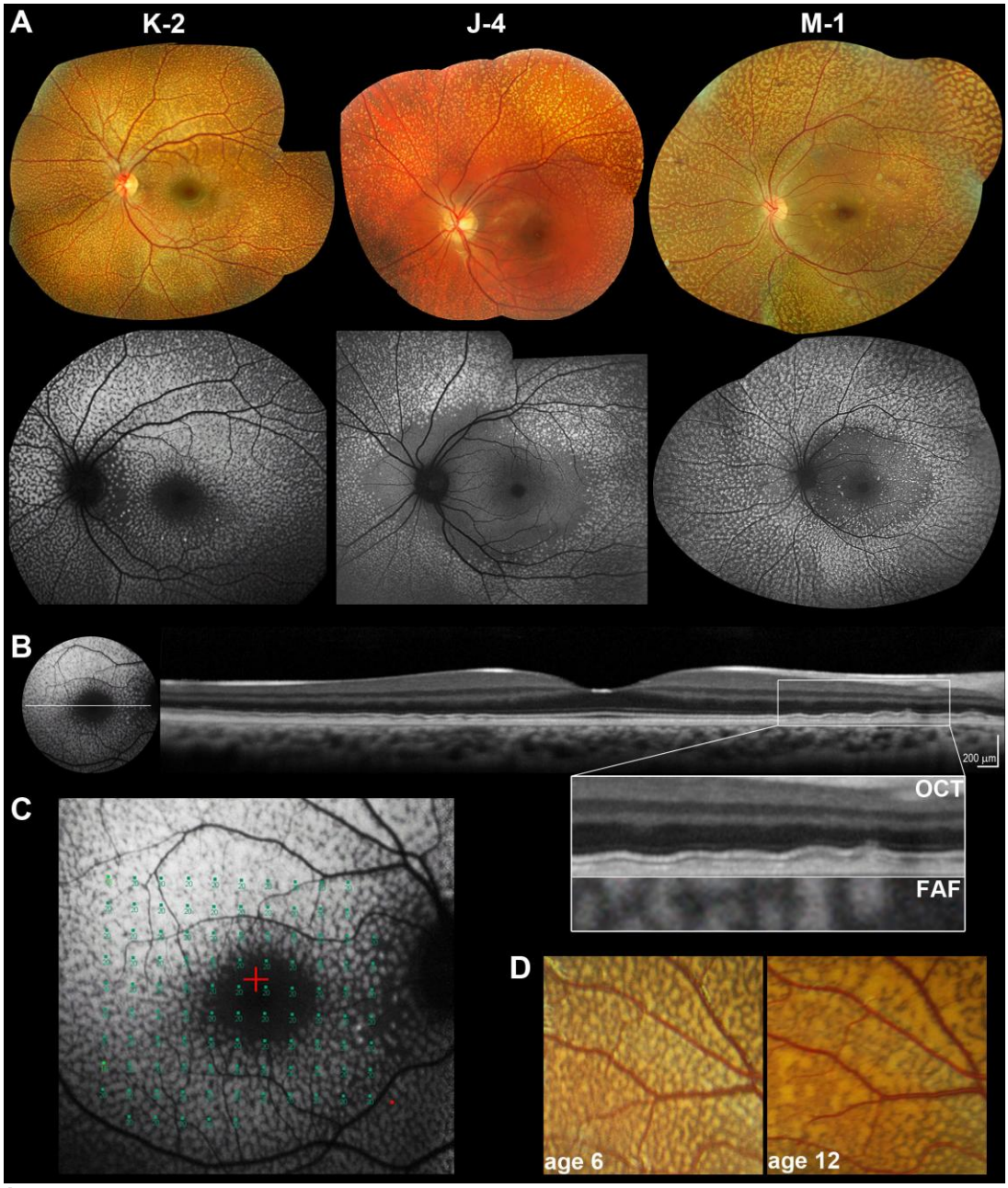

Figure 3-27.
[A] Colour photographs and corresponding fundus autofluorescence images of the left fundi of subjects K-2 (aged 12), J-4 (aged 12) and M-1 (aged 39). On fundus photography, multiple yellow-white flecks of various sizes are observed. Fundus autofluorescence imaging reveals hyperautofluorescent lesions corresponding in location with the flecks. The macula is relatively spared in subjects J-3 and M-1 but not in K-2 where only the fovea appears not to be affected. This might reflect a more detrimental effect of the c p.Trp62X mutation in homozygous state (subject K-2) as opposed to homozygous missense (p.Gly45Cys in subject J-3), compound heterozygous missense and frameshift (p.Gly45Cys and c.383delA, p.Gln128ArgfsX88 in M-1) mutations.
[B] Fundus autofluorescence imaging and linear SD OCT scan of the left retina of subject K-2. Deep, discrete hyperreflective deposits, more obvious at the edge of the foveal scan are observed. Panel with enlarged image of boxed region shows outer retina and RPE in detail. The lesions are located posterior to the hyperreflective band corresponding to the photoreceptor IS/OS junction and do not disrupt it. An overlay of SD OCT with fundus autofluorescence image is also presented. Deposits are spatially associated with the hyperautofluorescent lesions thus, corresponding to the flecks.
[C] Functional assessment of the central retina in subject K-2. Static perimetry testing

(threshold sensitivities from 0 to 20 dB, test spot size Goldmann III) results overlaid with fundus autofluorescence imaging are presented. Retinal sensitivity was normal.
[D] Longitudinal data showing evolution of fleck-like lesions over time. Magnified view of fundus photographs from the left eye (vascular arcades) of subject K-2 at ages six and 12. Flecks increase in number and size and become more confluent.

DNA samples from the three affected siblings (subjects J-4, J-5 and J-6), their unaffected sister (subject J-3) and parents (subjects J-1 and J-2) were genotyped with the use of GeneChip Human Mapping 50K Xba Arrays (experiment conducted by Dr Zheng Li; section 2.4.18.2.1). The BRLMM genotype calling algorithm was used; CEL files were input and the threshold was set at 0.01 (section 2.5.4). The pedigree was consistent with the propagation of a single mutant allele from a recent ancestor such that affected individuals were autozygous for this allele and the unaffected sibling not. A python script interacting with a MySQL database was used to detect regions obeying this rule and rank them by genetic distance (section 2.5.4.3). Three chromosomal segments over 1 cM were identified (table 3-19): two regions on 1p (19 cM and 5 cM) and one region on 2q (14 cM).

Exon capture and high-throughput sequencing of DNA from subject J-6 was undertaken (Agilent SureSelect 38 Mb exome capture, Illumina HiSeq2000 sequencer; section 2.4.17). Reads were aligned to the hg19 human reference sequence (section 2.5.2.2); average sequencing depth on target was 72 with 87% of the targeted region covered with a minimum read depth of 10. Overall, 15,611 exonic sequence alterations with respect to the reference sequence were identified (table 3-20). Given the level of consanguinity in this family it was hypothesised that the trait is recessive and we focused on homozygous variants. Based on the prior belief that benign fleck retina-associated mutations are rare, calls with MAF over 0.5% in the 1000 genomes pilot dataset (20101123 release; 1094 genomes) or an internal set of 224 exomes (individuals with adult-onset neurodegenerative disease) were filtered. Subsequently, we focused on the three regions of homozygosity found by SNP arrays to be shared among affected family members; no loss-of-function variants were identified and three homozygous rare missense changes were detected: p.Gly45Cys in *PLA2G5*, p.Asn385Ser in *ECE1* and p.Arg241Gln in *NEU2* (table 3-20).

Simultaneously, a DNA sample was obtained from a previously reported case of benign fleck retina (K-2; V-3, family K in figure 3-26) [561]. There was evidence of parental consanguinity and homozygosity mapping using the Affymetrix Genome-Wide Human SNP Array 6.0 (sections 2.4.18.2.2 and 2.5.4.3) yielded four regions of homozygosity over 10 cM (table 3-19). The third largest segment (12 cM) encompassed one of the loci detected in family J. Thus, we focused on the *PLA2G5*:p.Gly45Cys and *ECE1*:p.Asn385Ser variants found within this shared region. On the basis of physiological relevance (Unigene and OMIM), the *PLA2G5* change appeared to be more likely to cause disease and Sanger sequencing of the open reading frame (exons 2 to 5, 138 amino acids, Ensembl transcript ENST00000375108) and intron-exon boundaries was undertaken in four unrelated individuals with benign fleck retina. Clinical and electrophysiological characteristics of two of these cases (K-2 and L-1) have been detailed in previous reports [560-561].

Biallelic *PLA2G5* variants were identified in three of four cases; all changes were novel (figure 3-26 and table 3-21). Notably, seven nonsynonymous sequence alterations (all with MAF <0.05%) and no loss-of-function *PLA2G5* variants have been previously reported (EVS, dbSNP135, 1000 genomes) or were identified in an internal set of 224 exomes (table 3-21). Subject K-2, a 12-year-old boy [561], was found to be homozygous for a p.Trp62X change, altering the last base of exon 3. Subject L-1, a 28-year-old female [560], was found to carry two changes in heterozygous state (p.Gly49Ser and p.Arg53X). PCR amplification and subsequent TA cloning of exon 3 (pGEM-T Easy Vector, Promega; sections 2.3, 2.4.7 and 2.4.13) demonstrated that these variants were present on different alleles. Two heterozygous changes were also identified in subject M-1, a 39-year-old female (p.Gly45Cys and c.383delA, p.Gln128ArgfsX88); these variants were also shown to be biallelic using a similar approach (long-range PCR and TA cloning of the 5 kb of DNA encompassing exons 3 to 5; experiment conducted by Dr Alice E Davidson). Interestingly, the p.Gly45Cys variant was detected in a homozygous state in the three affected members of family J. Both missense changes identified in

Table 3-18. Clinical characteristics and molecular pathology of subjects with benign fleck retina

Subject	Gender	Visual function* (age at examination)	Lipid levels (mmol/l)^	Other systemic findings	Molecular diagnosis, amino acid changes in *PLA2G5*
J-4	Female	Normal ERG, pERG, EOG (12)	not tested		p.[Gly45Cys];[Gly45Cys]
J-5	Female	Normal ERG, pERG, EOG (12)	not tested		p.[Gly45Cys];[Gly45Cys]
J-6	Male	Normal ERG, pERG, EOG (10)	not tested		p.[Gly45Cys];[Gly45Cys]
K-2	Male	Normal ERG, pERG [6][561] and MP1 (12)	LDL 3.6 mmol/l, total cholesterol 5.5 mmol/l	High BMI (31), allergic rhinitis	p.[Trp62X];[Trp62X]
L-1	Female	Normal ERG, EOG (12)[560]	not tested	High BMI	p.[Gly49Ser];[Arg53X]
M-1	Female	Normal ERG, pERG (37)	LDL 3.9 mmol/l, total cholesterol 6.3 mmol/l	High BMI (26)	p.[Gly45Cys];[Gln128Argfs*45]
N-1	Female	Normal ERG, pERG (10)	normal LDL, cholesterol	Normal BMI	[?];[?]

Subjects J-4, J-5, J-6 and K-2 are of South Asian origin and born to consanguineous parents; subject L-1 is of mixed Australian aboriginal and white descent; subject M-1 is of South Asian origin; subject N-1 is white British. All patients presented with abnormal retinal appearance on a routine eye test, were asymptomatic, reported no night blindness and had visual acuities of 0.2 logMAR (logarithm of the minimal angle of resolution) or better. Colour vision was normal in all eyes [evaluated using Farnsworth D-15 test (L-2)[560], HRR (K-2, M-1 and N-1) or Ishihara test plates (J-4, J-5, J-6, L-2,[560] M-1 and N-1). Subjects K-2 and L-1 had mild myopic astigmatism and subject M-1 is a high myope.
Subjects K-2 and M-1 had mild eosinophilia (0.45 and 0.64 x 10^9/l respectively; normal levels from 0.0 to 0.4 x 10^9/l).

*Visual function was evaluated using electrophysiology or perimetry (Nidek MP1, Goldmann III stimulus size)
^Normal levels are from 2.3 to 4.9 mmol/l for cholesterol and from 0.0 to 3.0 mmol/l for LDL.

Table 3-19. Segments of homozygosity yielded from homozygosity mapping in families A and B

Chromosome	From	To	Genetic Distance (Marshfield linkage map)	Reference
chr1	54,742,471 (rs590041)	64,361,979 (rs855824)	19 cM	Family J, regions >1 cM
chr2	232,025,284 (rs6437002)	236,731,624 (rs952608)	14 cM	
chr1	20,238,860 (rs3738122)	23,266,939 (rs1832047)	5 cM	
chr7	pter	8,546,068 (rs2189903)	15 cM	Family K, regions >10 cM
chr18	pter	4,925,739 (rs9961128)	12 cM	
chr1	18,477,450 (rs10796459)	24,578,011 (rs12407356)	12 cM	
chr1	110,701,174 (rs12118197)	144,989,739 (rs2590125)	11 cM	

Genotypes of subjects J-1, J-2, J-3, J-4, J-5 and J-6 were generated using the Affymetrix GeneChip Human Mapping 50K Array Xba (section 2.4.18.2.1). Genotypes of subject K-2 were generated using the Affymetrix Genome-Wide Human SNP Array 6.0 (section 2.4.18.2.2).

Table 3-20. Prioritization of variants identified by exome sequencing of DNA from patient J-6

	Total	Within regions of homozygosity (on the basis of exome sequencing data)	Within regions of homozygosity shared among affected but not unaffected siblings (on the basis of SNP genotyping data)
All variants.	15,611	1,223	81
Only NS/SS/I,	7,247	588	40
AND ≤ 0.5% MAF in 1000 genomes,	648	41	3
AND ≤ 0.5% MAF in internal database	580	36	3
AND are predicted to be loss of function	80	7	0

Variants presented were sequentially filtered on the basis of effect on protein sequence (synonymous or intronic variants were excluded), presence in the 1000 genomes project dataset (with ≤ 0.5% MAF; the 20101123 sequence and alignment release including 1094 individuals was used), presence in exomes from an internal database (with ≤ 0.5% MAF; DNA from 224 samples processed using the same tools as J-6) and being presumed to cause loss of protein function (nonsense, splice site variants and frameshifting insertions-deletions).

NS/SS/I, nonsynonymous, splice site or coding insertion-deletion variants.

Table 3-21. Summary of coding *PLA2G5* sequence variants identified here and elsewhere (EVS, 1000 genomes and dbSNP134)

Coding DNA variants		SIFT		PolyPhen-2		Blosum 62 score (-4 to 11)	Reference *(observed allele count)*
Nucleotide	**Protein**	**Prediction**	**Tolerance index (0 to 1)**	**Prediction**	**HumVar Score (0 to 1)**		
c.9 C>T	p.(=)	*not applicable*				6	1000 genomes [rs2020887], EVS *(1244/3632)*, this study
c.15 C>G	p.(=)	*not applicable*				4	EVS *(1/4877)*
c.48 T>C	p.(=)	*not applicable*				7	EVS *(1/4877)*
c.88 G>A	p.Glu30Lys	tolerated	0.78	Benign	0.03	1	EVS *(1/4877)*
c.102 G>T	p.(=)	*not applicable*				6	Bushman_pop [rs111762734]
c.108 C>T	p.(=)	*not applicable*				6	internal database *(1/448)*, EVS *(3/4875)*
c.110 C>G	p.Ala37Gly	tolerated	0.35	POD	0.97	0	EVS *(1/4877)*
c.133 G>T	**p.Gly45Cys**	intolerant	0.00	POD	1.00	-3	this study [families J and M]
c.144 C>T	p.(=)	*not applicable*				9	1000 genomes [rs11573265], EVS *(77/4801)*, this study
c.145 G>A	**p.Gly49Ser**	intolerant	0.02	POD	1.00	0	this study [family L]
c.157 C>T	**p.Arg53X**	*not applicable*				-4	this study [family L]
c.181 G>A	p.Asp61Asn	intolerant	0.01	POD	1.00	1	EVS *(1/4877)*
c.185 G>A	**p.Trp62X**	*not applicable*				-4	this study [family K]
c.292 G>A	p.Glu98Lys	intolerant	0.04	Benign	0.47	1	EVS *(1/4855)*
c.297 C>T	p.(=)	*not applicable*				6	EVS *(2/4876)*
c.311 A>C	p.His104Pro	tolerated	0.23	Benign	0.00	-2	EVS *(1/4877)*
c.312 T>C	p.(=)	*not applicable*				8	internal database *(1/448)*, EVS *(7/4871)*
c.368 G>A	p.Arg123Gln	tolerated	0.53	Benign	0.10	1	EVS *(2/4876)*
c.383delA	**p.Gln128ArgfsX88**	*not applicable*				-4	this study [family M]
c.402 C>T	p.(=)	*not applicable*				6	Bushman_pop [rs112000348]
c.406 C>T	p.Leu136Phe	tolerated	0.71	Benign	0.00	0	EVS *(1/4877)*

Bushman_pop denotes variants identified only among the four Bushmen genomes (Schuster *et al*.[563]). For internal database see text

benign fleck retina patients (p.Gly45Cys and p.Gly49Ser) were highly conserved among orthologs and paralogs.

PLA2G5 encodes group V PLA_2, a secreted PLA_2 first described in 1994 [564]. The PLA_2 superfamily includes a broad range of enzymes defined by their ability to catalyze the hydrolysis of the middle (*sn*-2) ester bond of glycerophospholipids and thus release potentially bioactive lipids, namely lysophospholipids and free fatty acids (arachidonic acid and others) [565-566]. PLA_2s have been subdivided into several classes, including secreted PLA_2s [567]. These are water-soluble, Ca^{2+}-requiring enzymes that contain Histidine and Aspartic acid catalytic dyads and have the ability to function during secretion (in the secretory compartment or in the extracellular space, in an autocrine or paracrine manner) or after internalization [568]. Based on selected structural determinants, secreted PLA_2s have been classified into six groups. Individual secreted PLA_2s exhibit unique enzymatic properties and show diverse tissue and cellular localizations; thus distinct physiological roles and nonredundant functions are likely [568]. *PLA2G5* is highly expressed in the eye and heart and present in other tissues including placenta, lung and brain (eyeSAGE, Unigene, [564, 569-573]). A number of human cells including macrophages, neutrophils, bronchial and renal tubular epithelium, subendocardial cells (cardiomyocytes) and interstitial fibroblasts of gastric submucosa have been shown to express *PLA2G5* [572, 574-578].

A variety of biological functions have been attributed to group V PLA_2. These are often related to the enzyme's ability to provide arachidonic acid for eicosanoid (prostaglandins, leukotriens and others) generation [576, 579]. Additional functions not directly related to lipid mediator biosynthesis have also been demonstrated; these include regulation of phagocytosis, foam cell formation and anti-bacterial activities [577, 580-581]. This combination of pro- and anti-inflammatory properties and the presence of cell type-specific functions suggest that group V PLA_2 has distinct anatomical and context dependent roles [574, 581]. Studies employing transgenic [582] and knock-out [583] mice have provided important insights into the role of group V PLA_2 in various pathophysiological events. Enzyme deficiency in *Pla2g5* null mice

leads to marked attenuation of airway inflammation (asthma [584-585] and acute respiratory distress syndrome [586]) and reduced atherosclerosis [587-588]. Conversely, as group V PLA_2 modulates immune complex clearance by stimulating phagocytosis, knockout mice demonstrate exacerbation of autoantibody-induced arthritis [581]. *Pla2g5* transgenic mice overexpressing *PLA2G5* die soon after birth due to aberrant hydrolysis of lung surfactant phospholipids [582]. Despite the growing body of research focusing on animal model studies, definite evidence for an *in vivo* role of group V PLA_2 in human tissues is lacking and it is likely that some biological functions are not conserved from mouse to human [568].

None of the studied patients reported a medical history of major or chronic illness (table 3-18). Patient K-2 experiences symptoms of mild seasonal allergic rhinitis and infrequently receives antihistamine tablets. A high body mass index was recorded in three patients. In both mutation-positive individuals tested (subjects K-2 and M-1), a blood test revealed slight eosinophilia and mildly elevated LDL and total cholesterol levels (table 3-18). Notably, an association of human *PLA2G5* haplotypes with total and LDL cholesterol has been previously reported [589]. Although there is strong *in vitro* evidence that group V PLA_2 is enzymatically active in serum and hydrolyses LDL [590], no effect on plasma lipoproteins was observed in mice with enzyme deficiency [587]. It is possible that the raised LDL levels are unrelated to the *PLA2G5* mutations and further studies would be of interest. It is however noteworthy that a phase II trial of varsepladib, an inhibitor of secreted PLA_2s (selectivity against group IIA, V and X PLA_2s) has demonstrated efficacy in reducing the concentrations of LDL cholesterol [591].

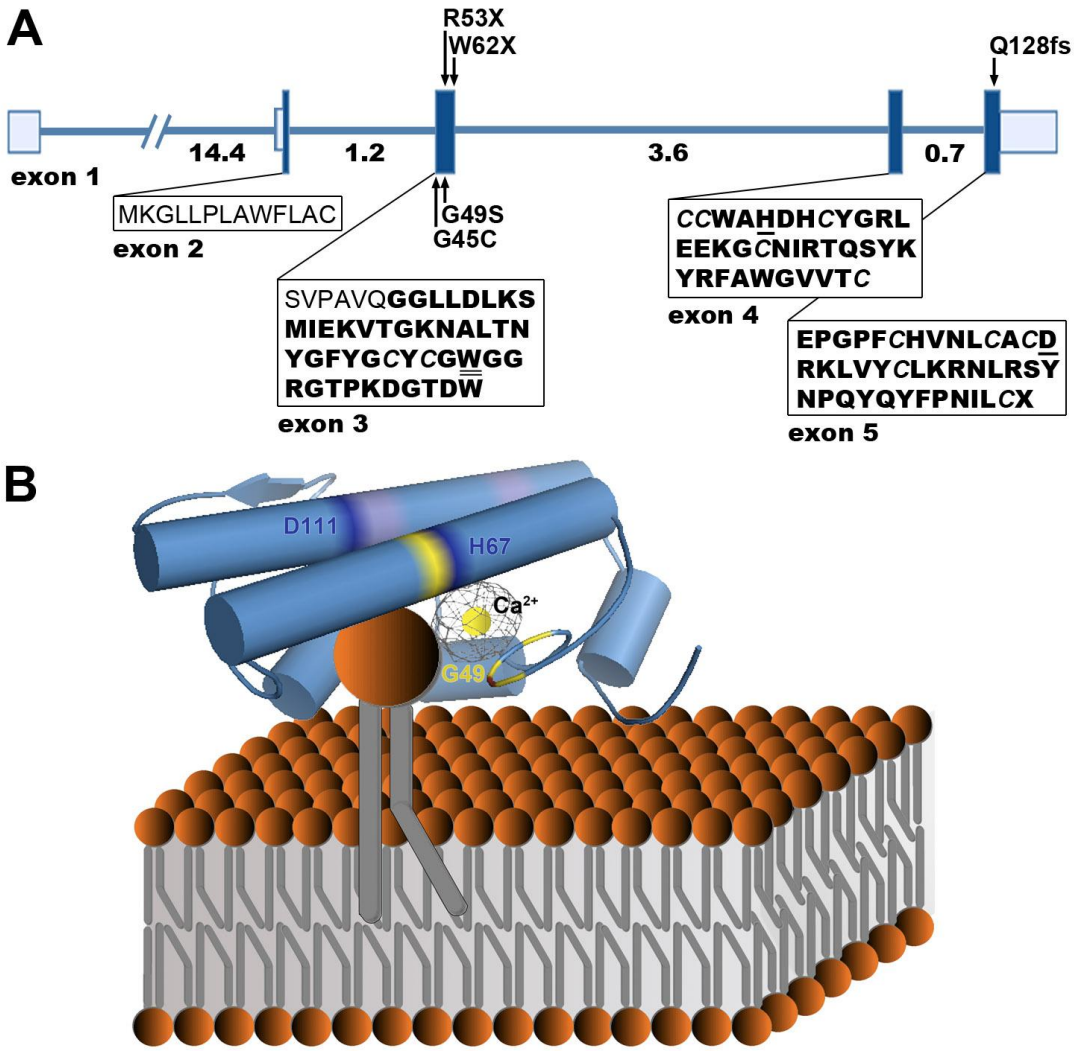

Figure 3-28. Structure of the *PLA2G5* gene and hypothetical model of human group V PLA_2 binding to a phospholipid membrane surface.
[A] Exons are depicted with boxes in which the shaded areas denote coding sequence and the unshaded areas denote 5' and 3' untranslated region. The amino acid sequence of the signal peptide is shown in normal font; the sequence of the 118-amino-acid mature enzyme after cleavage of the prepeptide is shown in bold font (Uniprot, [564]). Cystine residues forming the six disulfide bridges maintaining the enzyme's rigid three-dimensional structure are italicised (Uniprot, [564]). Amino acids responsible for interfacial binding (Tryptophan 50) [592] and catalytic activity(Histidine 67 and Aspartic Acid 111) [568] are underlined.
[B] A homology model of human group V PLA_2 (Protein Data Bank accession code 2ghn [593]) after hypothetical association with a phospholipid membrane is presented. Structural features of the, conserved among secreted PLA_2s, active site are highlighted; those include a catalytic Ca^{2+} ion bound by a peptide loop (yellow) and a catalytic dyad formed by amino acids His67 and Asp111 (dark blue) [568]. The Ca^{2+} coordination includes carbonyl backbone interactions from Tyr47, Gly49 and Gly51 as well as a shared bidentate interaction from Asp68 (amino acids coloured in yellow; Uniprot). Trp50, a key amino acid in the enzyme's interfacial binding surface (distinct from the active site) is highlighted in red; its indole chain contributes to the characteristic ability of group V PLA_2 to bind to both zwitterionic and anionic phospholipid vesicles [592]. Cationic residues towards the COOH end of the protein, also responsible for membrane binding, are coloured in purple [594].
PyMOL was used to view the human group V PLA_2 three-dimensional molecular structure (orthoscopic view, cartoon setting, cylindrical helices).

To gain insight into the function of group V PLA_2 in the retina, clinical investigations were performed in patients with mutations in *PLA2G5*. Firstly, *in vivo* cross sectional imaging using SD OCT (Spectralis HRA+OCT, Heidelberg Engineering) was undertaken. Deposit accumulation within the RPE monolayer and/or the area between the RPE and photoreceptor cells was observed (subjects K-2 and M-1; figure 3-27). Secondly, fundus autofluorescence imaging [147] (HRA2, Heidelberg Engineering) was utilised to provide insight into the molecular composition of the fleck-like lesions; hyperautofluorescent material, *i.e.* rich in lipofuscin or other fluorophores was observed (subjects J-4, J-5, J-6, K-2 and M-1; figure 3-27). Lipofuscin accumulation is a hallmark of aging in metabolically active cells including cardiac myocytes, neurons and RPE [595]. In the latter, the main source of lipofuscin is the undegradable components of phagocytosed photoreceptor outer segment discs [147, 596]. Excessive build-up has been associated with various forms of photoreceptor degeneration namely retinal dystrophies and age-related macular degeneration [147]. In order to assess the functional significance of abnormalities detected by fundus autofluorescence and SD OCT in benign fleck retina patients, fundus-controlled perimetry ("microperimetry"; MP1 Microperimeter, Nidek Technologies) was performed. Retinal sensitivity was normal in a 10-year-old patient even when areas corresponding to large flecks were stimulated (subject K-2; figure 3-27). This suggests that the compounds of lipofuscin accumulating in this condition have no or minimal functional consequences; this observation is supported by normal electrophysiological findings (table 3-18). Finally, fundus photography in subject K-2 at 6 and 12 years of age has documented an increase in number and size of retinal flecks (figure 3-27). This is not evident from cross sectional analysis across four decades and a genotype-phenotype correlation cannot be excluded (figure 3-27).

Despite Kolko *et al*. previously demonstrating high levels of *PLA2G5* mRNA expression within the rat retina [570], the precise protein localization is currently unknown. To determine this, immunohistochemical staining of human retinal tissue obtained from an 87-year-old male donor eye was performed (experiment designed and conducted by Dr Alice E Davidson).

Immunoreactivity was predominantly detected in the outer and inner plexiform layers (figure 3-29). This result is unexpected as the data (SD OCT, fundus autofluorescence imaging) indicate that the primary defect in patients with mutated group V PLA_2 is in close proximity to the RPE. More specifically, abnormal RPE phagocytosis could explain the level and autofluorescent nature of the fleck-like lesions (figure 3-27); this hypothesis is supported by previous reports that demonstrated the capacity of the protein to promote phagosome maturation in other tissues [580]. The inconsistency between protein localization in donor retina and site of structural change in patients is difficult to explain and future studies investigating group V PLA_2 staining in younger retinae should provide further insight.

No mutation was detected in the *PLA2G5* coding region and intron-exon boundaries of patient N-1, a 10-year-old girl with a typical benign fleck retina phenotype (rs2020887, a previously reported SNP, was found in heterozygous state). This finding suggests that benign fleck retina may be a genetically heterogeneous condition. Interestingly, group IB PLA_2, another conventional secretory phospholipase, has been shown to be expressed at similar levels and to have a comparable localization to group V PLA_2 within the rat retina [570]. *PLA2G1B* was therefore selected as a candidate gene and its coding region and intron-exon boundaries were screened; no variants were identified in patient N-1.

Retinal disease due to mutation in *PLA2G5* adds to a small group of human Mendelian disorders associated with genes encoding PLA_2s; these diseases involve neurodegeneration (mutations in *PLA2G6* and *PNPLA6*), abnormal lipid storage (mutations in *PNPLA2*) or platelet dysfunction (mutations in *PLA2G4A* and *PLA2G7*). Notably, *PLA2G7* encodes a lipoprotein-associated PLA_2 and its natural deficiency (caused by a functionally validated p.Val279Phe null allele; MAF from 4 to 18% in East Asian and around 0.03% in European populations) is not detrimental to human health with carriers having a low risk for coronary artery disease [597-598].

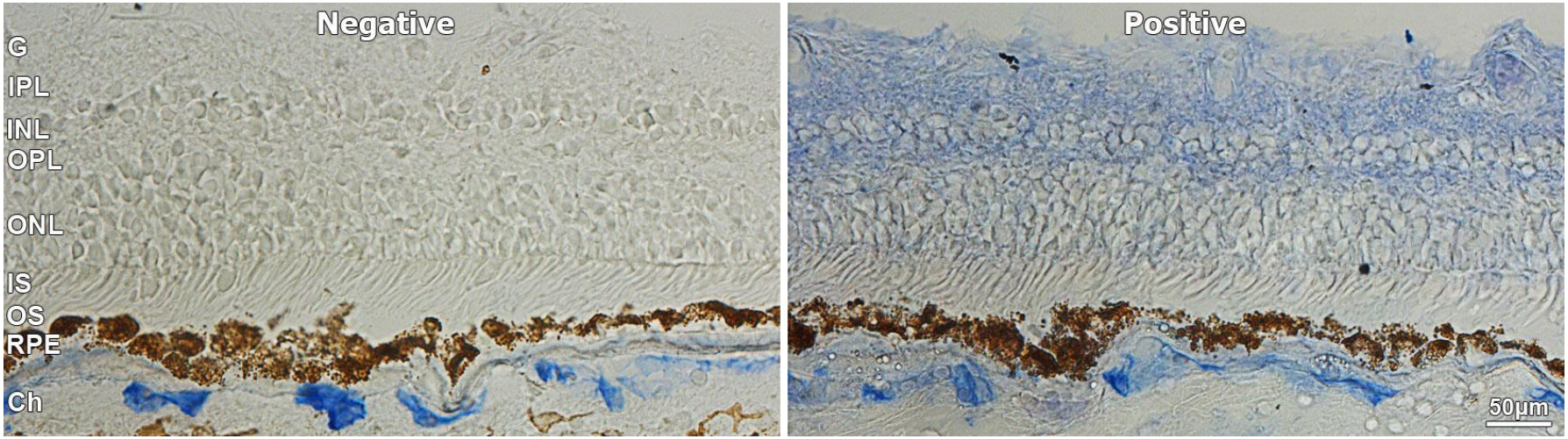

Figure 3-29. Localization of group V PLA_2 within a control human retinal tissue
Human retinal tissue from an 87-year-old male donor eye was obtained from the eye bank at MEH with the approval of Moorfields & Whittington Research Ethics Committee (06/Q0504/78) and embedded in optimal cutting temperature compound. Cryostat sections were cut at 10 µm and thaw-mounted onto charged slides. Immunohistochemistry was performed at room temperature to reveal group V PLA_2 localization using Mouse anti-Human PLA2G5 monoclonal antibody (LS-C11702, clone MCL-3G1, Lifespan Bioscience, Seattle, WA, USA) [586], at a dilution factor of 1 in 20. An alkaline phosphatase-conjugated avidin-biotin complex kit (Vectastain ABC-AP Mouse IgG kit, Vector Laboratories, Burlingame, CA, USA) was used as a secondary detection method according to manufacturer's guidelines. An additional quenching step was performed for 30 minutes to reduce autofluorescence using 1% levamisole.
Ch, Choroid; OS, photoreceptor outer segments; IS photoreceptor inner segment; ONL, outer nuclear layer; OPL, outer plexiform layer; INL, inner nuclear layer; IPL, inner plexiform layer; G ganglion cell layer. Scale bar is 50 µm.

4 GENERAL DISCUSSION

In 1977, in an address to the American Society of Human Genetics, Arno Motulsky highlighted that “genetics has given medicine a rich intellectual foundation and has made possible many practical medical applications” [599]. Thirty-five years later, genetic information continues to increase our understanding of disease mechanisms and to guide the development of novel therapeutic approaches. The present thesis focuses on Mendelian disorders (Motulsky in the same address claimed that “most data in this [monogenic trait] area are noncontroversial and accepted by all observers” [599]) and more specifically autosomal recessive retinal disease. Phenotypic data on five mechanistically distinct retinal disorders were collected (section 3.1) and defects in three molecules that have not been previously associated with recessive retinal disease were identified (section 3.2).

In this study, DNA samples from over 500 unrelated individuals affected with autosomal recessive retinal disease were available (section 2.1). Initially, subjects with distinctive clinical (sections 3.1.3 and 3.1.7) and/or electrophysiological features (sections 3.1.3, 3.1.4, 3.1.5 and 3.1.6) were selected and screened for previously associated with retinal disease candidate genes. Notably, a specific function has been assigned to the proteins encoded by most of the genes tested (including *SAG*, *RDH5*, *KCNV2*, *GRM6* and *OAT*). This facilitated the identification of features that have mechanistic relevance in individuals harbouring disease-causing mutations (for example the reduced fundus autofluorescence associated with *RDH5* variants, section 3.1.4.2.3). Furthermore, it allowed a more specific diagnosis of such individuals based on molecular and biochemical events rather than clinical appearance (for example *RDH5* retinopathy instead of fundus albipunctatus and *GRM6* retinopathy instead of autosomal recessive CSNB). Once a number of patients affected with a distinct disease subtype had been identified, additional clinical data were collected and an attempt to characterise the natural history of disease was made. This was often hindered by the cross-sectional nature of the study and the high degree of phenotypic variability observed. Explaining

this variability in symptoms and progression remains a major challenge and future studies should provide important insights into contributory genetic and environmental factors.

The “phenotype-oriented” method described above and elaborated in section 3.1 uses a robust pretest hypothesis as individuals were tested for a specific gene only if their clinical presentation was similar to the phenotype previously associated with this gene. Such an approach has important advantages and disadvantages. The main advantage is that the results, *i.e.* the observed DNA variation, are more likely to be meaningful and easier to place in context. The main disadvantage is the underestimation of the phenotypic variability associated with defects in a specific molecule. Furthermore, the role of a particular gene in human disease is not fully investigated. Approaches that are more unbiased and hypothesis-free are becoming increasingly available as a result of technological advances in microarray and sequencing technologies. These methods allow discoveries in previously unexplored places to be made. Such discoveries include:

(a) the identification of disease-causing variants in genes not previously associated with disease such as *TRPM1*, *KCNJ13* and *PLA2G5* (sections 3.2.3, 3.2.4 and 3.2.5).

(b) the expansion of the phenotypic spectrum caused by variants in genes that have been previously associated with disease. Likely examples from this study are a homozygous change in *RLBP1* detected in an individual with a mild fleck retina phenotype (hz18682, table 3-12, section 3.2.1; figure 4.1) as well as a variant, previously associated with rod monochromasy [344], identified in an individual with late-onset maculopathy (rs147876778; hz18502, table 3-13, section 3.2.2).

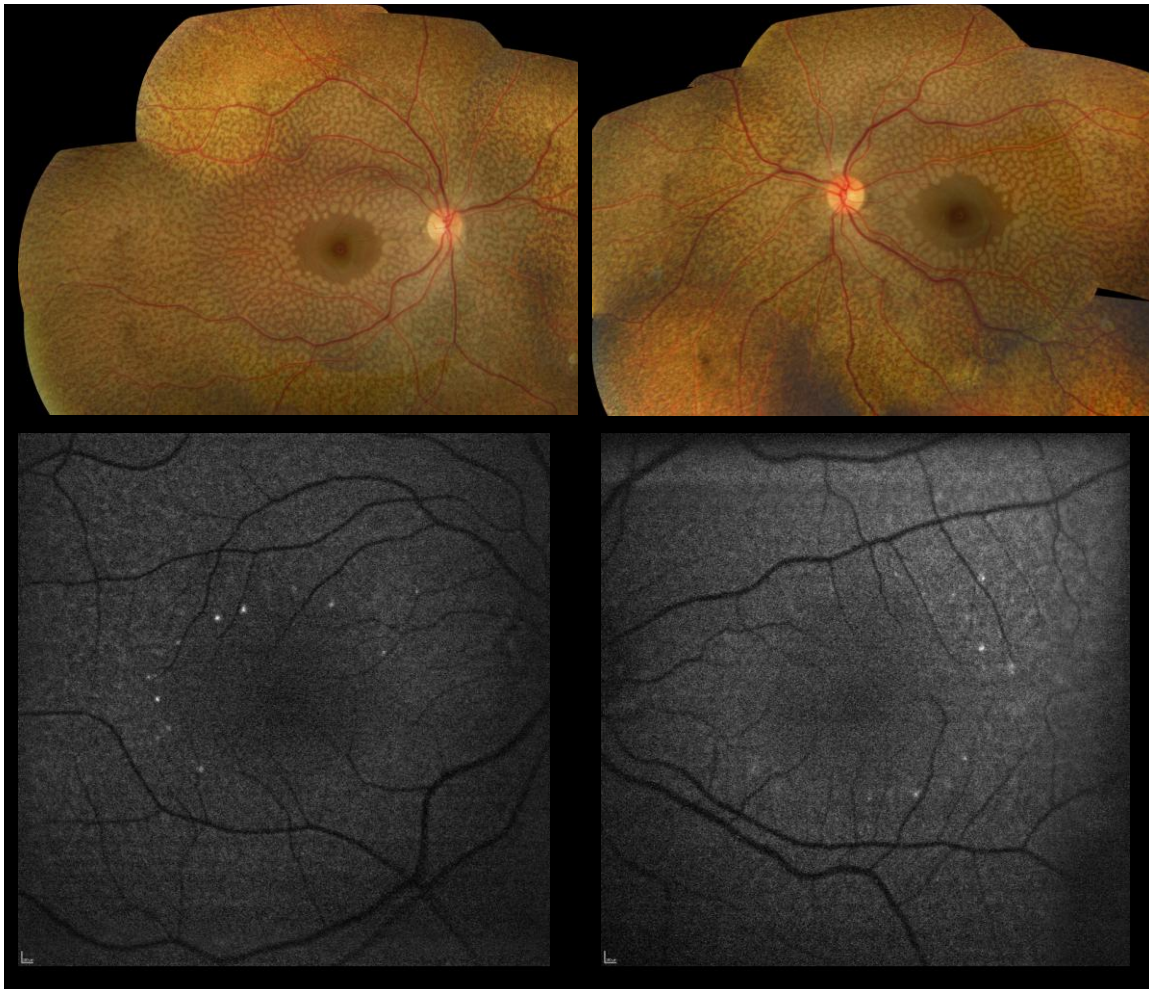

Figure 4-1. Fundus photographs and autofluorescence images from the left and right eyes of a 29-year-old individual. The patient reported night blindness from a very young age. Her parents are first cousins and she has two affected and four unaffected siblings. Colour vision and visual acuity were normal (0.0 logMAR and 17/17 Ishihara in each eye). Electrophysiological findings were in keeping with fundus albipunctatus (section 3.1.4) without evidence of cone system involvement. Screening of *RDH5* was negative. Homozygosity mapping (hz18682, table 3-12, section 3.2.1) revealed a region of homozygosity around *RLBP1*, a gene previously associated with progressive rod-cone degeneration (Bothnia dystrophy; see section 3.1.4). Subsequently, Sanger sequencing identified a homozygous p.Val11Ala variant in *RLBP1*; this sequence alteration has not been previously reported (1000 genomes, dbSNP, HGMD, EVS). It is likely that the p.Val11Ala change forms a hypomorphic allele associated with a significantly milder phenotype compared to the one associated with other *RLBP1* mutations [150, 600].

Some unexpected results may also be observed when genome-wide approaches are utilised. Examples from this study include:

(a) a proband with FEVR born to related parents in which exome sequencing identified compound heterozygous variants in the previously associated with FEVR gene *LRP5* [601-602] (hz19762, table 3-13, section 3.2.2);

(b) a pedigree with two individuals affected with FEVR (proband and her father's first cousin) in which one subject was found homozygous and one

heterozygous for the same splice site change in *TSPAN12* (hz17327, table 3-12, section 3.2.1). Notably, heterozygous frameshift, splice site, nonsense and missense mutations in *TSPAN12* are associated with dominantly inherited FEVR [603-604];

(c) a pedigree with three individuals affected with rod monochromacy (proband and two maternal aunts; figure 4-2) in which the proband was found to be homozygous for a previously reported disease-causing [343] variant in *CNGA3* (rs141386891; hz17857, table 3-12, section 3.2.1); both her aunts were found heterozygous for this change and homozygous for a different, also previously reported as disease-causing [344] variant in *CNGB3* (rs147876778). Surprisingly the proband's unaffected sister was also found homozygous for the *CNGA3* sequence alteration (MAF< 0.01% in EVS).

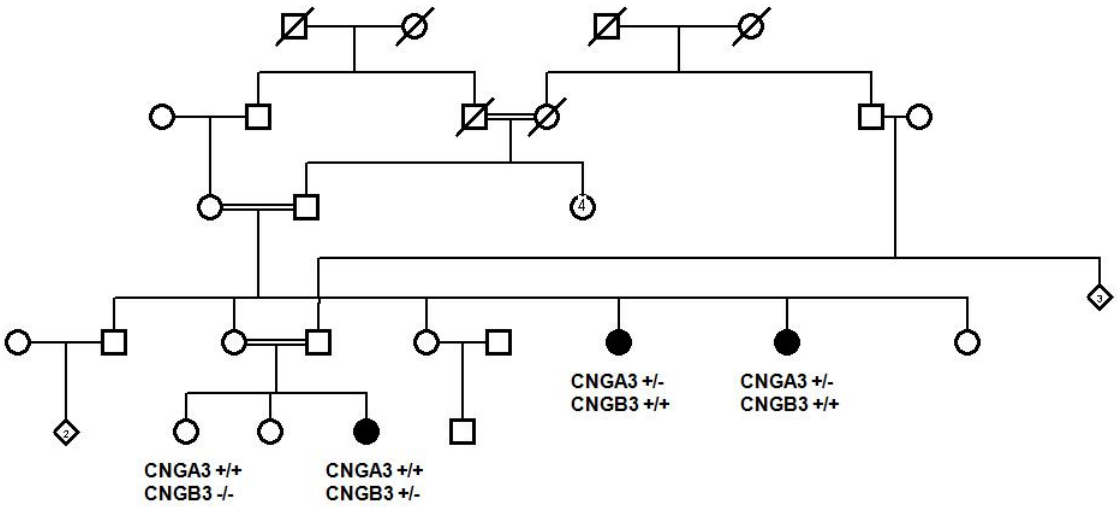

Figure 4-2. Pedigree and genetic testing results from a family segregating rod monochromasy.
CNGA3+ denotes presence of an allele harbouring a p.Arg437Cys.
CNGB3+ denotes presence on an allele harbouring a p.Arg403Gln.
+/+, homozygous; +/-, heterozygous

(d) a pedigree with three individuals affected with RP (two siblings and their first cousin; figure 4-3) in which one of the two siblings and her maternal cousin are homozygous for a previously reported [605] frameshift mutation in *RP1*. Intriguingly, the other affected sibling was found heterozygous for the same change (hz18655, table 3-12, section 3.2.1).

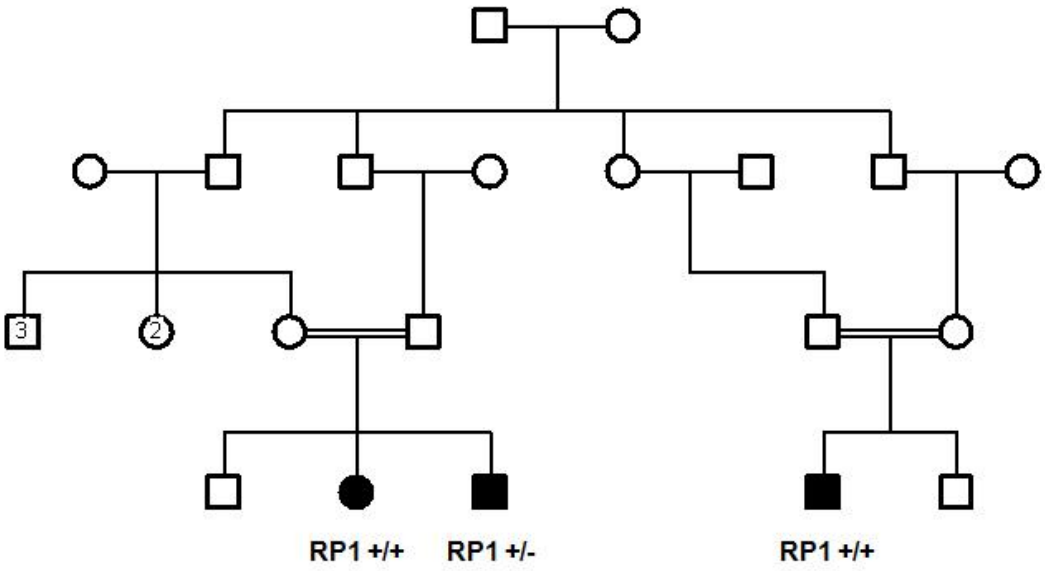

Figure 4-3. Pedigree and genetic testing results from a family segregating RP
RP1+ denotes presence on an allele harbouring a p.Glu487_Glu488delinsGluX.
+/+, homozygous; +/-, heterozygous.
See text for more details.

The trade-off of replacing informed but biased hypotheses (section 3.1) with unbiased but generic ones (section 3.2) is that every result must be treated with the skepticism that is appropriate for an ignorant hypothesis [104]. Therefore, additional, convincing evidence needs to be collected. Obtaining sufficient data is challenging and potentially unachievable for some true positive results. In this thesis, despite confidently imposing an autosomal recessive, Mendelian model and being able to apply powerful family-based filtering strategies (homozygosity mapping, linkage approaches), causality could not be established in the majority of families studied with microarrays or exome sequencing (section 3.2). It can be argued that only the low-hanging fruit were harvested and in retrospect, *TRPM1*, *KCNJ13* and *PLA2G5* may appear obvious candidate genes. Robinson *et al*. note that “a major problem in studying rare disease is that one can never be entirely certain that a given gene is in fact the sought after disease gene until a second unrelated individual is described with mutation in the same gene and a comparable phenotype” [96]. The main strength of this study has been the availability of a large number of families to screen in order to robustly associate a molecular defect with a phenotype. Although dealing with the explosive growth in the quantity and complexity of genomic data is often considered the major

challenge for the future, involving in genetic research and collecting DNA samples from as many affected individuals as possible is also key. Equally if not more important to those is to maintain a constant flow of basic research discoveries. Knowledge gained from basic research has significantly benefited this clinical study; if information has not been previously accumulated on the function of *TRPM1*, *KCNJ13* and *PLA2G5,* these would have probably been overlooked as candidate genes.

It seems inevitable that genetics and genomics will transform the way medicine is practiced. It is clear however that a substantial amount of research is needed before implementing “genomic medicine”. Gaining insight into genetic and phenotypic heterogeneity of disease is extremely important and the results presented in this thesis are a minor contribution towards ophthalmic care that focuses on predisposition testing, early detection and targeted therapy.

5 REFERENCES

1. Johannsen, W. (1909). Elemente der exakten Erblichkeitslehre.(Jena, Justav Fischer).
2. Sturtevant, A.H. (1965). A history of genetics.(Cold Spring Harbor, Cold Spring Harbor Laboratory Press).
3. Darwin, C. (1858). The Variation of Animals and Plants under Domestication.(London, John Murray).
4. Weiling, F. (1991). Historical study: Johann Gregor Mendel 1822-1884. Am J Med Genet *40*, 1-26.
5. Mendel, G. (1866). Versuche über pflanzen-hybriden. Verh Naturforsch Ver Brünn *IV für das Jahr 1865*, 3–47.
6. Bateson, W. (1906). The progress of genetic research. The 3rd International Conference on Genetics, Royal Horticultural Society, London.
7. Harper, P.S. (2005). William Bateson, human genetics and medicine. Hum Genet *118*, 141-151.
8. De Vries, H. (1900). Sur la loi de disjonction des hybrids. C R Acad Sci *130*, 845–847
9. De Vries, H. (1904). The evidence of evolution. Science *20*, 395-401.
10. Von Tschermak Seysenegg, E. (1900). Über künstliche Kreuzung bei Pisum sativum. Zeitschrift für das Landwirthschaftliche Versuchswesen in Oesterreich *3*, 465-555.
11. Correns, G.C. (1900). Mendel's regel über das verhalten der nachkommenschaft der rassenbastarde. Berichte der Deutschen Botanischen Gesellschaft *18*, 158-168.
12. De Vries, H. (1902). The origin of species by mutation. Science *15*, 721-729.
13. De Vries, H. (1914). The principles of the theory of mutation. Science *40*, 77-84.
14. De Vries, H. (1889). Intracellular pangenesis.(Chicago, The Open Court Publishing Company).
15. Churchill, F.B. (1974). William Johannsen and the genotype concept. J Hist Biol *7*, 5-30.
16. Roll-Hansen, N. (2009). Sources of Wilhelm Johannsen's genotype theory. J Hist Biol *42*, 457-493.
17. Bridges, C.B. (1921). Current maps of the location of the mutant genes of Drosophila melanogaster. Proc Natl Acad Sci U S A *7*, 127-132.
18. Kandel, E.R. (1999) Thomas Hunt Morgan at Columbia University: genes, chromosomes, and the origins of modern biology. Columbia Magazine: Living Legacies, *Fall 1999*.
19. Morgan, T.H. (1910). Sex limited inheritance in Drosophila. Science *32*, 120-122.
20. Morgan, T.H. (1911). The origin of five mutations in eye color in Drosophila and their modes of inheritance. Science *33*, 534-537.
21. Boveri, T. (1902). Über mehrpolige mitosen als mittel zur analyse des zellkerns. Verh phys-med Gesellsch Wurzburg *35*, 67–90.

22. Goldschmidt, R. (1916). Theodor Boveri. Science *43*, 263-270.
23. Sutton, W. (1902). On the morphology of the chromosome group in Brachystola magna. Biol Bull *4*, 24-39.
24. Morgan, T.H. (1915). Localization of the hereditary material in the germ cells. Proc Natl Acad Sci U S A *1*, 420-429.
25. Morgan, T.H., Sturtevant, A.H. Muller, H.J. Bridges, C.B. (1915). The mechanism of Mendelian heredity.(New York, Henry Holt).
26. Muller, H.J. (1916). The mechanism of crossing-over.(New York, The American Naturalist).
27. Sturtevant, A.H., Bridges, C.B., and Morgan, T.H. (1919). The spatial relations of genes. Proc Natl Acad Sci U S A *5*, 168-173.
28. Sturtevant, A.H. (1913). A third group of linked genes in Drosophila ampelophila. Science *37*, 990-992.
29. Haldane, J.B.S. (1919). The combination of linkage values and the calculation of distances between the loci of linked factors. J Genet *8*, 299-309.
30. Bridges, C.B. (1916). Non-disjunction as proof of the chromosome theory of heredity. Genetics *1*, 1-52.
31. Bridges, C.B. (1914). Direct proof through non-disjunction that the sex-linked genes of Drosophila are borne by the X-chromosome. Science *40*, 107-109.
32. Morgan, T.H. (1932). The rise of genetics. Science *76*, 261-267.
33. Tatum, E.L. and Beadle, G.W. (1942). Genetic control of biochemical reactions in Neurospora: an "aminobenzoicless" mutant. Proc Natl Acad Sci U S A *28*, 234-243.
34. Horowitz, N.H. (1995). One-gene, one-enzyme: remembering biochemical genetics. Protein Sci *4*, 1017-1019.
35. Hickman, M. and Cairns, J. (2003). The centenary of the one-gene one-enzyme hypothesis. Genetics *163*, 839-841.
36. Avery, O.T., Macleod, C.M., and McCarty, M. (1944). Studies on the chemical nature of the substance inducing transformation of Pneumococcal types: induction of transformation by a desoxyribonucleic acid fraction isolated from Pneumococcus yype III. J Exp Med *79*, 137-158.
37. Steinman, R.M. and Moberg, C.L. (1994). A triple tribute to the experiment that transformed biology. J Exp Med *179*, 379-384.
38. Morgan, T.H., Lynch, C.J. (1912). The linkage of two factors in Drosophila that are not sex-linked. Biol Bull *23*, 174-182.
39. Edwards, A.W.F. (2005). Linkage methods in human genetics before the computer. Hum Genet *118*, 515-530.
40. Bateson, W.S., E.R. Punnett,R.C. (1905). Experimental studies in the physiology of heredity. Rep Evol Com R Soc *II*, 1-131.
41. Wilson, E.B. (1911). The sex chromosomes. Arch Anat Entwicklungsmech *77*, 249-271.

42. Lock, R.H. (1906). Recent progress in the study of variation, heredity and evolution.(Boston, Adamant Media Corporation).
43. Edwards, A.W.F. (1996). The early history of the statistical estimation of linkage. Ann Hum Genet *60*, 237-249.
44. Engledow, F.L., Yule, G. U (1914). The determination of the best value of the coupling ratio from a given set of data. Proc Camb Phil Soc *17*, 436-440.
45. Edwards, A.W.F. (1997). Three early papers on eficient parametric estimation. Stat Sci *12*, 35-47.
46. Haldane, J.B.S. (1919). The probable errors of calculated linkage values, and the most accurte method for determining gametic from certain zygotic series. J Genet *20*.
47. Fisher, R.A. (1922). On the mathematical foundations of theoretical statistics. Philos Trans R Soc Lond *222*, 309-368.
48. Mohr, J. (1954). A study of linkage in man.(Copenhagen, Munksgaard).
49. Smith, C.A.B. (1986). The development of human linkage analysis. Ann Hum Genet *50*, 293-311.
50. Haldane, J.B.S., Smith, C.A.B. (1947). A new estimate of the linkage between the genes for colour-blindness and haemophilia in man. Ann Eugen *14*, 10-31.
51. Bell, J., Haldane,J.B.S. (1937). The linkage between the genes for colour-blindness and haemophilia in man. Proc R Soc Lond B *123*, 119–150.
52. Morton, N.E. (1955). Sequential tests for the detection of linkage. Am J Hum Genet *7*, 277-318.
53. Elston, R.C. and Stewart, J. (1971). A general model for the genetic analysis of pedigree data. Hum Hered *21*, 523-542.
54. Lander, E.S. and Green, P. (1987). Construction of multilocus genetic linkage maps in humans. Proc Natl Acad Sci U S A *84*, 2363-2367.
55. Ott, J. (2011). Writings on genetic linkage in the annals. Ann Hum Genet *75*, 344-347.
56. Simpson, H.R. (1958). The estimation of linkage on an electronic computer. Ann Hum Genet *22*, 356-361.
57. Ott, J. (1974). Estimation of the recombination fraction in human pedigrees: efficient computation of the likelihood for human linkage studies. Am J Hum Genet *26*, 588-597.
58. Lathrop, G.M.A.L., J.M. (1984). Estimation of recombination and genetic risks using several markers. Prog Clin Biol Res. *147*, 267-269.
59. O'Connell, J.R. and Weeks, D.E. (1995). The VITESSE algorithm for rapid exact multilocus linkage analysis via genotype set-recoding and fuzzy inheritance. Nat Genet *11*, 402-408.
60. Kruglyak, L., Daly, M.J., Reeve-Daly, M.P., and Lander, E.S. (1996). Parametric and nonparametric linkage analysis: a unified multipoint approach. Am J Hum Genet *58*, 1347-1363.
61. Li, H. and Schaid, D.J. (1997). GENEHUNTER: application to analysis of bipolar pedigrees and some extensions. Genet Epidemiol *14*, 659-663.

62. Gudbjartsson, D.F., Jonasson, K., Frigge, M.L., and Kong, A. (2000). Allegro, a new computer program for multipoint linkage analysis. Nat Genet *25*, 12-13.
63. Abecasis, G.R., Cherny, S.S., Cookson, W.O., and Cardon, L.R. (2002). Merlin: rapid analysis of dense genetic maps using sparse gene flow trees. Nat Genet *30*, 97-101.
64. Altshuler, D., Daly, M.J., and Lander, E.S. (2008). Genetic mapping in human disease. Science *322*, 881-888.
65. Ott, J., Kamatani, Y., and Lathrop, M. (2011). Family-based designs for genome-wide association studies. Nat Rev Genet *12*, 465-474.
66. Dawn Teare, M. and Barrett, J.H. (2005). Genetic linkage studies. Lancet *366*, 1036-1044.
67. Garrod, A.E. (1996). The incidence of alkaptonuria: a study in chemical individuality - 1902. Mol Med *2*, 274-282.
68. Dunwell, J.M. (2007). 100 years on: a century of genetics. Nat Rev Genet *8*, 231-235.
69. Farabee, W.C. (1903). Notes on negro albinism. Science *17*, 75.
70. Bateson, W. (1906). An address on Mendelian heredity and its application to man. Brain *29*, 157-179.
71. Donahue, R.P., Bias, W.B., Renwick, J.H., and McKusick, V.A. (1968). Probable assignment of the Duffy blood group locus to chromosome 1 in man. Proc Natl Acad Sci U S A *61*, 949-955.
72. Botstein, D., White, R.L., Skolnick, M., and Davis, R.W. (1980). Construction of a genetic linkage map in man using restriction fragment length polymorphisms. Am J Hum Genet *32*, 314-331.
73. Davies, K.E., Pearson, P.L., Harper, P.S., Murray, J.M., et al. (1983). Linkage analysis of two cloned DNA sequences flanking the Duchenne muscular dystrophy locus on the short arm of the human X chromosome. Nucleic Acids Res *11*, 2303-2312.
74. Cavenee, W.K., Dryja, T.P., Phillips, R.A., Benedict, W.F., et al. (1983). Expression of recessive alleles by chromosomal mechanisms in retinoblastoma. Nature *305*, 779-784.
75. Gusella, J.F., Wexler, N.S., Conneally, P.M., Naylor, S.L., et al. (1983). A polymorphic DNA marker genetically linked to Huntington's disease. Nature *306*, 234-238.
76. Royer-Pokora, B., Kunkel, L.M., Monaco, A.P., Goff, S.C., et al. (1986). Cloning the gene for an inherited human disorder, chronic granulomatous disease, on the basis of its chromosomal location. Nature *322*, 32-38.
77. Collins, F.S. (1992). Positional cloning: let's not call it reverse anymore. Nat Genet *1*, 3-6.
78. Gilissen, C., Hoischen, A., Brunner, H.G., and Veltman, J.A. (2011). Unlocking Mendelian disease using exome sequencing. Genome Biol *12*, 228.
79. Friend, S.H., Bernards, R., Rogelj, S., Weinberg, R.A., et al. (1986). A human DNA segment with properties of the gene that predisposes to retinoblastoma and osteosarcoma. Nature *323*, 643-646.

80. Riordan, J.R., Rommens, J.M., Kerem, B., Alon, N., et al. (1989). Identification of the cystic fibrosis gene: cloning and characterization of complementary DNA. Science *245*, 1066-1073.

81. Rommens, J.M., Iannuzzi, M.C., Kerem, B., Drumm, M.L., et al. (1989). Identification of the cystic fibrosis gene: chromosome walking and jumping. Science *245*, 1059-1065.

82. Kerem, B., Rommens, J.M., Buchanan, J.A., Markiewicz, D., et al. (1989). Identification of the cystic fibrosis gene: genetic analysis. Science *245*, 1073-1080.

83. Dryja, T.P., Mcgee, T.L., Reichel, E., Hahn, L.B., et al. (1990). A point mutation of the rhodopsin gene in one form of retinitis pigmentosa. Nature *343*, 364-366.

84. Aird, I., Bentall, H.H., Mehigan, J.A., and Roberts, J.A. (1954). The blood groups in relation to peptic ulceration and carcinoma of colon, rectum, breast, and bronchus; an association between the ABO groups and peptic ulceration. Br Med J *2*, 315-321.

85. Ingram, V.M. (1956). A specific chemical difference between the globins of normal human and sickle-cell anaemia haemoglobin. Nature *178*, 792-794.

86. Dipple, K.M. and McCabe, E.R. (2000). Phenotypes of patients with "simple" Mendelian disorders are complex traits: thresholds, modifiers, and systems dynamics. Am J Hum Genet *66*, 1729-1735.

87. Badano, J.L. and Katsanis, N. (2002). Beyond Mendel: an evolving view of human genetic disease transmission. Nat Rev Genet *3*, 779-789.

88. Antonarakis, S.E., Chakravarti, A., Cohen, J.C., and Hardy, J. (2010). Mendelian disorders and multifactorial traits: the big divide or one for all? Nat Rev Genet *11*, 380-384.

89. Antonarakis, S.E. and Beckmann, J.S. (2006). Mendelian disorders deserve more attention. Nat Rev Genet *7*, 277-282.

90. Miki, Y., Swensen, J., Shattuck-Eidens, D., Futreal, P.A., et al. (1994). A strong candidate for the breast and ovarian cancer susceptibility gene BRCA1. Science *266*, 66-71.

91. Wooster, R., Bignell, G., Lancaster, J., Swift, S., et al. (1995). Identification of the breast cancer susceptibility gene BRCA2. Nature *378*, 789-792.

92. Bell, G.I., Horita, S., and Karam, J.H. (1984). A polymorphic locus near the human insulin gene is associated with insulin-dependent diabetes mellitus. Diabetes *33*, 176-183.

93. Pericak-Vance, M.A., Bebout, J.L., Gaskell, P.C., Jr., Yamaoka, L.H., et al. (1991). Linkage studies in familial Alzheimer disease: evidence for chromosome 19 linkage. Am J Hum Genet *48*, 1034-1050.

94. Corder, E.H., Saunders, A.M., Strittmatter, W.J., Schmechel, D.E., et al. (1993). Gene dose of apolipoprotein E type 4 allele and the risk of Alzheimer's disease in late onset families. Science *261*, 921-923.

95. Risch, N. and Merikangas, K. (1996). The future of genetic studies of complex human diseases. Science *273*, 1516-1517.

96. Robinson, P.N., Krawitz, P., and Mundlos, S. (2011). Strategies for exome and genome sequence data analysis in disease-gene discovery projects. Clin Genet *80*, 127-132.

97. Kruglyak, L. (2008). The road to genome-wide association studies. Nat Rev Genet *9*, 314-318.

98. Maher, B. (2008). Personal genomes: the case of the missing heritability. Nature *456*, 18-21.

99. Manolio, T.A., Collins, F.S., Cox, N.J., Goldstein, D.B., et al. (2009). Finding the missing heritability of complex diseases. Nature *461*, 747-753.

100. Kaiser, J. (2010). Human genetics. Affordable 'exomes' fill gaps in a catalog of rare diseases. Science *330*, 903.

101. Bamshad, M.J., Ng, S.B., Bigham, A.W., Tabor, H.K., et al. (2011). Exome sequencing as a tool for Mendelian disease gene discovery. Nat Rev Genet *12*, 745-755.

102. Ng, S.B., Buckingham, K.J., Lee, C., Bigham, A.W., et al. (2010). Exome sequencing identifies the cause of a Mendelian disorder. Nat Genet *42*, 30-35.

103. Swami, M. (2010). Whole-genome sequencing identifies Mendelian mutations. Nat Rev Genet *11*, 313.

104. Cooper, G.M. and Shendure, J. (2011). Needles in stacks of needles: finding disease-causal variants in a wealth of genomic data. Nat Rev Genet *12*, 628-640.

105. Lander, E.S. and Botstein, D. (1987). Homozygosity mapping: a way to map human recessive traits with the DNA of inbred children. Science *236*, 1567-1570.

106. Hardy, G.H. (1908). Mendelian Proportions in a Mixed Population. Science *28*, 49-50.

107. Punnett, R.C. (1950). Early days of genetics. Heredity *4*, 1-10.

108. Edwards, A.W. (2008). G. H. Hardy (1908) and Hardy-Weinberg equilibrium. Genetics *179*, 1143-1150.

109. Weinberg, W. (1908). Über den Nachweis der Vererbung beim Menschen. Jahreshefte des Vereins für vaterländische Naturkunde in Württemberg *64*, 368–382.

110. Okasha, S. (2008). Population Genetics. The Stanford Encyclopedia of Philosophy.

111. Fisher, R.A. (1918). The correlation between relatives on the supposition of Mendelian inheritance. Transactions of the Royal Society of Edinburgh *52*, 399-433.

112. Piegorsh, W.W. (1990). Fisher's contributions to genetics and heredity, with special emphasis on the Gregor Mendel controversy. Biometrics *46*, 915-924.

113. Fisher, R.A. (1930). The genetical theory of natural selection.(Oxford, Clarendon Press).

114. Hill, W.G. (1996). Sewall Wright's "Systems of Mating". Genetics *143*, 1499-1506.

115. Wright, S. (1921). Systems of Mating I: the biometric relations between parent and offspring. Genetics *6*, 111-123.

116. Wright, S. (1921). Systems of Mating II: the effects of inbreeding on the genetic composition of a population. Genetics *6*, 124-143.

117. Wright, S. (1921). Systems of Mating III: assortative mating based on somatic resemblance. Genetics *6*, 144-161.

118. Wright, S. (1921). Systems of Mating IV: the effects of selection. Genetics *6*, 162-166.

119. Wright, S. (1921). Systems of Mating V: general considerations. Genetics *6*, 167-178.

120. Olby, R.C. (2000). Horticulture: the font for the baptism of genetics. Nat Rev Genet *1*, 65-70.

121. Sanfilippo, P.G., Hewitt, A.W., Hammond, C.J., and Mackey, D.A. (2011). The heritability of ocular traits. Surv Ophthalmol *55*, 561-583.

122. Visscher, P.M., Hill, W.G., and Wray, N.R. (2008). Heritability in the genomics era: concepts and misconceptions. Nat Rev Genet *9*, 255-266.

123. Lush, J.L. (1940). Intra-sire correlations or regressions of offspring on dam as a method of estimating heritability of characteristics. Proc Am Soc Anim Prod, 293-301.

124. Mcgee, T.L., Devoto, M., Ott, J., Berson, E.L., et al. (1997). Evidence that the penetrance of mutations at the RP11 locus causing dominant retinitis pigmentosa is influenced by a gene linked to the homologous RP11 allele. Am J Hum Genet *61*, 1059-1066.

125. Beit-Ya'acov, A., Mizrahi-Meissonnier, L., Obolensky, A., Landau, C., et al. (2007). Homozygosity for a novel ABCA4 founder splicing mutation is associated with progressive and severe Stargardt-like disease. Invest Ophthalmol Vis Sci *48*, 4308-4314.

126. Kondo, H., Hayashi, H., Oshima, K., Tahira, T., et al. (2003). Frizzled 4 gene (FZD4) mutations in patients with familial exudative vitreoretinopathy with variable expressivity. Br J Ophthalmol *87*, 1291-1295.

127. Thompson, D.A., McHenry, C.L., Li, Y., Richards, J.E., et al. (2002). Retinal dystrophy due to paternal isodisomy for chromosome 1 or chromosome 2, with homoallelism for mutations in RPE65 or MERTK, respectively. Am J Hum Genet *70*, 224-229.

128. Delettre, C., Lenaers, G., Griffoin, J.M., Gigarel, N., et al. (2000). Nuclear gene OPA1, encoding a mitochondrial dynamin-related protein, is mutated in dominant optic atrophy. Nat Genet *26*, 207-210.

129. Kajiwara, K., Berson, E.L., and Dryja, T.P. (1994). Digenic retinitis pigmentosa due to mutations at the unlinked peripherin/RDS and ROM1 loci. Science *264*, 1604-1608.

130. Gropman, A.L. and Adams, D.R. (2007). Atypical patterns of inheritance. Semin Pediatr Neurol *14*, 34-45.

131. Danchin, E., Charmantier, A., Champagne, F.A., Mesoudi, A., et al. (2011). Beyond DNA: integrating inclusive inheritance into an extended theory of evolution. Nat Rev Genet *12*, 475-486.

132. Levy, S., Sutton, G., Ng, P.C., Feuk, L., et al. (2007). The diploid genome sequence of an individual human. PLoS Biol *5*, e254.

133. Kidd, J.M., Cooper, G.M., Donahue, W.F., Hayden, H.S., et al. (2008). Mapping and sequencing of structural variation from eight human genomes. Nature *453*, 56-64.

134. Strachan, T. and Read, A.P. (2004). Human Molecular Genetics 3.(London, Garland Science).

135. Reich, D.E. and Lander, E.S. (2001). On the allelic spectrum of human disease. Trends Genet *17*, 502-510.

136. Arnheim, N. and Calabrese, P. (2009). Understanding what determines the frequency and pattern of human germline mutations. Nat Rev Genet *10*, 478-488.

137. Phillips, P.C. (2008). Epistasis - the essential role of gene interactions in the structure and evolution of genetic systems. Nat Rev Genet *9*, 855-867.

138. Jaeger, W. (1992). Horner's law. The first step in the history of the understanding of X-linked disorders. Ophthalmic Paediatr Genet *13*, 49-56.

139. Wright, A.F., Jay, B. (1994). Molecular genetics of inherited eye disorders.(Edinburgh, Harwood Academic Publishers).

140. Sheffield, V.C. and Stone, E.M. (2011). Genomics and the eye. N Engl J Med *364*, 1932-1942.

141. Rodieck, R.W. (1998). The first steps in seeing.(Sunderland, Massachusetts, Sinauer Associates Incorporation).

142. Boulton, M. and Dayhaw-Barker, P. (2001). The role of the retinal pigment epithelium: topographical variation and ageing changes. Eye (Lond) *15*, 384-389.

143. Mann, I. (1969). The Development of the Human Eye. BMA.

144. Terman, A. and Brunk, U.T. (2006). Oxidative stress, accumulation of biological 'garbage', and aging. Antioxid Redox Signal *8*, 197-204.

145. Boulton, M., McKechnie, N.M., Breda, J., Bayly, M., et al. (1989). The formation of autofluorescent granules in cultured human RPE. Invest Ophthalmol Vis Sci *30*, 82-89.

146. Eldred, G.E. and Katz, M.L. (1988). Fluorophores of the human retinal pigment epithelium: separation and spectral characterization. Exp Eye Res *47*, 71-86.

147. Schmitz-Valckenberg, S., Holz, F.G., Bird, A.C., and Spaide, R.F. (2008). Fundus autofluorescence imaging: review and perspectives. Retina *28*, 385-409.

148. Strauss, O. (2005). The retinal pigment epithelium in visual function. Physiol Rev *85*, 845-881.

149. Yamamoto, H., Simon, A., Eriksson, U., Harris, E., et al. (1999). Mutations in the gene encoding 11-cis retinol dehydrogenase cause delayed dark adaptation and fundus albipunctatus. Nat Genet *22*, 188-191.

150. Maw, M.A., Kennedy, B., Knight, A., Bridges, R., et al. (1997). Mutation of the gene encoding cellular retinaldehyde-binding protein in autosomal recessive retinitis pigmentosa. Nat Genet *17*, 198-200.

151. Bainbridge, J.W., Smith, A.J., Barker, S.S., Robbie, S., et al. (2008). Effect of gene therapy on visual function in Leber's congenital amaurosis. N Engl J Med *358*, 2231-2239.

152. Maguire, A.M., Simonelli, F., Pierce, E.A., Pugh, E.N., et al. (2008). Safety and efficacy of gene transfer for Leber's congenital amaurosis. N Engl J Med *358*, 2240-2248.

153. Cideciyan, A.V., Aleman, T.S., Boye, S.L., Schwartz, S.B., et al. (2008). Human gene therapy for RPE65 isomerase deficiency activates the retinoid cycle of vision but with slow rod kinetics. Proc Natl Acad Sci U S A *105*, 15112-15117.

154. Massey, S.C. (2006). Molecular genetics of retinal disase. In Retina, Ryan, S.J., ed. (St. Louis, Mosby), 43-82.

155. Bowmaker, J.K. and Dartnall, H.J. (1980). Visual pigments of rods and cones in a human retina. J Physiol *298*, 501-511.

156. Curcio, C.A., Sloan, K.R., Kalina, R.E., and Hendrickson, A.E. (1990). Human photoreceptor topography. J Comp Neurol *292*, 497-523.

157. Dryja, T.P., McGee, T.L., Berson, E.L., Fishman, G.A., et al. (2005). Night blindness and abnormal cone electroretinogram ON responses in patients with mutations in the GRM6 gene encoding mGluR6. Proc Natl Acad Sci U S A *102*, 4884-4889.

158. Bramall, A.N., Wright, A.F., Jacobson, S.G., and McInnes, R.R. (2010). The genomic, biochemical, and cellular responses of the retina in inherited photoreceptor degenerations and prospects for the treatment of these disorders. Annu Rev Neurosci *33*, 441-472.

159. Wright, A.F., Chakarova, C.F., Abd El-Aziz, M.M., and Bhattacharya, S.S. (2010). Photoreceptor degeneration: genetic and mechanistic dissection of a complex trait. Nat Rev Genet *11*, 273-284.

160. Den Hollander, A.I., Black, A., Bennett, J., and Cremers, F.P. (2010). Lighting a candle in the dark: advances in genetics and gene therapy of recessive retinal dystrophies. J Clin Invest *120*, 3042-3053.

161. Keeler, C.R. (2004). Babbage the unfortunate. Br J Ophthalmol *88*, 730-732.

162. Scanziani, M. and Hausser, M. (2009). Electrophysiology in the age of light. Nature *461*, 930-939.

163. Armington, J.C. (1974). The electroretinogram.(New York, Academic Press).

164. Holmgren, F. (1865). Metod att objectivera effektenav ljusintryck pa retina. Upsala Iakaref Forhandl, 177-191.

165. Hartline, H.K. (1925). The electrical response to illumiantion of the eye in intact animals, including the human subject; and in decerebrate preparations Am J Physiol, 600-612.

166. Dolwing, J.E. and Ratliff, F. (1967). Nobel prize: three named for medicine, physiology award (George Wald, Ragnar Granit and Haldan Keffer Hartline). Science *158*, 468-473.

167. Granit, R. (1933). The components of the retinal action potential in mammals and their relation to the discharge in the optic nerve. J Physiol *77*, 207-239.

168. Steinmetz, R.L., Haimovici, R., Jubb, C., Fitzke, F.W., et al. (1993). Symptomatic abnormalities of dark adaptation in patients with age-related Bruch's membrane change. Br J Ophthalmol *77*, 549-554.

169. Marmor, M.F., Fulton, A.B., Holder, G.E., Miyake, Y., et al. (2009). ISCEV standard for full-field clinical electroretinography (2008 update). Doc Ophthalmol *118*, 69-77.

170. Brown, M., Marmor, M., Vaegan, Zrenner, E., et al. (2006). ISCEV standard for clinical electro-oculography (EOG) 2006. Doc Ophthalmol *113*, 205-212.

171. Holder, G.E., Brigell, M.G., Hawlina, M., Meigen, T., et al. (2007). ISCEV standard for clinical pattern electroretinography, 2007 update. Doc Ophthalmol *114*, 111-116.

172. Odom, J.V., Bach, M., Brigell, M., Holder, G.E., et al. (2010). ISCEV standard for clinical visual evoked potentials, 2009 update. Doc Ophthalmol *120*, 111-119.

173. Brigell, M., Bach, M., Barber, C., Moskowitz, A., et al. (2003). Guidelines for calibration of stimulus and recording parameters used in clinical electrophysiology of vision. Doc Ophthalmol *107*, 185-193.

174. Hood, D.C., Bach, M., Brigell, M., Keating, D., et al. (2008). ISCEV guidelines for clinical multifocal electroretinography, 2007 edition. Doc Ophthalmol *116*, 1-11.

175. Wu, H., Cowing, J.A., Michaelides, M., Wilkie, S.E., et al. (2006). Mutations in the gene KCNV2 encoding a voltage-gated potassium channel subunit cause "cone dystrophy with supernormal rod electroretinogram" in humans. Am J Hum Genet *79*, 574-579.

176. Robson, A.G., Webster, A.R., Michaelides, M., Downes, S.M., et al. (2010). "Cone dystrophy with supernormal rod electroretinogram": a comprehensive genotype/phenotype study including fundus autofluorescence and extensive electrophysiology. Retina *30*, 51-62.

177. Milam, A.H., Rose, L., Cideciyan, A.V., Barakat, M.R., et al. (2002). The nuclear receptor NR2E3 plays a role in human retinal photoreceptor differentiation and degeneration. Proc Natl Acad Sci U S A *99*, 473-478.

178. Audo, I., Michaelides, M., Robson, A.G., Hawlina, M., et al. (2008). Phenotypic variation in enhanced S-cone syndrome. Invest Ophthalmol Vis Sci *49*, 2082-2093.

179. Holder, G.E. (2006). Principles and practice of clinical electrophysiology of vision.(Cambridge, Massachusetts, MIT Press).

180. Frishman, L.J. (2006). Electrogenesis of the electroretinogram. In Retina, Ryan, S.J., ed. (St. Louis, Mosby), 103-135.

181. Thau, W. (1942). Purkyne, a pioneer in ophthalmoscopy. Arch Ophthalmol *27*, 299-316.

182. Weale, R. (1994). On the invention of the ophthalmoscope. Doc Ophthalmol *86*, 163-166.

183. Keeler, C.R. (1997). 150 years since Babbage's ophthalmoscope. Arch Ophthalmol *115*, 1456-1457.

184. Pearce, J.M. (2009). The ophthalmoscope: Helmholtz's Augenspiegel. Eur Neurol *61*, 244-249.

185. Helmholtz, H. (1851). Beschreibung eines Augenspiegels zur untersuchung der netzhaut in lebenden auge.(Berlin, Förstner).

186. Wade, N.J. (2007). Image, eye, and retina. J Opt Soc Am A Opt Image Sci Vis *24*, 1229-1249.

187. Ruete, C.T.G. (1852). Der Augenspiegel und das optometer.(Göttingen, Druck und Verlag der Dieterichschen Buchhandlung).

188. Simonsz, H.J. (2004). Christian Theodor Georg Ruete: the first strabismologist, coauthor of listing's law, maker of the first ophthalmotrope and inventor of indirect fundoscopy. Strabismus *12*, 53-57.

189. Ravin, J.G. (2001). Allvar Gullstrand. Ophthalmology *108*, 1012.

190. Nordenson, J.W. (1962). Allvar Gullstrand (1862-1930). Doc Ophthalmol *16*, 283-337.

191. Coccius, E.A. (1853). Ueber die anwendung des augenspiegels nebst angabe eines neuen instruments.(Leipzig, Müller).

192. Jackman, W.T., Webster, J. D. (1886). On photographing the retina of the living human eye. Philadelphia Photographer *23*, 340-341.

193. Bennett, T.J. and Barry, C.J. (2009). Ophthalmic imaging today: an ophthalmic photographer's viewpoint - a review. Clin Experiment Ophthalmol *37*, 2-13.

194. Von Ruckmann, A., Fitzke, F.W., and Bird, A.C. (1995). Distribution of fundus autofluorescence with a scanning laser ophthalmoscope. Br J Ophthalmol *79*, 407-412.

195. Machemer, R., Norton, E.W., Gass, J.D., and Choromokos, E. (1970). Pseudofluorescence - a problem in interpretation of fluorescein angiograms. Am J Ophthalmol *70*, 1-10.

196. Webb, R.H., Hughes, G.W., and Pomerantzeff, O. (1980). Flying spot TV ophthalmoscope. Appl Opt *19*, 2991-2997.

197. Webb, R.H., Hughes, G.W., and Delori, F.C. (1987). Confocal scanning laser ophthalmoscope. Appl Opt *26*, 1492-1499.

198. Manivannan, A., Sharp, P.F., Phillips, R.P., and Forrester, J.V. (1993). Digital fundus imaging using a scanning laser ophthalmoscope. Physiol Meas *14*, 43-56.

199. Sharp, P.F. and Manivannan, A. (1997). The scanning laser ophthalmoscope. Phys Med Biol *42*, 951-966.

200. Sharp, P.F., Manivannan, A., Xu, H., and Forrester, J.V. (2004). The scanning laser ophthalmoscope - a review of its role in bioscience and medicine. Phys Med Biol *49*, 1085-1096.

201. Robson, A.G., Egan, C.A., Luong, V.A., Bird, A.C., et al. (2004). Comparison of fundus autofluorescence with photopic and scotopic fine-matrix mapping in patients with retinitis pigmentosa and normal visual acuity. Invest Ophthalmol Vis Sci *45*, 4119-4125.

202. Robson, A.G., Saihan, Z., Jenkins, S.A., Fitzke, F.W., et al. (2006). Functional characterisation and serial imaging of abnormal fundus autofluorescence in patients with retinitis pigmentosa and normal visual acuity. Br J Ophthalmol *90*, 472-479.

203. Wolf, S., Wolf-Schnurrbusch, U. E. K. (2007). Macular pigment measurement - theoretical background. In Atlas of Fundus Autofluorescence, Holz, F.G., et al., ed. (Heidelberg, Springer-Verlag), 55-61.

204. Subczynski, W.K., Wisniewska, A., and Widomska, J. (2010). Location of macular xanthophylls in the most vulnerable regions of photoreceptor outer-segment membranes. Arch Biochem Biophys *504*, 61-66.

205. Drexler, W. and Fujimoto, J.G. (2008). State-of-the-art retinal optical coherence tomography. Progress in Retinal and Eye Research *27*, 45-88.

206. Huang, D., Swanson, E.A., Lin, C.P., Schuman, J.S., et al. (1991). Optical coherence tomography. Science *254*, 1178-1181.

207. Swanson, E.A., Izatt, J.A., Hee, M.R., Huang, D., et al. (1993). In vivo retinal imaging by optical coherence tomography. Opt Lett *18*, 1864-1866.

208. Drexler, W., Morgner, U., Ghanta, R.K., Kartner, F.X., et al. (2001). Ultrahigh-resolution ophthalmic optical coherence tomography. Nat Med *7*, 502-507.

209. Drexler, W., Sattmann, H., Hermann, B., Ko, T.H., et al. (2003). Enhanced visualization of macular pathology with the use of ultrahigh-resolution optical coherence tomography. Arch Ophthalmol *121*, 695-706.

210. Fercher, A.F., Hitzenberger, C.K., Kamp, G., El-Zaiat, S.Y. (1995). Measurement of intraocular distances by backscattering spectral interferometry. Optics Communications, 43-48.

211. Costa, R.A., Skaf, M., Melo, L.A., Jr., Calucci, D., et al. (2006). Retinal assessment using optical coherence tomography. Progress in Retinal and Eye Research *25*, 325-353.

212. Wojtkowski, M., Leitgeb, R., Kowalczyk, A., Bajraszewski, T., et al. (2002). In vivo human retinal imaging by Fourier domain optical coherence tomography. J Biomed Opt *7*, 457-463.

213. Wojtkowski, M., Srinivasan, V., Fujimoto, J.G., Ko, T., et al. (2005). Three-dimensional retinal imaging with high-speed ultrahigh-resolution optical coherence tomography. Ophthalmology *112*, 1734-1746.

214. Sakata, L.M., Deleon-Ortega, J., Sakata, V., and Girkin, C.A. (2009). Optical coherence tomography of the retina and optic nerve - a review. Clin Experiment Ophthalmol *37*, 90-99.

215. Gabriele, M.L., Wollstein, G., Ishikawa, H., Xu, J., et al. (2010). Three dimensional optical coherence tomography imaging: Advantages and advances. Prog Retin Eye Res *29*, 556-579.

216. Ishikawa, H., Kim, J., Friberg, T.R., Wollstein, G., et al. (2009). Three-dimensional optical coherence tomography (3D-OCT) image enhancement with segmentation-free contour modeling C-mode. Invest Ophthalmol Vis Sci *50*, 1344-1349.

217. Potsaid, B., Gorczynska, I., Srinivasan, V.J., Chen, Y., et al. (2008). Ultrahigh speed spectral / Fourier domain OCT ophthalmic imaging at 70,000 to 312,500 axial scans per second. Opt Express *16*, 15149-15169.

218. Huang, J.C., Voaden, M.J., Zarbin, M.A., and Marshall, J. (2000). Morphologic preservation and variability of human donor retina. Curr Eye Res *20*, 231-241.

219. Gloesmann, M., Hermann, B., Schubert, C., Sattmann, H., et al. (2003). Histologic correlation of pig retina radial stratification with ultrahigh-resolution optical coherence tomography. Invest Ophthalmol Vis Sci *44*, 1696-1703.

220. Ishikawa, H., Stein, D.M., Wollstein, G., Beaton, S., et al. (2005). Macular segmentation with optical coherence tomography. Invest Ophthalmol Vis Sci *46*, 2012-2017.

221. Srinivasan, V.J., Monson, B.K., Wojtkowski, M., Bilonick, R.A., et al. (2008). Characterization of outer retinal morphology with high-speed, ultrahigh-resolution optical coherence tomography. Invest Ophthalmol Vis Sci *49*, 1571-1579.

222. Kaluzny, J.J., Wojtkowski, M., Sikorski, B.L., Szkulmowski, M., et al. (2009). Analysis of the outer retina reconstructed by high-resolution, three-dimensional spectral domain optical coherence tomography. Ophthalmic Surg Lasers Imaging *40*, 102-108.

223. Lujan, B.J., Roorda, A., Knighton, R.W., and Carroll, J. (2011). Revealing Henle's fiber layer using spectral domain optical coherence tomography. Invest Ophthalmol Vis Sci *52*, 1486-1492.

224. Yanisch-Perron, C., Vieira, J., and Messing, J. (1985). Improved M13 phage cloning vectors and host strains: nucleotide sequences of the M13mp18 and pUC19 vectors. Gene *33*, 103-119.

225. Sambrook, J. and Russell, D.W. (2001). Molecular Cloning: a laboratory manual.(Cold Spring Harbor, Cold Spring Harbor Laboratory Press).

226. Fleige, S. and Pfaffl, M.W. (2006). RNA integrity and the effect on the real-time qRT-PCR performance. Mol Aspects Med *27*, 126-139.

227. Schroeder, A., Mueller, O., Stocker, S., Salowsky, R., et al. (2006). The RIN: an RNA integrity number for assigning integrity values to RNA measurements. BMC Mol Biol *7*, 3.

228. Danna, K. and Nathans, D. (1971). Specific cleavage of simian virus 40 DNA by restriction endonuclease of Hemophilus influenzae. Proc Natl Acad Sci U S A *68*, 2913-2917.

229. Roberts, R.J. (2005). How restriction enzymes became the workhorses of molecular biology. Proc Natl Acad Sci U S A *102*, 5905-5908.

230. Weiss, B. and Richardson, C.C. (1967). Enzymatic breakage and joining of deoxyribonucleic acid; I. Repair of single-strand breaks in DNA by an enzyme system from Escherichia coli infected with T4 bacteriophage. Proc Natl Acad Sci U S A *57*, 1021-1028.

231. Thorne, H.V. (1966). Electrophoretic separation of polyoma virus DNA from host cell DNA. Virology *29*, 234-239.

232. Sharp, P.A., Sugden, B., and Sambrook, J. (1973). Detection of two restriction endonuclease activities in Haemophilus parainfluenzae using analytical agarose--ethidium bromide electrophoresis. Biochemistry *12*, 3055-3063.

233. Kleppe, K., Ohtsuka, E., Kleppe, R., Molineux, I., et al. (1971). Studies on polynucleotides. XCVI. Repair replications of short synthetic DNA's as catalyzed by DNA polymerases. J Mol Biol *56*, 341-361.

234. Mullis, K.B. (1990). The unusual origin of the polymerase chain reaction. Sci Am *262*, 56-61, 64-55.

235. Newton, C.R., Graham, A., Heptinstall, L.E., Powell, S.J., et al. (1989). Analysis of any point mutation in DNA. The amplification refractory mutation system (ARMS). Nucleic Acids Res *17*, 2503-2516.

236. Brock, T.D. (1997). The value of basic research: discovery of Thermus aquaticus and other extreme thermophiles. Genetics *146*, 1207-1210.

237. Chien, A., Edgar, D.B., and Trela, J.M. (1976). Deoxyribonucleic acid polymerase from the extreme thermophile Thermus aquaticus. J Bacteriol *127*, 1550-1557.

238. Lundberg, K.S., Shoemaker, D.D., Adams, M.W., Short, J.M., et al. (1991). High-fidelity amplification using a thermostable DNA polymerase isolated from Pyrococcus furiosus. Gene *108*, 1-6.

239. Schouten, J.P., McElgunn, C.J., Waaijer, R., Zwijnenburg, D., et al. (2002). Relative quantification of 40 nucleic acid sequences by multiplex ligation-dependent probe amplification. Nucleic Acids Res *30*, e57.

240. Frohman, M.A., Dush, M.K., and Martin, G.R. (1988). Rapid production of full-length cDNAs from rare transcripts: amplification using a single gene-specific oligonucleotide primer. Proc Natl Acad Sci U S A *85*, 8998-9002.

241. Ohara, O., Dorit, R.L., and Gilbert, W. (1989). One-sided polymerase chain reaction: the amplification of cDNA. Proc Natl Acad Sci U S A *86*, 5673-5677.

242. Loh, E.Y., Elliott, J.F., Cwirla, S., Lanier, L.L., et al. (1989). Polymerase chain reaction with single-sided specificity: analysis of T cell receptor delta chain. Science *243*, 217-220.

243. Holton, T.A. and Graham, M.W. (1991). A simple and efficient method for direct cloning of PCR products using ddT-tailed vectors. Nucleic Acids Res *19*, 1156.

244. Shuman, S. (1991). Recombination mediated by vaccinia virus DNA topoisomerase I in Escherichia coli is sequence specific. Proc Natl Acad Sci U S A *88*, 10104-10108.

245. Shuman, S. (1994). Novel approach to molecular cloning and polynucleotide synthesis using vaccinia DNA topoisomerase. J Biol Chem *269*, 32678-32684.

246. Wittwer, C.T., Reed, G.H., Gundry, C.N., Vandersteen, J.G., et al. (2003). High-resolution genotyping by amplicon melting analysis using LCGreen. Clin Chem *49*, 853-860.

247. Wittwer, C.T., Herrmann, M.G., Moss, A.A., and Rasmussen, R.P. (1997). Continuous fluorescence monitoring of rapid cycle DNA amplification. Biotechniques *22*, 130-131, 134-138.

248. Ririe, K.M., Rasmussen, R.P., and Wittwer, C.T. (1997). Product differentiation by analysis of DNA melting curves during the polymerase chain reaction. Anal Biochem *245*, 154-160.

249. Sanger, F., Air, G.M., Barrell, B.G., Brown, N.L., et al. (1977). Nucleotide sequence of bacteriophage phi X174 DNA. Nature *265*, 687-695.

250. Sanger, F., Nicklen, S., and Coulson, A.R. (1977). DNA sequencing with chain-terminating inhibitors. Proc Natl Acad Sci U S A *74*, 5463-5467.

251. Metzker, M.L. (2010). Sequencing technologies - the next generation. Nat Rev Genet *11*, 31-46.

252. Shendure, J. (2011). Next-generation human genetics. Genome Biol *12*, 408.

253. Margulies, M., Egholm, M., Altman, W.E., Attiya, S., et al. (2005). Genome sequencing in microfabricated high-density picolitre reactors. Nature *437*, 376-380.

254. Shendure, J., Porreca, G.J., Reppas, N.B., Lin, X., et al. (2005). Accurate multiplex polony sequencing of an evolved bacterial genome. Science *309*, 1728-1732.

255. Mamanova, L., Coffey, A.J., Scott, C.E., Kozarewa, I., et al. (2010). Target-enrichment strategies for next-generation sequencing. Nat Methods *7*, 111-118.

256. Gnirke, A., Melnikov, A., Maguire, J., Rogov, P., et al. (2009). Solution hybrid selection with ultra-long oligonucleotides for massively parallel targeted sequencing. Nat Biotechnol *27*, 182-189.

257. Clark, M.J., Chen, R., Lam, H.Y., Karczewski, K.J., et al. (2011). Performance comparison of exome DNA sequencing technologies. Nat Biotechnol *29*, 908-914.

258. Holt, R.A. and Jones, S.J. (2008). The new paradigm of flow cell sequencing. Genome Res *18*, 839-846.

259. Bentley, D.R., Balasubramanian, S., Swerdlow, H.P., Smith, G.P., et al. (2008). Accurate whole human genome sequencing using reversible terminator chemistry. Nature *456*, 53-59.

260. Cock, P.J., Fields, C.J., Goto, N., Heuer, M.L., et al. (2010). The Sanger FASTQ file format for sequences with quality scores, and the Solexa/Illumina FASTQ variants. Nucleic Acids Res *38*, 1767-1771.

261. Southern, E.M. (1975). Detection of specific sequences among DNA fragments separated by gel electrophoresis. J Mol Biol *98*, 503-517.

262. Schena, M., Shalon, D., Davis, R.W., and Brown, P.O. (1995). Quantitative monitoring of gene expression patterns with a complementary DNA microarray. Science *270*, 467-470.

263. Schena, M., Heller, R.A., Theriault, T.P., Konrad, K., et al. (1998). Microarrays: biotechnology's discovery platform for functional genomics. Trends Biotechnol *16*, 301-306.

264. Keck, J.L. and Berger, J.M. (2000). DNA replication at high resolution. Chem Biol *7*, R63-71.

265. Cheung, V.G. and Nelson, S.F. (1996). Whole genome amplification using a degenerate oligonucleotide primer allows hundreds of genotypes to be performed on less than one nanogram of genomic DNA. Proc Natl Acad Sci U S A *93*, 14676-14679.

266. Fodor, S.P., Read, J.L., Pirrung, M.C., Stryer, L., et al. (1991). Light-directed, spatially addressable parallel chemical synthesis. Science *251*, 767-773.

267. Cheung, V.G., Morley, M., Aguilar, F., Massimi, A., et al. (1999). Making and reading microarrays. Nat Genet *21*, 15-19.

268. Lipshutz, R.J., Fodor, S.P., Gingeras, T.R., and Lockhart, D.J. (1999). High density synthetic oligonucleotide arrays. Nat Genet *21*, 20-24.

269. Lander, E.S. (1999). Array of hope. Nat Genet *21*, 3-4.

270. Various Authors. (2002). The chipping forecast II. Nat Genet, 465-552.
271. Shumaker, J.M., Metspalu, A., and Caskey, C.T. (1996). Mutation detection by solid phase primer extension. Hum Mutat *7*, 346-354.
272. Pastinen, T., Partanen, J., and Syvanen, A.C. (1996). Multiplex, fluorescent, solid-phase minisequencing for efficient screening of DNA sequence variation. Clin Chem *42*, 1391-1397.
273. Zernant, J., Kulm, M., Dharmaraj, S., Den Hollander, A.I., et al. (2005). Genotyping microarray (disease chip) for Leber congenital amaurosis: detection of modifier alleles. Invest Ophthalmol Vis Sci *46*, 3052-3059.
274. Jaakson, K., Zernant, J., Kulm, M., Hutchinson, A., et al. (2003). Genotyping microarray (gene chip) for the ABCR (ABCA4) gene. Hum Mutat *22*, 395-403.
275. Litt, M. and Luty, J.A. (1989). A hypervariable microsatellite revealed by in vitro amplification of a dinucleotide repeat within the cardiac muscle actin gene. Am J Hum Genet *44*, 397-401.
276. Dib, C., Faure, S., Fizames, C., Samson, D., et al. (1996). A comprehensive genetic map of the human genome based on 5,264 microsatellites. Nature *380*, 152-154.
277. Schuelke, M. (2000). An economic method for the fluorescent labeling of PCR fragments. Nat Biotechnol *18*, 233-234.
278. Hagen, J.B. (2000). The origins of bioinformatics. Nat Rev Genet *1*, 231-236.
279. Hogeweg, P. and Hesper, B. (1978). Interactive instruction on population interactions. Comput Biol Med *8*, 319-327.
280. Hogeweg, P. (1978). Simulating the growth of cellular forms. Simulation, 90-96.
281. Van Zundert, M. (2009). Interview with Paulien Hogeweg. Interface: Developments in bioinformatics, 8-11.
282. Benton, D. (1996). Bioinformatics--principles and potential of a new multidisciplinary tool. Trends Biotechnol *14*, 261-272.
283. Luscombe, N.M., Greenbaum, D., and Gerstein, M. (2001). What is bioinformatics? A proposed definition and overview of the field. Methods Inf Med *40*, 346-358.
284. Bayat, A. (2002). Science, medicine, and the future: Bioinformatics. BMJ *324*, 1018-1022.
285. Attwood, T.K. and Miller, C.J. (2001). Which craft is best in bioinformatics? Comput Chem *25*, 329-339.
286. Kanehisa, M. and Bork, P. (2003). Bioinformatics in the post-sequence era. Nat Genet *33 Suppl*, 305-310.
287. Kibbe, W.A. (2007). OligoCalc: an online oligonucleotide properties calculator. Nucleic Acids Res *35*, W43-46.
288. Schadt, E.E., Linderman, M.D., Sorenson, J., Lee, L., et al. (2010). Computational solutions to large-scale data management and analysis. Nat Rev Genet *11*, 647-657.
289. Li, H. and Homer, N. (2010). A survey of sequence alignment algorithms for next-generation sequencing. Brief Bioinform *11*, 473-483.

290. Li, H., Handsaker, B., Wysoker, A., Fennell, T., et al. (2009). The Sequence Alignment/Map format and SAMtools. Bioinformatics *25*, 2078-2079.

291. Stitziel, N.O., Kiezun, A., and Sunyaev, S. (2011). Computational and statistical approaches to analyzing variants identified by exome sequencing. Genome Biol *12*, 227.

292. Fiume, M., Williams, V., Brook, A., and Brudno, M. (2010). Savant: genome browser for high-throughput sequencing data. Bioinformatics *26*, 1938-1944.

293. Robinson, J.T., Thorvaldsdottir, H., Winckler, W., Guttman, M., et al. (2011). Integrative genomics viewer. Nat Biotechnol *29*, 24-26.

294. Danecek, P., Auton, A., Abecasis, G., Albers, C.A., et al. (2011). The variant call format and VCFtools. Bioinformatics *27*, 2156-2158.

295. Wang, K., Li, M., and Hakonarson, H. (2010). ANNOVAR: functional annotation of genetic variants from high-throughput sequencing data. Nucleic Acids Res *38*, e164.

296. Wistow, G. (2006). The NEIBank project for ocular genomics: data-mining gene expression in human and rodent eye tissues. Progress in Retinal and Eye Research *25*, 43-77.

297. Bowes Rickman, C., Ebright, J.N., Zavodni, Z.J., Yu, L., et al. (2006). Defining the human macula transcriptome and candidate retinal disease genes using EyeSAGE. Invest Ophthalmol Vis Sci *47*, 2305-2316.

298. Blackshaw, S., Fraioli, R.E., Furukawa, T., and Cepko, C.L. (2001). Comprehensive analysis of photoreceptor gene expression and the identification of candidate retinal disease genes. Cell *107*, 579-589.

299. Blackshaw, S., Harpavat, S., Trimarchi, J., Cai, L., et al. (2004). Genomic analysis of mouse retinal development. PLoS Biol *2*, E247.

300. Chowers, I., Gunatilaka, T.L., Farkas, R.H., Qian, J., et al. (2003). Identification of novel genes preferentially expressed in the retina using a custom human retina cDNA microarray. Invest Ophthalmol Vis Sci *44*, 3732-3741.

301. Bortoluzzi, S., D'alessi, F., and Danieli, G.A. (2000). A novel resource for the study of genes expressed in the adult human retina. Invest Ophthalmol Vis Sci *41*, 3305-3308.

302. Sharon, D., Blackshaw, S., Cepko, C.L., and Dryja, T.P. (2002). Profile of the genes expressed in the human peripheral retina, macula, and retinal pigment epithelium determined through serial analysis of gene expression (SAGE). Proc Natl Acad Sci U S A *99*, 315-320.

303. Stohr, H., Mah, N., Schulz, H.L., Gehrig, A., et al. (2000). EST mining of the UniGene dataset to identify retina-specific genes. Cytogenet Cell Genet *91*, 267-277.

304. Swaroop, A. and Zack, D.J. (2002). Transcriptome analysis of the retina. Genome Biol *3*, 1022.

305. Corbo, J.C., Myers, C.A., Lawrence, K.A., Jadhav, A.P., et al. (2007). A typology of photoreceptor gene expression patterns in the mouse. Proc Natl Acad Sci U S A *104*, 12069-12074.

306. Katsanis, N., Worley, K.C., Gonzalez, G., Ansley, S.J., et al. (2002). A computational/functional genomics approach for the enrichment of the retinal transcriptome and the identification of positional candidate retinopathy genes. Proc Natl Acad Sci U S A *99*, 14326-14331.

307. Strunnikova, N.V., Maminishkis, A., Barb, J.J., Wang, F., et al. (2010). Transcriptome analysis and molecular signature of human retinal pigment epithelium. Hum Mol Genet *19*, 2468-2486.

308. Booij, J.C., Ten Brink, J.B., Swagemakers, S.M., Verkerk, A.J., et al. (2010). A new strategy to identify and annotate human RPE-specific gene expression. PLoS One *5*, e9341.

309. Kim, D.S., Ross, S.E., Trimarchi, J.M., Aach, J., et al. (2008). Identification of molecular markers of bipolar cells in the murine retina. J Comp Neurol *507*, 1795-1810.

310. Yoshida, S., Mears, A.J., Friedman, J.S., Carter, T., et al. (2004). Expression profiling of the developing and mature Nrl-/- mouse retina: identification of retinal disease candidates and transcriptional regulatory targets of Nrl. Hum Mol Genet *13*, 1487-1503.

311. Swiderski, R.E., Nishimura, D.Y., Mullins, R.F., Olvera, M.A., et al. (2007). Gene expression analysis of photoreceptor cell loss in bbs4-knockout mice reveals an early stress gene response and photoreceptor cell damage. Invest Ophthalmol Vis Sci *48*, 3329-3340.

312. Roesch, K., Jadhav, A.P., Trimarchi, J.M., Stadler, M.B., et al. (2008). The transcriptome of retinal Muller glial cells. J Comp Neurol *509*, 225-238.

313. Demos, C., Bandyopadhyay, M., and Rohrer, B. (2008). Identification of candidate genes for human retinal degeneration loci using differentially expressed genes from mouse photoreceptor dystrophy models. Mol Vis *14*, 1639-1649.

314. Hornan, D.M., Peirson, S.N., Hardcastle, A.J., Molday, R.S., et al. (2007). Novel retinal and cone photoreceptor transcripts revealed by human macular expression profiling. Invest Ophthalmol Vis Sci *48*, 5388-5396.

315. Corbo, J.C., Lawrence, K.A., Karlstetter, M., Myers, C.A., et al. (2010). CRX ChIP-seq reveals the cis-regulatory architecture of mouse photoreceptors. Genome Res *20*, 1512-1525.

316. Boguski, M.S., Lowe, T.M., and Tolstoshev, C.M. (1993). dbEST - database for "expressed sequence tags". Nat Genet *4*, 332-333.

317. Velculescu, V.E., Zhang, L., Vogelstein, B., and Kinzler, K.W. (1995). Serial analysis of gene expression. Science *270*, 484-487.

318. Geisert, E.E., Lu, L., Freeman-Anderson, N.E., Templeton, J.P., et al. (2009). Gene expression in the mouse eye: an online resource for genetics using 103 strains of mice. Mol Vis *15*, 1730-1763.

319. Yoshida, Y., Makita, Y., Heida, N., Asano, S., et al. (2009). PosMed (Positional Medline): prioritizing genes with an artificial neural network comprising medical documents to accelerate positional cloning. Nucleic Acids Res *37*, W147-152.

320. Korn, J.M., Kuruvilla, F.G., McCarroll, S.A., Wysoker, A., et al. (2008). Integrated genotype calling and association analysis of SNPs, common copy number polymorphisms and rare CNVs. Nat Genet *40*, 1253-1260.

321. Tisdall, J.D. (2001). Beginning Perl for Bioinformatics.(Sebastopol, CA, O'Reilly Media, Inc).

322. Stajich, J.E., Block, D., Boulez, K., Brenner, S.E., et al. (2002). The Bioperl toolkit: Perl modules for the life sciences. Genome Res *12*, 1611-1618.

323. Dubois, P. (2000). MySQL.(Indianapolis, New Riders Publishing).

324. Foundation', T.P.S. (2010). The python tutorial.

325. Stone, E.M. (2003). Finding and interpreting genetic variations that are important to ophthalmologists. Trans Am Ophthalmol Soc *101*, 437-484.

326. Mukhopadhyay, R., Sergouniotis, P.I., Mackay, D.S., Day, A.C., et al. (2010). A detailed phenotypic assessment of individuals affected by MFRP-related oculopathy. Mol Vis *16*, 540-548.

327. Mackay, D.S., Henderson, R.H., Sergouniotis, P.I., Li, Z., et al. (2010). Novel mutations in MERTK associated with childhood onset rod-cone dystrophy. Mol Vis *16*, 369-377.

328. Henderson, R.H., Mackay, D.S., Li, Z., Moradi, P., et al. (2011). Phenotypic variability in patients with retinal dystrophies due to mutations in CRB1. Br J Ophthalmol *95*, 811-817.

329. Sergouniotis, P.I., Sohn, E.H., Li, Z., McBain, V.A., et al. (2011). Phenotypic variability in RDH5 retinopathy (Fundus Albipunctatus). Ophthalmology *118*, 1661-1670.

330. Sergouniotis, P.I., Holder, G.E., Robson, A.G., Michaelides, M., et al. (2011). High-resolution optical coherence tomography imaging in KCNV2 retinopathy. Br J Ophthalmol.

331. Sergouniotis, P.I., Davidson, A.E., Lenassi, E., Devery, S.R., et al. (2012). Retinal structure, function, and molecular pathologic features in gyrate atrophy. Ophthalmology *119*, 596-605.

332. Den Hollander, A.I., Heckenlively, J.R., Van Den Born, L.I., De Kok, Y.J., et al. (2001). Leber congenital amaurosis and retinitis pigmentosa with Coats-like exudative vasculopathy are associated with mutations in the crumbs homologue 1 (CRB1) gene. Am J Hum Genet *69*, 198-203.

333. Hanein, S., Perrault, I., Gerber, S., Tanguy, G., et al. (2004). Leber congenital amaurosis: comprehensive survey of the genetic heterogeneity, refinement of the clinical definition, and genotype-phenotype correlations as a strategy for molecular diagnosis. Hum Mutat *23*, 306-317.

334. Den Hollander, A.I., Ten Brink, J.B., De Kok, Y.J., Van Soest, S., et al. (1999). Mutations in a human homologue of Drosophila crumbs cause retinitis pigmentosa (RP12). Nat Genet *23*, 217-221.

335. Thiagalingam, S., McGee, T.L., Weleber, R.G., Sandberg, M.A., et al. (2007). Novel mutations in the KCNV2 gene in patients with cone dystrophy and a supernormal rod electroretinogram. Ophthalmic Genet *28*, 135-142.

336. Haider, N.B., Jacobson, S.G., Cideciyan, A.V., Swiderski, R., et al. (2000). Mutation of a nuclear receptor gene, NR2E3, causes enhanced S cone syndrome, a disorder of retinal cell fate. Nat Genet *24*, 127-131.

337. Sharon, D., Sandberg, M.A., Caruso, R.C., Berson, E.L., et al. (2003). Shared mutations in NR2E3 in enhanced S-cone syndrome, Goldmann-Favre syndrome, and many cases of clumped pigmentary retinal degeneration. Arch Ophthalmol *121*, 1316-1323.

338. Coppieters, F., Leroy, B.P., Beysen, D., Hellemans, J., et al. (2007). Recurrent mutation in the first zinc finger of the orphan nuclear receptor NR2E3 causes autosomal dominant retinitis pigmentosa. Am J Hum Genet *81*, 147-157.

339. O'Connor, E., Allen, L.E., Bradshaw, K., Boylan, J., et al. (2006). Congenital stationary night blindness associated with mutations in GRM6 encoding glutamate receptor mGluR6. Br J Ophthalmol *90*, 653-654.

340. Zeitz, C., Labs, S., Lorenz, B., Forster, U., et al. (2009). Genotyping microarray for CSNB-associated genes. Invest Ophthalmol Vis Sci *50*, 5919-5926.

341. Shan, M., Dong, B., Zhao, X., Wang, J., et al. (2005). Novel mutations in the CYP4V2 gene associated with Bietti crystalline corneoretinal dystrophy. Mol Vis *11*, 738-743.

342. Lai, T.Y., Ng, T.K., Tam, P.O., Yam, G.H., et al. (2007). Genotype phenotype analysis of Bietti's crystalline dystrophy in patients with CYP4V2 mutations. Invest Ophthalmol Vis Sci *48*, 5212-5220.

343. Wissinger, B., Gamer, D., Jagle, H., Giorda, R., et al. (2001). CNGA3 mutations in hereditary cone photoreceptor disorders. Am J Hum Genet *69*, 722-737.

344. Michaelides, M., Aligianis, I.A., Ainsworth, J.R., Good, P., et al. (2004). Progressive cone dystrophy associated with mutation in CNGB3. Invest Ophthalmol Vis Sci *45*, 1975-1982.

345. Den Hollander, A.I., Koenekoop, R.K., Mohamed, M.D., Arts, H.H., et al. (2007). Mutations in LCA5, encoding the ciliary protein lebercilin, cause Leber congenital amaurosis. Nat Genet *39*, 889-895.

346. Den Hollander, A.I., Koenekoop, R.K., Yzer, S., Lopez, I., et al. (2006). Mutations in the CEP290 (NPHP6) gene are a frequent cause of Leber congenital amaurosis. Am J Hum Genet *79*, 556-561.

347. Sundin, O.H., Leppert, G.S., Silva, E.D., Yang, J.M., et al. (2005). Extreme hyperopia is the result of null mutations in MFRP, which encodes a Frizzled-related protein. Proc Natl Acad Sci U S A *102*, 9553-9558.

348. Adato, A., Vreugde, S., Joensuu, T., Avidan, N., et al. (2002). USH3A transcripts encode clarin-1, a four-transmembrane-domain protein with a possible role in sensory synapses. Eur J Hum Genet *10*, 339-350.

349. Akahori, M., Tsunoda, K., Miyake, Y., Fukuda, Y., et al. (2010). Dominant mutations in RP1L1 are responsible for occult macular dystrophy. Am J Hum Genet *87*, 424-429.

350. Schnur, R.E., Gao, M., Wick, P.A., Keller, M., et al. (1998). OA1 mutations and deletions in X-linked ocular albinism. Am J Hum Genet *62*, 800-809.

351. Baye, L.M., Nishimura, D. Y., Searby C. C., Avila A., Ayuso C., Valverde D., Stone E. M., Slusarski D. C., Sheffield V. C. (2009). Discovery and functional analysis of a new retinitis pigmentosa gene, C2orf71. The American Society of Human Genetics 59th Annual Meeting.

352. Nishimura, D.Y., Baye, L.M., Perveen, R., Searby, C.C., et al. (2010). Discovery and functional analysis of a retinitis pigmentosa gene, C2ORF71. Am J Hum Genet *86*, 686-695.

353. Collin, R.W., Safieh, C., Littink, K.W., Shalev, S.A., et al. (2010). Mutations in C2ORF71 cause autosomal-recessive retinitis pigmentosa. Am J Hum Genet *86*, 783-788.

354. Audo, I., Lancelot, M.E., Mohand-Said, S., Antonio, A., et al. (2011). Novel C2orf71 mutations account for approximately 1% of cases in a large French arRP cohort. Hum Mutat *32*, E2091-2103.

355. Hebrard, M., Manes, G., Bocquet, B., Meunier, I., et al. (2011). Combining gene mapping and phenotype assessment for fast mutation finding in non-consanguineous autosomal recessive retinitis pigmentosa families. Eur J Hum Genet *19*, 1256-1263.

356. Nei, M. and Roychoudhury, A.K. (1974). Sampling variances of heterozygosity and genetic distance. Genetics *76*, 379-390.

357. Nei, M. and Li, W.H. (1979). Mathematical model for studying genetic variation in terms of restriction endonucleases. Proc Natl Acad Sci U S A *76*, 5269-5273.

358. Tajima, F. (1989). Statistical method for testing the neutral mutation hypothesis by DNA polymorphism. Genetics *123*, 585-595.

359. Watterson, G.A. (1975). On the number of segregating sites in genetical models without recombination. Theor Popul Biol *7*, 256-276.

360. Webster, A.R., Heon, E., Lotery, A.J., Vandenburgh, K., et al. (2001). An analysis of allelic variation in the ABCA4 gene. Invest Ophthalmol Vis Sci *42*, 1179-1189.

361. Erali, M. and Wittwer, C.T. (2010). High resolution melting analysis for gene scanning. Methods *50*, 250-261.

362. Aguirre-Lamban, J., Riveiro-Alvarez, R., Garcia-Hoyos, M., Cantalapiedra, D., et al. (2010). Comparison of high-resolution melting analysis with denaturing high-performance liquid chromatography for mutation scanning in the ABCA4 gene. Invest Ophthalmol Vis Sci *51*, 2615-2619.

363. Van Der Stoep, N., Van Paridon, C.D., Janssens, T., Krenkova, P., et al. (2009). Diagnostic guidelines for high-resolution melting curve (HRM) analysis: an interlaboratory validation of BRCA1 mutation scanning using the 96-well LightScanner. Hum Mutat *30*, 899-909.

364. De Juan, I., Esteban, E., Palanca, S., Barragan, E., et al. (2009). High-resolution melting analysis for rapid screening of BRCA1 and BRCA2 Spanish mutations. Breast Cancer Res Treat *115*, 405-414.

365. Taylor, C.F. (2009). Mutation scanning using high-resolution melting. Biochem Soc Trans *37*, 433-437.

366. Dobrowolski, S.F., McKinney, J.T., Amat Di San Filippo, C., Giak Sim, K., et al. (2005). Validation of dye-binding/high-resolution thermal denaturation for the identification of mutations in the SLC22A5 gene. Hum Mutat *25*, 306-313.

367. Liew, M., Pryor, R., Palais, R., Meadows, C., et al. (2004). Genotyping of single-nucleotide polymorphisms by high-resolution melting of small amplicons. Clin Chem *50*, 1156-1164.

368. Palais, R.A., Liew, M.A., and Wittwer, C.T. (2005). Quantitative heteroduplex analysis for single nucleotide polymorphism genotyping. Anal Biochem *346*, 167-175.

369. Graham, R., Liew, M., Meadows, C., Lyon, E., et al. (2005). Distinguishing different DNA heterozygotes by high-resolution melting. Clin Chem *51*, 1295-1298.

370. Laurie, A.D., Smith, M.P., and George, P.M. (2007). Detection of factor VIII gene mutations by high-resolution melting analysis. Clin Chem *53*, 2211-2214.

371. Vandersteen, J.G., Bayrak-Toydemir, P., Palais, R.A., and Wittwer, C.T. (2007). Identifying common genetic variants by high-resolution melting. Clin Chem *53*, 1191-1198.

372. Eckert, K.A. and Kunkel, T.A. (1991). DNA polymerase fidelity and the polymerase chain reaction. PCR Methods Appl *1*, 17-24.

373. Linding, R., Russell, R.B., Neduva, V., and Gibson, T.J. (2003). GlobPlot: Exploring protein sequences for globularity and disorder. Nucleic Acids Res *31*, 3701-3708.

374. Kay, B.K., Williamson, M.P., and Sudol, M. (2000). The importance of being proline: the interaction of proline-rich motifs in signaling proteins with their cognate domains. FASEB J *14*, 231-241.

375. He, H.J., Wang, X.S., Pan, R., Wang, D.L., et al. (2009). The proline-rich domain of tau plays a role in interactions with actin. BMC Cell Biol *10*, 81.

376. Chaitin, M.H., Schneider, B.G., Hall, M.O., and Papermaster, D.S. (1984). Actin in the photoreceptor connecting cilium: immunocytochemical localization to the site of outer segment disk formation. J Cell Biol *99*, 239-247.

377. Xi, Q., Pauer, G.J., Marmorstein, A.D., Crabb, J.W., et al. (2005). Tubby-like protein 1 (TULP1) interacts with F-actin in photoreceptor cells. Invest Ophthalmol Vis Sci *46*, 4754-4761.

378. Rayment, I., Rypniewski, W.R., Schmidt-Base, K., Smith, R., et al. (1993). Three-dimensional structure of myosin subfragment-1: a molecular motor. Science *261*, 50-58.

379. Yamaki, K., Tsuda, M., Kikuchi, T., Chen, K.H., et al. (1990). Structural organization of the human S-antigen gene. cDNA, amino acid, intron, exon, promoter, in vitro transcription, retina, and pineal gland. J Biol Chem *265*, 20757-20762.

380. Kuhn, H., Hall, S.W., and Wilden, U. (1984). Light-induced binding of 48-kDa protein to photoreceptor membranes is highly enhanced by phosphorylation of rhodopsin. FEBS Lett *176*, 473-478.

381. Gurevich, V.V., Hanson, S.M., Song, X., Vishnivetskiy, S.A., et al. (2011). The functional cycle of visual arrestins in photoreceptor cells. Progress in Retinal and Eye Research *30*, 405-430.

382. Nakamura, B. (1920). Ueber ein neues phänomen der farbenveränderung des menschlichen augenhintergrundes in zusammenhang mit der fortschreitenden dunkeladaptation. Klin Monatsbl Augenheilkd *65*, 83-85.

383. Fuchs, S., Nakazawa, M., Maw, M., Tamai, M., et al. (1995). A homozygous 1-base pair deletion in the arrestin gene is a frequent cause of Oguchi disease in Japanese. Nat Genet *10*, 360-362.

384. Dryja, T.P. (2000). Molecular genetics of Oguchi disease, fundus albipunctatus, and other forms of stationary night blindness: LVII Edward Jackson Memorial Lecture. Am J Ophthalmol *130*, 547-563.

385. Nakazawa, M., Wada, Y., and Tamai, M. (1998). Arrestin gene mutations in autosomal recessive retinitis pigmentosa. Arch Ophthalmol *116*, 498-501.

386. Nakamachi, Y., Nakamura, M., Fujii, S., Yamamoto, M., et al. (1998). Oguchi disease with sectoral retinitis pigmentosa harboring adenine deletion at position 1147 in the arrestin gene. Am J Ophthalmol *125*, 249-251.

387. Sonoyama, H., Shinoda, K., Ishigami, C., Tada, Y., et al. (2011). Oguchi disease masked by retinitis pigmentosa. Doc Ophthalmol *123*, 127-133.

388. Hayashi, T., Tsuzuranuki, S., Kozaki, K., Urashima, M., et al. (2011). Macular dysfunction in Oguchi disease with the frequent mutation 1147delA in the SAG gene. Ophthalmic Res *46*, 175-180.

389. Yamamoto, S., Sippel, K.C., Berson, E.L., and Dryja, T.P. (1997). Defects in the rhodopsin kinase gene in the Oguchi form of stationary night blindness. Nat Genet *15*, 175-178.

390. Cideciyan, A.V., Zhao, X., Nielsen, L., Khani, S.C., et al. (1998). Null mutation in the rhodopsin kinase gene slows recovery kinetics of rod and cone phototransduction in man. Proc Natl Acad Sci U S A *95*, 328-333.

391. Maw, M., Kumaramanickavel, G., Kar, B., John, S., et al. (1998). Two Indian siblings with Oguchi disease are homozygous for an arrestin mutation encoding premature termination. Hum Mutat *Suppl 1*, S317-319.

392. Hashimoto, H. and Kishi, S. (2009). Shortening of the rod outer segment in Oguchi disease. Graefes Arch Clin Exp Ophthalmol *247*, 1561-1563.

393. Takada, M., Otani, A., Ogino, K., and Yoshimura, N. (2011). Spectral-domain optical coherence tomography findings in the Mizuo-Nakamura phenomenon of Oguchi disease. Retina *31*, 626-628.

394. Burstedt, M.S., Sandgren, O., Golovleva, I., and Wachtmeister, L. (2008). Effects of prolonged dark adaptation in patients with retinitis pigmentosa of Bothnia type: an electrophysiological study. Doc Ophthalmol *116*, 193-205.

395. Robson, A.G., Mengher, L.S., Tan, M.H., and Moore, A.T. (2009). An unusual fundus phenotype of inner retinal sheen in X-linked retinoschisis. Eye (Lond) *23*, 1876-1878.

396. Dryja, T.P., McEvoy, J.A., McGee, T.L., and Berson, E.L. (2000). Novel rhodopsin mutations Gly114Val and Gln184Pro in dominant retinitis pigmentosa. Invest Ophthalmol Vis Sci *41*, 3124-3127.

397. Nishiguchi, K.M., Sandberg, M.A., Kooijman, A.C., Martemyanov, K.A., et al. (2004). Defects in RGS9 or its anchor protein R9AP in patients with slow photoreceptor deactivation. Nature *427*, 75-78.

398. Michaelides, M., Li, Z., Rana, N.A., Richardson, E.C., et al. (2010). Novel mutations and electrophysiologic findings in RGS9- and R9AP-associated retinal dysfunction (Bradyopsia). Ophthalmology *117*, 120-127 e121.

399. Parker, R.O. and Crouch, R.K. (2010). Retinol dehydrogenases (RDHs) in the visual cycle. Exp Eye Res.

400. Lion, F., Rotmans, J.P., Daemen, F.J., and Bonting, S.L. (1975). Biochemical aspects of the visual process XXVII: stereospecificity of ocular retinol dehydrogenases and the visual cycle. Biochim Biophys Acta *384*, 283-292.

401. Jones, G.J., Crouch, R.K., Wiggert, B., Cornwall, M.C., et al. (1989). Retinoid requirements for recovery of sensitivity after visual-pigment bleaching in isolated photoreceptors. Proc Natl Acad Sci U S A *86*, 9606-9610.

402. Simon, A., Hellman, U., Wernstedt, C., and Eriksson, U. (1995). The retinal pigment epithelial-specific 11-cis retinol dehydrogenase belongs to the family of short chain alcohol dehydrogenases. J Biol Chem *270*, 1107-1112.

403. Simon, A., Romert, A., Gustafson, A.L., McCaffery, J.M., et al. (1999). Intracellular localization and membrane topology of 11-cis retinol dehydrogenase in the retinal pigment epithelium suggest a compartmentalized synthesis of 11-cis retinaldehyde. J Cell Sci *112*, 549-558.

404. Farjo, K.M., Moiseyev, G., Takahashi, Y., Crouch, R.K., et al. (2009). The 11-cis-retinol dehydrogenase activity of RDH10 and its interaction with visual cycle proteins. Invest Ophthalmol Vis Sci *50*, 5089-5097.

405. Mata, N.L., Radu, R.A., Clemmons, R.C., and Travis, G.H. (2002). Isomerization and oxidation of vitamin A in cone-dominant retinas: a novel pathway for visual-pigment regeneration in daylight. Neuron *36*, 69-80.

406. Jang, G.F., Van Hooser, J.P., Kuksa, V., McBee, J.K., et al. (2001). Characterization of a dehydrogenase activity responsible for oxidation of 11-cis-retinol in the retinal pigment epithelium of mice with a disrupted RDH5 gene. A model for the human hereditary disease fundus albipunctatus. J Biol Chem *276*, 32456-32465.

407. Driessen, C.A., Winkens, H.J., Hoffmann, K., Kuhlmann, L.D., et al. (2000). Disruption of the 11-cis-retinol dehydrogenase gene leads to accumulation of cis-retinols and cis-retinyl esters. Mol Cell Biol *20*, 4275-4287.

408. Simon, A., Lagercrantz, J., Bajalica-Lagercrantz, S., and Eriksson, U. (1996). Primary structure of human 11-cis retinol dehydrogenase and organization and chromosomal localization of the corresponding gene. Genomics *36*, 424-430.

409. Ripps, H. (1982). Night blindness revisited: from man to molecules. Proctor lecture. Invest Ophthalmol Vis Sci *23*, 588-609.

410. Marmor, M.F. (1990). Long-term follow-up of the physiologic abnormalities and fundus changes in fundus albipunctatus. Ophthalmology *97*, 380-384.

411. Sekiya, K., Nakazawa, M., Ohguro, H., Usui, T., et al. (2003). Long-term fundus changes due to fundus albipunctatus associated with mutations in the RDH5 gene. Arch Ophthalmol *121*, 1057-1059.

412. Yamamoto, H., Yakushijin, K., Kusuhara, S., Escano, M.F., et al. (2003). A novel RDH5 gene mutation in a patient with fundus albipunctatus presenting with macular atrophy and fading white dots. Am J Ophthalmol *136*, 572-574.

413. Carr, R.E. (1974). Congenital stationary nightblindness. Trans Am Ophthalmol Soc *72*, 448-487.

414. Lamb, T.D. and Pugh, E.N., Jr. (2004). Dark adaptation and the retinoid cycle of vision. Progress in Retinal and Eye Research *23*, 307-380.

415. Querques, G., Carrillo, P., Querques, L., Bux, A.V., et al. (2009). High-definition optical coherence tomographic visualization of photoreceptor layer and retinal flecks in fundus albipunctatus associated with cone dystrophy. Arch Ophthalmol *127*, 703-706.

416. Hayashi, T., Goto-Omoto, S., Takeuchi, T., Gekka, T., et al. (2006). Compound heterozygous RDH5 mutations in familial fleck retina with night blindness. Acta Ophthalmol Scand *84*, 254-258.

417. Nakamura, M., Lin, J., and Miyake, Y. (2004). Young monozygotic twin sisters with fundus albipunctatus and cone dystrophy. Arch Ophthalmol *122*, 1203-1207.

418. Nakamura, M. and Miyake, Y. (2002). Macular dystrophy in a 9-year-old boy with fundus albipunctatus. Am J Ophthalmol *133*, 278-280.

419. Nakamura, M., Hotta, Y., Tanikawa, A., Terasaki, H., et al. (2000). A high association with cone dystrophy in fundus albipunctatus caused by mutations of the RDH5 gene. Invest Ophthalmol Vis Sci *41*, 3925-3932.

420. Wada, Y., Abe, T., Fuse, N., and Tamai, M. (2000). A frequent 1085delC/insGAAG mutation in the RDH5 gene in Japanese patients with fundus albipunctatus. Invest Ophthalmol Vis Sci *41*, 1894-1897.

421. Gonzalez-Fernandez, F., Kurz, D., Bao, Y., Newman, S., et al. (1999). 11-cis retinol dehydrogenase mutations as a major cause of the congenital night-blindness disorder known as fundus albipunctatus. Mol Vis *5*, 41.

422. Hirose, E., Inoue, Y., Morimura, H., Okamoto, N., et al. (2000). Mutations in the 11-cis retinol dehydrogenase gene in Japanese patients with fundus albipunctatus. Invest Ophthalmol Vis Sci *41*, 3933-3935.

423. Wada, Y., Abe, T., Sato, H., and Tamai, M. (2001). A novel Gly35Ser mutation in the RDH5 gene in a Japanese family with fundus albipunctatus associated with cone dystrophy. Arch Ophthalmol *119*, 1059-1063.

424. Kuroiwa, S., Kikuchi, T., and Yoshimura, N. (2000). A novel compound heterozygous mutation in the RDH5 gene in a patient with fundus albipunctatus. Am J Ophthalmol *130*, 672-675.

425. Hotta, K., Nakamura, M., Kondo, M., Ito, S., et al. (2003). Macular dystrophy in a Japanese family with fundus albipunctatus. Am J Ophthalmol *135*, 917-919.

426. Nakamura, M., Skalet, J., and Miyake, Y. (2003). RDH5 gene mutations and electroretinogram in fundus albipunctatus with or without macular dystrophy: RDH5 mutations and ERG in fundus albipunctatus. Doc Ophthalmol *107*, 3-11.

427. Sato, M., Oshika, T., Kaji, Y., and Nose, H. (2004). A novel homozygous Gly107Arg mutation in the RDH5 gene in a Japanese patient with fundus albipunctatus with sectorial retinitis pigmentosa. Ophthalmic Res *36*, 43-50.

428. Iannaccone, A., Tedesco, S.A., Gallaher, K.T., Yamamoto, H., et al. (2007). Fundus albipunctatus in a 6-year old girl due to compound heterozygous mutations in the RDH5 gene. Doc Ophthalmol *115*, 111-116.

429. Niwa, Y., Kondo, M., Ueno, S., Nakamura, M., et al. (2005). Cone and rod dysfunction in fundus albipunctatus with RDH5 mutation: an electrophysiological study. Invest Ophthalmol Vis Sci *46*, 1480-1485.

430. Wang, C., Nakanishi, N., Ohishi, K., Hikoya, A., et al. (2008). Novel RDH5 mutation in family with mother having fundus albipunctatus and three children with retinitis pigmentosa. Ophthalmic Genet *29*, 29-32.

431. Hajali, M., Fishman, G.A., Dryja, T.P., Sweeney, M.O., et al. (2009). Diagnosis in a patient with fundus albipunctatus and atypical fundus changes. Doc Ophthalmol *118*, 233-238.

432. Driessen, C.A., Janssen, B.P., Winkens, H.J., Kuhlmann, L.D., et al. (2001). Null mutation in the human 11-cis retinol dehydrogenase gene associated with fundus albipunctatus. Ophthalmology *108*, 1479-1484.

433. Ruther, K., Janssen, B.P., Kellner, U., Janssen, J.J., et al. (2004). [Clinical and genetic findings in a patient with fundus albipunctatus]. Ophthalmologe *101*, 177-185.

434. Sohn, E.H., Li, Z., Robson, A.G., Wright, G., et al. (2008). The clinical characteristics of patients with retinal dysfunction due to biallelic mutation of RDH5. ARVO *49*, 3287.

435. Robson, A.G., Michaelides, M., Saihan, Z., Bird, A.C., et al. (2008). Functional characteristics of patients with retinal dystrophy that manifest abnormal parafoveal annuli of high density fundus autofluorescence; a review and update. Doc Ophthalmol *116*, 79-89.

436. Lorenz, B., Wabbels, B., Wegscheider, E., Hamel, C.P., et al. (2004). Lack of fundus autofluorescence to 488 nanometers from childhood on in patients with early-onset severe retinal dystrophy associated with mutations in RPE65. Ophthalmology *111*, 1585-1594.

437. Liden, M., Romert, A., Tryggvason, K., Persson, B., et al. (2001). Biochemical defects in 11-cis-retinol dehydrogenase mutants associated with fundus albipunctatus. J Biol Chem *276*, 49251-49257.

438. Imaizumi, M., Tatewaki, S.Y., Kimoto, K., Takaki, Y., et al. (2005). Disappearance of puncta after uveitis in an eye with fundus albipunctatus. Retina *25*, 1096-1098.

439. Maeda, A., Maeda, T., Sun, W., Zhang, H., et al. (2007). Redundant and unique roles of retinol dehydrogenases in the mouse retina. Proc Natl Acad Sci U S A *104*, 19565-19570.

440. Schatz, P., Preising, M., Lorenz, B., Sander, B., et al. (2010). Lack of autofluorescence in fundus albipunctatus associated with mutations in RDH5. Retina.

441. He, X., Lobsiger, J., and Stocker, A. (2009). Bothnia dystrophy is caused by domino-like rearrangements in cellular retinaldehyde-binding protein mutant R234W. Proc Natl Acad Sci U S A *106*, 18545-18550.

442. Audo, I., Robson, A.G., Holder, G.E., and Moore, A.T. (2008). The negative ERG: clinical phenotypes and disease mechanisms of inner retinal dysfunction. Surv Ophthalmol *53*, 16-40.

443. Wali, N. and Leguire, L.E. (1992). The photopic hill: a new phenomenon of the light adapted electroretinogram. Doc Ophthalmol *80*, 335-345.

444. Ueno, S., Kondo, M., Niwa, Y., Terasaki, H., et al. (2004). Luminance dependence of neural components that underlies the primate photopic electroretinogram. Invest Ophthalmol Vis Sci *45*, 1033-1040.

445. McBain, V.A., Egan, C.A., Pieris, S.J., Supramaniam, G., et al. (2007). Functional observations in vitamin A deficiency: diagnosis and time course of recovery. Eye (Lond) *21*, 367-376.

446. Kim, T.S., Maeda, A., Maeda, T., Heinlein, C., et al. (2005). Delayed dark adaptation in 11-cis-retinol dehydrogenase-deficient mice: a role of RDH11 in visual processes in vivo. J Biol Chem *280*, 8694-8704.

447. Driessen, C.A., Janssen, B.P., Winkens, H.J., Van Vugt, A.H., et al. (1995). Cloning and expression of a cDNA encoding bovine retinal pigment epithelial 11-cis retinol dehydrogenase. Invest Ophthalmol Vis Sci *36*, 1988-1996.

448. Wulff, H., Castle, N.A., and Pardo, L.A. (2009). Voltage-gated potassium channels as therapeutic targets. Nat Rev Drug Discov *8*, 982-1001.

449. Czirjak, G., Toth, Z.E., and Enyedi, P. (2007). Characterization of the heteromeric potassium channel formed by kv2.1 and the retinal subunit kv8.2 in Xenopus oocytes. J Neurophysiol *98*, 1213-1222.

450. Gouras, P., Eggers, H.M., and Mackay, C.J. (1983). Cone dystrophy, nyctalopia, and supernormal rod responses. A new retinal degeneration. Arch Ophthalmol *101*, 718-724.

451. Michaelides, M., Holder, G.E., Webster, A.R., Hunt, D.M., et al. (2005). A detailed phenotypic study of "cone dystrophy with supernormal rod ERG". Br J Ophthalmol *89*, 332-339.

452. Thomas, M.G., Kumar, A., Kohl, S., Proudlock, F.A., et al. (2011). High-resolution in vivo imaging in achromatopsia. Ophthalmology *118*, 882-887.

453. Grover, S., Murthy, R.K., Brar, V.S., and Chalam, K.V. (2009). Normative data for macular thickness by high-definition spectral-domain optical coherence tomography (spectralis). Am J Ophthalmol *148*, 266-271.

454. Ottschytsch, N., Raes, A., Van Hoorick, D., and Snyders, D.J. (2002). Obligatory heterotetramerization of three previously uncharacterized Kv channel alpha-subunits identified in the human genome. Proc Natl Acad Sci U S A *99*, 7986-7991.

455. Wissinger, B., Schaich, S., Baumann, B., Bonin, M., et al. (2011). Large deletions of the KCNV2 gene are common in patients with cone dystrophy with supernormal rod response. Hum Mutat *32*, 1398-1406.

456. Wang, Q., Curran, M.E., Splawski, I., Burn, T.C., et al. (1996). Positional cloning of a novel potassium channel gene: KVLQT1 mutations cause cardiac arrhythmias. Nat Genet *12*, 17-23.

457. Biervert, C., Schroeder, B.C., Kubisch, C., Berkovic, S.F., et al. (1998). A potassium channel mutation in neonatal human epilepsy. Science *279*, 403-406.

458. Maljevic, S., Naros, G., Yalcin, O., Blazevic, D., et al. (2011). Temperature and pharmacological rescue of a folding-defective, dominant-negative KV 7.2 mutation associated with neonatal seizures. Hum Mutat *32*, E2283-2293.

459. Jorge, B.S., Campbell, C.M., Miller, A.R., Rutter, E.D., et al. (2011). Voltage-gated potassium channel KCNV2 (Kv8.2) contributes to epilepsy susceptibility. Proc Natl Acad Sci U S A *108*, 5443-5448.

460. Jacobson, S.G., Aleman, T.S., Cideciyan, A.V., Sumaroka, A., et al. (2005). Identifying photoreceptors in blind eyes caused by RPE65 mutations: Prerequisite for human gene therapy success. Proc Natl Acad Sci U S A *102*, 6177-6182.

461. Thiadens, A.A., Den Hollander, A.I., Roosing, S., Nabuurs, S.B., et al. (2009). Homozygosity mapping reveals PDE6C mutations in patients with early-onset cone photoreceptor disorders. Am J Hum Genet *85*, 240-247.

462. Thiadens, A.A., Somervuo, V., Van Den Born, L.I., Roosing, S., et al. (2010). Progressive loss of cones in achromatopsia: an imaging study using spectral-domain optical coherence tomography. Invest Ophthalmol Vis Sci *51*, 5952-5957.

463. Sisk, R.A., Berrocal, A.M., and Lam, B.L. (2010). Loss of foveal cone photoreceptor outer segments in occult macular dystrophy. Ophthalmic Surg Lasers Imaging, 1-3.

464. Gomes, N.L., Greenstein, V.C., Carlson, J.N., Tsang, S.H., et al. (2009). A comparison of fundus autofluorescence and retinal structure in patients with Stargardt disease. Invest Ophthalmol Vis Sci *50*, 3953-3959.

465. Friedburg, C., Wissinger, B., Schambeck, M., Bonin, M., et al. (2011). Long-term follow-up of the human phenotype in three siblings with cone dystrophy associated with a homozygous p.G461R mutation of KCNV2. Invest Ophthalmol Vis Sci *52*, 8621-8629.

466. Wissinger, B., Dangel, S., Jagle, H., Hansen, L., et al. (2008). Cone dystrophy with supernormal rod response is strictly associated with mutations in KCNV2. Invest Ophthalmol Vis Sci *49*, 751-757.

467. Torti, C., Povazay, B., Hofer, B., Unterhuber, A., et al. (2009). Adaptive optics optical coherence tomography at 120,000 depth scans/s for non-invasive cellular phenotyping of the living human retina. Opt Express *17*, 19382-19400.

468. Murakoshi, H. and Trimmer, J.S. (1999). Identification of the Kv2.1 K+ channel as a major component of the delayed rectifier K+ current in rat hippocampal neurons. J Neurosci *19*, 1728-1735.

469. Smith, K.E., Wilkie, S.E., Stocker, M., and Hunt, D.M. (2010). Cone dystrophy with supernormal electroretinogram (CDSE): functional analysis of mutations in KCNV2 encoding the voltage-gated potassium channel subunit, Kv8.2. ARVO.

470. Zeitz, C. (2007). Molecular genetics and protein function involved in nocturnal vision. Expert Rev Ophthalmol, 467-485.

471. Schubert, G. and Bornschein, H. (1952). [Analysis of the human electroretinogram]. Ophthalmologica *123*, 396-413.

472. Karpe, G. (1945). The basis of clinical electroretinography. Acta Ophthalmol, 1-118.

473. Miyake, Y., Yagasaki, K., Horiguchi, M., Kawase, Y., et al. (1986). Congenital stationary night blindness with negative electroretinogram. A new classification. Arch Ophthalmol *104*, 1013-1020.

474. Bech-Hansen, N.T., Naylor, M.J., Maybaum, T.A., Sparkes, R.L., et al. (2000). Mutations in NYX, encoding the leucine-rich proteoglycan nyctalopin, cause X-linked complete congenital stationary night blindness. Nat Genet *26*, 319-323.

475. Li, Z., Sergouniotis, P.I., Michaelides, M., Mackay, D.S., et al. (2009). Recessive mutations of the gene TRPM1 abrogate ON bipolar cell function and cause complete congenital stationary night blindness in humans. Am J Hum Genet *85*, 711-719.

476. Van Genderen, M.M., Bijveld, M.M., Claassen, Y.B., Florijn, R.J., et al. (2009). Mutations in TRPM1 are a common cause of complete congenital stationary night blindness. Am J Hum Genet *85*, 730-736.

477. Audo, I., Kohl, S., Leroy, B.P., Munier, F.L., et al. (2009). TRPM1 is mutated in patients with autosomal-recessive complete congenital stationary night blindness. Am J Hum Genet *85*, 720-729.

478. Slaughter, M.M. and Miller, R.F. (1985). Characterization of an extended glutamate receptor of the on bipolar neuron in the vertebrate retina. J Neurosci *5*, 224-233.

479. Schiller, P.H. (2010). Parallel information processing channels created in the retina. Proc Natl Acad Sci U S A *107*, 17087-17094.

480. Masland, R.H. (2001). The fundamental plan of the retina. Nat Neurosci *4*, 877-886.

481. Sharpe, L.T. and Stockman, A. (1999). Rod pathways: the importance of seeing nothing. Trends Neurosci *22*, 497-504.

482. Zeitz, C., Van Genderen, M., Neidhardt, J., Luhmann, U.F., et al. (2005). Mutations in GRM6 cause autosomal recessive congenital stationary night blindness with a distinctive scotopic 15-Hz flicker electroretinogram. Invest Ophthalmol Vis Sci *46*, 4328-4335.

483. Zeitz, C., Forster, U., Neidhardt, J., Feil, S., et al. (2007). Night blindness-associated mutations in the ligand-binding, cysteine-rich, and intracellular domains of the metabotropic glutamate receptor 6 abolish protein trafficking. Hum Mutat *28*, 771-780.

484. Leifert, D., Todorova, M.G., Prunte, C., and Palmowski-Wolfe, A.M. (2005). LED-generated multifocal ERG ON- and OFF-responses in complete congenital stationary night blindness: a case report. Doc Ophthalmol *111*, 1-6.

485. Xu, X., Li, S., Xiao, X., Wang, P., et al. (2009). Sequence variations of GRM6 in patients with high myopia. Mol Vis *15*, 2094-2100.

486. Zhang, Q., Xiao, X., Li, S., Jia, X., et al. (2007). Mutations in NYX of individuals with high myopia, but without night blindness. Mol Vis *13*, 330-336.

487. Scholl, H.P., Langrova, H., Pusch, C.M., Wissinger, B., et al. (2001). Slow and fast rod ERG pathways in patients with X-linked complete stationary night blindness carrying mutations in the NYX gene. Invest Ophthalmol Vis Sci *42*, 2728-2736.

488. Simell, O. and Takki, K. (1973). Raised plasma-ornithine and gyrate atrophy of the choroid and retina. Lancet *1*, 1031-1033.

489. Takki, K. (1974). Gyrate atrophy of the choroid and retina associated with hyperornithinaemia. Br J Ophthalmol *58*, 3-23.

490. Takki, K.K. and Milton, R.C. (1981). The natural history of gyrate atrophy of the choroid and retina. Ophthalmology *88*, 292-301.

491. Peltola, K.E., Nanto-Salonen, K., Heinonen, O.J., Jaaskelainen, S., et al. (2001). Ophthalmologic heterogeneity in subjects with gyrate atrophy of choroid and retina harboring the L402P mutation of ornithine aminotransferase. Ophthalmology *108*, 721-729.

492. O'Donnell, J.J., Sandman, R.P., and Martin, S.R. (1978). Gyrate atrophy of the retina: inborn error of L-ornithin:2-oxoacid aminotransferase. Science *200*, 200-201.

493. Volpe, P., Sawamura, R., and Strecker, H.J. (1969). Control of ornithin delta-transaminase in rat liver and kidney. J Biol Chem *244*, 719-726.

494. Shen, B.W., Hennig, M., Hohenester, E., Jansonius, J.N., et al. (1998). Crystal structure of human recombinant ornithine aminotransferase. J Mol Biol *277*, 81-102.

495. Valle, D., Walser, M., Brusilow, S.W., and Kaiser-Kupfer, M. (1980). Gyrate atrophy of the choroid and retina: amino acid metabolism and correction of hyperornithinemia with an arginine-deficient diet. J Clin Invest *65*, 371-378.

496. Kaiser-Kupfer, M.I., Caruso, R.C., and Valle, D. (2002). Gyrate atrophy of the choroid and retina: further experience with long-term reduction of ornithine levels in children. Arch Ophthalmol *120*, 146-153.

497. Rao, G.N. and Cotlier, E. (1984). Ornithine delta-aminotransferase activity in retina and other tissues. Neurochem Res *9*, 555-562.

498. Wang, T., Milam, A.H., Steel, G., and Valle, D. (1996). A mouse model of gyrate atrophy of the choroid and retina. Early retinal pigment epithelium damage and progressive retinal degeneration. J Clin Invest *97*, 2753-2762.

499. Caruso, R.C., Nussenblatt, R.B., Csaky, K.G., Valle, D., et al. (2001). Assessment of visual function in patients with gyrate atrophy who are considered candidates for gene replacement. Arch Ophthalmol *119*, 667-669.

500. Liu, M.M., Tuo, J., and Chan, C.C. (2010). Gene therapy for ocular diseases. Br J Ophthalmol.

501. Howden, S.E., Gore, A., Li, Z., Fung, H.L., et al. (2011). Genetic correction and analysis of induced pluripotent stem cells from a patient with gyrate atrophy. Proc Natl Acad Sci U S A *108*, 6537-6542.

502. Wilson, D.J., Weleber, R.G., and Green, W.R. (1991). Ocular clinicopathologic study of gyrate atrophy. Am J Ophthalmol *111*, 24-33.

503. Meyer, C.H., Hoerauf, H., Schmidt-Erfurth, U., Roider, J., et al. (2000). [Correlation of morphologic changes between optical coherence tomography and topographic angiography in a case of gyrate atrophy]. Ophthalmologe *97*, 41-46.

504. Oliveira, T.L., Andrade, R.E., Muccioli, C., Sallum, J., et al. (2005). Cystoid macular edema in gyrate atrophy of the choroid and retina: a fluorescein angiography and optical coherence tomography evaluation. Am J Ophthalmol *140*, 147-149.

505. Vasconcelos-Santos, D.V., Magalhaes, E.P., and Nehemy, M.B. (2007). Macular edema associated with gyrate atrophy managed with intravitreal triamcinolone: a case report. Arq Bras Oftalmol *70*, 858-861.

506. Sharma, Y.R., Singh, D.V., Azad, R.V., and Pal, N. (2006). Gyrate atrophy with bilateral full thickness macular hole. Eye (Lond) *20*, 745-747.

507. Valle, D.L., Boison, A.P., Jezyk, P., and Aguirre, G. (1981). Gyrate atrophy of the choroid and retina in a cat. Invest Ophthalmol Vis Sci *20*, 251-255.

508. Mashima, Y.G., Weleber, R.G., Kennaway, N.G., and Inana, G. (1999). Genotype-phenotype correlation of a pyridoxine-responsive form of gyrate atrophy. Ophthalmic Genet *20*, 219-224.

509. Rohrschneider, K., Bultmann, S., and Springer, C. (2008). Use of fundus perimetry (microperimetry) to quantify macular sensitivity. Progress in Retinal and Eye Research *27*, 536-548.

510. Midena, E. (2007). Perimetry and the fundus: an introduction to microperimetry.(Thorofare, Slack Incorporated).

511. Zweifel, S.A., Engelbert, M., Laud, K., Margolis, R., et al. (2009). Outer retinal tubulation: a novel optical coherence tomography finding. Arch Ophthalmol *127*, 1596-1602.

512. Kaufman, D.L., Ramesh, V., McClatchey, A.I., Menkes, J.H., et al. (1990). Detection of point mutations associated with genetic diseases by an exon scanning technique. Genomics *8*, 656-663.

513. Brody, L.C., Mitchell, G.A., Obie, C., Michaud, J., et al. (1992). Ornithine delta-aminotransferase mutations in gyrate atrophy. Allelic heterogeneity and functional consequences. J Biol Chem *267*, 3302-3307.

514. Kaiser-Kupfer, M., Kuwabara, T., Uga, S., Takki, K., et al. (1983). Cataract in gyrate atrophy: clinical and morphologic studies. Invest Ophthalmol Vis Sci *24*, 432-436.

515. Takki, K. (1974). Differential diagnosis between the primary total choroidal vascular atrophies. Br J Ophthalmol *58*, 24-35.

516. Ho, G., Kumar, S., Min, X.S., Kng, Y.L., et al. (2009). Molecular imaging of retinal gliosis in transgenic mice induced by kainic acid neurotoxicity. Invest Ophthalmol Vis Sci *50*, 2459-2464.

517. Fujiwara, T., Imamura, Y., Giovinazzo, V.J., and Spaide, R.F. (2010). Fundus autofluorescence and optical coherence tomographic findings in acute zonal occult outer retinopathy. Retina *30*, 1206-1216.

518. Ma, N. and Streilein, J.W. (1998). Contribution of microglia as passenger leukocytes to the fate of intraocular neuronal retinal grafts. Invest Ophthalmol Vis Sci *39*, 2384-2393.

519. Ramesh, V., McClatchey, A.I., Ramesh, N., Benoit, L.A., et al. (1988). Molecular basis of ornithine aminotransferase deficiency in B6-responsive and -nonresponsive forms of gyrate atrophy. Proc Natl Acad Sci U S A *85*, 3777-3780.

520. Michaud, J., Thompson, G.N., Brody, L.C., Steel, G., et al. (1995). Pyridoxine-responsive gyrate atrophy of the choroid and retina: clinical and biochemical correlates of the mutation A226V. Am J Hum Genet *56*, 616-622.

521. Ohkubo, Y., Ueta, A., Ito, T., Sumi, S., et al. (2005). Vitamin B6-responsive ornithine aminotransferase deficiency with a novel mutation G237D. Tohoku J Exp Med *205*, 335-342.

522. Stone, E.M. (1998). Expanding the repertoire of RP genes. Nat Genet *19*, 311-313.

523. Sturtevant, A.H. (1913). The linear arrangement of six sex-linked factors in Drosophila, as shown by their mode of association. J Exp Zool *14*, 43-59.

524. Bellone, R.R., Brooks, S.A., Sandmeyer, L., Murphy, B.A., et al. (2008). Differential gene expression of TRPM1, the potential cause of congenital stationary night blindness and coat spotting patterns (LP) in the Appaloosa horse (Equus caballus). Genetics *179*, 1861-1870.

525. Bojang, P., Pearring, J.N., Gregg, R.G. (2009). Nyctalopin interacts with transient receptor potential channels in Yeast. ARVO 2009 Annual Meeting.

526. Shen, Y., Heimel, J.A., Kamermans, M., Peachey, N.S., et al. (2009). A transient receptor potential-like channel mediates synaptic transmission in rod bipolar cells. J Neurosci *29*, 6088-6093.

527. Hunter, J.J., Shao, J., Smutko, J.S., Dussault, B.J., et al. (1998). Chromosomal localization and genomic characterization of the mouse melastatin gene (Mlsn1). Genomics *54*, 116-123.

528. Ramsey, I.S., Delling, M., and Clapham, D.E. (2006). An introduction to TRP channels. Annu Rev Physiol *68*, 619-647.

529. Scott, K. and Zuker, C. (1998). TRP, TRPL and trouble in photoreceptor cells. Curr Opin Neurobiol *8*, 383-388.

530. Clapham, D.E., Runnels, L.W., and Strubing, C. (2001). The TRP ion channel family. Nat Rev Neurosci *2*, 387-396.

531. Clapham, D.E. (2003). TRP channels as cellular sensors. Nature *426*, 517-524.

532. Duncan, L.M., Deeds, J., Hunter, J., Shao, J., et al. (1998). Down-regulation of the novel gene melastatin correlates with potential for melanoma metastasis. Cancer Res *58*, 1515-1520.

533. Dhingra, A., Fina, M.E., Neinstein, A., Ramsey, D.J., et al. (2011). Autoantibodies in melanoma-associated retinopathy target TRPM1 cation channels of retinal ON bipolar cells. J Neurosci *31*, 3962-3967.

534. Kondo, M., Sanuki, R., Ueno, S., Nishizawa, Y., et al. (2011). Identification of autoantibodies against TRPM1 in patients with paraneoplastic retinopathy associated with ON bipolar cell dysfunction. PLoS One *6*, e19911.

535. Den Hollander, A.I., Roepman, R., Koenekoop, R.K., and Cremers, F.P.M. (2008). Leber congenital amaurosis: genes, proteins and disease mechanisms. Progress in Retinal and Eye Research *27*, 391-419.

536. Sergouniotis, P.I., Davidson, A.E., Mackay, D.S., Li, Z., et al. (2011). Recessive mutations in KCNJ13, encoding an inwardly rectifying potassium channel subunit, cause leber congenital amaurosis. Am J Hum Genet *89*, 183-190.

537. Doring, F., Derst, C., Wischmeyer, E., Karschin, C., et al. (1998). The epithelial inward rectifier channel Kir7.1 displays unusual K+ permeation properties. J Neurosci *18*, 8625-8636.

538. Krapivinsky, G., Medina, I., Eng, L., Krapivinsky, L., et al. (1998). A novel inward rectifier K+ channel with unique pore properties. Neuron *20*, 995-1005.

539. Partiseti, M., Collura, V., Agnel, M., Culouscou, J.M., et al. (1998). Cloning and characterization of a novel human inwardly rectifying potassium channel predominantly expressed in small intestine. FEBS Lett *434*, 171-176.

540. Hibino, H., Inanobe, A., Furutani, K., Murakami, S., et al. (2010). Inwardly rectifying potassium channels: their structure, function, and physiological roles. Physiol Rev *90*, 291-366.

541. Nakamura, N., Suzuki, Y., Sakuta, H., Ookata, K., et al. (1999). Inwardly rectifying K+ channel Kir7.1 is highly expressed in thyroid follicular cells, intestinal epithelial cells and choroid plexus epithelial cells: implication for a functional coupling with Na+,K+-ATPase. Biochem J *342*, 329-336.

542. Kusaka, S., Inanobe, A., Fujita, A., Makino, Y., et al. (2001). Functional Kir7.1 channels localized at the root of apical processes in rat retinal pigment epithelium. J Physiol *531*, 27-36.

543. Hejtmancik, J.F., Jiao, X., Li, A., Sergeev, Y.V., et al. (2008). Mutations in KCNJ13 cause autosomal-dominant snowflake vitreoretinal degeneration. Am J Hum Genet *82*, 174-180.

544. Tateno, T., Nakamura, N., Hirata, Y., and Hirose, S. (2006). Role of C-terminus of Kir7.1 potassium channel in cell-surface expression. Cell Biol Int *30*, 270-277.

545. Hirose, T., Lee, K.Y., and Schepens, C.L. (1974). Snowflake degeneration in hereditary vitreoretinal degeneration. Am J Ophthalmol *77*, 143-153.

546. Edwards, A.O. (2008). Clinical features of the congenital vitreoretinopathies. Eye (Lond) *22*, 1233-1242.

547. Lee, M.M., Ritter, R., 3rd, Hirose, T., Vu, C.D., et al. (2003). Snowflake vitreoretinal degeneration: follow-up of the original family. Ophthalmology *110*, 2418-2426.

548. Lang, G.E., Laudi, B., and Pfeiffer, R.A. (1991). [Autosome dominant vitreoretinal dystrophy with skeletal dysplasia in one generation]. Klin Monbl Augenheilkd *198*, 207-214.

549. Gheiler, M., Pollack, A., Uchenik, D., Godel, V., et al. (1982). Hereditary snowflake vitreoretinal degeneration. Birth Defects Orig Artic Ser *18*, 577-580.

550. Robertson, D.M., Link, T.P., and Rostvold, J.A. (1982). Snowflake degeneration of the retina. Ophthalmology *89*, 1513-1517.

551. Pollack, A., Uchenik, D., Chemke, J., and Oliver, M. (1983). Prophylactic laser photocoagulation in hereditary snowflake vitreoretinal degeneration. A family report. Arch Ophthalmol *101*, 1536-1539.

552. Chen, C.J., Everett, T.K., and Marascalco, D. (1986). Snowflake degeneration: an independent entity or a variant of retinitis pigmentosa? South Med J *79*, 1216-1223.

553. Tao, X., Avalos, J.L., Chen, J., and Mackinnon, R. (2009). Crystal structure of the eukaryotic strong inward-rectifier K+ channel Kir2.2 at 3.1 A resolution. Science *326*, 1668-1674.

554. Thomas, P., Ye, Y., and Lightner, E. (1996). Mutation of the pancreatic islet inward rectifier Kir6.2 also leads to familial persistent hyperinsulinemic hypoglycemia of infancy. Hum Mol Genet *5*, 1809-1812.

555. Simon, D.B., Karet, F.E., Rodriguez-Soriano, J., Hamdan, J.H., et al. (1996). Genetic heterogeneity of Bartter's syndrome revealed by mutations in the K+ channel, ROMK. Nat Genet *14*, 152-156.

556. Scholl, U.I., Choi, M., Liu, T., Ramaekers, V.T., et al. (2009). Seizures, sensorineural deafness, ataxia, mental retardation, and electrolyte imbalance (SeSAME syndrome) caused by mutations in KCNJ10. Proc Natl Acad Sci U S A *106*, 5842-5847.

557. Plaster, N.M., Tawil, R., Tristani-Firouzi, M., Canun, S., et al. (2001). Mutations in Kir2.1 cause the developmental and episodic electrical phenotypes of Andersen's syndrome. Cell *105*, 511-519.

558. Gass, J.D. (1997). Stereoscopic atlas of macular disease: diagnosis and treatment.(St Louis, Mosby).

559. Sabel Aish, S.F. and Dajani, B. (1980). Benign familial fleck retina. Br J Ophthalmol *64*, 652-659.

560. Isaacs, T.W., Mcallister, I.L., and Wade, M.S. (1996). Benign fleck retina. Br J Ophthalmol *80*, 267-268.

561. Audo, I., Tsang, S.H., Fu, A.D., Barnes, J.A., et al. (2007). Autofluorescence imaging in a case of benign familial fleck retina. Arch Ophthalmol *125*, 714-715.

562. Galindo-Ferreiro, A., Sanabria, M.R., Garcia, E.P., Coco-Martin, R.M., et al. (2010). Benign fleck retinal findings on multifocal ERG, microperimetry, and OCT. Ophthalmic Surg Lasers Imaging *41*, e1-5.

563. Schuster, S.C., Miller, W., Ratan, A., Tomsho, L.P., et al. (2010). Complete Khoisan and Bantu genomes from southern Africa. Nature *463*, 943-947.

564. Chen, J., Engle, S.J., Seilhamer, J.J., and Tischfield, J.A. (1994). Cloning and recombinant expression of a novel human low molecular weight Ca(2+)-dependent phospholipase A2. J Biol Chem *269*, 2365-2368.

565. Six, D.A. and Dennis, E.A. (2000). The expanding superfamily of phospholipase A(2) enzymes: classification and characterization. Biochim Biophys Acta *1488*, 1-19.

566. Dennis, E.A. (1994). Diversity of group types, regulation, and function of phospholipase A2. J Biol Chem *269*, 13057-13060.

567. Murakami, M., Taketomi, Y., Miki, Y., Sato, H., et al. (2011). Recent progress in phospholipase A research: from cells to animals to humans. Prog Lipid Res *50*, 152-192.

568. Lambeau, G. and Gelb, M.H. (2008). Biochemistry and physiology of mammalian secreted phospholipases A2. Annu Rev Biochem *77*, 495-520.

569. Valentin, E., Singer, A.G., Ghomashchi, F., Lazdunski, M., et al. (2000). Cloning and recombinant expression of human group IIF-secreted phospholipase A(2). Biochem Biophys Res Commun *279*, 223-228.

570. Kolko, M., Christoffersen, N.R., Barreiro, S.G., and Bazan, N.G. (2004). Expression and location of mRNAs encoding multiple forms of secretory phospholipase A2 in the rat retina. J Neurosci Res *77*, 517-524.

571. Cupillard, L., Koumanov, K., Mattei, M.G., Lazdunski, M., et al. (1997). Cloning, chromosomal mapping, and expression of a novel human secretory phospholipase A2. J Biol Chem *272*, 15745-15752.

572. Seeds, M.C., Jones, K.A., Duncan Hite, R., Willingham, M.C., et al. (2000). Cell-specific expression of group X and group V secretory phospholipases A(2) in human lung airway epithelial cells. Am J Respir Cell Mol Biol *23*, 37-44.

573. Suzuki, N., Ishizaki, J., Yokota, Y., Higashino, K., et al. (2000). Structures, enzymatic properties, and expression of novel human and mouse secretory phospholipase A(2)s. J Biol Chem *275*, 5785-5793.

574. Masuda, S., Murakami, M., Ishikawa, Y., Ishii, T., et al. (2005). Diverse cellular localizations of secretory phospholipase A2 enzymes in several human tissues. Biochim Biophys Acta *1736*, 200-210.

575. Masuda, S., Murakami, M., Mitsuishi, M., Komiyama, K., et al. (2005). Expression of secretory phospholipase A2 enzymes in lungs of humans with pneumonia and their potential prostaglandin-synthetic function in human lung-derived cells. Biochem J *387*, 27-38.

576. Kim, K.P., Rafter, J.D., Bittova, L., Han, S.K., et al. (2001). Mechanism of human group V phospholipase A2 (PLA2)-induced leukotriene biosynthesis in human neutrophils. A potential role of heparan sulfate binding in PLA2 internalization and degradation. J Biol Chem *276*, 11126-11134.

577. Balestrieri, B. and Arm, J.P. (2006). Group V sPLA2: classical and novel functions. Biochim Biophys Acta *1761*, 1280-1288.

578. Murakami, M., Masuda, S., Shimbara, S., Ishikawa, Y., et al. (2005). Cellular distribution, post-translational modification, and tumorigenic potential of human group III secreted phospholipase A(2). J Biol Chem *280*, 24987-24998.

579. Munoz, N.M., Kim, Y.J., Meliton, A.Y., Kim, K.P., et al. (2003). Human group V phospholipase A2 induces group IVA phospholipase A2-independent cysteinyl leukotriene synthesis in human eosinophils. J Biol Chem *278*, 38813-38820.

580. Balestrieri, B., Maekawa, A., Xing, W., Gelb, M.H., et al. (2009). Group V secretory phospholipase A2 modulates phagosome maturation and regulates the innate immune response against Candida albicans. J Immunol *182*, 4891-4898.

581. Boilard, E., Lai, Y., Larabee, K., Balestrieri, B., et al. (2010). A novel anti-inflammatory role for secretory phospholipase A2 in immune complex-mediated arthritis. EMBO Mol Med *2*, 172-187.

582. Ohtsuki, M., Taketomi, Y., Arata, S., Masuda, S., et al. (2006). Transgenic expression of group V, but not group X, secreted phospholipase A2 in mice leads to neonatal lethality because of lung dysfunction. J Biol Chem *281*, 36420-36433.

583. Satake, Y., Diaz, B.L., Balestrieri, B., Lam, B.K., et al. (2004). Role of group V phospholipase A2 in zymosan-induced eicosanoid generation and vascular permeability revealed by targeted gene disruption. J Biol Chem *279*, 16488-16494.

584. Munoz, N.M., Meliton, A.Y., Arm, J.P., Bonventre, J.V., et al. (2007). Deletion of secretory group V phospholipase A2 attenuates cell migration and airway hyperresponsiveness in immunosensitized mice. J Immunol *179*, 4800-4807.

585. Giannattasio, G., Fujioka, D., Xing, W., Katz, H.R., et al. (2010). Group V secretory phospholipase A2 reveals its role in house dust mite-induced allergic pulmonary inflammation by regulation of dendritic cell function. J Immunol *185*, 4430-4438.

586. Munoz, N.M., Meliton, A.Y., Meliton, L.N., Dudek, S.M., et al. (2009). Secretory group V phospholipase A2 regulates acute lung injury and neutrophilic inflammation caused by LPS in mice. Am J Physiol Lung Cell Mol Physiol *296*, L879-887.

587. Bostrom, M.A., Boyanovsky, B.B., Jordan, C.T., Wadsworth, M.P., et al. (2007). Group v secretory phospholipase A2 promotes atherosclerosis: evidence from genetically altered mice. Arterioscler Thromb Vasc Biol *27*, 600-606.

588. Boyanovsky, B., Zack, M., Forrest, K., and Webb, N.R. (2009). The capacity of group V sPLA2 to increase atherogenicity of ApoE-/- and LDLR-/- mouse LDL in vitro predicts its atherogenic role in vivo. Arterioscler Thromb Vasc Biol *29*, 532-538.

589. Wootton, P.T., Arora, N.L., Drenos, F., Thompson, S.R., et al. (2007). Tagging SNP haplotype analysis of the secretory PLA2-V gene, PLA2G5, shows strong association with LDL and oxLDL levels, suggesting functional distinction from sPLA2-IIA: results from the UDACS study. Hum Mol Genet *16*, 1437-1444.

590. Rosengren, B., Jonsson-Rylander, A.C., Peilot, H., Camejo, G., et al. (2006). Distinctiveness of secretory phospholipase A2 group IIA and V suggesting unique roles in atherosclerosis. Biochim Biophys Acta *1761*, 1301-1308.

591. Rosenson, R.S., Hislop, C., McConnell, D., Elliott, M., et al. (2009). Effects of 1-H-indole-3-glyoxamide (A-002) on concentration of secretory phospholipase A2 (PLASMA study): a phase II double-blind, randomised, placebo-controlled trial. Lancet *373*, 649-658.

592. Han, S.K., Kim, K.P., Koduri, R., Bittova, L., et al. (1999). Roles of Trp31 in high membrane binding and proinflammatory activity of human group V phospholipase A2. J Biol Chem *274*, 11881-11888.

593. Winget, J.M., Pan, Y.H., and Bahnson, B.J. (2006). The interfacial binding surface of phospholipase A2s. Biochim Biophys Acta *1761*, 1260-1269.

594. Murakami, M., Shimbara, S., Kambe, T., Kuwata, H., et al. (1998). The functions of five distinct mammalian phospholipase A2S in regulating arachidonic acid release. Type IIa and type V secretory phospholipase A2S are functionally redundant and act in concert with cytosolic phospholipase A2. J Biol Chem *273*, 14411-14423.

595. Terman, A., Kurz, T., Navratil, M., Arriaga, E.A., et al. (2010). Mitochondrial turnover and aging of long-lived postmitotic cells: the mitochondrial-lysosomal axis theory of aging. Antioxid Redox Signal *12*, 503-535.

596. Wing, G.L., Blanchard, G.C., and Weiter, J.J. (1978). The topography and age relationship of lipofuscin concentration in the retinal pigment epithelium. Invest Ophthalmol Vis Sci *17*, 601-607.

597. Jang, Y., Waterworth, D., Lee, J.E., Song, K., et al. (2011). Carriage of the V279F null allele within the gene encoding Lp-PLA is protective from coronary artery disease in South Korean males. PLoS One *6*, e18208.

598. Song, K., Nelson, M.R., Aponte, J., Manas, E.S., et al. (2011). Sequencing of Lp-PLA2-encoding PLA2G7 gene in 2000 Europeans reveals several rare loss-of-function mutations. Pharmacogenomics J.

599. Motulsky, A.G. (1978). Medical and human genetics 1977: trends and directions. Am J Hum Genet *30*, 123-131.

600. Burstedt, M.S., Sandgren, O., Holmgren, G., and Forsman-Semb, K. (1999). Bothnia dystrophy caused by mutations in the cellular retinaldehyde-binding protein gene (RLBP1) on chromosome 15q26. Invest Ophthalmol Vis Sci *40*, 995-1000.

601. Toomes, C., Bottomley, H.M., Jackson, R.M., Towns, K.V., et al. (2004). Mutations in LRP5 or FZD4 underlie the common familial exudative vitreoretinopathy locus on chromosome 11q. Am J Hum Genet *74*, 721-730.

602. Jiao, X., Ventruto, V., Trese, M.T., Shastry, B.S., et al. (2004). Autosomal recessive familial exudative vitreoretinopathy is associated with mutations in LRP5. Am J Hum Genet *75*, 878-884.

603. Nikopoulos, K., Gilissen, C., Hoischen, A., Van Nouhuys, C.E., et al. (2010). Next-generation sequencing of a 40 Mb linkage interval reveals TSPAN12 mutations in patients with familial exudative vitreoretinopathy. Am J Hum Genet *86*, 240-247.

604. Poulter, J.A., Ali, M., Gilmour, D.F., Rice, A., et al. (2010). Mutations in TSPAN12 cause autosomal-dominant familial exudative vitreoretinopathy. Am J Hum Genet *86*, 248-253.

605. Riazuddin, S.A., Zulfiqar, F., Zhang, Q., Sergeev, Y.V., et al. (2005). Autosomal recessive retinitis pigmentosa is associated with mutations in RP1 in three consanguineous Pakistani families. Invest Ophthalmol Vis Sci *46*, 2264-2270.

606. Malécot, G. (1948). Les mathématiques de l'hérédité.(Paris, Masson et Cie).

607. Wright, S. (1922). Coefficients of inbreeding and relationship. American Naturalist, 330-338.

608. Wright, S. (1950). Genetical structure of populations. Nature *166*, 247-249.

609. Bittles, A. (2001). Consanguinity and its relevance to clinical genetics. Clin Genet *60*, 89-98.

610. Ott, J. (1999). Analysis of human genetic linkage.(Baltimore, John Hopkins University Press).

611. Karlin, S. and Liberman, U. (1978). Classifications and comparisons of multilocus recombination distributions. Proc Natl Acad Sci U S A *75*, 6332-6336.

612. McPeek, M.S. and Speed, T.P. (1995). Modeling interference in genetic recombination. Genetics *139*, 1031-1044.

613. Renwick, J.H. (1969). Progress in mapping human autosomes. Br Med Bull *25*, 65-73.

614. Hodge, S.E., Flodman, P.L., Duryea, M.F., and Spence, M.A. (1998). Estimating recombination fraction separately for males and females: a counterintuitive result. Hum Hered *48*, 42-48.

615. Kong, A., Gudbjartsson, D.F., Sainz, J., Jonsdottir, G.M., et al. (2002). A high-resolution recombination map of the human genome. Nat Genet *31*, 241-247.

616. Browning, S.R. (2000). A Monte Carlo approach to calculating probabilities for continuous identity by descent data. J Appl Prob, 850-864.

617. Liberman, U. and Karlin, S. (1984). Theoretical models of genetic map functions. Theor Popul Biol *25*, 331-346.

618. Zhao, H., McPeek, M.S., and Speed, T.P. (1995). Statistical analysis of chromatid interference. Genetics *139*, 1057-1065.

619. Bennett, J.H. (1954). The distribution of heterogeneity upon inbreeding. J R Stat Soc *16*, 88-99.

620. Bailey, N.Y.J. (1961). Introduction to the mathematical theory of genetic linkage. (Oxford, Clarendon Press), 200-203.

621. Morgan, T.H. (1928). The theory of genes.(New Haven, Yale University Oress).

622. Kosambi, D.D. (1944). The estimation of map distances from recombination values. Ann Eugen, 172-175.

623. Spiegel, M.R. (1975). Schaum's outline of theory and problems of probability and statistics. (New York, McGraw-Hill), 38-42.

624. Grinstead, C.M. and Snell, J.M. (1997). Introduction to probability. 285-293.

625. Erlang, A.K. (1917). Solution of some problems in the theory of probabilities of significance in automatic telephone exchanges. The Post Office Electrical Engineers' Journal 189-197.

626. Hillier, F.S. and Lieberman, G.J. (2005). Introduction to operations research. (Boston, McGraw Hill), 798-800.

6 APPENDIX

6.1 Computing Probabilities for Continuous Autozygous Segments in Consanguineous Pedigrees

6.1.1 Coefficient of Inbreeding and Consanguinity

Wright's (section 1.1.1.4) coefficient of inbreeding, *f* (as redefined by Malécot), is the probability of two alleles at any locus in an individual being autozygous [606-607]. Wright's equation for calculating *f* is [607-608]:

$f = \sum[(1/2)^m (1+f_a)]$

where *f* is the coefficient of inbreeding for the person in question, f_a is the coefficient of inbreeding for the common ancestor, *m* is the total number of zygotes in the path and $\sum$ represents the sum for all common ancestor alleles. Common ancestors are assumed to be non-inbred and unrelated; therefore, $f_a = 0$.

Consanguineous marriage is most commonly defined as a union between a couple related as second cousins or closer, equivalent to a coefficient of inbreeding in their progeny of $f \geq 0.0156$ [609].

6.1.2 Crossing Over

In diploid eukaryotes, during meiosis, each of the two (paternal and maternal) homologous chromosome copies duplicates to form two pairs of strands (chromatids). All four resulting strands line up together forming a very tight bundle. During the prophase of meiosis I, homologs separate from each other at most places but maintain one or more zones of physical contact known as chiasmata (figure 6-1). Chiasmata reflect the occurrence of crossover between chromatids, *i.e.* breakage of the double helix in one paternal and one maternal

chromatid and joining of maternal and paternal ends. While chiasmata can be observed cytogenetically, crossovers are a feature of genetic marker maps [610]. Correspondence between cytological chiasmata and genetic crossing-over is assumed although this assumption is not absolutely accurate [611]. It is also assumed that the two chromatids involved in any particular crossover cannot be the two copies of a single homologous chromosome (sister chromatids) [612]. The fact that chiasmata are more frequent in female meioses [613-615] is ignored in this analysis.

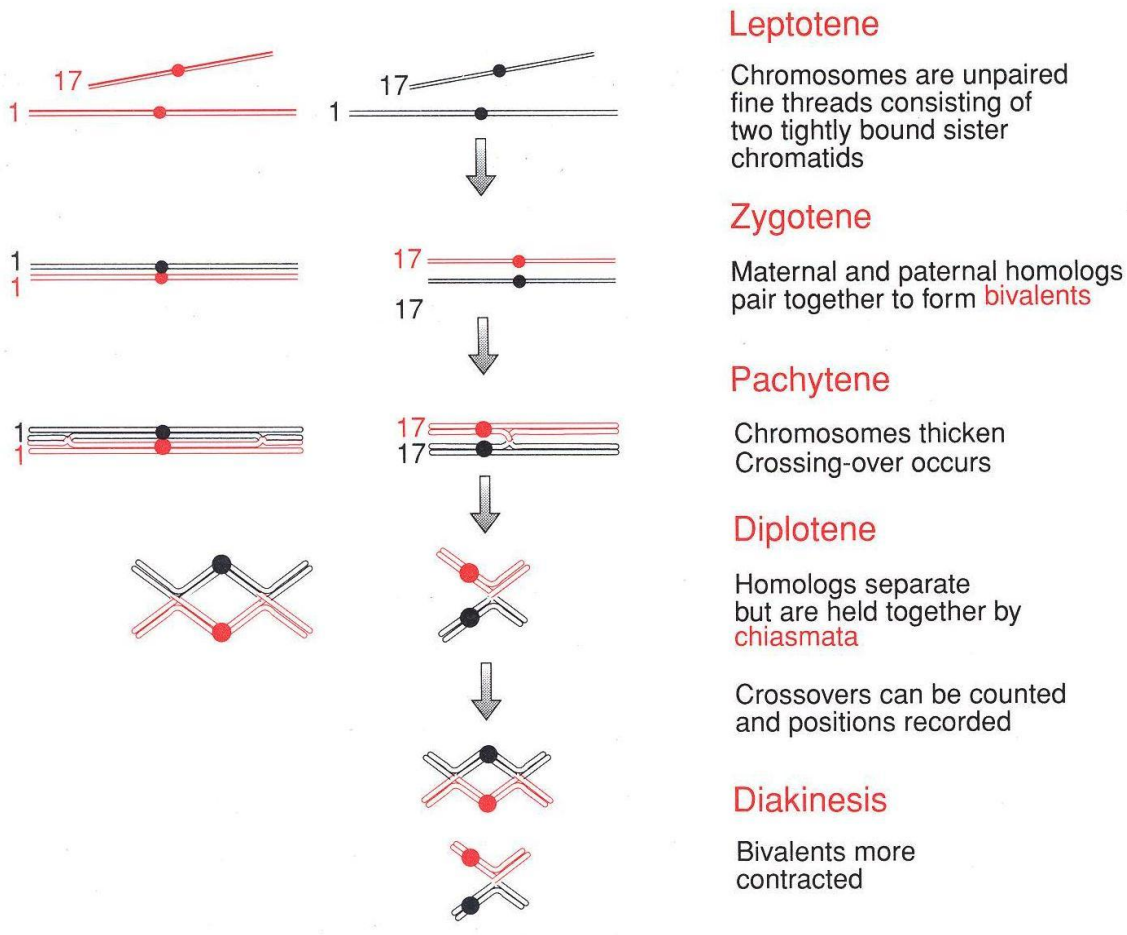

Figure 6-1. The five stages of prophase in meiosis.
Two pairs of homologs are shown (chromosomes 1 and 17) [134].

It is known that the locations of multiple crossovers on a chromosome at meiosis are not independent but exhibit crossover interference, operating whenever crossover events fail to occur completely "at random" [616]. Crossover interference may be of two types: (a) chiasma interference (positive or negative) which reflects the influence on formation of a new chiasma by an

existing chiasma and (b) chromatidal interference which refers to the correlation of the two chromatides of the next crossover event to those that participated in the preceding or neighboring crossover [617]. There is little consistent evidence of chromatid interference [618] and it is assumed to be zero.

6.1.3 Map Distance

For simplicity purposes this section mainly focuses on two-point analysis. Crossovers may lead to what is known as “homologous recombination” and the following relation holds between crossover and recombination: an odd number of crossover points between two loci on a gamete leads to recombination whereas an even point leads to nonrecombination [610]. Recombination fraction (*θ;* see also section 1.1.1.2) expresses the probability that an odd number of crossovers (recombination) will take place between two loci during meiosis. By definition, however far apart the loci are, θ cannot exceed 0.5; therefore, it is not an additive distance measure. The major reason for this nonadditivity is the occurrence of multiple crossovers between the loci making them either linked (recombination fraction $0 \leq \theta < 0.5$) or not linked ($\theta = 0.5$). It is the average number of crossovers between loci that serves as a stochastic measure of distance between loci. The nonadditive recombination fraction θ can be converted into an additive map distance $x = f(\theta)$ using transformations called mapping functions. The map distance (in Morgans) between two chromosomal points *a* and *b* is denoted by x_{ab} and is defined as the expected (average) number of crossovers per meiosis occurring in a gamete in [*a, b*] [611]. Another definition is: genetic map length equals one half of the expected number of chiasmata in the given region of the germ plasm. This can be explained by the fact that an offspring receives one of the four chromatids; hence, assuming no interference, each chiasma resolves as a crossover in the offspring with probability one half, independent of the resolution of other chiasmata [616, 619].

The main method for constructing map functions is the differential equation method introduced by Haldane in 1919; this makes two assumptions: (a) any

recombination frequency θ can be regarded as a function $\theta = \theta(x)$ of the map distance x of the segment in question; (b) the recombination frequency is approximately equal to map distance for short intervals, *i.e.*, $\theta(x) \approx x$ for x small [29, 611, 617].

Using these assumptions many different map functions have been developed, each one assuming different mechanisms of crossover interference and generated by various specifications of a parameter called coefficient of coincidence $C(x)$ [620].

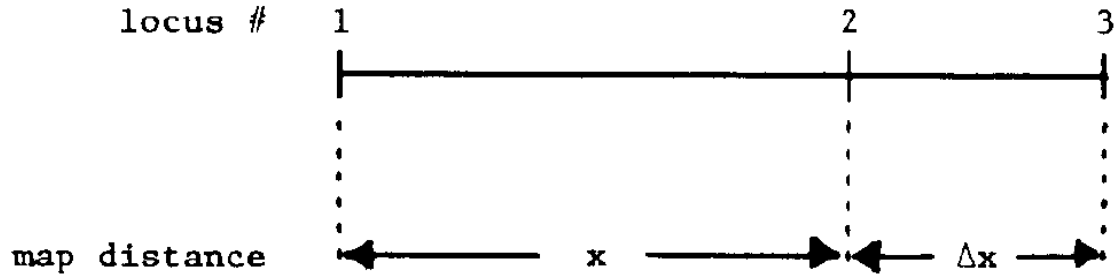

Figure 6-2. Map distance schematic.

To understand $C(x)$, consider three loci as shown in figure 6-2 and let the corresponding recombination frequencies between the loci be $\theta_{12} = \theta(x)$, $\theta_{13} = \theta(x+\Delta x)$, $\theta_{23} = \theta(\Delta x)$. If $C(x, \Delta x)$ is the coefficient of coincidence between the interval $(0, x)$ and the increment $(x, x+\Delta x)$, then $C(x, \Delta x)$ is given by the following equation [617]:

$$\theta(x+\Delta x) = \theta(x) + \theta(\Delta x) - 2C(x, \Delta x)\, \theta(x)\, \theta(\Delta x).$$

The most commonly used functions are found in table 6-1.

Table 6-1. Main map functions

Source	Coefficient of coincidence (interference)	Map function
Haldane [29]	1	$\theta = (1-e^{-2x})/2$
Morgan [621]	0	$\theta = x$
Kosambi [622]	2 $\theta(x)$	$\theta = (e^{4x}-1)/(e^{4x}+1)$

Haldane's function represents the case of no interference [$C(x) = 1$], whereas Morgan's function $\theta(x) = x$ represents complete interference [$C(x) = 0$] such that a crossover event occurring in one interval precludes its occurrence in any subsequent small interval. Coefficient of coincidence in Kosambi's function [$C(x) = 2\,\theta(x)$] assumes that for long segments with $\theta \rightarrow 1/2$ interference vanishes ($C \rightarrow 1$), whereas for short segments ($\theta \rightarrow 0$) the degree of interference becomes complete ($C \rightarrow 0$) [617].

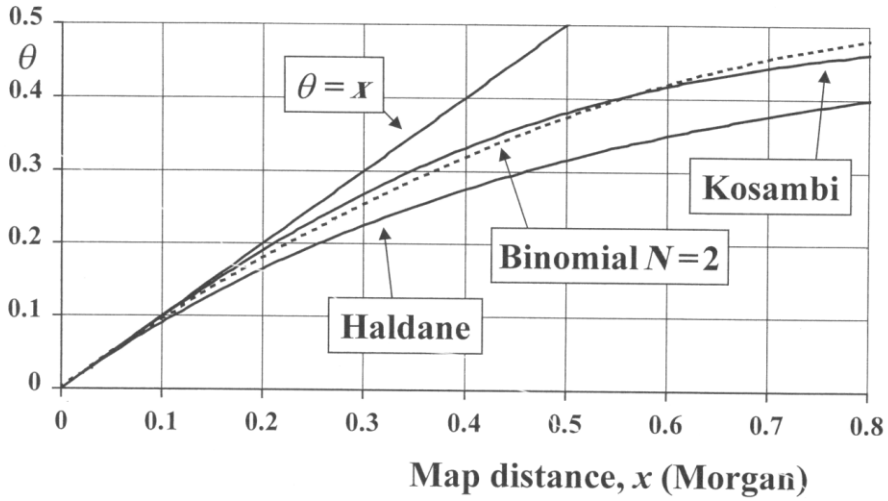

Figure 6-3. Graphs of Morgan ($\theta = x$), Haldane and Kosambi functions (modified from [610]). For small distances (with $\theta \leq 0.05$), any map function is appropriate.

6.1.4 Probability Distribution of Autozygous Fragments

Let a length x cM of a chromosome be considered as divided into a very large number N of small equal portions Δx ($x = N\,\Delta x$). As Δx is very small, the map distance Δx equals the recombination frequency $\theta(\Delta x)$ (see figure 6-3).

A random variable is a variable whose value is a numerical outcome. As map distance $x \in (0; +\infty)$ is a continuous random variable, its relative likelihood to

occur at a given point in the observation space is described by its probability density function [623]. Let f(x) be the probability density function of x with f(x) ≥ 0 and $\int_0^{+\infty} f(x)\,dx = 1$. The probability $P(X)$ of X having a value between a and b is given by the integral of its probability density function from a to b:

$P\ (a < X < b) = \int_a^b f(x)dx$

In a similar fashion, the probability of X being between x and $x + \Delta x$ is:

$P\ (x \le X \le x+\Delta x) = \int_x^{x+\Delta x} f(u)\ du$

From the geometric interpretation of the definite integral, for small Δx, we have:

$P\ (x \le X \le x+\Delta x) = \int_x^{x+\Delta x} f(u)\ du = f(x)\ \Delta x$ (equation 1)

Let the following functions of $x \in (0; +\infty)$ be defined as follows:
$P_0\ (x)$ as the probability of no recombination in an interval of genetic distance x; $P_1\ (x)$ as the probability of at least one crossover in an interval of genetic distance x.

From figure 6-3 and as Δx is small (with the probability of over two crossovers being close to 0) we have:
$P_0\ (\Delta x) = 1 - P_1\ (\Delta x) = 1 - \theta(\Delta x) = 1 - \Delta x$

As $x = N\ \Delta x$, assuming no interference (Haldane's model), the probability of no recombination in x equals the probability of no recombination in each of the N Δx-sized intervals making

$P_0\ (x) = [P_0\ (\Delta x)]^N = (1 - \Delta x)^N$ (equation 2)

Let #1 in figure 6-2 be a heterozygous marker at the q tip (point 0 of the genetic distance) of a chromosome in a noninbred individual (common ancestor). The probability that #1 will be identical by descent along two distinct

paths (paternal and maternal) involving in total *m* meioses from this single ancestor is $f = (1/2)^m$

For *m* meioses, the probability of observing a continuous identical by descent segment of size *X* (from locus #1 to locus #3) equals the probability of no crossover between #1 and #2 in *m* meioses [$P_{0m}(x)$] and at least one crossover in the very small interval between #2 and #3 [$P_{1m}(\Delta x)$].

$$P\,(x \le X \le x+\Delta x) = P_{0m}\,(x)\;P_{1m}\,(\Delta x) \qquad \text{(equation 3)}$$

Using equation 2, $P_{0m}\,(x)$ and $P_{1m}\,(\Delta x)$ are calculated as follows:

$$P_{0m}\,(x) = [P_0\,(x)]^m = \{[P_0\,(\Delta x)]^N\}^m = (1-\Delta x)^{Nm}$$

As $N = \frac{x}{\Delta x}$

$$P_{0m}\,(x) = [(1-\Delta x)^{\frac{1}{\Delta x}}]^{mx} \qquad \text{(equation 4)}$$

$$P_{1m}\,(\Delta x) = 1 - P_{0m}(\Delta x) = 1 - [P_0(\Delta x)]^m = 1 - (1-\Delta x)^m \qquad \text{(equation 5)}$$

Applying the formula $a^n - b^n = (a-b)(a^{n-1} + a^{n-2}\,b + a^{n-3}\,b^2 + \ldots + b^{n-1})$ for $a=1$, $b=1-\Delta x$ and $n=m$ in equation 5, we get:

$$P_{1m}\,(\Delta x) = 1^m - (1-\Delta x)^m = 1^{m-1} + 1^{m-2}(1-\Delta x) + \ldots + (1-\Delta x)^{m-1} \qquad \text{(equation 6)}$$

Combining equations 1, 3, 4 and 6 we have:

$$f(x)\,\Delta x = [(1-\Delta x)^{\frac{1}{\Delta x}}]^{mx}\;[1^{m-1} + 1^{m-2}(1-\Delta x) + \ldots + (1-\Delta x)^{m-1}]\,\Delta x \quad \rightarrow$$

$$f(x) = [(1-\Delta x)^{\frac{1}{\Delta x}}]^{mx}\;[1^{m-1} + 1^{m-2}(1-\Delta x) + \ldots + (1-\Delta x)^{m-1}] \qquad \text{(equation 7)}$$

For $\Delta x \to 0$ we have:

$\lim_{\Delta x \to 0}[(1-\Delta x)^{\frac{1}{\Delta x}}]^{mx} = e^{-mx}$ (from the definition of the number *e*) and

$\lim_{\Delta x \to 0}[1^{m-1} + 1^{m-2}(1-\Delta x) + \ldots + (1-\Delta x)^{m-1}] \approx m$.

Therefore equation 7 becomes:

$$f(x) = m\,e^{-mx} \qquad \text{(equation 8)}$$

The probability density function of equation 8 is for a spot *x* cM from point 0. For an arbitrary point in the genome were autozygosity is observed, let *x* and *y*, both in the interval (0, +∞), be the genetic distances to its left and right side till the next crossover. If f_x and f_y are the probability density functions for these two variables, we have shown that

$f_x(x) = f_y(x) = m\, e^{-mx}$

For $z = x + y$ we have [624]:

$$f_z(z) = \int_0^{+\infty} f_x(z-y)\, f_y(y)\mathrm{d}y = \int_0^z m\, e^{-m(z-y)}\ m\ e^{-my}\mathrm{d}y = \int_0^z m^2\, e^{-mz}\mathrm{d}y\ \ m^2 \rightarrow$$

$$f_z(z) = m^2\ z\ e^{-mz} \qquad \text{(equation 9)}$$

This is an Erlang-2 (k=2) distribution [625-626] of $z \in (0; +\infty)$ with a mean $\mu = \frac{k}{m} = \frac{2}{m}$ and a variance $\mathrm{var}(z) = \frac{k}{m^2} = \frac{2}{m^2}$ where m being the total number of meioses from the founder.

6.2 Python Code for Homozygosity Mapping

The program is running on a Ubuntu 10.04 Linux machine (144.82.133.7) with python 2.6.5, MySQL 5.1 and a python-mysqldb 1.2.2-7ubuntu1 module. After connecting to mysql (`$mysql –u username –p`), two databases ("panos2" [`mysql> CREATE DATABASE panos2;`] and "panos3" [`mysql> CREATE DATABASE panos3; `] should be created. To use type plum or, preferably, plum --rs.

Input files are comma-separated values (CSV) files containing either annotation information (downloaded from http://www.affymetrix.com; for Genome-Wide Human SNP Array 6.0, relevant file can be downloaded from http://www.affymetrix.com/support/technical/byproduct.affx?product=genomewidesnp_6]) or genotyping data from an individual (typically output from the Affymetrix Genotyping Console Software [http://www.affymetrix.com/browse/level_seven_software_products_only.jsp?productId=131535&categoryId=35625#1_1]. The latter CSV file should be arranged so that the first column corresponds to ProbeSetID, the second to Code (AA, AB, BB, NoCall) and the fourth to DbSnpRsID.

```
#!/usr/bin/env python
# encoding: utf-8

import sys
import os
import MySQLdb


def printOptions():

        print "\n2010B PLUM\n"
        print "Make a choice:"
        print "1. Import new family member to database"
        print "2. Generate the input data for a family"
        print "3. Run the script for a family"
        print "4. Make a csv file from a table"
        print "5. Find common areas between families"
        print "6. Import new annotation file"
        print "7. Delete data"
        print "8. Quit"
        print "Your Choice: ",
        answer = sys.stdin.readline()
        if answer.split('\n')[0] == '1':
                return 1
        elif answer.split('\n')[0] == '2':
                return 2
        elif answer.split('\n')[0] == '3':
                return 3
        elif answer.split('\n')[0] == '4':
                return 4
        elif answer.split('\n')[0] == '5':
                return 5
        elif answer.split('\n')[0] == '6':
                return 6
        elif answer.split('\n')[0] == '7':
                return 7
        elif answer.split('\n')[0] == '8':
                return 8
        else:
                print "Please chose one of the available choices"
                printOptions()


def checkTable(db,tableName):
        sqlQuery = 'SHOW TABLES'
        cursor = db.cursor()
        cursor.execute(sqlQuery)
        result = cursor.fetchall()
        exists = 0
        for table in result:
                if table[0] == tableName:
```

```
                        exists = 1
        cursor.close()
        return exists


def initialDBSetup(db,DBchoice):
        cursor = db.cursor()

        create_families_query = 'CREATE TABLE families ( \
        FamilyID varchar(50) NOT NULL,\
        FatherID varchar(50) DEFAULT NULL, \
        MotherID varchar(50) DEFAULT NULL, \
        IndividualID1 varchar(50) DEFAULT NULL, \
        IndividualID2 varchar(50) DEFAULT NULL, \
        IndividualID3 varchar(50) DEFAULT NULL, \
        IndividualID4 varchar(50) DEFAULT NULL, \
        IndividualID5 varchar(50) DEFAULT NULL, \
        IndividualID6 varchar(50) DEFAULT NULL, \
        IndividualID7 varchar(50) DEFAULT NULL, \
        IndividualID8 varchar(50) DEFAULT NULL, \
        IndividualID9 varchar(50) DEFAULT NULL, \
        IndividualID10 varchar(50) DEFAULT NULL, \
        PRIMARY KEY (FamilyID) \
        ) ENGINE=MyISAM DEFAULT CHARSET=utf8'
        cursor.execute(create_families_query)

        if DBchoice == 0:
                create_annotation_query = 'CREATE TABLE annotation ( \
                ProbeSetID varchar(20) NOT NULL, \
                DbSnpRsID varchar(20) NOT NULL, \
                Chromosome varchar(2) NOT NULL, \
                ChromosomeStart varchar(7) NOT NULL, \
                CytoBand varchar(10) NOT NULL, \
                GeneticMap varchar(255) NOT NULL, \
                PRIMARY KEY (ProbeSetID) \
                ) ENGINE=MyISAM DEFAULT CHARSET=utf8'
        else:
                create_annotation_query = 'CREATE TABLE annotation ( \
                ProbeSetID varchar(20) NOT NULL, \
                DbSnpRsID varchar(20) NOT NULL, \
                Chromosome varchar(2) NOT NULL, \
                ChromosomeStart varchar(7) NOT NULL, \
                CytoBand varchar(10) NOT NULL, \
                GeneticMap varchar(255) NOT NULL, \
                PRIMARY KEY (DbSnpRsID) \
                ) ENGINE=MyISAM DEFAULT CHARSET=utf8'
        cursor.execute(create_annotation_query)

        create_families_status_query = 'CREATE TABLE families_status ( \
        FamilyID varchar(50) NOT NULL,\
        IndividualID1 varchar(5) DEFAULT NULL, \
        IndividualID2 varchar(5) DEFAULT NULL, \
```

```
        IndividualID3 varchar(5) DEFAULT NULL, \
        IndividualID4 varchar(5) DEFAULT NULL, \
        IndividualID5 varchar(5) DEFAULT NULL, \
        IndividualID6 varchar(5) DEFAULT NULL, \
        IndividualID7 varchar(5) DEFAULT NULL, \
        IndividualID8 varchar(5) DEFAULT NULL, \
        IndividualID9 varchar(5) DEFAULT NULL, \
        IndividualID10 varchar(5) DEFAULT NULL, \
        PRIMARY KEY (FamilyID) \
        ) ENGINE=MyISAM DEFAULT CHARSET=utf8'
        cursor.execute(create_families_status_query)

        db.commit()
        cursor.close()


def importFamilyMember(db,DBchoice):
        # read the id of the individual and check for correct input
        while 1:
                print "Individual ID: ",
                individualID = sys.stdin.readline()
                try:
                        individualID = int(individualID.split('\n')[0])
                        print 'Numeric values not allowed'
                except Exception, e:
                        individualID = individualID.split('\n')[0]
                        break

        # read the type of the individual father/mother/child
        exit = False
        while not exit:
                print "Individual Type ('f' for father/'m' for mother/'c' for child): ",
                individualType = sys.stdin.readline()
                individualType = individualType.split('\n')[0]
                if individualType == "f" or individualType == "m":
                        break
                # if it is a child check if it is affected or unaffected
                if  individualType == "c":
                        while 1:
                                print "Status ('aff' for affected/'unaff' for unaffected): ",
                                status = sys.stdin.readline()
                                status = status.split('\n')[0]
                                if status == "aff" or status == "unaff":
                                        exit = True
                                        break

        # read the family ID; all individuals of the same family need to have the same family ID, otherwise a new family will be created

        while 1:
                print "Enter the family ID of the individual.\nThe family ID needs to be the SAME\nfor all family members otherwise\na new family will
be created\nFamily ID: ",
                familyID = sys.stdin.readline()
```

```
                try:
                        familyID = int(familyID.split('\n')[0])
                        print 'Numeric values not allowed'
                except Exception, e:
                        familyID = familyID.split('\n')[0]
                        break
        # read the path of the data file of the individual
        fileNameOK = False
        while not fileNameOK:
                print "Full path of text file: ",
                filePath = sys.stdin.readline()
                filePath = filePath.split('\n')[0]
                if os.path.isfile(filePath):
                        fileNameOK = True
                else:
                        print 'File does not exist'

        # check if individual exists; if not import it

        if checkTable(db,individualID) == 0:
                cursor = db.cursor()
                # check if the family with the given ID exists or not
                check_family_query = 'SELECT * FROM families WHERE familyID=\''+familyID+'\''
                cursor.execute(check_family_query)
                results = cursor.fetchall()
                nrows = int(cursor.rowcount)
                check = 1
                column_number = -1
                if nrows == 0: # family does not exist insert a row in the families table
                        insert_families_query = 'INSERT INTO families VALUES ("%s", null, null, null, null, null, null, null, null, null, null, null,
null)'%(familyID)
                        cursor.execute(insert_families_query)

                        insert_families_status_query = 'INSERT INTO families_status VALUES ("%s", null, null, null, null, null, null, null, null, null,
null)'%(familyID)
                        cursor.execute(insert_families_status_query)

                if individualType == "f": # individual is the father
                        update_families_father_query = 'UPDATE families SET FatherID=\''+individualID+'\' WHERE familyID=\''+familyID+'\''
                        cursor.execute(update_families_father_query)
                        column_number = 1

                elif individualType == "m": # individual is the mother
                        update_families_mother_query = 'UPDATE families SET MotherID=\''+individualID+'\' WHERE familyID=\''+familyID+'\''
                        cursor.execute(update_families_mother_query)
                        column_number = 2

                else: # individual is a child
                        if nrows == 0: # no other children exist till now because the family was just created
                                update_families_child_query = 'UPDATE families SET IndividualID1=\''+individualID+'\' WHERE familyID=\''+familyID+'\''
                                cursor.execute(update_families_child_query)
```

```
                                update_families_status_child_status_query = 'UPDATE families_status SET IndividualID1=\''+status+'\' WHERE
familyID=\''+familyID+'\''
                                cursor.execute(update_families_status_child_status_query)
                        else:
                                # other children already exist and we need to find the first individualID{number} available
                                # scan all columns to see the first empty individual and update the entry
                                column_number = 3
                                while column_number < 12:
                                        if results[0][column_number] == None:
                                                update_families_individualID_query = 'UPDATE families SET IndividualID'+str(column_number-
2)+'=\''+individualID+'\' WHERE familyID=\''+familyID+'\''
                                                cursor.execute(update_families_individualID_query)
                                                update_families_status_individualID_status_query = 'UPDATE families_status SET
IndividualID'+str(column_number-2)+'=\''+status+'\' WHERE familyID=\''+familyID+'\''
                                                cursor.execute(update_families_status_individualID_status_query)
                                                break
                                        column_number += 1
                                # there is a limit that allows only families with maximum 10 children. tough luck
                                if column_number == 12:
                                        print 'Individual not imported. Already 10 children exist in the database.'
                                        check = 0
                if check == 1: # create table for the individual

                        if DBchoice == 0:
                                create_individual_query = 'CREATE TABLE '+individualID+' ( \
                                ProbeSetID varchar(20) NOT NULL, \
                                Code varchar(7) NOT NULL, \
                                Confidence varchar(10) NOT NULL, \
                                DbSnpRsID varchar(20) NOT NULL, \
                                PRIMARY KEY (ProbeSetID) \
                                ) ENGINE=MyISAM DEFAULT CHARSET=utf8'
                        else:
                                create_individual_query = 'CREATE TABLE '+individualID+' ( \
                                ProbeSetID varchar(20) NOT NULL, \
                                Code varchar(7) NOT NULL, \
                                Confidence varchar(10) NOT NULL, \
                                DbSnpRsID varchar(20) NOT NULL, \
                                PRIMARY KEY (DbSnpRsID) \
                                ) ENGINE=MyISAM DEFAULT CHARSET=utf8'
                        cursor.execute(create_individual_query)
                        try:
                                load_data_query = 'LOAD DATA LOCAL INFILE \''+filePath+'\' INTO TABLE '+individualID+' FIELDS TERMINATED BY \'\t\'
LINES TERMINATED BY \'\r\n\' IGNORE 6 LINES'
                                cursor.execute(load_data_query)
                        except Exception, e:
                                print 'File could not be imported...'
                                drop_table_query = 'DROP TABLE '+individualID
                                cursor.execute(drop_table_query)
                                if column_number == 1:
                                        update_families_father_query = 'UPDATE families SET FatherID=NULL WHERE familyID=\''+familyID+'\''
                                        cursor.execute(update_families_father_query)
                                elif column_number == 2:
```

```
                                        update_families_mother_query = 'UPDATE families SET MotherID=NULL WHERE familyID=\''+familyID+'\''
                                        cursor.execute(update_families_mother_query)
                                else:

                                        update_families_individualID_query = 'UPDATE families SET IndividualID'+str(column_number-2)+'=NULL WHERE
familyID=\''+familyID+'\''
                                        cursor.execute(update_families_individualID_query)
                                        update_families_status_individualID_status_query = 'UPDATE families_status SET IndividualID'+str(column_number-
2)+'=NULL WHERE familyID=\''+familyID+'\''
                                        cursor.execute(update_families_status_individualID_status_query)

                db.commit()
                cursor.close()
        # if member exists print message
        else:
                print 'Individual '+individualID+' already exists in the database'


def generateInputData(db,DBchoice):
        cursor = db.cursor()
        drop_children_query = 'DROP TABLE IF EXISTS children'
        cursor.execute(drop_children_query)
        familiesID_query = 'SELECT familyID from families'
        cursor.execute(familiesID_query)
        families = cursor.fetchall()
        exit = False
        while not exit:
                for f in families:
                        print f[0]
                exit2 = False
                while not exit2:
                        print "Family ID: ",
                        familyID = sys.stdin.readline()
                        try:
                                familyID = int(familyID.split('\n')[0])
                                print 'Numeric values not allowed'
                        except Exception, e:
                                familyID = familyID.split('\n')[0]
                                for f in families:
                                        if f[0] == familyID:
                                                exit = True
                                                exit2 = True
                                                break
        aff = [] # list with all the affected Individual IDs
        unaff = [] # list with all the unaffected Individual IDs
        sqlQuery3 = 'SELECT * from families_status WHERE familyID=\''+familyID+'\''
        cursor.execute(sqlQuery3)
        results = cursor.fetchall()
        print results[0]
        i = 1
        while i < 11:
                if results[0][i] == "aff":
```

```
                aff.append(i)
        if results[0][i] == "unaff":
                unaff.append(i)
        i += 1
print aff
print unaff

# if affected children exist
if aff.__len__() > 0:
        sqlQuery4 = 'SELECT '
        for a in aff:
                sqlQuery4 += 'IndividualID'+str(a)+','
        sqlQuery4 = sqlQuery4.strip(',')
        sqlQuery4 += ' FROM families WHERE familyID=\''+familyID+'\''
        cursor.execute(sqlQuery4)
        aff = cursor.fetchall()[0]
        # create a temporary table called affected to join all the affected individuals to
        if DBchoice == 0:
                sqlQuery6 = 'CREATE TABLE affected ( ProbeSetID varchar(20) NOT NULL, '
                sqlQuery7 = 'INSERT INTO affected SELECT '+aff[0]+'.ProbeSetID,'
        else:
                sqlQuery6 = 'CREATE TABLE affected ( DbSnpRsID varchar(20) NOT NULL, '
                sqlQuery7 = 'INSERT INTO affected SELECT '+aff[0]+'.DbSnpRsID,'
        i = 0
        while i < aff.__len__():
                sqlQuery6 += 'Code'+str(i+1)+' varchar(7) DEFAULT NULL, Confidence'+str(i+1)+' varchar(10) DEFAULT NULL, '
                sqlQuery7 += aff[i]+'.Code,'+aff[i]+'.Confidence,'
                i += 1
        if DBchoice == 0:
                sqlQuery6 += 'PRIMARY KEY (ProbeSetID) ) ENGINE=MyISAM DEFAULT CHARSET=utf8'
        else:
                sqlQuery6 += 'PRIMARY KEY (DbSnpRsID) ) ENGINE=MyISAM DEFAULT CHARSET=utf8'
        print sqlQuery6+'\n'
        cursor.execute(sqlQuery6)

        sqlQuery7 = sqlQuery7.strip(',')
        sqlQuery7 += ' FROM '+aff[0]
        i = 1
        while i < aff.__len__():
                if DBchoice == 0:
                        sqlQuery7 += ' INNER JOIN '+aff[i]+' ON '+aff[i-1]+'.ProbeSetID = '+aff[i]+'.ProbeSetID'
                else:
                        sqlQuery7 += ' INNER JOIN '+aff[i]+' ON '+aff[i-1]+'.DbSnpRsID = '+aff[i]+'.DbSnpRsID'
                i += 1
        print sqlQuery7+'\n'
        cursor.execute(sqlQuery7)

# if unaffected children exist
if unaff.__len__() > 0:
        sqlQuery5 = 'SELECT '
        for u in unaff:
                sqlQuery5 += 'IndividualID'+str(u)+','
```

```
        sqlQuery5 = sqlQuery5.strip(',')
        sqlQuery5 += ' FROM families WHERE familyID=\''+familyID+'\''
        cursor.execute(sqlQuery5)
        unaff = cursor.fetchall()[0]

        # create a temporary table called unaffected to join all the affected individuals to
        if DBchoice == 0:
                sqlQuery8 = 'CREATE TABLE unaffected ( ProbeSetID varchar(20) NOT NULL, '
                sqlQuery9 = 'INSERT INTO unaffected SELECT '+unaff[0]+'.ProbeSetID,'
        else:
                sqlQuery8 = 'CREATE TABLE unaffected ( DbSnpRsID varchar(20) NOT NULL, '
                sqlQuery9 = 'INSERT INTO unaffected SELECT '+unaff[0]+'.DbSnpRsID,'
        i = 0
        while i < unaff.__len__():
                sqlQuery8 += 'Code'+str(i+1)+' varchar(7) DEFAULT NULL, Confidence'+str(i+1)+' varchar(10) DEFAULT NULL, '
                sqlQuery9 += unaff[i]+'.Code,'+unaff[i]+'.Confidence,'
                i += 1
        if DBchoice == 0:
                sqlQuery8 += 'PRIMARY KEY (ProbeSetID) ) ENGINE=MyISAM DEFAULT CHARSET=utf8'
        else:
                sqlQuery8 += 'PRIMARY KEY (DbSnpRsID) ) ENGINE=MyISAM DEFAULT CHARSET=utf8'
        print sqlQuery8+'\n'
        cursor.execute(sqlQuery8)

        sqlQuery9 = sqlQuery9.strip(',')
        sqlQuery9 += ' FROM '+unaff[0]
        i = 1
        while i < unaff.__len__():
                if DBchoice == 0:
                        sqlQuery9 += ' INNER JOIN '+unaff[i]+' ON '+unaff[i-1]+'.ProbeSetID = '+unaff[i]+'.ProbeSetID'
                else:
                        sqlQuery9 += ' INNER JOIN '+unaff[i]+' ON '+unaff[i-1]+'.DbSnpRsID = '+unaff[i]+'.DbSnpRsID'
                i += 1
        print sqlQuery9+'\n'
        cursor.execute(sqlQuery9)

# join the affected and/or unaffected children in one table called children
if DBchoice == 0:
        sqlQuery10 = 'CREATE TABLE children ( ProbeSetID varchar(20) NOT NULL, '
else:
        sqlQuery10 = 'CREATE TABLE children ( DbSnpRsID varchar(20) NOT NULL, '
i = 0
while i < aff.__len__() + unaff.__len__():
        sqlQuery10 += 'Code'+str(i+1)+' varchar(7) DEFAULT NULL, Confidence'+str(i+1)+' varchar(10) DEFAULT NULL, '
        i += 1
if DBchoice == 0:
        sqlQuery10 += 'PRIMARY KEY (ProbeSetID) ) ENGINE=MyISAM DEFAULT CHARSET=utf8'
else:
        sqlQuery10 += 'PRIMARY KEY (DbSnpRsID) ) ENGINE=MyISAM DEFAULT CHARSET=utf8'
print sqlQuery10+'\n'
cursor.execute(sqlQuery10)
sqlQuery11 = ''
```

```
if aff.__len__() > 0 and unaff.__len__() > 0:
        sqlQuery11 = 'INSERT INTO children SELECT '
        if DBchoice == 0:
                if aff.__len__() > 0:
                        sqlQuery11 += 'affected.ProbeSetID, '
                else:
                        sqlQuery11 += 'unaffected.ProbeSetID, '
        else:
                if aff.__len__() > 0:
                        sqlQuery11 += 'affected.DbSnpRsID, '
                else:
                        sqlQuery11 += 'unaffected.DbSnpRsID, '
        i = 0
        while i < aff.__len__():
                sqlQuery11 += 'affected.Code'+str(i+1)+',affected.Confidence'+str(i+1)+','
                i += 1
        i = 0
        while i < unaff.__len__():
                sqlQuery11 += 'unaffected.Code'+str(i+1)+',unaffected.Confidence'+str(i+1)+','
                i += 1
        sqlQuery11 = sqlQuery11.strip(',')
        if DBchoice == 0:
                sqlQuery11 += ' from affected inner join unaffected on affected.ProbeSetID = unaffected.ProbeSetID'
        else:
                sqlQuery11 += ' from affected inner join unaffected on affected.DbSnpRsID = unaffected.DbSnpRsID'
elif aff.__len__() > 0 and unaff.__len__() == 0:
        sqlQuery11 = 'INSERT INTO children SELECT * from affected'
else:
        sqlQuery11 = 'INSERT INTO children SELECT * from unaffected'
        print sqlQuery11+'\n'
cursor.execute(sqlQuery11)
sqlQuery12 = 'DROP TABLE IF EXISTS affected'
sqlQuery13 = 'DROP TABLE IF EXISTS unaffected'
cursor.execute(sqlQuery12)
cursor.execute(sqlQuery13)

# join the parents if they exist
sqlQuery14 = 'SELECT FatherID,MotherID from families WHERE familyID=\''+familyID+'\''
cursor.execute(sqlQuery14)
results = cursor.fetchall()[0]
sqlQuery15 = 'SELECT '
fatherExists = False
motherExists = False
if results[0] != None:
        print 'Father exists'
        if DBchoice == 0:
                sqlQuery15 += results[0]+'.ProbeSetID,'+results[0]+'.Code as FatherCode,'+results[0]+'.Confidence as FatherConfidence,'
        else:
                sqlQuery15 += results[0]+'.DbSnpRsID,'+results[0]+'.Code as FatherCode,'+results[0]+'.Confidence as FatherConfidence,'
        fatherExists = True
if results[1] != None:
        print 'Mother exists'
```

```
                motherExists = True
                if fatherExists:
                        sqlQuery15 += results[1]+'.Code as MotherCode,'+results[1]+'.Confidence as MotherConfidence,'
                else:
                        if DBchoice == 0:
                                sqlQuery15 += results[1]+'.ProbeSetID,'+results[1]+'.Code as MotherCode,'+results[1]+'.Confidence as MotherConfidence,'
                        else:
                                sqlQuery15 += results[1]+'.DbSnpRsID,'+results[1]+'.Code as MotherCode,'+results[1]+'.Confidence as MotherConfidence,'
        i = 0;
        while i < aff.__len__() + unaff.__len__():
                sqlQuery15 += 'children.Code'+str(i+1)+', children.Confidence'+str(i+1)+','
                i += 1
        sqlQuery15 = sqlQuery15.strip(',')
        if DBchoice == 0:
                if fatherExists and motherExists:
                        sqlQuery15 += ' FROM '+results[0]+' INNER JOIN children ON '+results[0]+'.ProbeSetID = children.ProbeSetID INNER JOIN
'+results[1]+' ON children.ProbeSetID = '+results[1]+'.ProbeSetID'
                elif fatherExists and not motherExists:
                        sqlQuery15 += ' FROM '+results[0]+' INNER JOIN children ON '+results[0]+'.ProbeSetID = children.ProbeSetID'
                elif motherExists and not fatherExists:
                        sqlQuery15 += ' FROM '+results[1]+' INNER JOIN children ON '+results[1]+'.ProbeSetID = children.ProbeSetID'
                else:
                        sqlQuery15 = 'SELECT * from children'
        else:
                if fatherExists and motherExists:
                        sqlQuery15 += ' FROM '+results[0]+' INNER JOIN children ON '+results[0]+'.DbSnpRsID = children.DbSnpRsID INNER JOIN
'+results[1]+' ON children.DbSnpRsID = '+results[1]+'.DbSnpRsID'
                elif fatherExists and not motherExists:
                        sqlQuery15 += ' FROM '+results[0]+' INNER JOIN children ON '+results[0]+'.DbSnpRsID = children.DbSnpRsID'
                elif motherExists and not fatherExists:
                        sqlQuery15 += ' FROM '+results[1]+' INNER JOIN children ON '+results[1]+'.DbSnpRsID = children.DbSnpRsID'
                else:
                        sqlQuery15 = 'SELECT * from children'
        print sqlQuery15+'\n'

        # create a table for the familyID
        sqlQuery18 = 'DROP TABLE IF EXISTS '+familyID
        cursor.execute(sqlQuery18)

        sqlQuery2 = 'CREATE TABLE '+familyID+' ( \
                ProbeSetID varchar(20) NOT NULL, \
                DbSnpRsID varchar(20) NOT NULL, \
                Chromosome varchar(2) DEFAULT NULL, \
                ChromosomeStart varchar(7) DEFAULT NULL, \
                CytoBand varchar(10) DEFAULT NULL, \
                GeneticMap varchar(255) DEFAULT NULL,'

        sqlQuery16 = 'INSERT INTO '+familyID+' SELECT annotation.ProbeSetID,\
        annotation.DbSnpRsID,\
        annotation.Chromosome,\
        annotation.ChromosomeStart,\
        annotation.Cytoband,\
```

```
        annotation.GeneticMap,'
        if fatherExists:
                sqlQuery16 += 'temp.FatherCode,temp.FatherConfidence,'
                sqlQuery2 += 'FatherCode varchar(7) DEFAULT NULL, FatherConfidence varchar(10) DEFAULT NULL,'
        if motherExists:
                sqlQuery16 += 'temp.MotherCode,temp.MotherConfidence,'
                sqlQuery2 += 'MotherCode varchar(7) DEFAULT NULL, MotherConfidence varchar(10) DEFAULT NULL,'
        i = 0;
        while i < aff.__len__() + unaff.__len__():
                sqlQuery16 += 'temp.Code'+str(i+1)+', temp.Confidence'+str(i+1)+','
                sqlQuery2 += 'Code'+str(i+1)+' varchar(7) DEFAULT NULL, Confidence'+str(i+1)+' varchar(10) DEFAULT NULL,'
                i += 1
        sqlQuery16 += 'NULL, NULL, NULL'
        if DBchoice == 0:
                sqlQuery16 += ' FROM annotation INNER JOIN ('+sqlQuery15+') AS temp ON annotation.ProbeSetID = temp.ProbeSetID WHERE
CAST(annotation.GeneticMap AS DECIMAL(20,15)) AND temp.ProbeSetID NOT LIKE \"AFFX-%\"' #ORDER BY annotation.Chromosome'
        else:
                sqlQuery16 += ' FROM annotation INNER JOIN ('+sqlQuery15+') AS temp ON annotation.DbSnpRsID = temp.DbSnpRsID WHERE
CAST(annotation.GeneticMap AS DECIMAL(20,15)) #ORDER BY annotation.Chromosome'
        sqlQuery2 += 'homoz varchar(20) DEFAULT NULL,' \
                'linkage varchar(20) DEFAULT NULL,' \
                'mendel varchar(20) DEFAULT NULL,'
        if DBchoice == 0:
                sqlQuery2 += ' PRIMARY KEY (ProbeSetID) \
                ) ENGINE=MyISAM DEFAULT CHARSET=utf8'
        else:
                sqlQuery2 += ' PRIMARY KEY (DbSnpRsID) \
                ) ENGINE=MyISAM DEFAULT CHARSET=utf8'
        print sqlQuery2+'\n'
        cursor.execute(sqlQuery2)
        print sqlQuery16+'\n'
        cursor.execute(sqlQuery16)

        # sqlQuery17 = 'DROP TABLE IF EXISTS children'
        # cursor.execute(sqlQuery17)
        db.commit()
        cursor.close()


def importNewAnnotationFile(db):
        cursor = db.cursor()
        fileNameOK = False
        while not fileNameOK:
                print "Full path of text file: ",
                filePath = sys.stdin.readline()
                filePath = filePath.split('\n')[0]
                if os.path.isfile(filePath):
                        fileNameOK = True
                else:
                        print 'File does not exist'
        while 1:
                print 'Choose the Genetic Map you want to be imported (1/2/3): ',
```

```
                GMchoice = sys.stdin.readline()
                GMchoice = GMchoice.split('\n')[0]
                if GMchoice == '1' or GMchoice == '2' or GMchoice == '3':
                        GMchoice = int(GMchoice)
                        break
                else:
                        print 'Please choose 1, 2 or 3'
        annotationFILE = open(filePath,'r')
        outputPath = os.path.dirname(filePath)
        if outputPath.__len__() > 0:
                outputPath += '/'+os.path.basename(filePath).split('.csv')[0]+'_short.csv'
        else:
                outputPath = os.path.basename(filePath).split('.csv')[0]+'_short.csv'
        outputFILE = open(outputPath,'w')
        count = 0
        sqlQuery = 'TRUNCATE TABLE annotation'
        cursor.execute(sqlQuery)
        for line in annotationFILE:
                if count > 21:
                        newline =
line.split('\"')[1]+','+line.split('\"')[3]+','+line.split('\"')[5]+','+line.split('\"')[7]+','+line.split('\"')[13]+','+line.split('\"')[23]+'\n'
                        outputFILE.write(newline)
                        if count > 24 and line.split('\"')[23] != "---" and line.split('\"')[1].find('AFFX') == -1:
                                sqlQuery2 = 'INSERT IGNORE INTO annotation VALUES ("%s", "%s", "%s", "%s", "%s",
"%s")'%(line.split('\"')[1],line.split('\"')[3],line.split('\"')[5],line.split('\"')[7],line.split('\"')[13],line.split('\"')[23].split('///')[GMchoic
e-1].split('//')[0].strip(' '))
                                cursor.execute(sqlQuery2)
                count += 1
        outputFILE.close()
        annotationFILE.close()
        db.commit()
        cursor.close()


def makeCSVfile(db):
        cursor = db.cursor()
        showFamiliesQuery = 'SELECT familyID FROM families'
        cursor.execute(showFamiliesQuery)
        results = cursor.fetchall()
        print "Available Families: "
        for table in results:
                        print table[0]
        print "Name of Table: ",
        tableName = sys.stdin.readline()
        tableName = tableName.split('\n')[0]
        found = False
        for table in results:
                if table[0] == tableName:
                        found = True
                        break

        if found:
```

```
                fileName = tableName+'.csv'
                outputFILE = open(fileName,'w')
                print 'Reading from Database...'
                sqlQuery2 = 'SELECT * from '+tableName
                cursor.execute(sqlQuery2)
                results = cursor.fetchall()
                print 'Exporting Data...'
                for row in results:
                        # print row
                        line = ''
                        allNoCall = True
                        for k in range(6,row.__len__()-3,2):
                                if row[k] != 'NoCall':
                                        allNoCall = False
                                        break
                        if not allNoCall:
                                for field in row:
                                        if field != None:
                                                field = field.strip('\r')
                                                line += field+','
                                        else:
                                                line += 'NULL,'
                                line = line.strip(',')
                                outputFILE.write(line+'\n')
                outputFILE.close()
                print 'File '+fileName+' created succesfully at '+os.getcwd()
        else:
                print 'Table \''+tableName+'\' not found'
        db.commit()
        cursor.close()


def homoz(dataList,father,mother,affected,unaffected):
        """
        dataList: a list with the Codes of the family members
        father: boolean that defines father existanse in the data
        mother: boolean that defines mother existanse in the data
        affected: number of affected children
        unaffected: number of unaffected children
        """
        if father and not mother:
                dataList.insert(1,'NoCall')
        if mother and not father:
                dataList.insert(0,'NoCall')
        if not mother and not father:
                dataList.insert(0,'NoCall')
                dataList.insert(0,'NoCall')
        # Affected
        callaff = 0
        geno = ''
        for n in range(2,2 + affected):
                if dataList[n] != 'NoCall':
```

```
                        if geno == '': # first affected
                                geno = dataList[n]
                        elif geno != dataList[n]:
                                return 'EXAFF'
                        callaff += 1
        if geno == 'AB':
                return 'EXAUTO'

        # Parents
        hetparent = 0
        for n in range(0,2):
                if dataList[n] == 'AB':
                        hetparent += 1
        meioses = hetparent * (callaff - 1)
        if hetparent < 2:
                return 'LINK_'+str(meioses)

        # Unaffected
        callunaff = 0
        for n in range(2 + affected,2 + affected + unaffected):
                if dataList[n] != 'NoCall':
                        if dataList[n] == geno:
                                return 'EXUNAFF'
                        callunaff += 1
        meioses = meioses + 2 * callunaff
        return 'LINK_'+str(meioses)


def linkage(dataList,father,mother,affected,unaffected):
        """
        dataList: a list with the Codes of the family members
        father: boolean that defines father existanse in the data
        mother: boolean that defines mother existanse in the data
        affected: number of affected children
        unaffected: number of unaffected children
        """
        if father and not mother:
                dataList.insert(1,'NoCall')
        if mother and not father:
                dataList.insert(0,'NoCall')
        if not mother and not father:
                dataList.insert(0,'NoCall')
                dataList.insert(0,'NoCall')

        # Affected
        geno = ''
        callaff = 0
        for n in range(2,2 + affected):
                if dataList[n] != 'NoCall':
                        if geno == '':
                                geno = dataList[n]
                        elif geno != dataList[n]:
```

```
                                return 'EXAFF'
                        callaff += 1

        # Parents
        hetparent = 0
        for n in range(0,2):
                if dataList[n] == 'AB':
                        hetparent += 1

        meioses = hetparent * (callaff - 1)
        if hetparent < 2:
                return 'LINK_'+str(meioses)

        # Unaffected
        callunaff = 0
        for n in range(2 + affected,2 + affected + unaffected):
                if dataList[n] != 'NoCall':
                        if dataList[n] == geno and geno != 'AB':
                                return 'EXUNAFF'
                        callunaff += 1
        meioses = meioses + 2 * callunaff
        return 'LINK_'+str(meioses)


def mendel(dataList,father,mother):
        if father and not mother:
                dataList.insert(1,'NoCall')
        if mother and not father:
                dataList.insert(0,'NoCall')
        if not mother and not father:
                dataList.insert(0,'NoCall')
                dataList.insert(0,'NoCall')

        dad1 = ''
        mom1 = ''
        dad2 = ''
        mom2 = ''

        if dataList[0] == 'NoCall':
                dad1 = 'NoCall'
        else:
                dad1 = dataList[0][0:1]
                dad2 = dataList[0][1:2]
        if dataList[1] == 'NoCall':
                mom1 = 'NoCall'
        else:
                mom1 = dataList[1][0:1]
                mom2 = dataList[1][1:2]

        # loop through children
        errors = 0
        a1 = ''
```

```
        a2 = ''
        flag = ''
        for n in range(2,dataList.__len__()):
                if dataList[n] != 'NoCall':
                        a1 = dataList[n][0:1]
                        a2 = dataList[n][1:2]
                        flag = 'Error'
                        # trial one a1 from dad, a2 from mom
                        if dad1 == 'NoCall' or a1 == dad1 or a1 == dad2:
                                if mom1 == 'NoCall' or a2 == mom1 or a2 == mom2:
                                        flag = 'OK'
                        # trial two a2 from dad and a1 from mom
                        if dad1 == 'NoCall' or a2 == dad1 or a2 == dad2:
                                if mom1 == 'NoCall' or a1 == mom1 or a1 == mom2:
                                        flag = 'OK'
                        if flag == 'Error':
                                errors += 1
        if errors == 0:
                return 'MenOK'
        else:
                return 'Error_'+str(errors)


def runFunction(db,func,DBchoice,famID=-1):
        cursor = db.cursor()
        familyID = ''
        if famID == -1:
                sqlQuery = 'SELECT familyID FROM families'
                cursor.execute(sqlQuery)
                results = cursor.fetchall()
                print 'Available families: '
                found = False
                while not found:
                        for table in results:
                                print table[0]
                        while 1:
                                print "Select Family ID: ",
                                familyID = sys.stdin.readline()
                                try:
                                        familyID = int(familyID.split('\n')[0])
                                        print 'Numeric values not allowed'
                                except Exception, e:
                                        familyID = familyID.split('\n')[0]
                                        break
                        for table in results:
                                if table[0] == familyID:
                                        found = True
                                        break
                        if not found:
                                print 'Not a valid Family ID:'
        else:
                familyID = famID
```

```
if func != 3:
        while 1:
                print "Threshold: ",
                Threshold = sys.stdin.readline()
                try:
                        Threshold = float(Threshold.split('\n')[0])
                        break
                except Exception, e:
                        print 'Needs to be numeric'
print 'Loading data from the database...'
affected = 0
unaffected = 0
father = False
mother = False
sqlQuery2 = 'SELECT * FROM families_status WHERE familyID=\''+familyID+'\''
cursor.execute(sqlQuery2)
results = cursor.fetchall()[0]
affected = results.count('aff')
unaffected = results.count('unaff')
sqlQuery3 = 'SELECT * FROM families WHERE familyID=\''+familyID+'\''
cursor.execute(sqlQuery3)
results = cursor.fetchall()[0]
if results[1] != None:
        father = True
if results[2] != None:
        mother = True
sqlQuery5 = 'SELECT DISTINCT Chromosome FROM '+familyID+' WHERE Chromosome <> \"--\" AND Chromosome <> \"MT\" ORDER BY Chromosome'
cursor.execute(sqlQuery5)
chromosomeList = cursor.fetchall()
summaryFileName = familyID
resultTableName = familyID
countMembers = 0
if father:
        countMembers += 1
if mother:
        countMembers += 1
countMembers += affected + unaffected
countMembers *= 2
if func == 1:
        summaryFileName += '_homoz_summary.csv'
        resultTableName += '_homoz'
else:
        summaryFileName += '_linkage_summary.csv'
        resultTableName += '_linkage'
summaryFILE = open(summaryFileName,'w')
dropTableQuery = 'DROP TABLE IF EXISTS '+resultTableName
cursor.execute(dropTableQuery)
createResultTableQuery = 'CREATE TABLE '+resultTableName+' ( \
          id int(11) NOT NULL AUTO_INCREMENT,\
          ProbeSetID varchar(20) NOT NULL,\
          DbSnpRsID varchar(20) NOT NULL,\
          Chromosome varchar(2) NOT NULL,\
```

```
          GeneticMap varchar(255) NOT NULL,\
          GeneticDifference varchar(255) DEFAULT NULL,\
          PRIMARY KEY (id)\
        ) ENGINE=MyISAM DEFAULT CHARSET=utf8'
cursor.execute(createResultTableQuery)
if func == 3:
        print 'Running mendel...'
for chromosome in chromosomeList:
        GeneticDifference = 0
        countRowsInbetween = 0
        chromosome = chromosome[0]
        if func == 1:
                print 'Running homoz for chromosome '+chromosome+'...'
        if func == 2:
                print 'Running linkage for chromosome '+chromosome+'...'
        sqlQuery6 = 'SELECT * FROM '+familyID+' WHERE Chromosome=\''+chromosome+'\' ORDER BY CAST(GeneticMap AS DECIMAL(20,15))'
        cursor.execute(sqlQuery6)
        results = cursor.fetchall()
        firstGMValue = 5000000.0
        isFirstLINK = False
        lastGMValue = 5000000.0
        countRow = -1
        firstRow = -1
        notAllLINK = False
        for row in results:
                countRow += 1
                i = 6
                dataList = []
                while i < 6 + countMembers:
                        dataList.append(row[i])
                        i += 2
                func_result = '-89778'
                if func == 1:
                        func_result = homoz(dataList,father,mother,affected,unaffected)
                        if DBchoice == 0:
                                sqlQuery7 = 'UPDATE '+familyID+' SET homoz=\''+func_result+'\' WHERE ProbeSetID=\''+row[0]+'\''
                        else:
                                sqlQuery7 = 'UPDATE '+familyID+' SET homoz=\''+func_result+'\' WHERE DbSnpRsID=\''+row[1]+'\''
                        cursor.execute(sqlQuery7)
                elif func == 2:
                        func_result = linkage(dataList,father,mother,affected,unaffected)
                        if DBchoice == 0:
                                sqlQuery7 = 'UPDATE '+familyID+' SET linkage=\''+func_result+'\' WHERE ProbeSetID=\''+row[0]+'\''
                        else:
                                sqlQuery7 = 'UPDATE '+familyID+' SET linkage=\''+func_result+'\' WHERE DbSnpRsID=\''+row[1]+'\''
                        cursor.execute(sqlQuery7)
                else:
                        func_result = mendel(dataList,father,mother)
                        if DBchoice == 0:
                                sqlQuery7 = 'UPDATE '+familyID+' SET mendel=\''+func_result+'\' WHERE ProbeSetID=\''+row[0]+'\''
                        else:
                                sqlQuery7 = 'UPDATE '+familyID+' SET mendel=\''+func_result+'\' WHERE DbSnpRsID=\''+row[1]+'\''
```

```
                        cursor.execute(sqlQuery7)
                if func == 1 or func == 2:
                        if func_result.find('LINK_') > -1:
                                currentGMValue = float(row[5])
                                if isFirstLINK == False:
                                        firstGMValue = currentGMValue
                                        firstRow = countRow
                                        isFirstLINK = True
                                lastGMValue = currentGMValue
                                countRowsInbetween += 1
                        else:
                                notAllLINK = True
                                GeneticDifference = lastGMValue - firstGMValue
                                firstGMValue = 5000000.0
                                lastGMValue = 5000000.0
                                if GeneticDifference >= Threshold:
                                        sqlQuery7 = 'SELECT * FROM '+familyID+' WHERE Chromosome=\''+chromosome+'\' ORDER BY CAST(GeneticMap AS
DECIMAL(20,15)) LIMIT '+str(firstRow)+','+str(countRowsInbetween)
                                        print 'Found one area with '+str(countRowsInbetween)+' rows and Genetic difference:
'+str(GeneticDifference)
                                        cursor.execute(sqlQuery7)
                                        interestingRows = cursor.fetchall()
                                        line = ''
                                        for field in interestingRows[0]:
                                                if field != None:
                                                        field = field.strip('\r')
                                                        line += field+','
                                        line = line.strip(',')
                                        summaryFILE.write(line+'\n')
                                        line = line.split(',')
                                        insertResultsQuery = 'INSERT INTO '+resultTableName+' VALUES (null, \"'+line[0]+'\", \"'+line[1]+'\",
\"'+line[2]+'\", \"'+line[5]+'\", null)'
                                        cursor.execute(insertResultsQuery)
                                        line = ''
                                        for field in interestingRows[-1]:
                                                if field != None:
                                                        field = field.strip('\r')
                                                        line += field+','
                                        line += str(GeneticDifference)
                                        summaryFILE.write(line+'\n\n')
                                        line = line.split(',')
                                        insertResultsQuery = 'INSERT INTO '+resultTableName+' VALUES (null, \"'+line[0]+'\", \"'+line[1]+'\",
\"'+line[2]+'\", \"'+line[5]+'\", \"'+str(GeneticDifference)+'\")'
                                        cursor.execute(insertResultsQuery)
                                isFirstLINK = False
                                firstRow = -1
                                GeneticDifference = 0
                                countRowsInbetween = 0
                # check in case there is an interesting area ending at the end of the chromosome
                if func_result.find('LINK_') > -1:
                        if not notAllLINK:
                                GeneticDifference = float(results[-1][5]) - float(results[0][5])
```

```
                                firstRow = 0
                        if GeneticDifference >= Threshold:
                                sqlQuery7 = 'SELECT * FROM '+familyID+' WHERE Chromosome=\''+chromosome+'\' ORDER BY CAST(GeneticMap AS DECIMAL(20,15))
LIMIT '+str(firstRow)+','+str(countRowsInbetween)
                                print 'Found one area with '+str(countRowsInbetween)+' rows and Genetic difference: '+str(GeneticDifference)
                                cursor.execute(sqlQuery7)
                                interestingRows = cursor.fetchall()
                                line = ''
                                for field in interestingRows[0]:
                                        if field != None:
                                                field = field.strip('\r')
                                                line += field+','
                                line = line.strip(',')
                                summaryFILE.write(line+'\n')
                                line = line.split(',')
                                insertResultsQuery = 'INSERT INTO '+resultTableName+' VALUES (null, \"'+line[0]+'\", \"'+line[1]+'\", \"'+line[2]+'\",
\"'+line[5]+'\", null)'
                                cursor.execute(insertResultsQuery)
                                line = ''
                                for field in interestingRows[-1]:
                                        if field != None:
                                                field = field.strip('\r')
                                                line += field+','
                                line += str(GeneticDifference)
                                summaryFILE.write(line+'\n\n')
                                line = line.split(',')
                                insertResultsQuery = 'INSERT INTO '+resultTableName+' VALUES (null, \"'+line[0]+'\", \"'+line[1]+'\", \"'+line[2]+'\",
\"'+line[5]+'\", \"'+str(GeneticDifference)+'\")'
                                cursor.execute(insertResultsQuery)
        summaryFILE.close()
        print 'File '+summaryFileName+' created succesfully at '+os.getcwd()
        db.commit()
        cursor.close()


def deleteIndividual(db):
        cursor = db.cursor()
        getAllFamiliesQuery = 'SELECT * from families'
        cursor.execute(getAllFamiliesQuery)
        families = cursor.fetchall()
        for family in families:
                for member in range(1,13):
                        if family[member] != None:
                                print family[member]
        while 1:
                print "Individual ID: ",
                individualID = sys.stdin.readline()
                try:
                        individualID = int(individualID.split('\n')[0])
                        print 'Numeric values not allowed'
                except Exception, e:
                        individualID = individualID.split('\n')[0]
```

```
                if checkTable(db,individualID) == 1:
                        break
                else:
                        print 'Individual does not exist'
deleteTableQuery = 'DROP TABLE '+individualID
cursor.execute(deleteTableQuery)
column_name  = ''
child = False
familyID = ''
member = 0
for family in families:
        for member in range(1,13):
                if family[member] == individualID:
                        familyID = family[0]
                        if member == 1:
                                column_name = 'FatherID'
                        elif member == 2:
                                column_name = 'MotherID'
                        else:
                                column_name = 'IndividualID'+str(member-2)
                                child = True
                        break
if child:
        familyList = []
        for i in range(0,member):
                familyList.append(family[i])
        for i in range(member+1,family.__len__()):
                familyList.append(family[i])
        familyList.append(None)
        deleteFamilyQuery = 'DELETE FROM families WHERE FamilyID=\"'+familyID+'\"'
        cursor.execute(deleteFamilyQuery)
        insertFamilyQuery = 'INSERT INTO families VALUES ('
        for f in familyList:
                if f == None:
                        insertFamilyQuery+='null,'
                else:
                        insertFamilyQuery+='\"'+str(f)+'\"'
                        insertFamilyQuery+=','
        insertFamilyQuery = insertFamilyQuery.strip(',')
        insertFamilyQuery+=')'
        cursor.execute(insertFamilyQuery)
        member-=2
        getFamilyStatusQuery = 'SELECT * from families_status WHERE FamilyID=\"'+familyID+'\"'
        cursor.execute(getFamilyStatusQuery)
        family = cursor.fetchall()[0]
        familyList = []
        for i in range(0,member):
                familyList.append(family[i])
        for i in range(member+1,family.__len__()):
                familyList.append(family[i])
        familyList.append(None)
        deleteFamilyQuery = 'DELETE FROM families_status WHERE FamilyID=\"'+familyID+'\"'
```

```
                cursor.execute(deleteFamilyQuery)
                insertFamilyQuery = 'INSERT INTO families_status VALUES ('
                for f in familyList:
                        if f == None:
                                insertFamilyQuery+='null,'
                        else:
                                insertFamilyQuery+='\"'+str(f)+'\"'
                                insertFamilyQuery+=','
                insertFamilyQuery = insertFamilyQuery.strip(',')
                insertFamilyQuery+=')'
                cursor.execute(insertFamilyQuery)
        else:
                updateParentQuery = 'UPDATE families SET '+column_name+'=null WHERE FamilyID=\"'+familyID+'\"'
                cursor.execute(updateParentQuery)
        db.commit()
        cursor.close()


def deleteFamily(db):
        cursor = db.cursor()
        sqlQuery = 'SELECT familyID FROM families'
        cursor.execute(sqlQuery)
        results = cursor.fetchall()
        print 'Available families: '
        found = False
        while not found:
                for table in results:
                        print table[0]
                while 1:
                        print "Select Family ID: ",
                        familyID = sys.stdin.readline()
                        try:
                                familyID = int(familyID.split('\n')[0])
                                print 'Numeric values not allowed'
                        except Exception, e:
                                familyID = familyID.split('\n')[0]
                                break
                for table in results:
                        if table[0] == familyID:
                                found = True
                                break
                if not found:
                        print 'Not a valid Family ID:'
        getAllIndividuals = 'SELECT * FROM families WHERE FamilyID=\"'+familyID+'\"'
        cursor.execute(getAllIndividuals)
        family = cursor.fetchall()[0]
        for i in range(1,family.__len__()):
                if family[i] != None:
                        deleteTableQuery = 'DROP TABLE '+family[i]
                        cursor.execute(deleteTableQuery)
        deleteFamilyEntry = 'DELETE FROM families WHERE FamilyID=\"'+familyID+'\"'
        cursor.execute(deleteFamilyEntry)
```

```
        deleteFamilyStatusEntry = 'DELETE FROM families_status WHERE FamilyID=\"'+familyID+'\"'
        cursor.execute(deleteFamilyStatusEntry)
        deleteTableQuery = 'DROP TABLE '+familyID
        cursor.execute(deleteTableQuery)
        db.commit()
        cursor.close()


def compareFamilies(db,DBchoice):
        cursor = db.cursor()
        sqlQuery = 'SELECT familyID FROM families'
        cursor.execute(sqlQuery)
        results = cursor.fetchall()
        print 'Available families: '
        found = False
        while not found:
                for table in results:
                        print table[0]
                while 1:
                        print "Select the first Family ID: ",
                        familyID1 = sys.stdin.readline()
                        try:
                                familyID1 = int(familyID.split('\n')[0])
                                print 'Numeric values not allowed'
                        except Exception, e:
                                familyID1 = familyID1.split('\n')[0]
                                break
                for table in results:
                        if table[0] == familyID1:
                                found = True
                                break
                if not found:
                        print 'Not a valid Family ID:'
        found = False
        fList = []
        for table in results:
                fList.append(table[0])
        fList.remove(familyID1)
        while not found:
                for table in fList:
                        print table
                while 1:
                        print "Select the second Family ID: ",
                        familyID2 = sys.stdin.readline()
                        try:
                                familyID2 = int(familyID.split('\n')[0])
                                print 'Numeric values not allowed'
                        except Exception, e:
                                familyID2 = familyID2.split('\n')[0]
                                break
                for table in fList:
                        if table == familyID2:
```

```
                        found = True
                        break
        if not found:
                print 'Not a valid Family ID:'
while 1:
        print "Compare them based on: "
        print "1. homoz"
        print "2. linkage"
        print "Your Choice: ",
        choice = sys.stdin.readline()
        choice = choice.split('\n')[0]
        choiceS = ''
        if choice == '1':
                choiceS = 'homoz'
                break
        elif choice == '2':
                choiceS = 'linkage'
                break
        else:
                print "Please chose one of the following"
family1R = familyID1+'_'+choiceS
family2R = familyID2+'_'+choiceS
if checkTable(db,family1R) == 0:
        print choiceS+' has not run for family '+familyID1+'. Run now?'
        while 1:
                print '1. Run '+choiceS+' for family '+familyID1
                print '2. Exit'
                print "Your Choice: ",
                yc = sys.stdin.readline()
                yc = yc.split('\n')[0]
                if yc == '1':
                        runFunction(db,int(choice),DBchoice,familyID1)
                        break
                elif yc == '2':
                        sys.exit(0)
                        break
                else:
                        print "Please chose one of the following"
if checkTable(db,family2R) == 0:
        print choiceS+' has not run for family '+familyID2+'. Run now?'
        while 1:
                print '1. Run '+choiceS+' for family '+familyID2
                print '2. Exit'
                print "Your Choice: ",
                yc = sys.stdin.readline()
                yc = yc.split('\n')[0]
                if yc == '1':
                        runFunction(db,int(choice),DBchoice,familyID2)
                        break
                elif yc == '2':
                        sys.exit(0)
                        break
```

```
                        else:
                                print "Please chose one of the following"
        print 'About to compare family '+familyID1+' with family '+familyID2+' based on '+choiceS
        sqlQuery5 = 'SELECT DISTINCT Chromosome FROM '+family1R+' WHERE Chromosome IN (SELECT DISTINCT Chromosome FROM '+family2R+')'
        cursor.execute(sqlQuery5)
        chromosomeList = cursor.fetchall()
        resultsFile = 'results_'+familyID1+'_'+familyID2+'_'+choiceS+'.csv'
        resultsFILE = open(resultsFile, 'w')
        line = 'Chromosome,GeneticMap Start,GeneticMap End,Genetic Difference\n'
        resultsFILE.write(line)
        for chromosome in chromosomeList:
                chromosome = chromosome[0]
                fam1ResultsQuery = 'SELECT ProbeSetID,DbSnpRsID,Chromosome,GeneticMap FROM '+family1R+' WHERE Chromosome=\"'+chromosome+'\" ORDER BY
CAST(GeneticMap AS DECIMAL(20,15))'
                cursor.execute(fam1ResultsQuery)
                fam1Results = cursor.fetchall()
                fam2ResultsQuery = 'SELECT ProbeSetID,DbSnpRsID,Chromosome,GeneticMap FROM '+family2R+' WHERE Chromosome=\"'+chromosome+'\" ORDER BY
CAST(GeneticMap AS DECIMAL(20,15))'
                cursor.execute(fam2ResultsQuery)
                fam2Results = cursor.fetchall()
                # print fam1Results
                i = 0
                fam1R = []
                fam2R = []
                while i < fam1Results.__len__() - 1:
                        fam1R.append((fam1Results[i],fam1Results[i+1]))
                        i+=2
                i = 0
                while i < fam2Results.__len__() - 1:
                        fam2R.append((fam2Results[i],fam2Results[i+1]))
                        i+=2
                fam = fam1R
                fam.extend(fam2R)
                def compareThem(a,b):
                        return int(float(a[0][3]) - float(b[0][3]))

                fam = sorted(fam,cmp=compareThem)
                j = 0
                while j < fam.__len__() - 1:
                        highEnd = float(fam[j][1][3])
                        nextLow = float(fam[j+1][0][3])
                        nextHigh = float(fam[j+1][1][3])
                        count = 0
                        while highEnd >= nextLow:
                                if highEnd >= nextHigh:
                                        print 'Found Common: '+str(nextLow)+' - '+str(nextHigh)+' for Chromosome '+chromosome+' with Genetic
Difference: '+str(nextHigh - nextLow)
                                        line = chromosome+','+str(nextLow)+','+str(nextHigh)+','+str(nextHigh - nextLow)+'\n'
                                        resultsFILE.write(line)
                                else:
                                        print 'Found Common: '+str(nextLow)+' - '+str(highEnd)+' for Chromosome '+chromosome+' with Genetic Difference:
'+str(highEnd - nextLow)
```

```
                                        line = chromosome+','+str(nextLow)+','+str(nextHigh)+','+str(nextHigh - nextLow)+'\n'
                                        resultsFILE.write(line)
                                j += 1
                                count += 1
                                try:
                                        nextLow = float(fam[j+1][0][3])
                                        nextHigh = float(fam[j+1][1][3])
                                except Exception, e:
                                        break
                        j = j + 1 - count
        resultsFILE.close()
        print 'Comparison Results file '+resultsFile+' created succesfully at '+os.getcwd()
        db.commit()
        cursor.close()


def main():
        # database credentials and information
        try:
                db = MySQLdb.connect(host="localhost", user="root", passwd="root", db="panos2", local_infile=1)
        except Exception, e:
                print 'Cannot connect to MYSQL server. Make sure its running and check your settings.'
                sys.exit(-1)
        DBchoice = 0
        if sys.argv.__len__() == 2:
                if sys.argv[1] == '--rs':
                        try:
                                db = MySQLdb.connect(host="localhost", user="root", passwd="root", db="panos3", local_infile=1)
                        except Exception, e:
                                print 'Cannot connect to MYSQL server. Make sure its running and check your settings.'
                                sys.exit(-1)
                        DBchoice = 1
        # if the basic tables dont exist in the database initialize the database by creating them
        if checkTable(db,'families') == 0 and checkTable(db,'families_status') == 0 and checkTable(db,'annotation') == 0:
                print "Initializing database..."
                initialDBSetup(db,DBchoice)
                print "Done"
        else:
                print "Database already initialized"

        # print the menu and get the user's choice
        choice = printOptions()
        if choice == 1:
                # import new family member
                importFamilyMember(db,DBchoice)
        elif choice == 2:
                # generate input data for a family
                generateInputData(db,DBchoice)
        elif choice == 3:
                # run homoz or linkage or mendel for a family
                while 1:
                        print "Which function do you want to run?: "
```

```
                        print "1. homoz"
                        print "2. linkage"
                        print "3. mendel"
                        print "4. homoz and linkage"
                        print "Your Choice: ",
                        choice = sys.stdin.readline()
                        choice = choice.split('\n')[0]
                        if choice == '1' or choice == '2' or choice == '3':
                                runFunction(db,int(choice),DBchoice)
                                break
                        elif choice == '4':
                                runFunction(db,1,DBchoice)
                                runFunction(db,2,DBchoice)
                                break
                        else:
                                print "Please chose one of the following"
        elif choice == 4:
                # dump the data to a CSV file
                makeCSVfile(db)
        elif choice == 5:
                compareFamilies(db,DBchoice)
        elif choice == 6:
                # import a new annotation file
                importNewAnnotationFile(db)
        elif choice == 7:
                while 1:
                        print "What do you want to delete?: "
                        print "1. individual"
                        print "2. whole family"
                        print "Your Choice: ",
                        choice = sys.stdin.readline()
                        choice = choice.split('\n')[0]
                        if choice == '1':
                                deleteIndividual(db)
                                break
                        elif choice == '2':
                                deleteFamily(db)
                                break
                        else:
                                print "Please chose one of the following"
        elif choice == 8:
                print 'Quiting...'
                sys.exit(0)
        else:
                print "WRONG INPUT"
        db.close()

if __name__ == '__main__':
        main()
```

6.3 Publications Related to This Thesis

As first author

Sergouniotis PI, Davidson AE, Lenassi E, Devery SR, Moore AT, Webster AR. Retinal structure, function, and molecular pathologic features in gyrate atrophy. Ophthalmology. Ophthalmology. 2012 Mar; 119(3): 596-605. PMID: 22182799

Sergouniotis PI, Davidson AE, Mackay DS, Lenassi E, Li Z, Robson AG, Yang X, Kam JH, Isaacs TW, Holder GE, Jeffery G, Beck JA, Moore AT, Plagnol V, Webster AR. Biallelic mutations in *PLA2G5*, encoding group V phospholipase A_2, cause benign fleck retina. Am J Hum Genet. 2011 Dec; 89(6): 782-91. PMID: 22137173

Sergouniotis PI, Robson AG, Li Z, Devery S, Holder GE, Moore AT, Webster AR. A phenotypic study of congenital stationary night blindness (CSNB) associated with mutations in the *GRM6* gene. Acta Ophthalmol. 2011 Oct 19 [Epub ahead of print]. PMID: 22008250

Sergouniotis PI, Davidson AE, Mackay DS, Li Z, Yang X, Plagnol V, Moore AT, Webster AR. Recessive mutations in *KCNJ13*, encoding an inwardly rectifying potassium channel subunit, cause Leber congenital amaurosis. Am J Hum Genet. 2011 Jul 15; 89(1): 183-90. PMID: 21763485

Sergouniotis PI, Holder GE, Robson AG, Michaelides M, Webster AR, Moore AT. High-resolution optical coherence tomography imaging in *KCNV2* retinopathy. Br J Ophthalmol. 2011 May 10 [Epub ahead of print]. PMID: 21558291

Sergouniotis PI, Sohn EH, Li Z, McBain VA, Wright GA, Moore AT, Robson AG, Holder GE, Webster AR. Phenotypic variability in *RDH5* retinopathy

(Fundus Albipunctatus). Ophthalmology. 2011 Aug; 118(8): 1661-70. PMID: 21529959

Sergouniotis PI, Davidson AE, Sehmi K, Webster AR, Robson AG, Moore AT. Mizuo-Nakamura phenomenon in Oguchi disease due to a homozygous nonsense mutation in the *SAG* gene. Eye (Lond). 2011 Aug; 25(8): 1098-101. PMID: 21494281

Sergouniotis PI, Li Z, Mackay DS, Wright GA, Borman AD, Devery SR, Moore AT, Webster AR. A survey of DNA variation of *C2ORF71* in probands with progressive autosomal recessive retinal degeneration and controls. Invest Ophthalmol Vis Sci. 2011 Mar 30; 52(3): 1880-6. PMID: 20811058

As co-author

Poulter J, Davidson AE, Ali M, Gilmour DF, Parry D, Mintz-Hittner HA, Carr I, Bottomley HM, Long V, Downey LM, **Sergouniotis PI**, Wright GA, MacLaren RE, Moore AT, Webster AR, Inglehearn CF, Toomes C. Recessive mutations in *TSPAN12* cause retinal dysplasia and severe familial exudative vitreoretinopathy (FEVR). Invest Ophthalmol Vis Sci. 2012 Mar 16. [Epub ahead of print]. PMID: 22427576

Mackay DS, Ocaka LA, Borman AD, **Sergouniotis PI**, Henderson RH, Moradi P, Robson AG, Thompson DA, Webster AR, Moore AT. Screening of *SPATA7* in patients with Leber congenital amaurosis and severe childhood-onset retinal dystrophy reveals disease-causing mutations. Invest Ophthalmol Vis Sci. 2011 May 9; 52(6): 3032-8. PMID: 21310915

Davidson AE, **Sergouniotis PI**, Burgess-Mullan R, Hart-Holden N, Low S, Foster PJ, Manson FD, Black GC, Webster AR. A synonymous codon variant in two patients with autosomal recessive bestrophinopathy alters in vitro splicing of *BEST1*. Mol Vis. 2010 Dec 31; 16: 2916-22. PMID: 21203346

Henderson RH, Mackay DS, Li Z, Moradi P, **Sergouniotis P**, Russell-Eggitt I, Thompson DA, Robson AG, Holder GE, Webster AR, Moore AT. Phenotypic variability in patients with retinal dystrophies due to mutations in *CRB1*. Br J Ophthalmol. 2011 Jun; 95(6): 811-7. PMID: 20956273

Mukhopadhyay R, **Sergouniotis PI**, Mackay DS, Day AC, Wright G, Devery S, Leroy BP, Robson AG, Holder GE, Li Z, Webster AR. A detailed phenotypic assessment of individuals affected by *MFRP*-related oculopathy. Mol Vis. 2010 Mar 26; 16: 540-8. PMID: 20361016

Mackay DS, Henderson RH, **Sergouniotis PI**, Li Z, Moradi P, Holder GE, Waseem N, Bhattacharya SS, Aldahmesh MA, Alkuraya FS, Meyer B, Webster AR, Moore AT. Novel mutations in *MERTK* associated with childhood-onset rod cone dystrophy. Mol Vis. 2010 Mar 9; 16: 369-77. PMID: 20300561

Li Z, **Sergouniotis PI**, Michaelides M, Mackay DS, Wright GA, Devery S, Moore AT, Holder GE, Robson AG, Webster AR. Recessive mutations of the gene *TRPM1* abrogate ON bipolar cell function and cause complete congenital stationary night blindness in humans. Am J Hum Genet. 2009 Nov; 85(5): 711-9. PMID: 19878917